

Chitosan Nanoplexes For Target siRNA Delivery

Dissertation
zur Erlangung des Doktorgrades
der Mathematisch – Naturwissenschaftlichen Fakultät
der Eberhard Karls Universität Tübingen

vorgelegt von

Andra Guțoia

aus Galați, Rumänien

Tübingen

2015

Tag der mündlichen Prüfung:

17.12.2015

Dekan:

Prof. Dr. Wolfgang Rosenstiel

1. Gutachter:

Prof. Dr. Stefan Laufer

2. Gutachter:

Prof. Dr. Dieter Stoll

Acknowledgements

Completing a PhD takes courage, perseverance, and discipline, but mostly this thesis has been kept on track and seen through to completion with the support and encouragement of numerous great people.

I would like to express my sincere appreciation to my “Doktorvater”, Prof. Stefan Laufer for your guidance, constant support, and many insightful discussions throughout this project.

I am very fortunate to have had Prof. Dieter Stoll as my NMI supervisor. I have learned a great deal from your perspective on research, sharp insight, your personal integrity, and expectations of excellence. I am deeply grateful for the effort you have put in my thesis correction, for taking the time to go into detail and giving me very helpful feedback.

I am grateful to Prof. Rumen Krastev, Dr. Simona Margutti and Prof. Hugo Hämmerle for giving me the opportunity to work at the NMI and introducing me to the biomaterials world. Simona you have influenced the course of my PhD work and life in many ways. Your drive, positive thinking, scientific knowledge and problem solving skills have been invaluable to me throughout my PhD. Rumen, your guidance and discussions on any issues that arose is greatly appreciated. I always felt I could count on you. Prof. Hämmerle, I would like to thank you for financing my work at the NMI and for your support to complete the linker story.

There are two people that need to be mentioned especially, Dr. Hanna Hartmann and Dr. Liane Schuster, *the tandem team!* Your contribution to my understanding of cell cytotoxicity, uptake, knockdown, antibody fragment synthesis, *in vitro* cell behaviour, and many more, was very valuable and is greatly appreciated. Hanna, I am extremely thankful for your constant support and understanding on scientific and personal matters.

A good support system is important for survival during the PhD. I was lucky to be a part of the Biomaterials group, a source of friendships as well as good advice and collaboration. I would like to say thank you to Elsa Arefaine (the LbL expert and a valuable friend that was always there for me), Marcus Hermann (extremely knowledgeable in just about everything), Dr. Xin Xiong (extremely giving – even if he tries to hide it), Alex Wilsdorf (the “new” PhD student, or the third PhD student of the Biomaterials group – thank you for all your support and generosity). I would like also to thank: Alex Rudt (for the help with the chitosan_PEG solubility tests and for all the help with the German translations), Kerstin Frey (for the help with the cytotoxicity assay), Andreas Früh (for the help with the chitosan_PEG solubility

tests), Nina Baldassi, Fatima Nouredine, Lili Sun, Dr. Dominic Stadel (for the cell experiments), Elke Rist (for helping me out with the cell experiments on short notice).

During my PhD I had the pleasure to work also with other groups at the NMI such as Dr. Jens Goepfert (thank you for the scientific discussions and planning of the ELISA experiments), Dr. Bart van den Berg, Benedikt Lang and Kerstin Pohl (I am so grateful for the help with MS analysis of the antibody fragment, for the help with the calculations), Felix Emele and Philipp Kaiser (thank you for the help with the single chain fragment antibody production and detection), Philipp Kammerlohr (I am deeply grateful for the your patient help with the GPC and IR), Christopher Pynn and David Eisen (my friend and companion during the long hours at the NMI), Sandra Maier (thank you for giving me some of the best news of my PhD – the MS of the small chemical inhibitor_linker system and all the LC-MS analytics), Christian Freudigmann, Cornelia Sommersdorf, Nico Weber, Ramona Samba (you were a great support at the NMI and I value our friendship).

A special thank you goes to Felix Niethammer! You have been a fountain of knowledge in regards to HPLC, MALDI, MS in general. Thank you for helping me with all the HPLC purifications and analysis, MALDI measurements, and for the fruitful scientific discussions.

I am grateful also to Prof. Laufer's group at the University of Tübingen, my second PhD family: Gerd Helms (help with the NMR, and many great discussions), Ellen Pfaffenrot (thank you for sharing with me the "working place"), Marcel Günther (thank you for the NMR key, Mestrenova software and nice time during the weekend in the lab), Dr. Matthias Gehringen and Michael Forster (great discussions, FTIR help, NMR access), Dr. Raimund Nieß (thank you for the support with all the administrative assistance), Katharina Bauer (thank you for always making me feel welcome the university) and all the other past and current members. In this context I would like to thank particularly Karin Ward for her administrative support.

Thank you to Prof. Roland Kontermann and his group at the Institute of Cell Biology and Immunology, University of Stuttgart, for providing the scFv'LCH3 construct and giving advice for its expression.

The great collaboration with Prof. Pieter Van den Veken and his group at the University of Antwerp lead to the design, synthesis and characterization of the *novel* FAP small chemical inhibitor_linker system. Thank you for the reliable and professional support.

In the challenging moments of my PhD, I was lucky to count on the support and motivation of Dr. Teodora Miclaus. Thank you for the protein corona, DLS discussions and proof reading, for the many articles, and for introducing me to the wonderful world of tennis.

Towards the end of the thesis some great people were by my side and would like to thank them for the technical support (Ramona Dima, Ruxandra Vilag) and proof reading parts of my thesis (Dr. Ross Cunningham, David Hiemstra, and Peter Jones).

A heart felt thank you to my friend, my partner in crime, my Roland. I am grateful for your support, the long weekends in the lab, the long scientific discussions, for helping with the translations, for putting up with me during the challenging times.

I finish with the most basic source of my life energy, my family. Although at times it was hard, they always offered me their unconditional support. They were investing, encouraging, engaged in the process, and always made an effort to understand what I am working on and how I am doing.

List of abbreviations

°C	grad Celsius
A	ampere
ANOVA	analysis of variance
BSA	bovines Serum Albumin
CAAC	Cu catalyzed azide alkyne cycloaddition
ACN	acetonitrile
CCM	cell culture medium
chi	chitosan
Cu	copper
DA	degree of acteylation
DD	degree of deacetylation
DNA	Deoxyribonucleic acid
DOPE	1,2-dioleoyl- <i>sn</i> -glycero-3-phosphoethanolamine
DPP	dipeptidyl peptidase
dsRNA	double stranded RNA
ECM	extracelullar matrix
ER	endoplasmic reticulum
FAP	fibroblast activation protein
FBGC	foreign body giant cells
FBR	foreign body response

FCS	fetal calf serum
FPLC	fast protein liquid chromatography
FTIR	fourier transform infrared
GFP	green fluorescence protein
GlcN	D-glucosamine
GlcNAc	N-glucosamine
GPC	gel permeation chromatography
HCCA	alpha-cyano-4-hydroxycinamic acid
His	hexahistidyl tag
HSP47	heat shock protein 47
IMAC	immobilized metal ion affinity chromatography
KBr	potassium bromide
LbL	layer-by-layer
M_N	number average molecular weight
mRNA	messenger RNA
M_w	molecular weight
N/P	nitrogen/phosphate ratio
NMR	nuclear magnetic resonance
NP	nanoplex
PAA	poly(aspartic acid)
PBS	phosphate buffer saline
PEG	Poly(ethyleneglycol)

PEI	polyethylenimine
PEM	polyelectrolyte multilayer
PREP	prolyl oligopeptidase
QCM	quartz crystal microbalance
Rh	hydrodynamic radius
RISC	RNA induced silencing complex
RNA	ribonucleic acid
RNAi	RNA interference
rpm	rotations per minute
RT	room temperature
scFv	single chain fragment
siRNA	small interference RNA
SPAAC	strain-promoted azide alkyne cycloaddition
TFA	trifluoroacetic acid
TPP	tripolyphosphate
V _H	heavy chain
V _L	light chain
ζ	zeta potential
η	intrinsic viscosity

INDEX

ABSTRACT	5
ZUSAMMENFASSUNG	7
1. INTRODUCTION	9
1.1. Biomaterials	9
1.2. RNA interference (RNAi) based therapy.....	11
1.3. Polymeric based siRNA delivery.....	15
1.4. Chitosan for oligonucleotide complexation	16
1.5. Chitosan:siRNA nanoplex formation	17
1.6. Physiological barriers for chitosan: siRNA nanoplex delivery	18
1.7. Chitosan modifications	21
1.7.1. Chitosan Poly(ethylene glycol) (PEG) modification	24
1.7.2. Chitosan modifications for specific targeted nanoplex delivery	25
1.7.3. Bioconjugation techniques.....	28
1.7.4. Orthogonal conjugation chemistry based on 1,3 –dipolar cycloadditions.....	32
1.8. Layer-by-layer coating and release	35
2. AIM OF THE PRESENT STUDY	38
3. RESULTS.....	39
3.1. Influence of molecular weight (M_w) and degree of deacetylation (DD) on the physico-chemical properties of chitosan for nanoplex formation.....	39
3.1.1. Alkaline deacetylation of chitosan	39
3.1.2. Analytical characterization of deacetylated chitosans.....	41
3.1.3. Chitosan siRNA nanoplexes	46
3.2. Chitosan – PEG synthesis and physicochemical characteristics	48
3.2.1. Synthesis of chitosan with different degrees of substitution (DS)	48
3.2.2. Analytical characterization of PEGylated chitosan.....	49
3.2.3. Influence of the DS on the solubility of mPEG-chitosan copolymer in aqueous buffers	53
3.2.4. Influence of the mPEG DS on the formation of chitosan_PEG siRNA nanoplexes	54
3.2.5. PEGylated chitosans cell viability	56
3.2.6. Effect of the dynamic cell environment on the properties of PEGylated chitosan:siRNA nanoplexes properties	57
3.2.7. Cellular uptake of chitosan and Chi_PEG:siRNA.....	67
3.3. Knockdown of chitosan and chi_PEG:siRNA nanoplexes	70

3.4. Targeted delivery of siRNA nanoplexes to specific cells	72
3.4.1. Electrostatic interaction of scFv'LCH3 target protein and nanoplex surface	72
3.4.2. Chemistry of the linker system.....	73
3.4.3. Bioconjugation of biological targets via a free thiol group to the maleimide linker system.....	82
3.4.4. Chemical inhibitor for specific cell targeting	92
3.4.5. Chitosan_PEG_N3.....	96
3.4.6. Functionality of the scFv'LCH3 after bioconjugation to the linker system.....	101
3.5. Layer by layer	103
3.5.1. Build-up of (HA/Ch) ₂ (HA/NP) _n PEM layer	103
3.5.2. NPs release over time	104
4. DISCUSSION.....	106
4.1. The optimal chitosan for siRNA delivery	106
4.2. Impact of the PEGylation on the chitosan siRNA delivery system	107
4.3. Targeting of the chitosan_PEG siRNA delivery system	113
4.4. Local delivery via LBL coating and release.....	119
5. CONCLUSIONS.....	121
6. MATERIALS AND METHODS	124
6.1. Materials	124
6.1.1. Table 14. Different siRNA's.....	128
6.1.2. E.coli bacteria	129
6.1.3. Medium for bacterial culture	129
6.1.4. Buffers and solutions.....	130
6.2. Biological and biochemical methods.....	132
6.2.1. Chi, Chi_PEG and NP cell viability.....	132
6.2.2. Cell culture for immunocytochemistry.....	132
6.2.3. Immunocytochemistry	132
6.2.4. Expression and purification of scFv'36LCH3.....	133
6.2.5. Antibody fragment characterization	136
6.3. Physico-chemical methods	137
6.3.1. Nanoplex formation and characterization	137
6.3.2. Stability measurement of chitosan/siRNA nanoplexes	137
6.3.3. Fluorescence Quenching Assay	138
6.3.4. Build-up of (HA/Chi) ₂ (HA/NP) _n PEM	138
6.3.5. Release of chi_PEG:siRNA ^{Tye563} over time	139
6.4. Analytical chemistry methods.....	139
6.4.1. NMR – Spectroscopy	139
6.4.2. Gel permeation chromatography (GPC).....	140
6.4.3. Fourier transform infrared (FT-IR).....	141

6.4.4.	Solubility measurement via UV/VIS	141
6.4.5.	LC-MS/ESI and direct injection ESI	141
6.4.6.	MALDI	141
6.4.7.	HPLC	141
6.4.8.	Quartz crystal microbalance (QCM)	142
6.5.	Statistical analysis.....	142
7.	EXPERIMENTAL SECTION.....	143
7.1.	Deacetylated chitosan	143
7.2.	Synthesis of mPEG grafted chitosan: Reaction conditions.....	143
7.3.	Synthesis of the linker system	144
8.	APPENDIX	153
8.1.	Functionality of the bioconjugated linker_FAP chemical inhibitor (UAMC 1533)	153
9.	REFERENCES	154

Part of my work was published in

Fine-tuning of PEG-chitosan/siRNA nanoplexes for efficient gene silencing

Andra Guţoiaia*, Liane Schuster*, Simona Margutti, Stefan Laufer, Burkhard Schlosshauer,
Rumen Krastev, Dieter Stoll, Hanna Hartmann

Submitted manuscript

Abstract

In recent years biopharmaceutical companies have started to turn their attention towards small interfering RNA (siRNA) therapeutics, as they offer a strategy to address therapeutically interesting targets that are not “druggable” with classic small molecule inhibitors. siRNAs can be easily adapted to any target of interest; they operate upstream of the protein production by silencing the messenger RNA (mRNA) before it is translated into pathogenic or disease-related proteins.

However, the successful application of siRNA based therapy strongly depends on the development of an efficient delivery system to (1) specifically target a particular cell type, (2) protect the siRNA from ribonucleases enzymatic degradation, (3) be taken up by the cells, and (4) release the siRNA in the cytoplasm where the targeted mRNA is located. Therefore, the main focus of this study was to design, synthesize and characterize an efficient and specific delivery system for siRNA.

Chitosan is a versatile, biocompatible and biodegradable polymer with high positive charge density. As such, it can be modified and optimized with various domains, thus proving to be very suitable as a gene delivery system. Despite the advantage of being biocompatible and biodegradable, chitosan has also some drawbacks, one of them being low solubility at physiological pH which can influence the formation of nanoplex (NP) aggregation.

Upon contact with biological fluids, chitosan:siRNA NP may unspecifically interact with the charged biological components. Therefore, chitosan was first conjugated with increasing grafting ratios of hydrophilic polyethylene glycol (PEG). The systematical analysis of various chitosan_PEGs enabled the identification of a defined PEG ratio with a low impact on the advantageous physicochemical characteristics of chitosan NP, whilst maintaining high gene transfection efficiency.

Further work was focused on a specific targeting of the NP. Two different strategies were pursued: targeting with a small molecule inhibitor as well as targeting via a specific antibody fragment. The exposed position of the targeting moiety on the surface of the NP, outside of any shielding effect, is one of the basic requirements for the effective addressing of the target. Therefore the main building block of the linker system had to be based on a spacer system. PEG was the obvious choice as the spacer moiety due to the positive results with

chitosan_PEG NP. A heterofunctional linker system was developed, with one end selective to the targeting moiety and other end selective to the modified chitosan.

The siRNA delivery system was designed with the aim of incorporating the NP on the surface of implantable medical devices. Therefore, a layer-by-layer coating approach of solid surfaces was tested with chitosan_PEG/siRNA NP with regards to layer deposition and release of the NP over time.

Overall, this study provided a delivery system with high transfection efficiency, achieved by an optimized PEG ratio. The developed system was further modified for specific cell targeting with both biological molecules and chemical inhibitors via a highly flexible heterofunctional linker system. Together with the layer by layer coating, the basis for a highly flexible and efficient targeted siRNA delivery system was successfully developed, providing a broad know-how for the further development of various siRNA delivery systems.

Zusammenfassung

Während der letzten Jahre bestand ein verstärktes Interesse der biopharmazeutischen Industrie an der Entwicklung RNA-Interferenz basierter Therapeutika, größtenteils mittels siRNA (small interfering RNA). Diese Technologie bietet die Möglichkeit therapeutisch interessante Targets zu adressieren, welche mit den klassischen Ansätzen der niedermolekularen Wirkstoffe gar nicht oder nur mit unzureichender Spezifität inhibiert werden können. siRNA Wirkstoffe können für jedes Target optimiert werden. Sie greifen immer innerhalb der jeweiligen Proteinsynthese in die Proteinbiosynthese ein, indem sie die messengerRNA (mRNA) für das therapeutisch relevante Targetprotein abbauen. Dadurch wird die Expression des krankheitsrelevanten Targetproteins verhindert oder stark reduziert. Allerdings hängt die erfolgreiche Anwendung von siRNA basierten Therapien stark von der Entwicklung geeigneter und effizienter Transportsysteme ab, welche (1) eine spezifische Zelladressierung gewährleisten (2) die siRNA vor enzymatischem Abbau durch Ribonukleasen schützen (3) eine effiziente *Zellaufnahme* ermöglichen (4) siRNA spezifisch im Zytoplasma freisetzen. Das Ziel dieser Studie war das Design, Synthese und Charakterisierung eines effizienten und spezifischen siRNA Transportsystems.

Chitosan ist ein vielseitiges, biokompatibles, sowie biologisch abbaubares Polymer mit hoher Ladungsdichte. Als solches kann dieses vielseitig modifiziert und optimiert werden und eignet sich daher besonders als Wirkstoff-Transportsystem. Trotz der Vorteile der Biokompatibilität und biologischen Abbaubarkeit, hat Chitosan auch nachteilige Aspekte. Einer dieser Herausforderungen ist die geringe Löslichkeit unter physiologischen Bedingungen, mit Einfluss auf die Aggregation der Nanoplexe. Desweiteren, können die Chitosan-siRNA Nanoplexe in einer biologischen Matrix unspezifische Wechselwirkungen mit biologischen geladenen Komponenten eingehen. Um diesen Effekten entgegen zu wirken, wurde Chitosan in verschiedenen Substitutionsgraden mit Polyethylenglykol konjugiert. Die Untersuchung verschiedener Pegylierungsgrade von Chitosan ergab einen definierten Pegylierungsgrad mit geringem Einfluss auf die vorteilhaften Eigenschaften von Chitosan.

Ein weiterer Schwerpunkt dieser Arbeit lag auf der spezifischen Adressierung der Nanoplexe (NP), damit diese nur von speziellen Zielzellen aufgenommen werden. Zwei verschiedene Ansätze wurden hierbei verfolgt, zum einen die Adressierung mit Hilfe eines niedermolekularen Inhibitors zum anderen durch ein spezifisches Antikörper-Fragment. Eine exponierte Lage dieser Targeting-Moleküle auf der NP-Oberfläche, außerhalb jeglicher

Abschirmungseffekte, ist eine der Grundvoraussetzungen für eine erfolgreiche Adressierung des Zielsystems. Daher basierte einer der essentiellen Teilstrukturen des nötigen Linkersystems auf einem Spacer. Durch die positiven Ergebnisse mit Chitosan PEG NP, lag es nahe PEG auch als Spacersystem zu verwenden. Basierend hierauf wurde ein heterofunktionales Linkersystem aufgebaut, zum einen selektiv gegenüber dem zu kuppelnden Targetingmolekül, zum andere gegenüber modifiziertem Chitosan.

Das erarbeitete siRNA Transportsystem wurde mit dem Ziel entworfen die NP in die Oberfläche medizinischer Implantate zu integrieren. Es wurde daher ein layer by layer Beschichtungsverfahren mit chitosan_PEG/siRNA NP getestet, im Hinblick auf die Schichtablagerung und die zeitabhängige NP Freisetzung.

Im Verlauf dieser Arbeit wurde ein Transportsystem mit hoher Transfektionseffizienz über ein optimiertes Pegylierungsverhältnis entwickelt. Das System wurde mit Hilfe eines biologischen Antikörper-Fragments, bzw. eines niedermolekularen Inhibitors im Hinblick auf dessen Spezifität weiter optimiert. Zusammen mit dem getesteten Beschichtungsverfahren wurden neue wissenschaftliche Erkenntnisse für die Entwicklung verschiedenster siRNA Transportsysteme gewonnen, die als Basis eines hoch flexiblen und spezifischen siRNA Transportsystems angewendet werden können.

1. Introduction

1.1. Biomaterials

Throughout history the idea of inserting foreign objects into the human body has emerged numerously. The earliest known examples of medical use include suturing of wounds and replacement of teeth with materials of biological origin. Since then carefully selected and manufactured materials to recover or replace physiologic disabilities have been well established [1-3]. Scientists categorized these materials in three primary types, *metallic*, being based on the metallic bond, *ceramic*, based on a mixture of ionic and covalent bonds and *polymeric*, based on covalent bonds. Each of these categories contained many subdivisions. However, these boundaries between material classes have now been eroded; those substances derived from clear, chemically defined primary interatomic and intermolecular bonds are being replaced by those of greater structural complexity [4]. In a similar way biomaterials are broadly defined as materials intended to interact with biological systems to “evaluate, treat, augment or replace any tissue, organ or function of the body” [5].

Synthetic and natural biomaterials are now being used for various medical applications such as tissue cultures [6], synthetic skin [7], hybrid organs [8], synthetic blood vessels [9], artificial hearts [10], cardiac pacemakers [11], drug delivery systems [12-14], wires and pins for bone treatments, total artificial joint implants [15], skull reconstruction [16], dental and maxillofacial applications [17]. Although their bulk properties should not be ignored, their contact to the cells and tissues via their surface is of utmost importance. The characterization of the material interaction with cells was, frequently based on biocompatibility, initiation of tissue ingrowth into the material’s void space or host tissue integration properties [18].

The clinical application of many of the implantable devices developed in recent years is still a critical issue due to the foreign body reaction (FBR). Even though, the ability of the body to protect itself against foreign bodies such as toxic components, bacterial toxins and allergens is regarded as an advantage, for an implant this reaction can be very detrimental. The formation of a fibrotic capsule on the surface of an implanted medical device can lead to the impairment or failure to perform its functions (Figure 1) [19, 20].

Already after the first contact with the tissue, proteins from blood and interstitial fluid are adsorbed on the implant surface. A process referred to as biofouling. The proteins are mainly fibrinogen and immunoglobulin. The protein layer is a trigger for the activation of the

coagulation cascade of the complement of platelets and immune cells. Phagocytic cells such as neutrophils and macrophages are the first ones trying to destroy or eliminate the foreign body. This is not possible due to the size of the implant and the nature of the material. This leads to the so-called "frustrated phagocytosis", resulting in the fusion of macrophages to polymorph nuclear cells creating the foreign body giant cells (FBGCs), which generate fusogenic cell phenotype or macrophages at the implant surface. This macrophage phenotype produces a variety of cytokines which lead to the recruitment and activation of fibroblasts as in normal wound healing. The ongoing activity of enteric FBGCs leads to prolonged fibroblast activation and excessive deposition of extracellular matrix (ECM) and ultimately to the formation of a fibrotic capsule surrounding the entire implant [21].

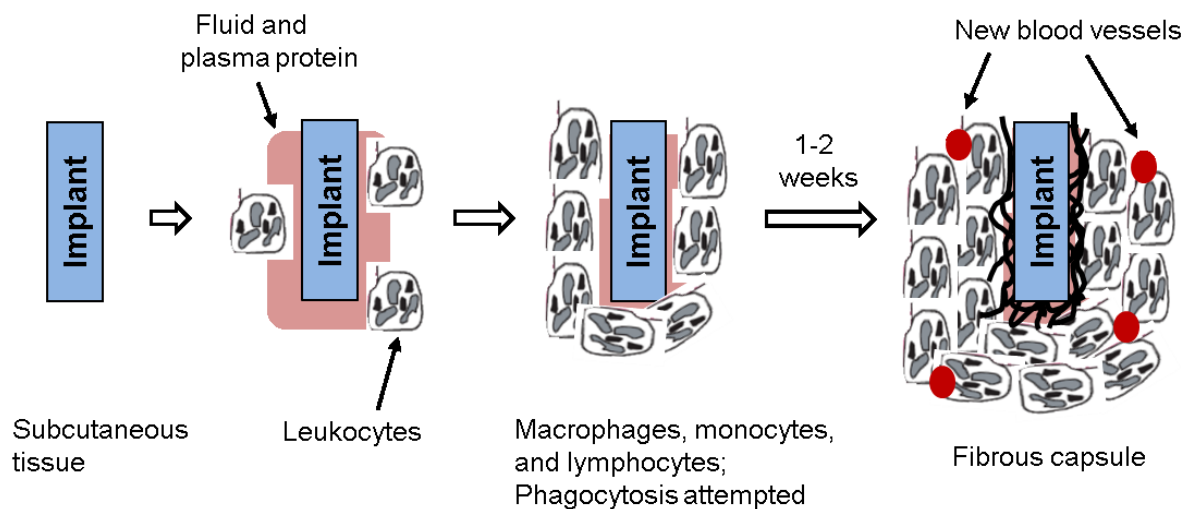


Figure 1. Formation of fibrotic capsule around implanted biosensors [22]. The implant is immediately covered by plasma proteins. Leucocytes recognize the foreign environment and attract other immune cells. As large implants cannot be eliminated by phagocytosis, foreign body giant cells are formed which recruit fibroblasts. In the end the entire implant is packed in a capsule of fibrotic tissue.

Biocompatibility of an implant therefore influences the extent, intensity and duration of inflammation and wound healing processes. Size, shape and mainly chemical and physical properties of the surface material determine the biocompatibility of an implant. Polymers have great potential to construct or to coat biomaterials for applications in biomedicine, pharmaceuticals and biotechnology. Their chemical modifications lead to the synthesis of materials with diverse physical and mechanical properties. Furthermore, stimuli-responsive polymers are engineered to undergo chemical or physical transitions in response to specific

external triggers. One such example could be bio-degradation over time. Another advantage of using polymers for implant surfaces is the possibility of adding or incorporating active substances at the surface either via covalent bonds or via a layer-by-layer approach [23]. Such a bioactive implant surface with incorporated active substances could target the foreign body response in order to trigger the healing process, but prevent it from evolving to the formation of the fibrous capsule.

1.2. RNA interference (RNAi) based therapy

The concept behind gene therapy is based on the use of nucleic acids as drugs with the aim of restoring or shutting down a specific cellular function. In contrast to conventional drugs that often focus on the treatment of clinical symptoms, gene therapy provides an alternative treatment which tries to fix a genetic dysfunction at its source [24]. Proteins for example are responsible for a variety of the physical and dynamic properties of a cell. Defects in the protein function or regulation contribute to or are even the cause of many diseases. Therefore, a significant number of drugs today are designed to selectively inactivate proteins by interfering with the enzymatic activity of the target protein, relying on distinct binding pockets of proteins. Oligonucleotides are molecules that operate upstream of the protein production in a cell. They target genes directly and can be stably integrated into chromosomes. But transient knockout of genetic information is easier to become “druggable”. Such therapies usually target mRNA – the carrier of genetic information before translation [25, 26]. Because mRNAs encode all cellular proteins, oligonucleotides targeting mRNA could prove to be effective for targets and disease that are not treatable by current drugs and are caused by the overexpression of single proteins [27, 28]. The cellular RNA interference (RNAi) mechanism starts with the enzymatic degradation of the double-stranded RNAs (dsRNA) into 21-22 nucleotides long dsRNAs, known as small interfering RNAs (siRNAs) (see Figure 2). These are included in the RNA induced silencing complex (RISC) with so-called Argonauts proteins. Within the RISC, the siRNA is unwound, the sense strand is discarded, and the antisense or guide strand binds to mRNA. When siRNA is fully complementary to its target, the endonuclease Argonaut 2 – a component of the RISC - cleaves the mRNA within the hybridization site preventing the translation of genetic information into the targeted protein. The remaining sections of the mRNA are degraded and the RISC complex will further degrade the next mRNA strand [29-33]

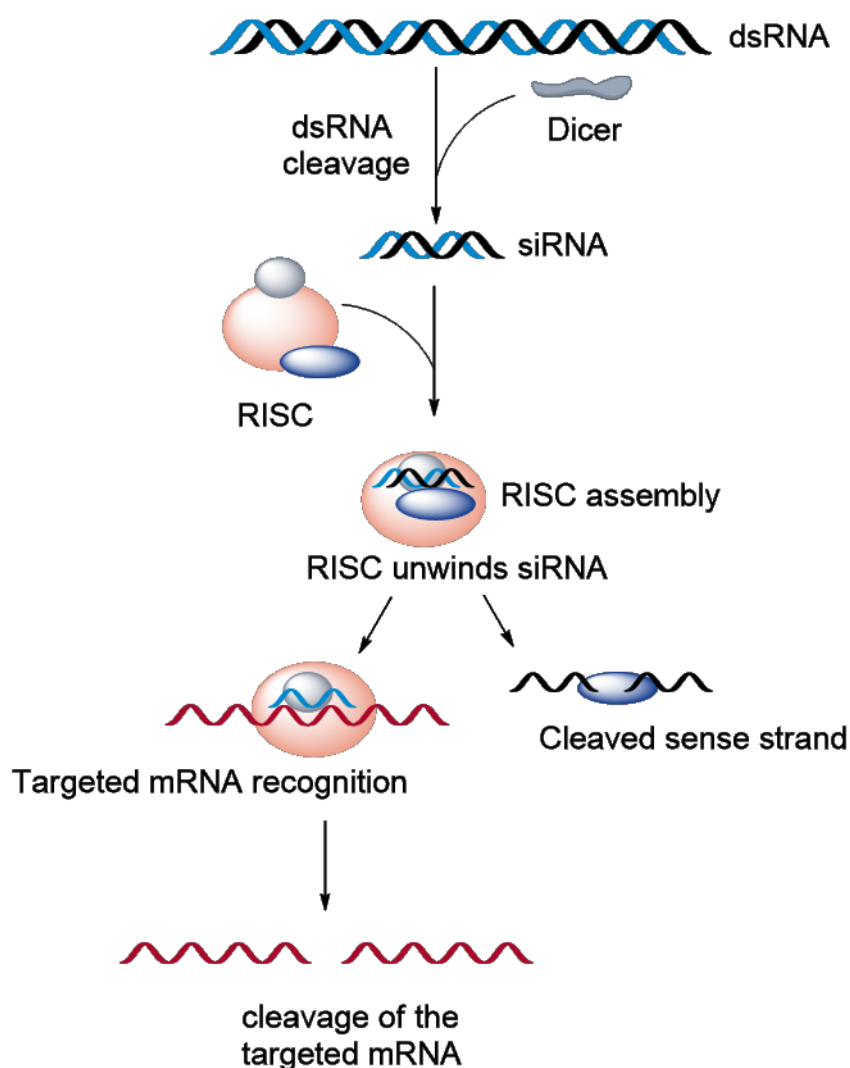


Figure 2. Scheme of the mechanism of cellular RNA interference. dsRNA is cleaved by an enzyme (“dicer”) into short dsRNA fragments known as siRNA. These short dsRNA fragments are then bound to Argonaut proteins building the so called RISC. In this complex one siRNA strand (sense strand) is degraded whereas the other one is bound to the RISC complex and serves as a template for the binding of homologous mRNA. RISC targets complementary single stranded mRNA by its bound antisense siRNA fragment and then degrades the bound mRNA by the so called “slicer” proteins.

RNAi is an endogenous biological pathway which regulates protein expression in many eukaryotes at the mRNA level. RNAi is a key process in gene silencing and defense against viral infections. Furthermore, RNAi allows the development of efficient drugs [34]. As siRNA is part of the catalytic RISC complex it mediates the silencing of many mRNAs. The very small concentrations of siRNAs can minimize the risk of adverse side effects often caused by the use of high drug dosages. In sharp contrast to small molecules, which have very diverse chemical properties and therefore pharmacological challenges that are very specific to

each drug candidate, the chemical uniformity of all siRNAs enables to use the know-how from the development of one siRNA drug candidate to establish an entire therapeutic platform for siRNA delivery [35, 36].

Even though the biomedical potential of siRNA is very promising, the side effects cannot be excluded. siRNA can lead to „off-target” effects on gene expression [37] as well as inducing the immune response [38, 39]. The sequence-specific „off-target” effect is caused by hybridization of other mRNA than the target one, while the sequence-unspecific „off-target” effect is induced by binding to proteins [28, 40]. However, it was shown that by slightly modifying the oligonucleotide design the „off-target” effect could be avoided without compromising the potency of siRNA [38, 41]. The immune stimulation can also be avoided either by careful oligonucleotide modifications [42] or by using delivery systems that shield siRNA and avoid interaction with immune cells [43].

siRNA could be used for coatings on the surface of implants[44] in order to target the anti-inflammatory response[45] without interfering with the reendothelialization of the device. The foreign body response to the implanted device leads to the formation of an extracellular matrix (ECM). One main component of the ECM is collagen which binds cells together and forms a reservoir for hormones and growth factors. There are several types of collagen found in different tissues optimized for their specific local function [46]. Collagen biosynthesis is a multi-step complex process that includes both intracellular and extracellular events (Figure 3) [47]. During the processing and folding steps within the endoplasmic reticulum (ER) heat shock protein 47 (HSP47) plays an important role. This chaperone specifically binds to collagen and ensures the correct folding. HSP47 is assumed to protect against premature degradation of the unfolded procollagen. In addition, it stabilizes the still immature procollagen during transport from the ER to the Golgi apparatus. It is also known that the HSP47 expression is increased in fibrotic disease which makes it a perfect target to manipulate collagen production [47-50]. Therefore, in order to circumvent the formation of fibrotic collagen, it is necessary to reduce collagen synthesis rates locally. The chaperone HSP47 is one of the best characterized target molecules for the RNA interference. Furthermore, two groups have already shown, through in vitro experiments as well as experiments in a rat model, that the HSP47 knockdown has an inhibitory effect on collagen secretion in liver fibrosis [49, 51, 52].

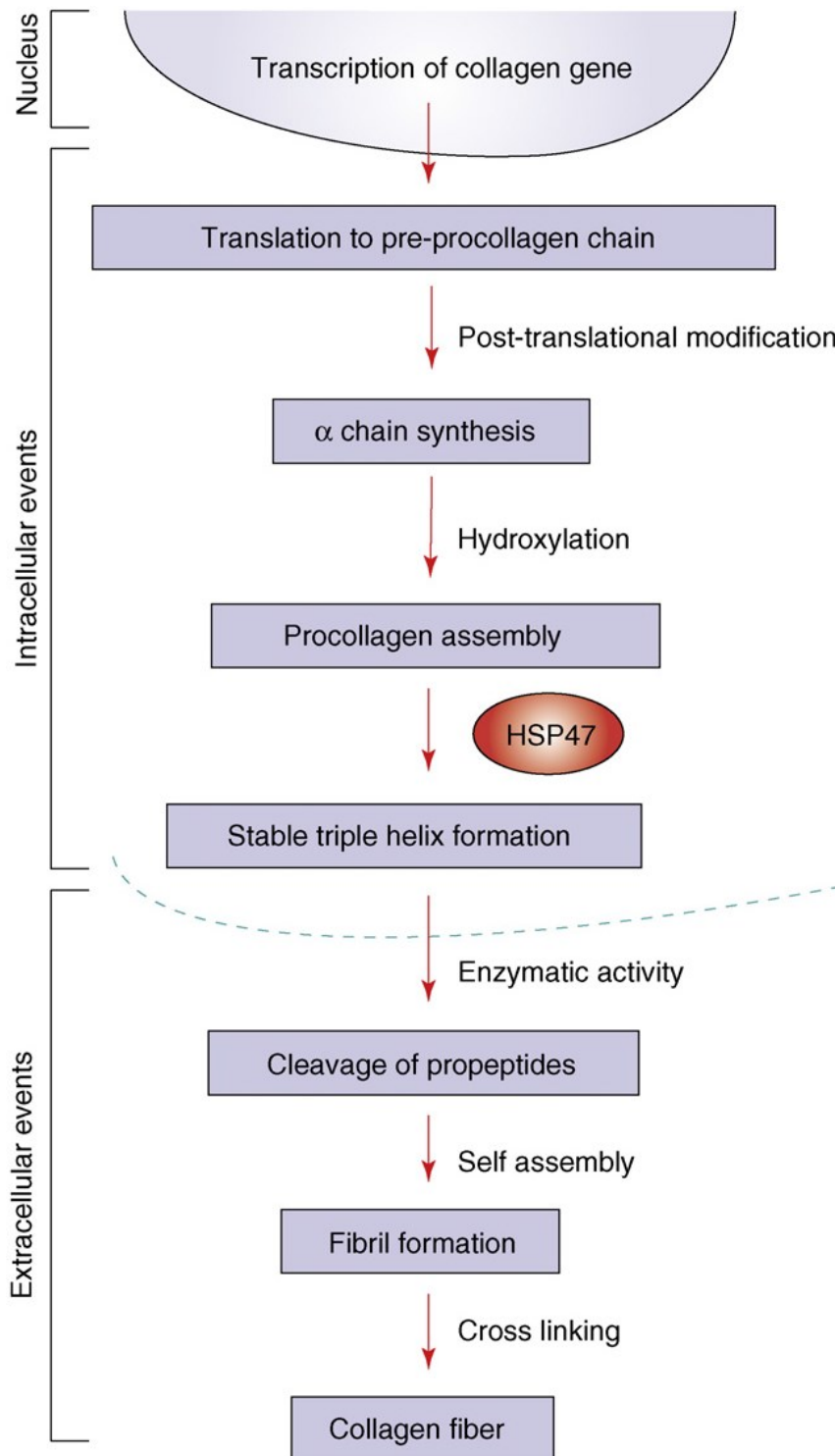


Figure 3. Modell of multi-step intracellular and extracellular events of fibrillar collagen synthesis. Step 1. Transcription of collagen gene. Step 2. Synthesis of α chains of pre-procollagen on ribosomes and ER. Step 3. Hydroxylation of proline residues to hydroxyproline and lysine residues to hydroxylysine. Step 4. Glycosylation of some of the hydroxylysine residues. Step 5. Assembly of three α chains to form procollagen. HSP47 is involved in correct folding and assembly of procollagen molecules to the stable triple helix structure. Step 6. Procollagen is transported to the extracellular space across the Golgi complex by exocytosis. Step 7. Cleavage of registration peptides by procollagen N- and C-proteinases. Step 8. Self-assembly and polymerization into collagen fibrils. Step 9. Cross-linkage between fibrils to form collagen fibers [47].

1.3. Polymeric based siRNA delivery

siRNA delivery is challenging due to its fast degradation by ubiquitous endogenous ribonucleases in biological fluids. Unmodified siRNA is also rapidly eliminated from blood by the kidneys [53]. In addition, the physicochemical properties of siRNAs (negative charge and size of: ~13 kDa) hinder the permeation of the equally negative charged “grease-like” barrier of the cell membrane in order to reach the cytoplasm, their site of action [29, 49]. Therefore, the success of RNAi therapy is dependent on a safe, stable and specific transport in the blood stream and high transfection efficiency.

Viral systems are very efficient for *in vitro* and *in vivo* transfection. However they pose considerable risk by activation of the immune system, such as triggering an interferon response or activation of coagulation and complement factors. There is also the risk of mutations by integration of expression cassettes in the host genome which can cause the development of cancer [29, 49, 54, 55]. Non-viral vectors produced from lipids or polymers, on the other hand, can provide a safer alternative to viral systems with lower costs, potential for rapid production at a larger scale, ability to modify or attach targeting ligands, and potential for repeated administration [56, 57].

Despite effective transfection into cells, liposomes have shown a relatively low encapsulation efficiency with poor storage, stability and rapid clearance from the blood [58]. Once inside the cells, they do not prevent degradation of nucleic acids within endosomes. To account for this, cationic liposomes have been coated with lipids such as DOPE (1,2-dioleoyl-sn-glycero-3-phosphoethanolamine) facilitating endosomal release of the complex [59-61] or cholesterol was inserted between the lipid bilayers to increase the rigidity of the liposomes [62]. However, lipid-based delivery still maintained several drawbacks including minimal control of degradation rates and targeting difficulty [56].

Non-viral systems based on cationic polymers have been extensively used as an alternative for nucleic acid delivery. Some of the advantages of polymeric delivery systems are: minimal immune response, targeting capability, controllable degradability, low costs and most importantly the possibility to easily modify them. Variations in chemical composition, structure, and molecular weight can provide changes in size, charge, hydrophobicity/hydrophilicity, and degradation rate of polymer/nucleic acid complexes [56, 63, 64]. Cationic polymers are generally divided into natural and synthetic polymers. One of the most commonly used synthetic polymers is polyethylenimine (PEI), which has a high

transfection efficiency and endosomal escape [65]. However, its use is limited by the cytotoxic effects [66]. Nanoparticles made of natural polymers such as chitosan and atelocollagen [67, 68] have been additionally exploited due to a better cytotoxicity profile, but slightly lower transfection efficiencies [63].

1.4. Chitosan for oligonucleotide complexation

In recent years, chitosan has become one of the most widely used non-viral delivery systems for nucleic acids. Its high positive charge density, versatility, biocompatibility, and biodegradability set chitosan apart from other polymeric nanocarriers [58, 69]. In physiological conditions chitosan can be readily digested by either lysozymes or chitinases, which are produced by the normal flora in the human intestine and can be detected in the blood as well [58]. This makes chitosan highly eligible for applications in the pharmaceutical field.

Chitosan is mainly produced by the alkaline de-*N*-acetylation of chitin, the second most abundant polysaccharide in nature after cellulose [70]. Chitin is primarily sourced from crustacean and insect shells [71]. It has a randomly distributed β -1-4 linked *D*-glucosamine (GlcN) and *N*-acetyl-*D*-glucosamine (GlcNAc) structure (Figure 4) with a pKa of 6.2 – 7.0 of the *D*-glucosamine unit. This means that chitosan is protonated at pH values lower than \sim 6.5 and can only be solubilized by slightly acidic conditions [72]. The high charge density of chitosan at pH levels below the pKa can also be seen as an advantage for polyplex preparation and endo-lysosomal escape, whereas a low charge density at pH 7.0 - 7.4 contributes to low cytotoxicity and may facilitate the intracellular release of the genetic material [73]

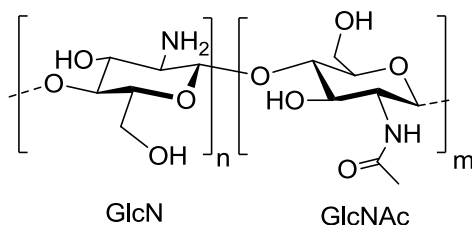


Figure 4. Chitosan structure: *N*-acetyl-*D*-glucosamine (GlcNAc) and *D*-glucosamine (GlcN) are randomly distributed in the linear polysaccharide.

The two most important structural parameters that influence chitosan's solubility and most of its physicochemical properties like protonation, are the degree of deacetylation and the molecular weight [74].

The degree of deacetylation (DD) offers information about the average amount of D-glucosamines available to interact with the nucleic acids and strongly influences degradability [75], inflammation [76] and immune modulation of chitosan [77, 78]. For siRNA delivery a higher DD is necessary to effectively bind the short length and stiff molecular topology of siRNA. High DD ($\geq 80\%$) is mandatory to complex siRNA and form efficient nanoparticles [58]. Malmo *et al.* [79] even formed siRNA nanoplexes using fully deacetylated chitosan which showed more efficient silencing than partially deacetylated chitosan with a DD $> 85\%$ because of the high number of charges. However, an excessive high DD will result in slower degradation rates [80]. Liu *et al.* [69] were able to formulate siRNA nanoplexes with a low DD (54%) chitosan. Nevertheless, this yielded low transfection efficiency of H1299 GFP cells due to lacking nanoplex stability [53].

Chitosan molecular weight (M_w) also strongly impacts the biological and physicochemical characteristics of nanoplexes. Its chains can influence the nanoplex stability which is crucial for siRNA protection before and after cell internalization, but should be low enough to permit the nucleic acid release once it reaches the cytosol [53]. Low M_w chitosan (~ 10 kDa) may be able to form nanoplexes with DNA but has short chain lengths which worsen siRNA complexation [69, 81]. Complete siRNA binding could only be observed with 25 to 80 kDa chitosan [81, 82]. Therefore, a high M_w chitosan would better entangle siRNA which will result in a more compact binding and a better protection from enzymatic degradation [69, 83]. Conversely, a chitosan with M_w which is too high may be too long to form suitable nanoplexes. Ragelle *et al.* [53] summarize in their review that chitosan molecules with 5–10 times the chain length of siRNA (M_w of ~ 13 kDa) are feasible to form suitable NPs.

1.5. Chitosan:siRNA nanoplex formation

There are three known methods for siRNA nanoplex formation in solution: complexation, ionic gelation using for example tripolyphosphate (TPP) and chitosan for siRNA entrapment and adsorption of siRNA onto the surface of preformed chitosan nanoplexes [58]. The later method raises concerns regarding nucleic acid protection against degradation [84]. The complexation technique relies on the electrostatic interactions between the positively charged

chitosan and negatively charged nucleic acids [69, 83, 85]. The ionic gelation method is based on the inclusion of a small polyion such as tripolyphosphate (TPP) in the nucleic acid solution that acts as an ionic cross-linker upon mixing with chitosan [77, 86, 87]. Katas *et al.* [88] reported a better transfection efficiency of chitosan-TPP:siRNA compared to chitosan:siRNA complexes for CHO K1 and HEK 293 cell lines. However, they also reported a higher loss of cell viability for chitosan-TPP:siRNA in comparison to chitosan:siRNA nanoplexes. There is no clear indication on which type of nanoplex formation leads to nanoplexes with the best transfection efficiency for a broad application range.

Once the DD and Mw are optimized for the specific chitosan delivery system and a preparation method is defined, the ratio between the number of positive charges in the polymer and the negative charges in siRNA needs to be taken into consideration and calculated [83]. This amine (N) to phosphate (P) ratio has a major impact on the nanoplex size. It was reported, that with a higher N/P ratio the siRNA nanoplexes were in the range of 100 nm, whereas 200 nm NPs were obtained at a lower N/P ratio (5/1–10/1) [83, 89]. Higher N/P ratios (50/1–150/1) proved to enable the successful and efficient EGFP knockdown in 1299 human lung carcinoma cells, in comparison to lower N/P ratios of 2/1 and 10/1 [53, 58, 69].

1.6. Physiological barriers for chitosan: siRNA nanoplex delivery

In the current thesis, chitosan:siRNA nanoplexes are designed to be incorporated into surface structures of medical implants. Therefore, their delivery is done locally at the site of implantation with a maximum dosage in comparison to systemic delivery [53]. Nevertheless, upon introduction into physiological fluids, either cell culture medium *in vitro* or, the body fluids *in vivo*, nanoplexes will encounter a hostile environment [90] (Figure 5). In such an environment, siRNA can be easily degraded by ribonucleases resulting in a loss of mRNA activity and knockdown. Therefore, the first function which has to be covered by the chitosan nanoplexes is to safely deliver the siRNA to the cell membrane.

The second barrier is the extracellular membrane. The naked anionic siRNA is unable to cross the negatively charged cell membrane due to both, its size and the electrostatic repulsions [91]. Therefore, the cationic chitosan must be able to bind and condense siRNA into small nanoplexes (100 – 300 nm) maintaining an overall positive charge at the nanoplex to facilitate cell uptake. However, studies showed that these two parameters only indirectly influence cell

uptake and ultimately transfection efficiency. Upon introduction into physiological fluids, the positive charge of the cationic nanocarrier and its size influence the formation of a protein corona on the surface of the nanopolyplex [92, 93]. The first *in vitro* studies on chitosan/DNA nanoplexes indicated that serum proteins in fetal calf serum – (FCS) had no inhibitory effect on chitosan DNA binding [94]. Further investigations showed that actually the FCS in cell culture medium enhanced the efficacy of the transfection [77, 95-98]. Nimesh *et al.* [96]

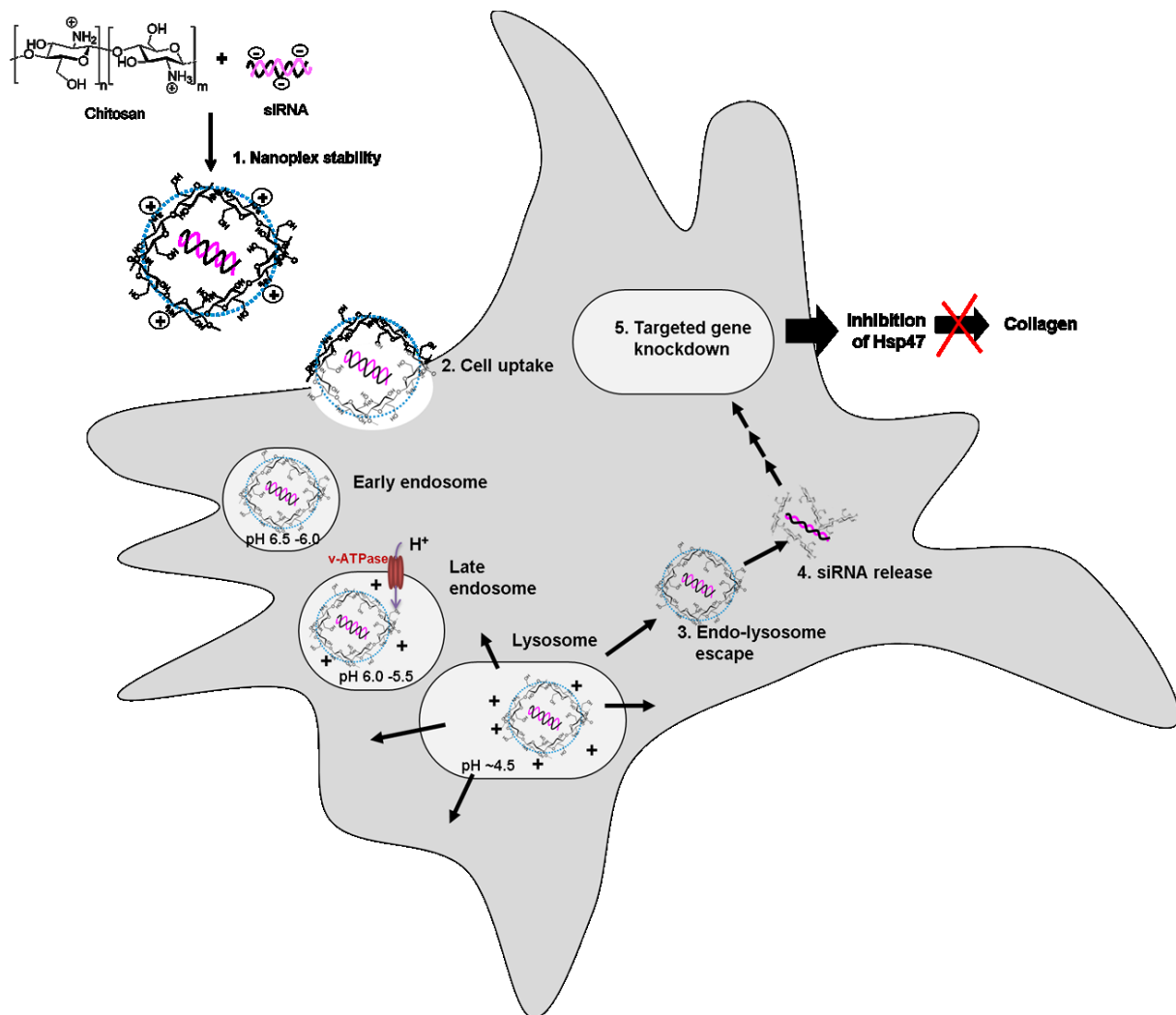


Figure 5. Physiological barriers for chitosan/siRNA nanoplex delivery. (1) Nanoplex formation in aqueous buffer and stability in the extracellular biological environment. Dependent on the components of the cell culture medium a protein layer is formed on the nanoplex surface (“protein corona”). (2) Cell uptake. (3) Escape from the endo-lysosome. (4) Disassembly and release of the nucleic acid payload into the cytosol. (5) Knockdown of the targeted gene product mRNA leading to the inhibition of e.g. Hsp47 chaperon protein production and ultimately the inhibition of collagen synthesis.

tested chitosan:DNA nanoplex formation at different pH values from 6.5 to 7.4 in cell culture medium with and without 10% FCS. The results showed that at pH 6.5, no matter if FCS was

present or not, the nanoplexes showed the best cellular uptake. Furthermore, at pH 7.1 and 7.4 the presence of large aggregates could be noticed near the cell membrane. Sato *et al.* [97] showed that an increased percentage of FCS (>20%) resulted in a decrease of transfection efficiency. Therefore, it seems that the positive charge of chitosan is important for the stability of the nanoplexes, but the uptake is promoted by the molecules on the nanoplexes surface.

The third barrier is the endosomal release into the intracellular environment. Within the endocytosis pathway nanoplexes will be exposed to dynamic pH environments. From an extracellular pH of ~7.0 chitosan:siRNA nanoplexes are enclosed in the early endosome at pH values between 6.0 – 6.5. In the late endosome the pH values are between 5.5 – 6.0 due to the action of an ATPase proton-pump in the vesicle membrane [99, 100]. The late endosome fuses with the lysosome which is even more acidic with a pH value of ~4.5 [100]. The most widely known endosome escape model for oligonucleotide delivery to the cytosol is the “proton sponge hypothesis” first describe by Behr *et al.* [101] It describes the ability of a polycation to swell and rupture vesicles by raising intra-vesicular osmotic pressure through proton buffering coupled to a concomitant influx of negatively charged ions such as Cl⁻ [77, 102]. However, chitosan nanoplexes are not able to escape the endo-lysosome pathway very quickly due to the proton sponge effect. In comparison to polyethyleneimine (PEI) delivery systems which show a rapid endosomal release (~4h) chitosan has a much slower release of ~12 to 24h [103, 104]. This late onset of oligonucleotide release [105] might be due to a lower linear charge density and a weaker membrane disrupting ability of chitosan [77]. Thibault *et al.* [104] traced the intracellular trafficking of chitosan:DNA systems via the dextran pulse-chase fluorescent dextran lysosomal staining which revealed the very fast transport of the nanoplexes from the endosome to the lysosome within ~4h, respecting the kinetics of the endosomal fusion with lysosomes [106]. The nanoplexes were colocalized in the lysosome for 8-12h until they were gradually released to the cytosol. Using double labeled FRET analysis Thibault *et al.* could observe that there was a direct correlation between the stability of the nanoplexes and their decondensation in the lysosome. The high Mw chitosan with a high DD was the most stabilizing and had the slowest decondensation and lysosome escape. The low Mw chitosan with a low DD was the least stabilizing chitosan and had the fastest decondensation which effected the DNA degradation inside the endosome. The chitosan with a good balance between Mw and DD showed the best transfection efficiency. Therefore, it is assumed that the lysosomal-escape of chitosan nanoplexes is due to the increase in vesicular

osmolarity by lysosomal enzyme induced degradation products of chitosan [75, 105] or due to the hydrostatic membrane destabilization [107]. Nevertheless, there are discrepancies between studies that hypothesise that the nanoplexes are transported in the lysosomes [103-105, 108] and studies suggesting chitosan nanoplexes do not transit the lysosome at all [109, 110]. The lack of consensus between the above studies could stem in part from the use of different methodologies for transfection and lysosomal staining, including different cell types, transfection pH or the use of an acidophilic LysoTracker dye versus dextran. In this context, it is important to note, that inhibition of lysosomal acidification will abolish LysoTracker fluorescence and acidophilic partitioning [111]. Therefore, this agent may not be an accurate marker of lysosomes when loaded with polycations endowed with a proton buffering capacity such as PEI [112] and chitosan [95] that can prevent lysosomal acidification [77, 104].

The fourth barrier in the siRNA delivery is the release from the chitosan nanoplex after reaching the cytosol. siRNA must be able to dissociate from the polycation. The competition with cytoplasmic polyanions [113] and the partial degradation of enzyme-labile biodegradable chitosan in the lysosome [75, 114] might facilitate the decomplexation in the cytosol [77]. However, this mechanism is not yet fully understood.

1.7. Chitosan modifications

In order to overcome the different siRNA delivery barriers, chitosan can be modified with various functional domains. On the chitosan backbone two groups are particularly susceptible to chemical modification: the free amine on the N-deacetylated glucosamine and the hydroxyl groups linked to the glucopyranose ring. The primary amines are more reactive in comparison to the hydroxyl groups. However, they are the basis for electrostatic interactions with the anionic phosphate groups of siRNA needed for nanoplex formation. Therefore, the modification of these primary amino groups may generate steric hindrance as well as a decrease in the number of positive charges available for nanoplex formation.

Chitosan modifications are focused mainly on adding functional domains to the polymer chain which enhance the solubility at physiological pH. This influences the colloidal stability of the siRNA nanoplexes as well. Furthermore, more specific modifications can be performed which incorporate targeting ligands for a more specific delivery or add endo-lysosomal

domains for a faster release of the oligonucleotide into the cytosol or fluorescent labels which enable live cell tracking of the nanoplexes.

Buschman *et al.* [77] summarized the chitosan modifications at the primary amine on the N-deacetylated glucosamine for the majority of the chitosan applications (see Figure 6). Furthermore, the review of Ragelle *et al.* [53] summarized in a table some of the chitosan modifications made specifically for siRNA delivery (Table 1)

Table 1. Chitosan derivatives for siRNA delivery from literature [53]. The table lists the modifications and their benefits for siRNA delivery applications.

Derivatives of chitosan	Improvements	References
Trimethyl chitosan (TMC)	Increased solubility pH independence	[115-117]
Thiolated/TMC	Increased extracellular stability by formation of intra and intermolecular disulfide bonds; enhanced intracellular release	[118]
Glycol chitosan	Increased stability	[119, 120]
PEGylation	Increase solubility and stability	[121, 122]
Guanidinylation	Improved cellular uptake by mimicking the cell penetrating peptide trans-membrane activity	[123]

INTRODUCTION

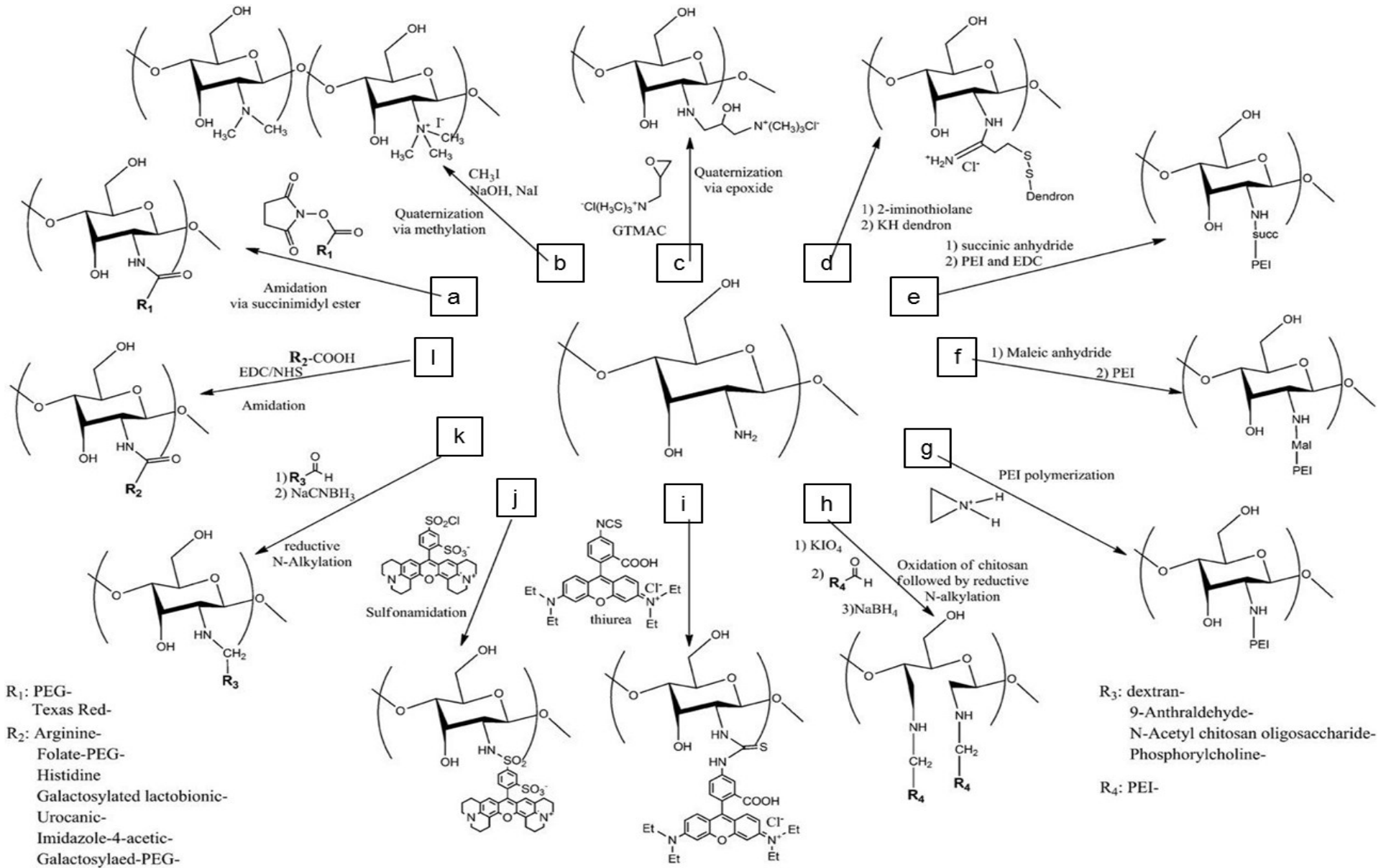


Figure 6. Modifications of the chitosan primary amine from literature [77] a) enhance of pharmacokinetics [124] b) c) solubility [125-127] d) endosomal escape [128] e) f) g) h) increase transfection efficiency [129] i) j) a) texas red: fluorescence [130] k) dextran: enhance complex stability [131], phosphorylcholine: enhance uptake [132]; 9-anthraldehyde: fluoresce [133]; N-acetylchitosan oligosaccharide aldehyde terminated: colloidal stability [134]; phosphorylcholine-glyceraldehyde: solubility [132] l) arginine: enhance uptake [135]; folate PEG: enhance pharmacokinetic and cancer cell recognition [135]; histidine, urocanic acid: endosomal escape [135-137]; galactosylated lactobionic acid, galactosylated-PEG: target liver cells [131].

1.7.1. Chitosan Poly(ethylene glycol) (PEG) modification

The functional modification of chitosan with hydrophilic PEG polymers is a strategy widely used because of its unique physicochemical properties. PEG has minimum interfacial free energies with water, extensive hydration, good conformational flexibility and large excluded volume [138]. PEG can enhance chitosan solubility at higher pH values, increase stability of the nanoplexes in the biological environment and prevent inter-nanoplex aggregation [139-142]. Furthermore, it is known to increase bioavailability, reduce cytotoxicity and decrease immunogenicity of nanoparticles [143, 144].

Chitosan_PEG nanoplexes form two compartments: the inner core via electrostatic interactions between the chitosan and the nucleic acids and a hydrophilic PEG layer serving as sterically stabilizing barrier [145-147]. The tightly bound interfacial hydration coating can prevent direct contact between the surface and the proteins in the biological environments. However, it has been shown that PEGylation reduces, but does not completely exclude protein binding to the nanoplexes [148]. Ebbesen *et al.* [149] hypothesize that small proteins may penetrate a thin polymer coating and adsorb to the underlying substrate, whereas larger proteins may adsorb at the upper layers if not sufficiently dense resulting in long range interactions between protein and nanoplex surface. Zheng *et al.* [138] showed that the protein repulsion ability decreased when the PEG substitution increased from 7% to 29% using the same PEG chain length of 2 kDa. Furthermore, Mao *et al.* [150] showed that PEI-(PEG_{5kDa})₄ and PEI-(PEG_{20kDa})₁ siRNA nanoplexes could better protect the siRNA against RNase digestion and had a positive influence on the transfection efficiency of NIH13T3 fibroblast cells in comparison to PEG_{550Da} with a higher PEG chain density at the nanoplex surface. Therefore, the protein resistance and the successful transfection efficiency depend on the PEG surface coverage and chain lengths [138, 144, 151]. The results of Chao *et al.* [152] revealed that it is actually the distance between two PEG molecules, which influences the protein adsorption.

1.7.2. Chitosan modifications for specific targeted nanoplex delivery

The targeted delivery of chitosan siRNA nanoplexes can not only reduce the siRNA accumulation in other cells, but it also minimizes the dose required to achieve a desired therapeutic effect. The specific delivery of siRNA to a particular cell type can be achieved by grafting a ligand onto the nanoplex surface, which will then recognize a receptor expressed by the cell [53]. The ligand could be conjugated to the chitosan amino groups via a broad range of modifications. However, the number of positive charges available on chitosan for nanoplex formation has to be high enough to enable sufficient electrostatic interaction between oligonucleotide and chitosan. Furthermore, the impact of a modification could change nanoplex characteristics such as size, charge, stability and cytotoxicity. The availability of the ligand to interact with its target is dependent on the physicochemical properties of the ligand and the interactions with the nanoplex surface [53, 153]. Therefore, PEG has been widely used as spacer between a targeting ligand and a cationic polymer (see Table 2) [154].

Table 2. Examples of PEG-conjugated copolymers for targeted delivery of oligonucleotide loaded nanoparticles to different cell types.

Gene carrier	Target Cells	References
BPEI-g-PEG-RGD	Vascular endothelial cells (angiogenesis)	[155]
Lactose-PEG-g-PLL	Hepatocytes	[156, 157]
Galactose-PEG-g-PLL	Hepatocytes	[158]
Folate-PEG-g-PLL	Cancer cells	[159]
Folate-PEG-folate-g-PEI	Cancer cells	[160, 161]
Folate-PEG-g-chitosan	Cancer cells	[162]
Biotin-PEG-g-chitosan	Brain endothelial cells (Blood Brain Barrier)	[163]
RGD-PEG-g-chitosan	Thrombocytes	[164]
Poly-L-Arginine-PEG-g-chitosan	epithelial cells (adenocarcinoma)	[165]

1.7.2.1. Fibroblast targeting

In order to successfully prevent the formation of ECM on implantable pharmaceutical devices, siRNA can be used to inhibit collagen synthesis specifically. As the collagen protein is produced by fibroblasts it is desirable to address this target cells directly via a cell specific cell surface protein. A suitable candidate seems to be the fibroblast activation protein (FAP).

FAP or separase (surface expressed protease) is a type II transmembrane protein with an extracellular C-terminal region followed by a single hydrophobic transmembrane domain and a short cytoplasmic tail [166]. It belongs to the serine protease family and exhibits dipeptidyl peptidase and endopeptidase activity, catalyzed by the same active site [167]. FAP is selectively expressed during fetal development [168], in reactive stromal fibroblasts of epithelial cancers [169], granulation tissue of healing wounds, and malignant cells of bone and soft tissue sarcomas [170]. The activation of fibroblasts, as happens in wound healing and fibrosis, results in an overexpression of FAP which makes it an interesting target molecule to specifically address active fibroblasts during fibroblast encapsulation [49]. Conversely, resting fibrocytes in normal adult tissues generally lack detectable FAP expression and would not be addressed by FAP targeted drug delivery [168].

Until now various ligands, such as proteins, peptides [171, 172], folic acid [173], antibodies [174] or single chain fragment antibodies [175], have been conjugated to polymeric delivery systems, including chitosan, in order to target specific cells. Messerschmidt *et al.* [176] in Prof. Kontermann's group at the University of Stuttgart developed novel single chain fragments (scFv) for immunoliposomes to target FAP. The insertion of the scFv into the lipid coat was achieved by a defined and site-directed coupling through a genetically engineered additional cysteine residue in the scFv protein. In the current study, the scFv used as a targeting ligand had a hexahistidyl-tag incorporated into the peptide linker between heavy and light chain fragments together with a cysteine residue at position 3 (scFv'LCH3) (see Figure 7) [177]. The Mw of the scFv'LCH3 is 56 kDa as a dimer and 28 as a monomer.

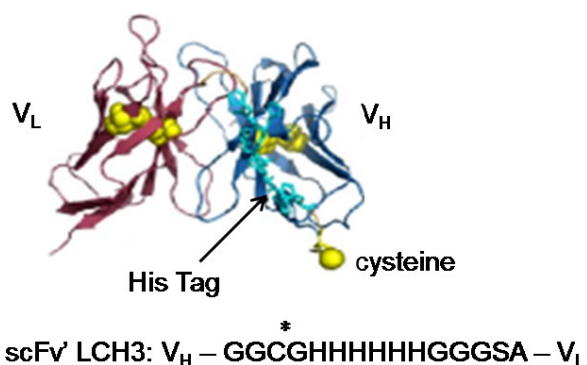


Figure 7. Structure of scFv LCH3 construct, visualized with PyMol by Dr. Messerschmidt *et al.* [177]. The sequence of the linker between heavy (V_H) and light (V_L) protein fragment had a cysteine residue at position 3 and a hexahistidyl-tag to enable metal-chelate affinity purification of the expressed protein and detection by anti-His-tag antibodies.

Small molecules such as carbohydrates, folate and cholesterol have also been used as targeting ligands. Therefore, the use of small potent and selective chemical inhibitor of cell membrane proteins might also be a viable targeting concept for specific cell delivery of drug molecules. Nanoplexes are mostly internalized via endocytosis. Therefore, once in the proximity of the target cells, a chemical inhibitor covalently attached to a nanoplex could bind the drug delivery system tightly to the surface of the desired cells, promoting a concentrated specific uptake of the siRNA delivery system.

Jansen *et al.* [167] in the group of Prof. Van der Veken at the University of Antwerp optimized a drug library based on N-acylated glycy-(2-cyano)pyrrolidines to identify inhibitors with higher potency and selectivity for FAP against compared to dipeptidyl peptidases (DPPs) and prolyl oligopeptidase (PREP) (Figure 8). Structure activity relationship studies identified different influences of modifications at the N-acyl group and the 2-cyanopyrrolidine residue [167, 178]. As a result they reported compounds that displayed low nanomolar inhibitory potency and high selectivity for FAP with respect to related DPPs, DPPIV, DPP9, DPPII, and PREP.

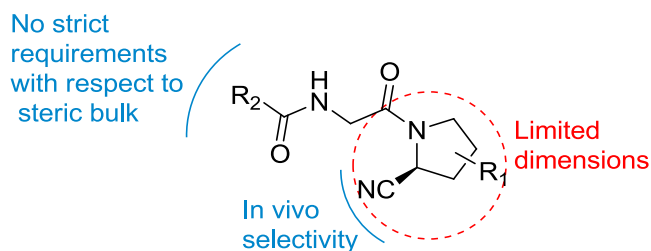


Figure 8. Structure activity relationship of N-acylated glycy-(2-cyano)pyrrolidine based FAP inhibitors. The 2-cyanopyrrolidine is essential for in vivo activity of the inhibitor, as it binds to the FAP. Therefore, the attachment of the inhibitor to polymers or nanoplex surfaces must be done at the glycy part of the molecules.

The structure of the chemical inhibitor was not revealed. The only information provided was that compound UAMC 1533 (the inhibitor) contains a linker group with an azide moiety at the glycy end. Its potency and selectivity is shown in Table 3. Its molecular weight is 524.57. UAMC 1533 had a yellowish appearance and was >95% pure on LC-MS.

Table 3. Potency and selectivity of UAMC as provided by the group of Prof. Van den Veecken.

Compd	IC ₅₀ (μM)						SI (FAP/PREP)*
	FAP	DPP IV	DPP8	DPP9	DPP II	PREP	
UAMC	0.0051 ±0.0003	>100	>100	>100	>25	>100	>20

*SI stands for "Selectivity Index" (calculated as $[IC_{50}(PREP)/IC_{50}(FAP)]$)

1.7.3. Bioconjugation techniques

Bioconjugation involves the linking of two or more molecules to form a novel complex having the combined properties of its individual components, mostly with at least one protein as biomolecule. Natural or synthetic compounds with their individual activities can be chemically combined to create unique substances possessing carefully engineered characteristics. Reactive functionalities on crosslinking reagents, tags, and probes provide the means to specifically label certain target groups on ligands, peptides, proteins, carbohydrates, lipids, synthetic polymers, nucleic acids, and oligonucleotides [179].

The intense research over the last decades provides a broad spectrum of different applications with specific targeting of functional groups under biorelevant and biocompatible conditions.

Functional groups in biomolecules like thiol-, amino- or hydroxyl groups can be directly addressed. Another approach is to incorporate unnatural functional groups into the target ligand without interfering with naturally occurring functional groups which are present in a living organism. Additional important requirements of these, so called “bioorthogonal reactions” are, chemoselectivity, high reaction rates and the operability under physiological conditions (water, high salt concentrations, reducing conditions, no toxic additives). As an example, azides are biologically inert and react specifically with alkynes in [3+2] cycloadditions under physiological conditions. Introduction of these unnatural functional groups is mostly done via the first approach of bioconjugation, by direct addressing of functional groups with reactive tags. These tags are bearing the corresponding unnatural functional group, which has to be inert to the “tagging-reaction” itself.

The most predominantly used internal and external chemical functionalization strategies are shown in Figure 9. Many modifications of the shown reactions were further developed over the years in order to improve specificity, reactivity and efficacy, such as the use of cyclo- instead of linear alkynes.

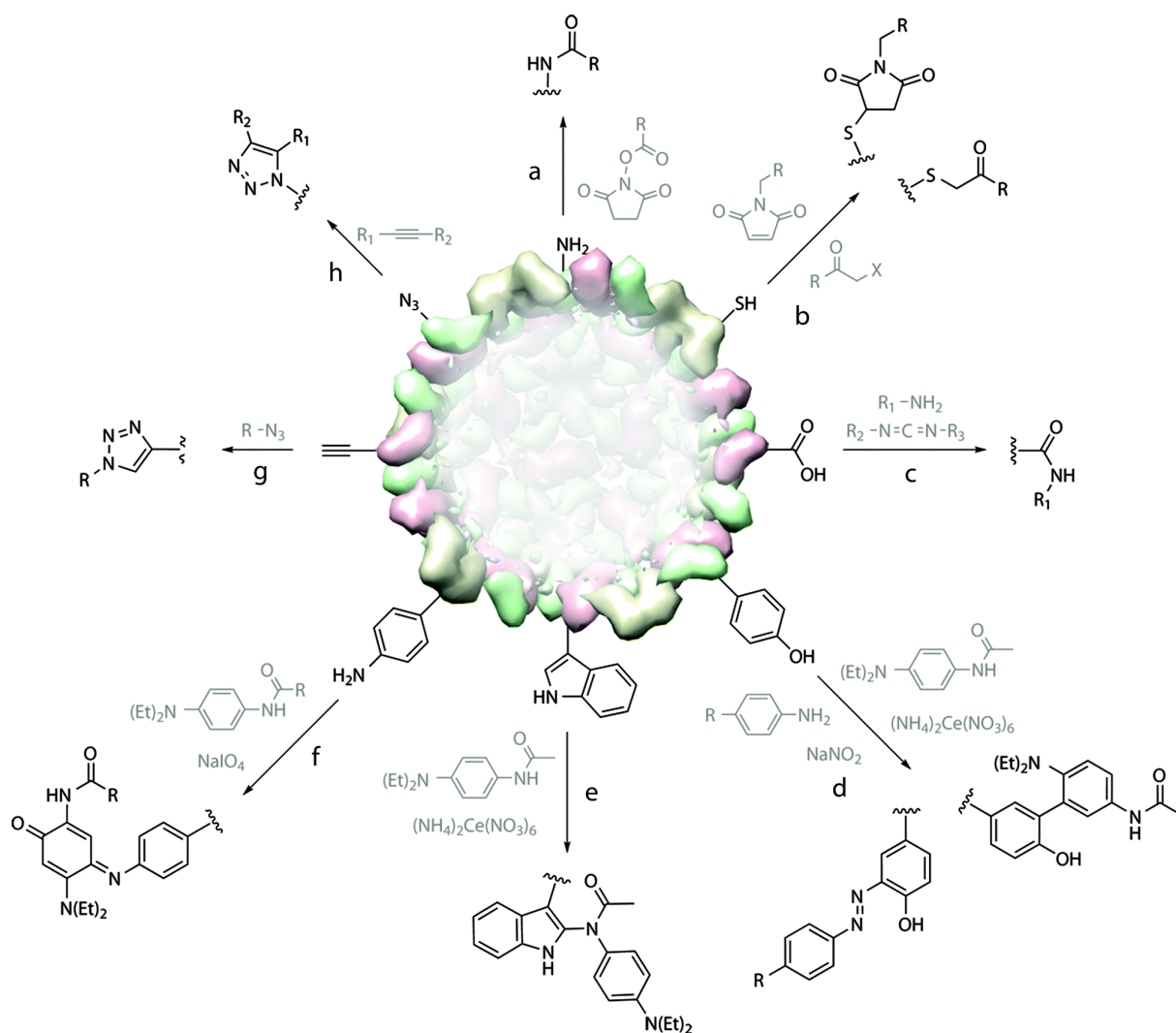


Figure 9. Depiction of the most predominantly used internal and external chemical functionalization reactions from protein-based bioconjugation strategies [180].

Short overview over the basic methods commonly used in protein bioconjugation techniques (see to Figure 9):

(a) The ϵ -amino groups of *lysine* can be amidated via N-hydroxysuccinimide esters in a classical amidation reaction.

(b) The free *thiol* residue of a cysteine can react specifically with maleimides in a Michael-reaction, forming stable thioethers. Alternatively the thiol can be reacted in a nucleophilic substitution to halogen-substituted usually iodated acetamides.

(c) *Glutamic* and *aspartic acids* can be activated with carbodiimides to reactive intermediates, mostly O-acylisourea intermediates, which undergo amidation with the corresponding amines under release of the corresponding urea among the available carbodiimides, EDC is preferred, due to its water solubility.

(d) *Tyrosine*. The phenol ring is a low reactive group but reacts with electrophiles especially diazonium salts in a very sensitive and specific manner. Diazonium coupling uses a phenyldiazonium salt electron withdrawing substitution in 4 position increases reaction rates. Another quite often used technique is the oxidative coupling of a phenylene diamine. Mannich condensations are also feasible site-specific reactions at tyrosine residues. Another approach to address tyrosine, less selective would use the phenolate ion, which can be easily generated under alkaline conditions, followed by alkylation or acylation reactions by using a variety of bioconjugate reagents.

(e) + (f) *Tryptophan* and *phenylalanine*, the two non-polar aromatic amino acids can be modified via oxidative coupling of a phenylene diamine derivative, similar to that shown for tyrosine.

(g) *Homopropargyl glycine* is a non-natural amino acid which can react in a [3+2] Huisgen cycloaddition between the alkyne and azide.

h) *Azidohomoalanine* can react via [3+2] cycloaddition between an alkyne and the azide with inverted functionalities to the reaction shown in (g).

The copper (Cu) catalyzed alkyne-azide Huisgen cycloaddition (g+h) (CuAAC) represents one of the most emblematic approaches of the “click chemistry” reactions. The “click” concept is based on fulfilling set of stringent criteria: wide in scope, give high yields, generate no or limited byproducts that can be removed by non-chromatographic methods, be stereoselective, take place in biologically benign conditions (aqueous solution, ambient temperature, and near physiologic pH [181]). Four main groups were originally defined on these basis: (i) additions to carbon - carbon multiple bonds (such as epoxidation, dihydroxylation, aziridination, and sulfonyl halide addition, but also Michael additions), (ii) carbonyl chemistry of the „non-aldol” type (such as formation of ureas, thioureas, aromatic heterocycles, oxime ethers, hydrazones, and amides), (iii) cycloadditions of unsaturated species (especially 1,3-dipolar cycloaddition reactions, but also the Diels - Alder reactions), (iv) nucleophilic substitution chemistry (particularly ring-opening reactions of strained

heterocyclic electrophiles such as epoxides, aziridines, aziridiniumions, and episulfoniumions) [182]. These “click” reactions constitute a toolbox for efficient coupling methodologies that can take place in a one-pot approach or in a sequential manner. These characteristics and advantages meet the increasing demand for multi-functional biomaterials that can mimic complicated synergistic signaling cascades inherent within biological environments [183].

1.7.4. Orthogonal conjugation chemistry based on 1,3 –dipolar cycloadditions

The 1,3-dipolar cycloaddition of 1,3-dipole azide and a dipolarophile like an alkyne (Huisgen 1,3 dipolar cycloaddition) can be done via Cu(I) promoted synthesis as well as via strain promoted 1,3 dipolar cycloaddition. The click chemistry of non-activated alkynes, such as terminal alkynes, needs high temperatures to overcome the activation barrier. Therefore catalyzed modifications are usually considered, which allow the reaction to take place at room temperature and also in aqueous solvent systems. Two of the most efficient transition metal catalysts known in literature are copper and ruthenium [184] (with rate acceleration of up to 10^7 to 10^8) [185]. However, in this type of reaction Cu (I) complexes are usually the catalysts of choice.

The mechanism of this type of ‘click chemistry’ reaction proceeds via the π - π interaction between a 1,3 dipole and a dipolarophile. The 2 π -electrons of the dipolarophile (the alkyne) and the 4 electrons of the dipolar compound (the azide) participate in a concerted, pericyclic shift, yielding 5 membered heterocycles (the triazole) as regioisomers (depending on electronic and steric effects) via a Hückel aromatic transition state as shown in Figure 10.

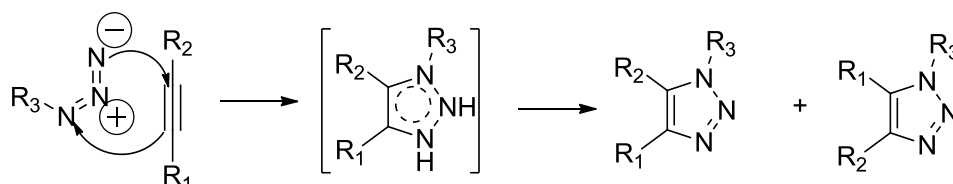


Figure 10. Mechanism of 1,3-dipolar reaction between alkyne and azide [185]. The 1,3-dipole of the azide shifts electrons to the alkyne system which shifts and electron pair to the azide dipole at the same time in a $4\pi+2\pi$ symmetry allowed the pericyclic concerted cycloaddition reaction. This forms the 6π – electron Huckel aromatic transition state which finally yields different regioisomers.

A condition for such a reaction to take place is a certain similarity of the interacting HOMO and LUMO orbitals of dipole and dipolarophile, depending on the relative orbital energies of both the dipolarophile and the dipole. According to the HOMO-LUMO interactions, the reaction is divided into three subclasses, type I-III [186] (Figure 11).

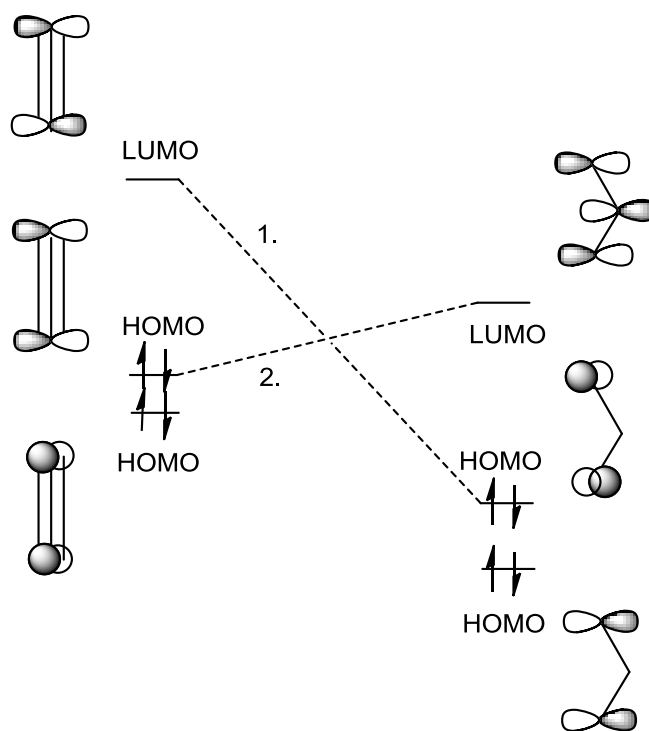


Figure 11. HOMO-LUMO interactions of the dipole and dipolarophile for type I-III 1,3-dipolar cycloaddition reactions. The energy levels of HOMO and LUMO define three different subtypes of 1,3-dipolar cycloadditions. The reaction with the lowest HOMO-LUMO energy gap is preferred. The influence of different electron drawing and pulling groups is therefore different for the three reaction types. Dashed lines show overlapping HOMO-LUMO pairs (1: Type I, II; 2: Type III, II) [186].

The reaction pathway via type I, II or III is always determined according to the lowest HOMO-LUMO energy gap.

The type I reactions are characterized by a high-lying HOMO of the 1,3-dipole which is overlapping with the LUMO of the dipolarophile (dashed line 1). Dipoles of this class refer to the class of HOMO-controlled or nucleophilic dipoles. In this case the reaction rates are accelerated by electron withdrawing groups lowering the LUMO of the dipolarophile (alkyne) while electron donating groups can decelerate the reaction (overlapping according to dashed line 1) (Figure 11).

Type II reactions are characterized by a mixture of HOMO-LUMO interactions. Due to similar energy gaps both interactions either HOMO (dipole)-LUMO (dipolarophile) as well as LUMO (dipole)-HOMO (dipolarophile) are possible. Both electron donating (highering HOMO) as well as electron withdrawing groups (lowering LUMO) on the dipolarophile are accelerating the reaction. Azides are included in these classes of dipolarophiles, the so called ambiphlic or HOMO-LUMO controlled dipoles (overlapping according to dashed line 1 or 2).

Type III is similar to inverse demand Diels-Alder reactions [187]. The low-lying LUMO of the dipole interacts with the HOMO of the dipolarophile (dashed line 2 in diagram). Electron withdrawing groups on the dipolarophile decelerate, while electron donating groups accelerates the reaction rates.

In all cases the HOMO-LUMO energy gap can be significantly lowered with catalysts such as copper as already mentioned above. This type of reaction is often referred as copper (I) catalyzed azide alkyne click chemistry reaction (CuAAC). The lowering of the HOMO-LUMO energy gap leads to highly efficient conversions with high reaction rates, deserving the name “click-reaction”.

An alternative for lowering the activation barrier of alkyne towards azide coupling is the use of activated ring strained alkynes. The so called strain-promoted azide-alkyne cycloaddition (SPAAC) was first reported by Bertozzi *et. al* [188] (Figure 12 a). The ring strain (18 kcal/mol of ring strain) activation is high enough to allow the azide-alkyne conjugation without the need of Cu-reagents as catalysts in high reaction rates. Cyclooctyne is the smallest stable ring strained alkyne with lowered HOMO-LUMO gap, allowing an efficient reaction at room temperature. Therefore, SPAAC represents one of the main bioorthogonal reactions and has found broad application in material sciences [189], chemical biology and *in vivo* imaging [188, 190-192]. In order to increase the reaction rates of the SPAAC, a number of structurally varied cyclooctyne derivatives, such as difluorinated cyclooctyne (DIFO) [193], dibenzocyclooctynols (DIBO) [194], dibenzoazacyclooctyne (DIBAC) [195], Biarylazacyclooctynones (BARAC) [196], bicycle[6.1.0]nonyne (BCN) [197] have been developed (Figure 12 b).

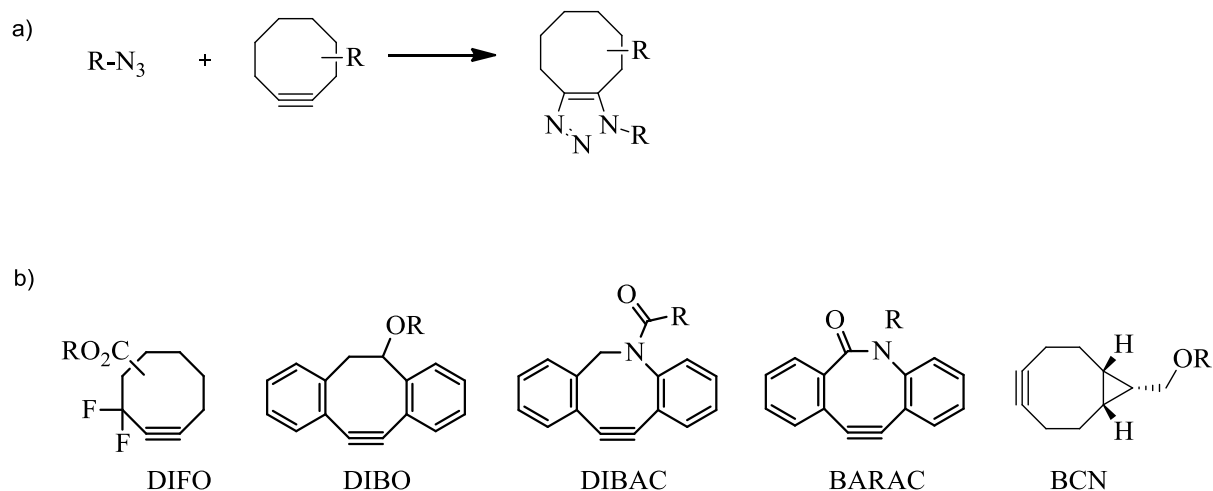


Figure 12. a) Strain promote azide alkyne cycloaddition (SPAAC), b) various activated cyclooctyne derivatives used for bioconjugation such as difluorinated cyclooctyne (DIFO), dibenzocyclooctynols (DIBO), dibenzoazacyclooctyne (DIBAC), Biarylazacyclooctynones (BARAC), bicyclo[6.1.0]nonyne (BCN).

Other known bioorthogonal reactions are the Staudinger ligation via the corresponding phosphine, yielding an amide linkage [179, 180], tetrazine ligation, nitron dipole, norbornene, and oxanorbornadiene cycloaddition, tetrazole photoclick chemistry, and quadricyclane ligation [198].

1.8. Layer-by-layer coating and release

The successful integration of an implant with the surrounding living tissue and its overall performance is influenced by the biological response to the device surface. Therefore, interactive coatings allow modifications of the implant surface in order to modulate and control the preferred biological interactions.

The layer-by-layer (LbL) adsorption technique is an established, simple and versatile approach for the formation of controlled bottom-up multilayer thin-films on surfaces of various chemistry and shape [199-202]. Important applications of LbL coatings include controlling cellular and bacterial adhesion[203], as well as delivery of bioactive molecules at the interface of a biomedical device and biological tissue, such as surfaces of orthopedic implants, urinary catheters or cardiovascular stents [204].

This technique is based on the alternate adsorption of oppositely charged materials, mainly via electrostatic interactions [205, 206] (Figure 13 A). Each adsorption leads to a charge

inversion at the surface, resulting in the continuous building up of a layer system of tunable characteristics in terms of composition and thickness (number of layers), surface charge, permeability and elasticity [207, 208]. The most commonly used polyelectrolytes are poly(ethyleneimine), poly(allylamine) hydrochloride, poly(diallyldimethylammonium chloride), poly(sodium styrenesulfonate), poly(sodium vinylsulfonate), poly(acrylic acid), and chitosan. Furthermore, the LbL film fabrication under mild aqueous conditions enables the immobilization of biomolecules with preserved activity such as dyes, proteins[209], lipids [210], nucleic acids [44, 45, 202, 211-213], (nano)particles [214], and enzymes (Figure 13 B). In a similar manner to the control of the film thickness, the amount of functional molecules can be controlled by the increase in the number of deposited layers. Furthermore, the release rate of drugs or biomolecules from the multilayers can be “controlled in a wide range from several seconds to several weeks by changing the nature of biodegradable building blocks, or by applying environmental cues, including temperature, pH, ionic strength, light or electrochemical stimuli” [204].

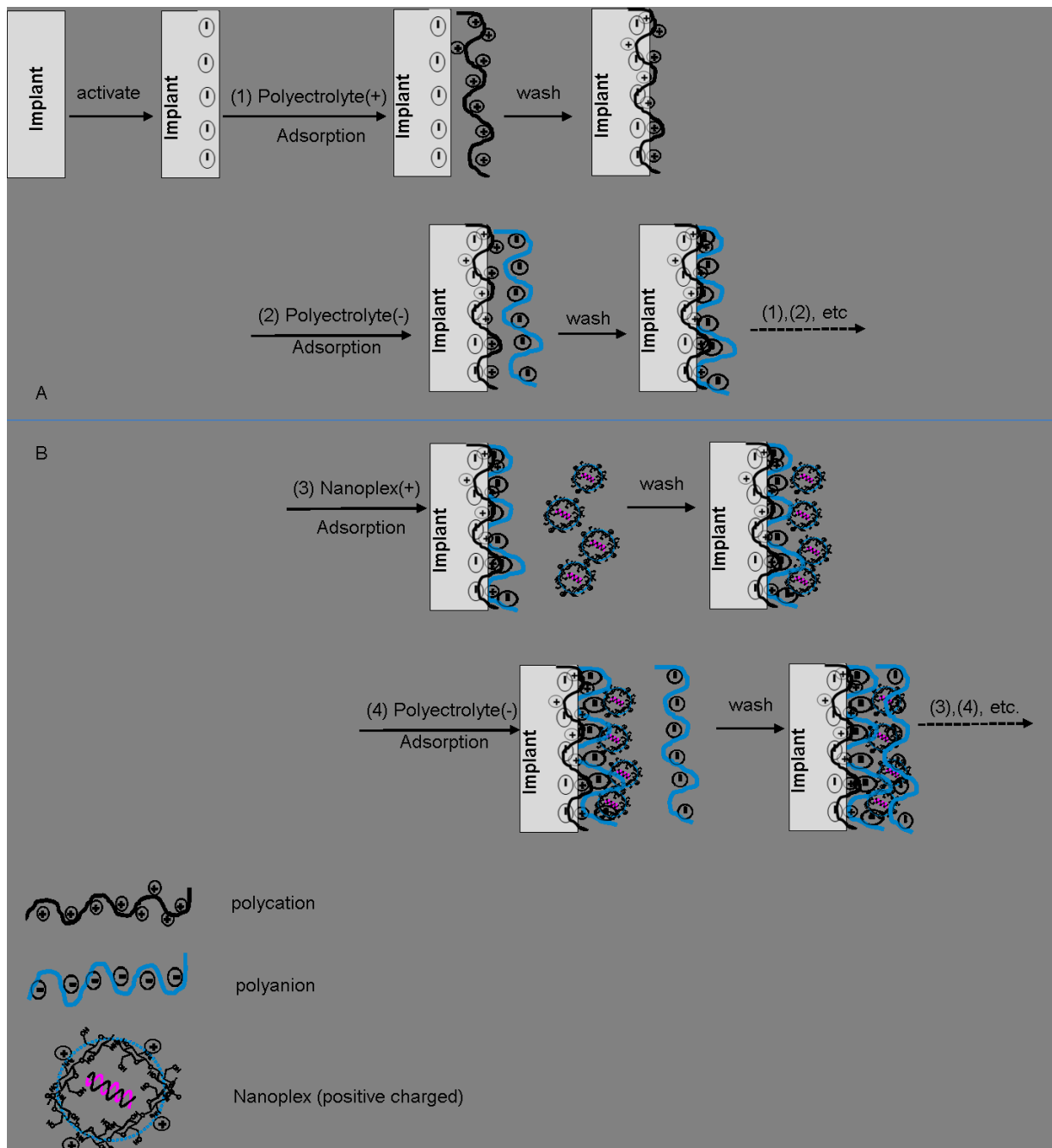


Figure 13. Schematic representation of the LbL deposition of oppositely charged polymers for the surface modification of implants. (A) After the activation of the surface, the multilayer coating is built up via repetitive exposure to dilute polycation and polyanion solutions. (B) Nanoplexes for example can also be inserted in the film. At a certain pH nanoplexes, such as chitosan/siRNA, are positively charged and can be absorbed via electrostatic interactions on the surface of a negatively charged layer. The film coating can be further developed by alternate adsorption of positively charged nanoplex solution and polyanion solution. The implant can be of different composition, size, and shape (stents, orthopedic implants, dental implants, biosensors, etc.).

2. Aim of the present study

The clinical application of many of the pharmaceutical implantable devices developed in recent years is still a critical issue due to the foreign body response. The current approaches to reduce the development of fibrosis have an overall anti-inflammatory effect or attempt to neutralize disease-associated proteins through direct binding without removing them. siRNA oligonucleotides are molecules that operate upstream of the protein production. They target mRNA – the carrier of genetic information before it is translated into proteins. Therefore, the delivery of siRNA to the inflammation site before the fibrotic capsule is formed might prevent the failure impairment or failure to perform.

This thesis is divided in three parts:

- 1) Design, synthesis and optimization of a chitosan:siRNA delivery system stable in extracellular environment, able to protect the siRNA from degradation, with nanoplex size in the range of 100 to 300 nm for a good cellular uptake, able to escape from the endo-lysosomal pathway before degradation and unstable enough to release siRNA once in the cytosol.
- 2) Targeting of the chitosan:siRNA delivery system. Therefore, a multifunctional linker needs to be developed in order to bind the targeting molecule to the nanoplex surface.
- 3) Coating of the solid surfaces with chitosan:siRNA nanoplexes via a layer-by-layer approach.

The physico-chemical properties of the established nanoplexes will be correlated with their biological behavior. The biological experiments performed by Dr. Schuster (NMI) or by the group at the University of Antwerp will be also attached in the results section of the thesis correspondently marked.

3. Results

3.1. Influence of molecular weight (M_w) and degree of deacetylation (DD) on the physico-chemical properties of chitosan for nanoplex formation

High M_w chitosans form longer and more flexible molecules, whereas the lower M_w chitosan form shorter and stiffer molecular chains. Therefore, chain length has a high impact on polymer properties and influences for example the formation of siRNA nanoplexes. Furthermore, the charge density correlates to the binding capacity of siRNA. It is directly correlated to the percentage of deacetylated primary amine groups along the molecular chain (degree of deacetylation – DD).

3.1.1. Alkaline deacetylation of chitosan

As sufficient nanoplex stability is necessary for extracellular siRNA protection and disassembly is needed to release the gene after the endosome escape, an appropriate balance needs to be achieved between the length of the chitosan molecules and the amount of deacetylated groups. Therefore, commercially available low and medium M_w chitosan (Aldrich) was characterized and modified to generate a library of chitosans with DD $\leq 80\%$ and M_w between 70-380 kDa (Figure 15, Table 4).

The increase in the DD of chitosan, the number of primary amine groups in position C_2 of the D – glucosamine monomers leads to a modification of M_w as well. The approach chosen was the alkaline deacetylation, using strong NaOH solutions (40-50% NaOH) at high temperatures (60-110 °C) and increasing time intervals (4 – 24 h) (Figure 15, Table 4). The kinetics of deacetylation and polymer chain degradation can be optimized by screening different temperatures and testing different hydrolysis times. The alkaline solution detaches the acetyl groups by the nucleophilic addition of hydroxide ions to the carbonyl groups, separating the N – acetyl – D – glucosamine at position C_2 into CH_3COO^- and the NH_2 – group. In the partial range of the FT-IR spectrum (1300 – 1800 cm^{-1}) the β form of the native chitosan could be identified. The 1652 cm^{-1} band was attributed to the stretching vibration of C=O (amide I) and 1558 cm^{-1} band corresponded to the NH bending (amide II), which both can be used to measure the N-acetyl group contents [215, 216]. In the case of α -chitin the amide I band (1652 cm^{-1}) would be split into a doublet from two type of H-bonds in which C=O are involved, whereas for the β -chitin and β -chitosan, respectively, it was shifted to a single peak indicating much weaker intermolecular hydrogen bonds (Figure 14) [216].

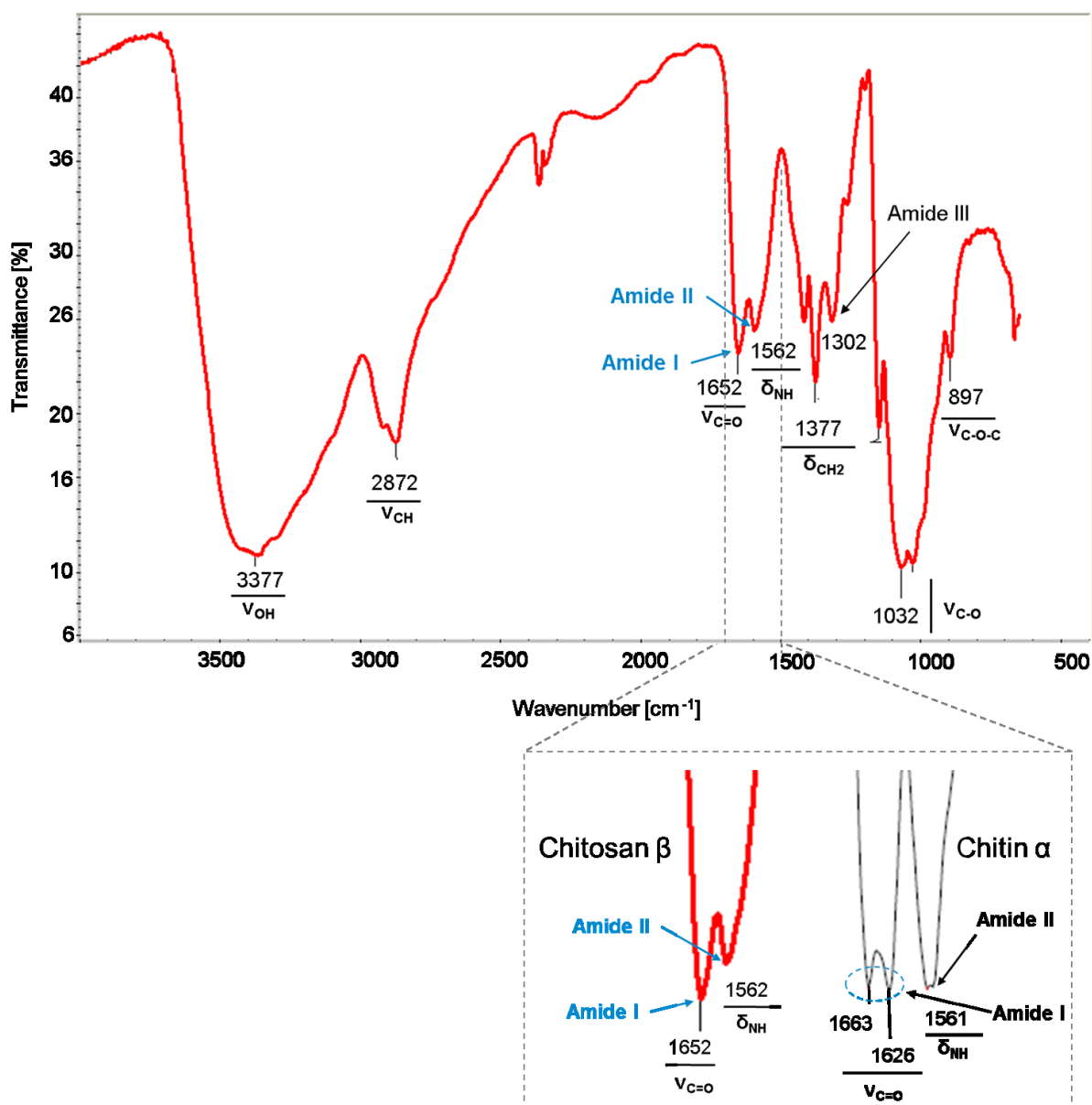


Figure 14. FTIR spectrum of commercially available chitosan (Aldrich). The broad absorption band at 3377 cm^{-1} is attributed to the O-H stretching vibrations. At 2872 cm^{-1} the methylene C-H band showed absorption. The 1652 cm^{-1} stretching vibration corresponds to the amide I (hydrogen bond in a C=O group with the NH group of the adjacent chain) and 1562 cm^{-1} corresponds to amide II (in-plane N-H bending and C-N stretching mode). The CH bending, symmetric CH_3 deformation and CH_2 wagging bands appear at 1377 and 1302 cm^{-1} . The bands ranging from 1032 to 1163 cm^{-1} are attributed to the asymmetric bridge oxygen and C-O stretching and the vibration of NH_2 appears at 897 cm^{-1} . The zoom in of the stretching vibration of C=O and bending of NH in the β -chitosan Aldrich was compared to the zoom in of the same region from the literature α -chitin to clearly show the differences between the α and β structure.

In case of β -chitosan, the deacetylation is supposed to be fast due to its weak hydrogen bonding and the resulting residual acetyl groups are distributed randomly on the chitosan

polymer chain [217]. As the IR data of the commercial chitosan showed β – type characteristics, short time intervals were chosen for the reaction 4, 8 and 24h (Table 4).

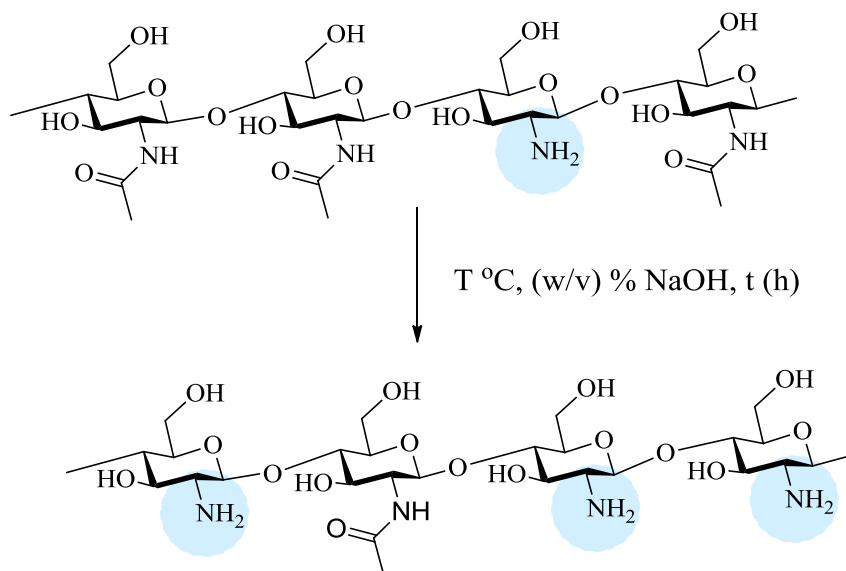


Figure 15. Alkaline deacetylation of chitosan using strong NaOH solutions (40-50% NaOH) at high temperatures (60-110 °C). Increasing time intervals provide different DD.

3.1.2. Analytical characterization of deacetylated chitosans

The primary amine content was determined by ^1H NMR. The degree of deacetylation was calculated with the method proposed by Hirai *et al.* [218], using the signals from protons H_2 , H_3 , H_4 , H_5 , H_6 of the sugar moieties to quantify the hexoses in chitosan and the peak of the three acetyl protons in the N-acetyl-glucosamine to quantify the acetyl groups (Figure 16, Table 4).

Polymer chains did not show the same degree of polymerization and molar mass, and H_1 H_2 signals show different chemical shift dependent on the neighboring acetylated or free amino groups. Whereas the H_2 in deacetylated chitosan is fully separated at 3.0 ppm, the H_2 signal in acetylated chitosan was part of the signal group of H_{2-6} (A) and H_{3-6} (D). The H_1 , A signal was detected at ~ 4.5 ppm whereas the H_1 , D signal could not be separated from the strong HOD peak at 4.7 ppm. Therefore, the results from the gel permeation chromatography (GPC) presented in Table 4 were used to calculate usual polymer parameters such as number-average

molecular weight M_N , weight-average molecular weight M_W , polydispersity defined as M_W divided by M_N , intrinsic viscosity η and the hydrodynamic radius R_h .

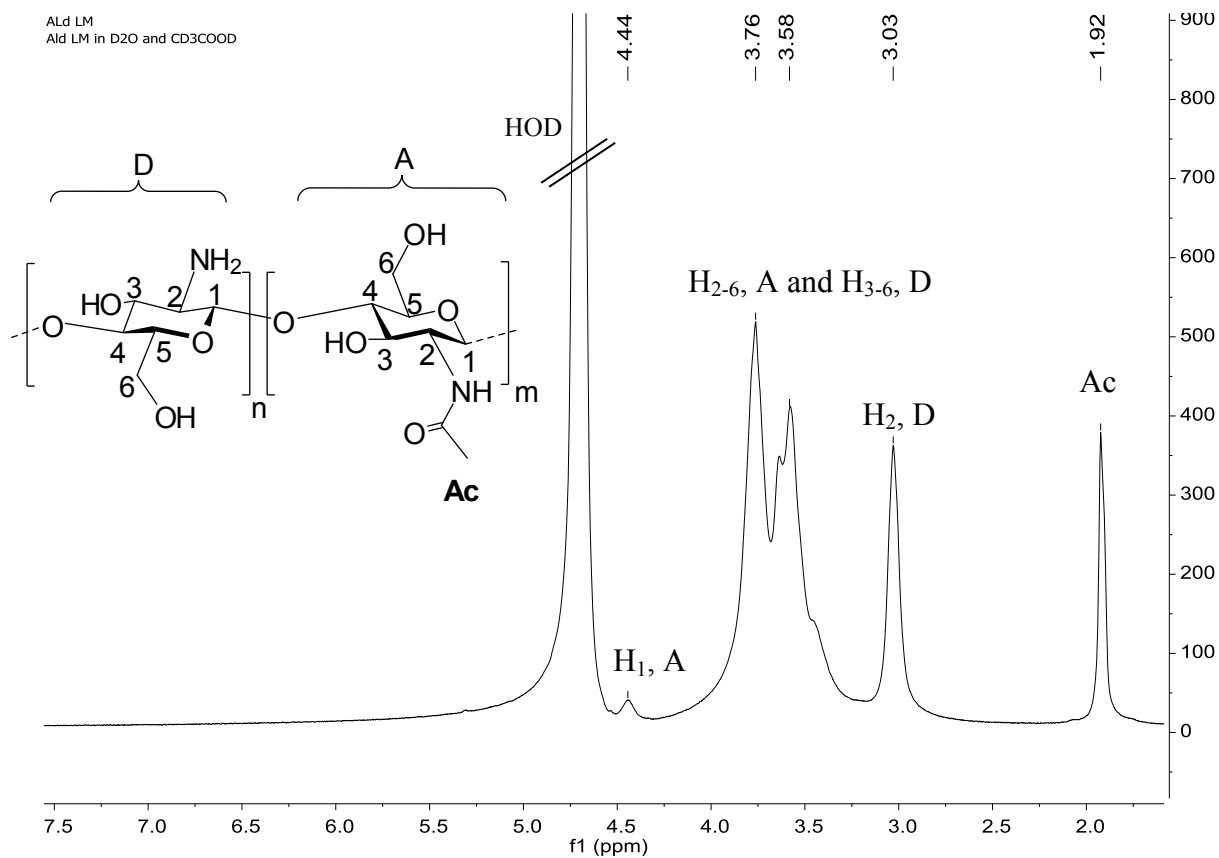


Figure 16. ^1H NMR reference spectrum of chitosan (low molecular weight Aldrich) dissolved in 2% CD_3COOD in D_2O . The H_1 of the acetylated unit (H_1, A) appears at ~ 4.5 ppm while H_1 in the acetylated glucosamine unit (H_1, A) should appear at ~ 5 ppm which can't always be seen. Signals from H_2 to H_6 overlap between 3.3 and 4.1 ppm, however, H_2 of the deacetylated unit (H_2, D) can be found separated at 3 ppm. The acetyl protons (Ac) appear at 1.9 ppm.

Table 4. Chitosan parameters measured and calculated based on the data from gel permeation chromatography (GPC) and ^1H NMR^a for different starting materials and deacetylation conditions: number average molecular weight M_N , weight-average molecular weight M_W , intrinsic viscosity η , hydrodynamic radius R_h , degree of deacetylation measured by NMR DD_{NMR} , integration of the H_{2-6} protons of sugar monomers $I_{\text{H2-H6}}$, the integration of the acetyl protons I_{Ac} was defined as 1.

<i>RN (DD;Mw)</i>	<i>Batch number</i>	<i>Starting material NaOH (w/v) % /T °C/t(h)</i>	<i>M_N [kDa]</i>	<i>M_W[kDa]</i>	<i>M_W/M_N</i>	<i>η [dL/g]</i>	<i>R_h [nm]</i>	<i>I_{H2-H6}^b</i>	<i>^cDD_{NMR} %</i>
Chi (80;165)	Aldrich Low	-	103 ±24	165 ±13	2.3 ±0.5	2.38 ±0.13	18.5 ±0.62	10	80
Chi (85;379)	Aldrich Med	-	314 ±11	379 ±18	1.2 ±0.1	6.04 ±0.41	32.2 ±1.02	13	85
Chi (83;122)	ANG115236b	Ald Low (40/60/4)	54 ±16	122 ±20	2.3 ±0.4	1.74 ±0.07	13.5 ±0.92	12	83
Chi (85;110)	ANG115236a	Ald Low (40/60/8)	53 ±7	110 ±15	2.1 ±0.4	1.72 ±0.09	13.1 ±0.32	13	85
Chi (88;135)	ANG115235b	Ald Low (40/110/4)	54 ±7	135 ±21	2.5 ±0.1	1.36 ±0.03	12.5 ±0.70	16	88
Chi (90;96)	ANG115235a	Ald Low (40/110/8)	47 ±14	96 ±21	2.1 ±0.2	1.56 ±0.15	12.4 ±1.01	20	90
Chi (92;73)	ANG115251a	ANG115235a (50/60/24)	43 ±1	73 ±2	1.7 ±0.1	1.67 ±0.04	11.7 ±0.10	25	92
Chi (90;276)	ANG115275a	Ald Medium (50/110/4)	184 ±3	276 ±2	1.5 ±0.0	6.70 ±0.10	29.8 ±0.13	20	90
Chi (94;245)	ANG115275b	Ald Medium (50/110/8)	154 ±7	245 ±11	1.6 ±0.1	6.03±0.04	27.3 ±0.24	32	94

a) chitosan samples dissolved in 20μL CD₃COOD and 980μL D₂O; b) 10% failure range c) $DD = 100 - \left(\frac{1/3 \times I_{\text{Ac}}}{1/6 \times I_{(\text{H2-H6})}} \times 100 \right)$

As the values of the DD and M_w of the starting materials were rather broad (DD: 75-85% and M_w : low), it was necessary to characterize them before further modifications. The low M_w Aldrich chitosan (Ald Low) with DD of 80% and M_w of 165kDa was deacetylated to give 5 new chitosan samples with higher DD and lower M_w . The first 2 samples, deacetylated with a solution of 40% NaOH at 60 °C for 4h and 8h, yielded a slight increase in the degree of deacetylation compared to the starting material. However, the differences between these two samples were barely noticeable. This indicated the necessity of higher temperatures or longer reaction times. When the reaction was performed at 110 °C the degree of deacetylation increased up to 90% after 8h reaction time. Significant differences could be noticed for the M_w which decreased from 165 kDa to 73 kDa. This M_w decrease was assumed to be mainly due to the decrease in number of acetyl groups. However the 96 kDa average molecular weight in the case of Chi (90; 96) must be also due to a depolmerization of the chitosan during deacetylation. Therefore, it was interesting to investigate the influence of temperature and reaction time on the depolymerization. Chi (90; 96) was further deactylated at 60 °C for 24h at a slightly higher concentrated NaOH solution (50%). A small percentage increase in the DD but a 23 kDa decrease could be noticed after the prolonged reaction times. In the end the deacetylation of the Ald Low starting material yielded chitosans with DD of up to 92%, but with M_w lower than 100 kDa. Therefore, Ald Medium starting material was also deacetylated under the same conditions and yielded chitosan with >90% DD and M_w higher than 200 kDa. The heterogenous reaction was performed at 110 °C with a NaOH 50% solution at 2 time interval 4 and 8h under conditions which showed best results for the Ald Low chitosan before. As expected the chitosan incubated for 8h in the previously mentioned conditions had a higher DD than the one left in 50% NaOH for only 4h. The M_w decreased from 379 kDa to 276 kDa (4h) or 245 kDa (8h), and the DD for both chitosans reached values higher of 90% (4h) and 94% (8h) which were feasible for the preparation of the siRNA nanoplexes.

The decrease of the intrinsic viscosity η was proportional to the decrease in M_w . The chitosans with M_w lower than 170 kDa reported η values \sim 2 dL/g while the chitosans with higher M_w showed η values in the range of \sim 6 dL/g. These results were expected, because of the chitosan hydrogen bonds of which form a superstructure that is only going to increase in complexity with an increase in molecular weight. As the hydrodynamic radius R_h is calculated based on the η and M_w values, it also decreased proportionally to the M_w . For M_w

between 73 kDa and 165 kDa, the R_h values decreased from 18 nm to ~12 nm. For M_w between 245 kDa and 379 kDa the R_h increased from 27 nm to 32 nm.

The dispersion of the molar – mass or average molecular weight within a polymer was calculated by dividing the M_w to the M_n . The results for all modified chitosan samples indicated a distribution of the relative M_w with a dispersity value ~2 which differed not much from the dispersity of the starting material.

To assess the impact of both M_w and DD on the charge of the chitosan polymer chain, samples were solubilized in 0.3 M CH_3COONa buffer at pH 5.5 and the zeta potential (ζ) was measured via ZetaSizer (Figure 17).

While chi with a DD of 80% had the lowest zeta potential with 29 mV, chi with a DD of 92% reached a positive charge of 62.1 mV. Even if the DD had the major influence on the zeta potential, the M_w seemed to have had some impact also. The charge of the chitosan with a DD of 90% was ~17 mV higher than the zeta potential of a chitosan with the same DD but a much lower M_w of ~96 kDa. Furthermore, it was shown that with a high M_w (276 kDa) and a DD of 90%, the charge of the polymer was ~19 mV higher than for a chitosan with a DD of 92 % but a lower M_w of 73 kDa.

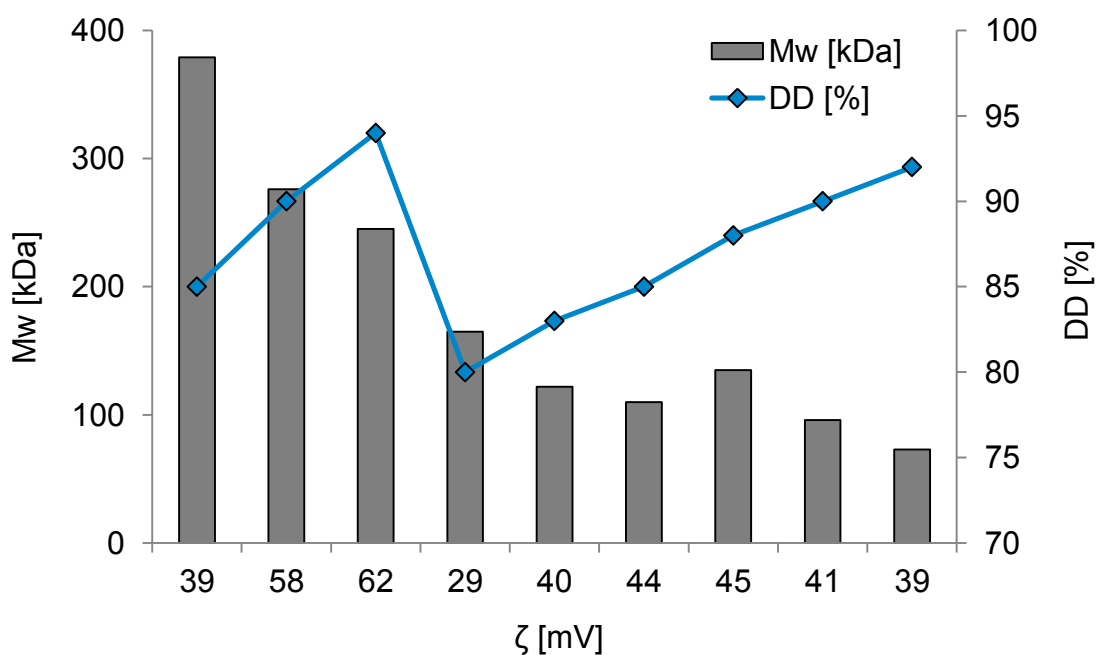


Figure 17. Effect of M_w and DD on the zeta potential ζ of the chitosan polymer chain. Both M_w (grey columns) and DD (blue markers) showed to have an influence on the ζ .

The results of the deacetylated chitosans offered a clear picture of the influence of the DD and Mw on the polydispersity, viscosity and charge of the polymer chain. These parameters were used to investigate which physicochemical factors have the largest influence on nanoplex formation.

3.1.3. Chitosan siRNA nanoplexes

Chitosan:siRNA nanoplexes were formed via electrostatic interactions between positively charged amino groups of chitosan and negatively charged phosphate groups of siRNA at pH 5.5. In order to generate stable nanoparticles, an excess of amino groups had to be considered for complexation of siRNA. The nitrogen/phosphate ratio (N/P) chosen was 50/1 and 100/1, meaning 50 or 100 positive charges (amines) to one negative charge (phosphate group). As Chi (90; 96) and Chi (92; 73) had a similar zeta potential to other Chi (90; 276) and Chi (94; 245), but lower M_w , they were not chosen for the nanoplex formation.

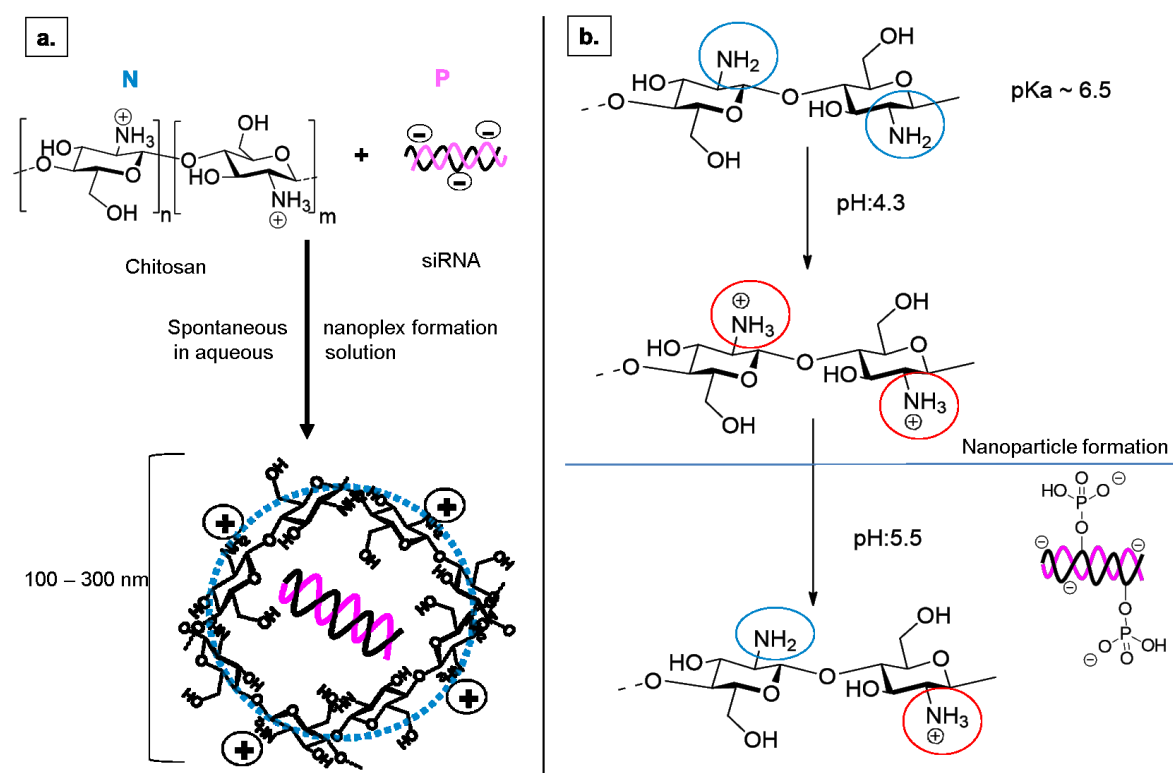


Figure 18. a) General scheme of chitosan:siRNA nanoplex formation b) Detailed representation of the complex formation via electrostatic interactions at a pH of 5.5 due to pH dependent generation of positively charged ammonium groups in chitosan.

The structural chitosan parameters described in subchapter 3.1.2 can influence the successful formation of siRNA nanoplexes and ultimately the transfection efficiency. By measuring and comparing both the size and the charge of the nanoplex the optimal chitosan M_w and DD could be chosen for siRNA – complex formation.

The size of the nanoplexes is important for cellular uptake and in the case of siRNA nanocarriers it should be between 100 and 300 nm [69, 219]. The results summarized in Table 5 revealed for all chitosan:siRNA formulations a size average lower than 300 nm, between 165 and 260 nm. The minimum size for N/P 100 and 50 was for nanoplexes formed with chitosan with a M_w of ~ 250 kDa with a DD 94%, followed by chitosan with a ~ M_w 280 kDa with a DD 90% and chitosan with M_w 165 with a DD of 80%. The nanoplexes formed with chitosan M_w 379 kDa had the highest size at both N/P ratios.

The surface charge of the nanoplexes must also be taken into consideration as it can influence the stability of the nanoplexes, sterically inhibits the agglomerate formation between the nanoplexes and can influence the transfection efficiency. As it can be seen in Table 5, all nanoplexes had a positive charge higher than 9 mV. The decrease in charge of the chitosan samples before and after nanoplex formation confirms the electrostatic interactions between the polycation and the negatively charged siRNA phosphate groups. Similar to the nanoplex size M_w correlation, at N/P 50 the highest zeta potential resulted from nanoplexes formed with chitosan with a M_w of ~ 250 kDa with a DD 94% and chitosan with a ~ M_w 280 kDa with a DD 90%. The increase in zeta potential clearly correlated to the increase in DD in the case of nanoplexes formed at N/P 50 and chitosan alone. At N/P 100 the highest zeta potential resulted from nanoplexes formed with chitosan with a M_w of ~ 120 kDa and a DD 83%, followed by chitosan with a M_w of ~ 380 kDa and a DD 85%.

Table 5. z-Average diameter (size) and zeta potential (ζ) of the chi/siRNA nanoplexes formed via electrostatic interactions at N/P ratios 50 and 100 and measured by ZetaSizer..

<i>RN (DD;M_w)</i>	<i>Batch</i>	<i>Chitosan alone</i> ζ (mV)	<i>N/P 50</i>		<i>N/P 100</i>	
			<i>Size (nm)</i>	ζ (mV)	<i>Size (nm)</i>	ζ (mV)
Chi (80;165)	Ald Low	29	184	9.41	216.7	16.6
Chi (83;122)	ANG115236b	40.2	233.8	9.67	259.2	23.1
Chi (85;110)	ANG115236a	43.9	234,0	12,0	244.1	16.4
Chi (85;379)	Ald Medium	39.3	250,4	11,7	253,6	21,9
Chi (90;276)	ANG115275a	57.6	164.6	21.1	191.7	19.4
Chi (94;245)	ANG115275b	62.1	215.2	18.9	171.9	20.4

The detailed characterization of the chitosan with different M_w and DD pointed towards using a chitosan with a higher DD (92 – 94 %) and M_w between 200 and 250 kDa. As PEGylation increases M_w of the polymer, it was decided to purchase chitosan Hepe with a M_w of 165 kDa and 92.6 % DD to get the final M_w of PEG_chitosan in the desired range. This chitosan not only fitted the structural parameters required for the siRNA delivery system, but it was also tested microbiologically and the protein content was as low as 0.5%. Chitosan Hepe was also characterized via GPC and 1H NMR (Table 6).

3.2. Chitosan – PEG synthesis and physicochemical characteristics

3.2.1. Synthesis of chitosan with different degrees of substitution (DS)

N-hydroxysuccinimidyl methoxy PEG 5 kDa was selected to be grafted on chitosan at low substitution ratios. As previous investigations proved that, both chain length and graft density of PEG have an impact on nanoparticle formation and can influence the efficient transfection of nucleic acids[150]. The long PEG chain will allow the siRNA to interact with positively charged chitosan without interference. However, the PEG chains reduce protein adsorption on

the nanoplex. The D-glucosamine units of chitosan can be modified by chemical derivatization of the amine or hydroxyl groups. The higher activity of the amino group at C-2 compared to the hydroxyl groups at C-6 and C-3 results in a specific reaction with the PEG succinimidyl ester (

Figure 19).

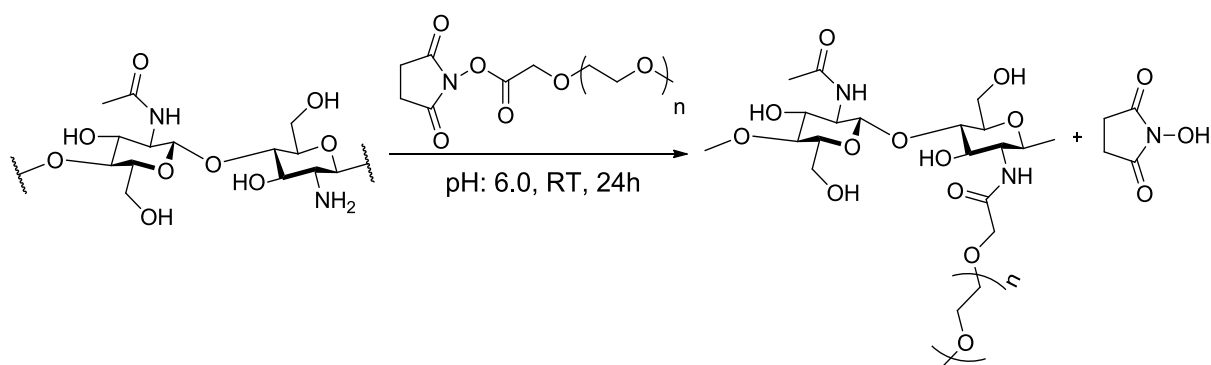


Figure 19. Synthesis of chitosan_PEG. Deacetylated chitosan was modified at pH 6.0 using NHS-methoxy PEG at different degrees of substitution.

At slightly acidic pH the amino groups of deacetylated chitosan can be modified by N-hydroxy succinimidyl methoxy PEG in a specific reaction. As the PEG grafting is done via amidation of the amine moiety at deacetylated chitosan, the ratio of substitution might affect the stability of the nanoplexes. High substitution ratios lead to a decrease in protonable groups which could interact with the negatively charged siRNA phosphate groups. To test this, five different chitosan_PEG copolymers were synthesized with increasing degrees of PEG substitution. The higher percentage of PEG grafting was generated by increasing the amount of the activated methoxy PEG derivative. To remove the excess of mPEG-NHs, hydrolyzed mPEG-carboxylic acid, and 1-hydroxypyrrolidine-2,5-dione side product, the resulting copolymer was dialyzed against deionized water using a dialysis membrane of 50 kDa MWCO.

3.2.2. Analytical characterization of PEGylated chitosan

After derivatization, the formation of new bonds on the amino group was identified by characterizing the copolymer in terms of its molecular weight and degree of substitution. ^1H

NMR spectra of the raw materials (chitosan Heppe and mPEG_{5kDa}-NHS ester) and the mPEG-grafted chitosan copolymer were compared to identify specific signals for the grafted groups. Specific mPEG signals were identified between 3.5 ppm and 4.3 ppm with the protons of the methoxy group at ~3.3 ppm. The peak related to the protons of the N-hydroxysuccinimide was methoxy present at ~2.7 ppm only in the activated form of the raw material. It was no longer present in the chitosan-PEG copolymer spectra. The signals of the three acetyl protons in the N-acetyl-glucosamine groups could be distinguished from the PEG peaks in the chi_PEG sample at ~1.9 ppm. Integration of this chitosan specific signal and the PEG specific OCH₃ singlet of the grafted mPEG chitosans were used for the determination of the degree of substitution of the grafted copolymer (Figure 20).

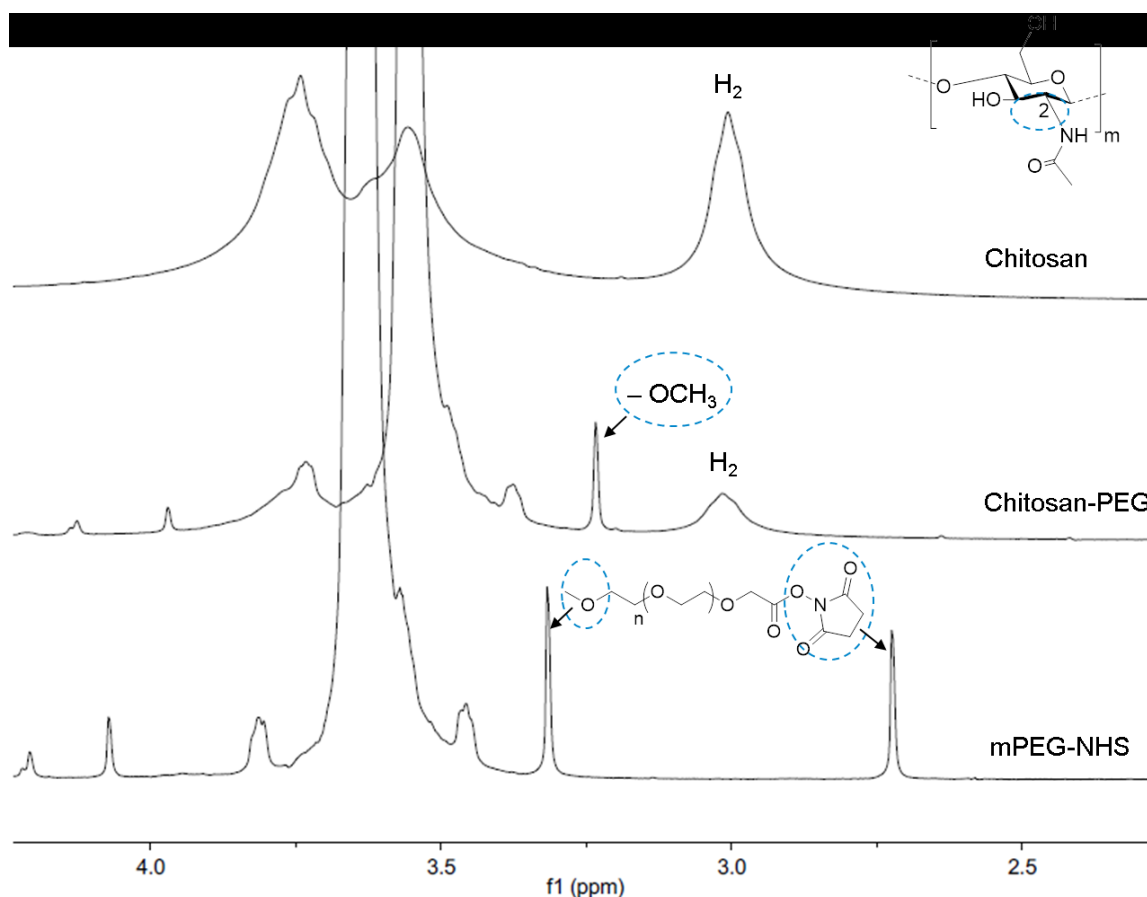


Figure 20. ¹H spectra of mPEG-NHS ester, chitosan and Chi-PEG copolymer in 2% CD₃COOD/D₂O. Specific signals from groups of the grafted PEG derivatives were identified in the range between 3.5 – 4.3 ppm (zoomed region) ¹H – signals from the methoxy group were detected at 3.3 ppm and were used for the quantification of PEG grafts on the chitosan-PEG copolymer.

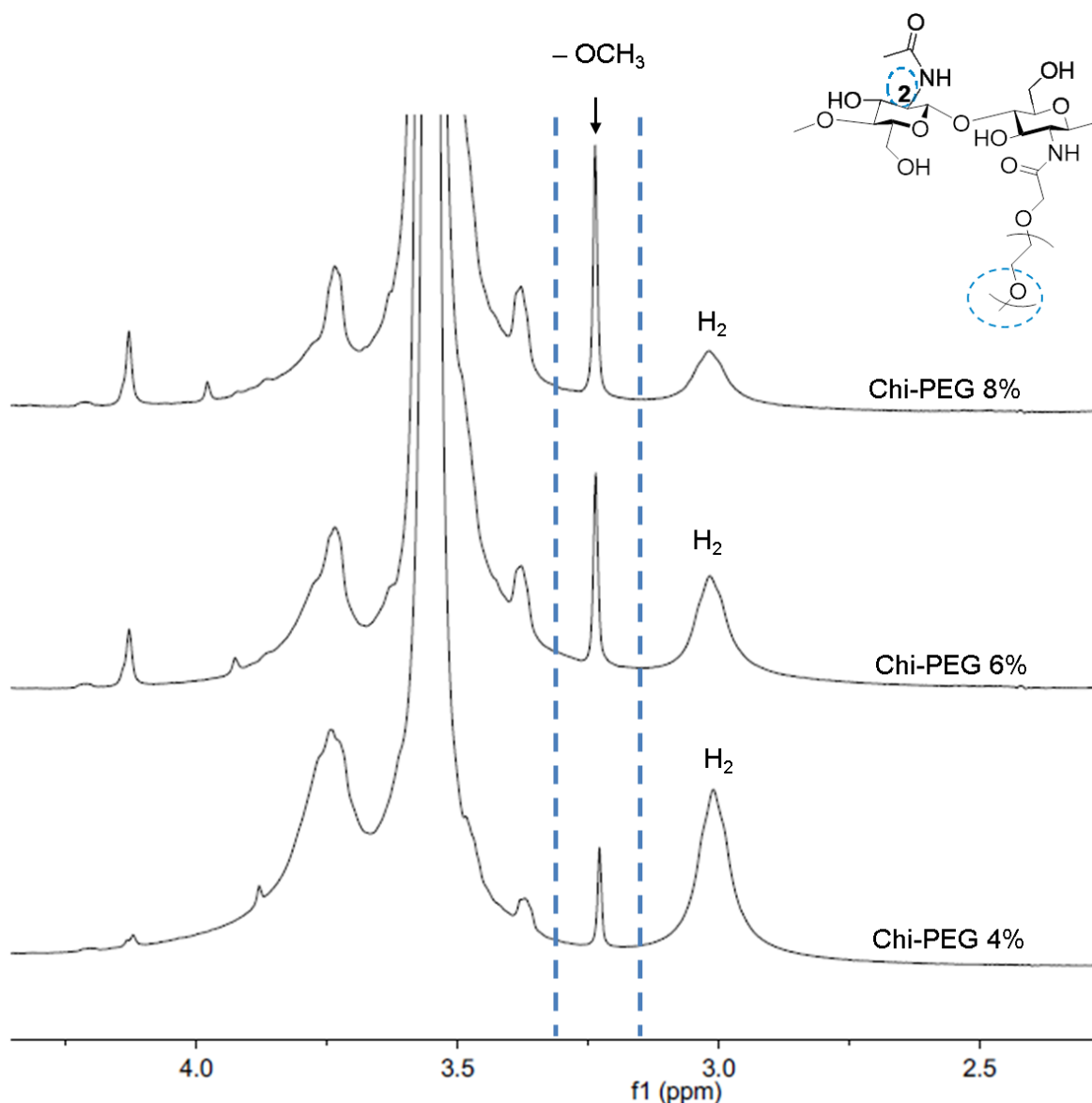


Figure 21. Overlay of $^1\text{H-NMR}$ spectra chi-PEG at DS 4%, 6% and 8%. Specific signals of the protons in the $-\text{OCH}_3$ group of the PEG graft at ~ 3.3 ppm were integrated and the grafting yield was calculated relating to the specific signal of the acetyl protons of *N*-acetylated glucosamine moieties of chitosan.

The grafting of PEG to the chitosan was also measured using gel permeation chromatography (GPC) by the increase in M_w calculated from right angle light scattering data and the decrease in retention time. The degree of PEG substitution was calculated from the M_w difference of the final chi-PEG copolymers and the M_w of the raw materials. The summarized results show that the degree of substitution of mPEG from GPC was similar to the value obtained by ^1H NMR (Table 6).

Table 6. Chitosan-PEG parameters measured and calculated from results of GPC and ¹H NMR analyses. Average molecular weight M_N , weight-average molecular weight M_w , intrinsic viscosity η , hydrodynamic radius Rh measured by GPC. Degree of substitution of mPEG expressed as moles/moles measured by ¹H NMR. S.D= standard deviation; RN=reference number;

RN	Batch number	mPEG/Chi-NH ₂ [mol/mol]	Mn ±S.D[kDa]	Mw ±S.D [kDa]	Mw/Mn ±S.D	η ±S.D [dL/g]	Rh ±S.D [nm]	DD [%] ^a	I _{OC} _{H3}	DS of PEG mol [%] NMR ^b	GPC ^c
Chi (152; 92.6)	Chitosan Hepe	-	119 ±0.1	152 ±1.1	1.3 ±0.01	3.8 ±0.19	20.4 ±0.13	92.6	-	-	-
1.5% PEG	ANG142958	0.06	131 ±0.7	161 ±4.1	1.2 ±0.02	4.0 ±0.07	21.1 ±0.05	91.1	0.20	1.5	1.6
3% PEG	ANG142960	0.11	141 ±1.2	176 ±2.1	1.3 ±0.03	3.3 ±0.81	20.1 ±1.78	89.6	0.44	3.3	3.4
4% PEG	ANG142961	0.13	146 ±1.7	185 ±6.8	1.3 ±0.05	3.3 ±0.87	20.5 ±2.08	88.6	0.60	4.4	4.3
6% PEG	ANG142897	0.14	156 ±2.2	231 ±11.0	1.4 ±0.07	3.6 ±0.13	22.3 ±0.52	86.6	0.81	6.0	5.8
8% PEG	ANG142953	0.19	172 ±1.2	316 ±23.0	1.8 ±0.12	3.4 ±0.14	24.4 ±0.75	84.6	1.10	8.1	8.4

$$^a DD\% = DD_{chi}\% - ^b DS\%; \quad ^b DS = I_{OCH3} \times \left(\frac{\frac{1}{3} \times I_{Ac}}{\frac{1}{6} \times I(H2-H6)} \times 100 \right)_{chitosan\ Hepe}; \quad ^c DS = \frac{(Mw_{ChiPEG} - Mw_{Chi})/5000}{DP_{chi}}; \quad DP_{chi} = Mw_{chi}/Mn_{chi}$$

With increasing PEG grafting an increase in M_w was noticed as well as a decrease in the DD due to the D-glucosamine derivatization. The lowest DD was 85% for chi_PEG with an 8% DS. A higher amount of PEG would have reduced the number of protonable amino groups even further which influence the stability of the nanoplexes. The polydispersity of the samples was between 1.3 and 1.4 quite similar to the starting material. However, chi-PEG with the M_w/M_n equal to 1.8 showed an increase in polydispersity, which could have been caused by the steric hindrance of the PEG grafting. Polydispersity values lower than 1.5 correlate to polymers with narrow molecular weight distribution.

3.2.3. Influence of the DS on the solubility of mPEG-chitosan copolymer in aqueous buffers

Chitosan is considered to be a reversibly cross-linked polymer as it forms superstructures via hydrogen bonds. These bonds have to be broken in order to dissolve chitosan. Therefore, the more primary amino groups are available the better chitosan can dissolve under slightly acidic conditions. At pH values higher than 5.5, however, it is believed that grafting of PEG chains onto chitosan can improve its solubility. The resulting solubility at neutral or even basic pH values seemed to be dependent on the M_w of the chitosan, its DS and the length of the PEG chains [150, 220, 221].

In the present work the solubility of unmodified chitosan was compared to PEGylated chitosan copolymers with increasing amount of mPEG by measuring the transparency of a solution at 600 nm using a spectrophotometer. A lower absorbance at 600 nm indicated better chitosan solubility while a higher absorbance reflected more turbid samples due to aggregation and precipitation. Chitosan and its derivatives were all soluble in acidic pH buffer (

Figure 22). In the case of PEGylated chitosan with DS 4% and 8%, a low turbidity and high solubility was kept also at higher pH. At pH 7.0 the absorbance for the highest DS samples was almost the same as at pH 4.0. The transparency of the chitosan derivatives was starting to decrease at pH 9.6 from a slightly increased turbidity for 8% Chi-PEG to a practically insoluble unmodified chitosan showing significant absorption at 600 nm. With a 1.5% mPEG DS the solubility of chitosan increased more than 3 times at pH 7.0 and about 2 times at pH 9.6 compared to the unmodified chitosan. Therefore, the solubility of unmodified chitosan was considerably improved even by very low mPEG DS.

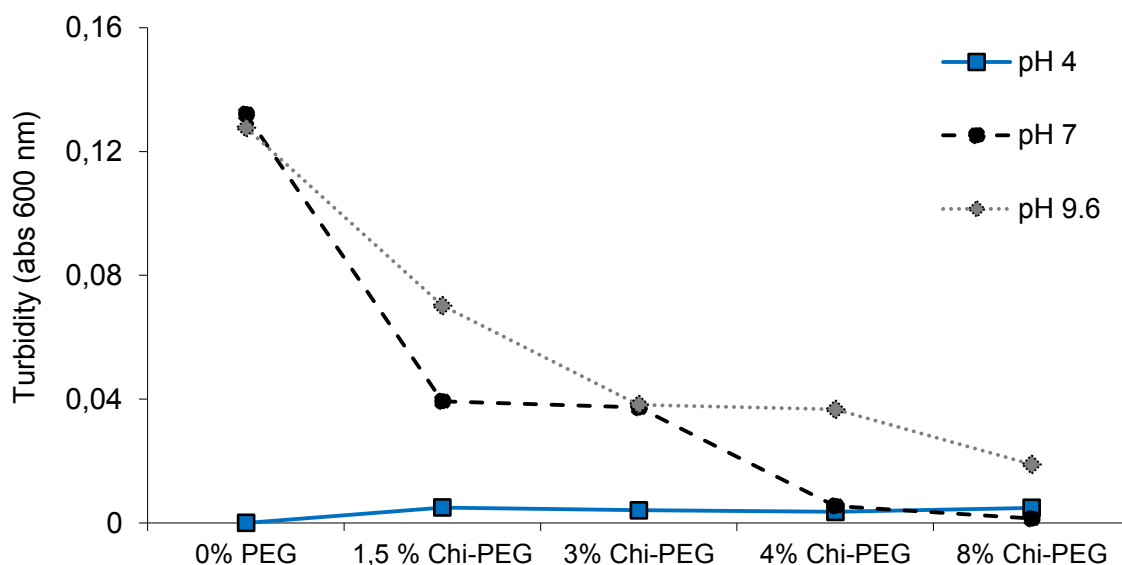


Figure 22. Solubility of chitosan and PEGylated chitosan at different DS in aqueous solutions at different pH measured as turbidity at 600nm. At acidic pH no significant turbidity was detected. At higher pH unmodified chi-PEG showed significant turbidity which was decreasing with increasing degree of PEGylation.

3.2.4. Influence of the mPEG DS on the formation of chitosan_PEG siRNA nanoplexes

Chitosan modifications of the primary amino groups might influence the stability of the nanoplexes. An increased PEGylation can lead to a lower number of positively charged groups and therefore to a lower complexation with siRNA via electrostatic interactions. Therefore, not only the DS was kept lower than 10% but also the ratio between the protonable amino groups (N) and phosphate groups (P) was kept constant for complex formation. The nanoplexes were formed with scrambled siRNA in 0.3 M CH₃COONa buffer at pH 5.5 at a constant N/P ratio of 25/1. This means, that in order to compensate for the lower overall cationic charge of PEGylated chitosans a higher amount of copolymer was added.

The stability of the chi_PEG siRNA nanoplexes was tested in a gel retardation assay. Unstable nanoplexes would release the siRNA in the agarose gel. Negatively charged siRNA would migrate to the cathode and a band in the lower part of the gel would be visible. All samples were treated either with RNase-free water which did not affect the complex stability, or with negatively charged polyaspartic acid (PAA), which displaced siRNA from the chitosan complex. Complete retardation of all complexes was observed whereas PAA-treated nanoparticles showed clearly the presence of free siRNA (Figure 23) (data provided by L.

Schuster NMI, Figure 4.21, page 75) [49]. At N/P 25/1 PEGylation at low DS had no negative effect on complex formation and stability for all tested PEGylation ratios. All chitosan siRNA nanoplexes were stable.

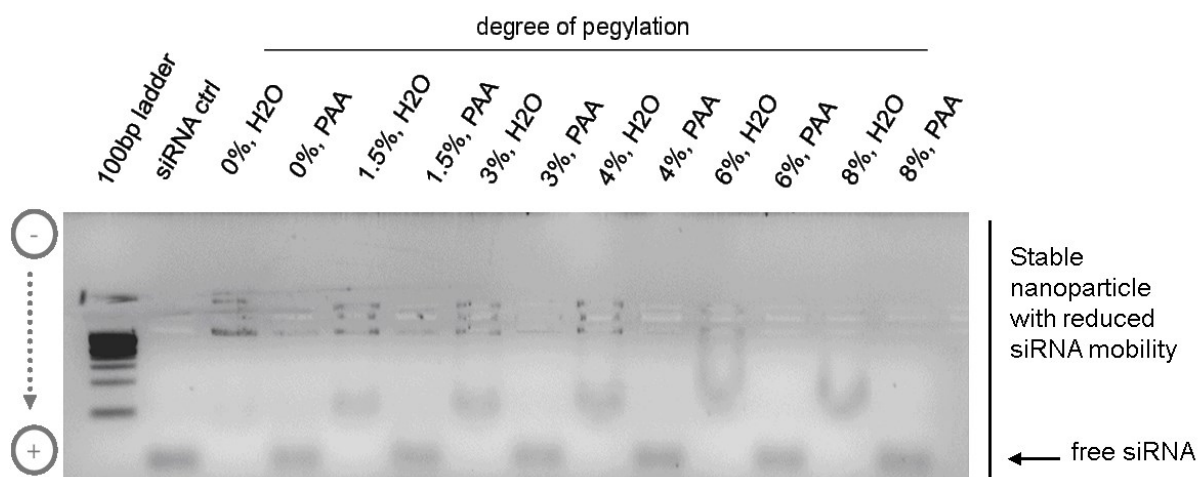


Figure 23. Gel retardation assay for the determination of nanoparticle stability. By means of differently modified chitosans and scr siRNA, nanoplexes were prepared. They were incubated with RNase-free water or with the complexation competitor PAA. The nanoplex samples were then loaded onto a 4% agarose gel and run for 90 min at 55 V. Subsequently, siRNA detection was performed with ethidium bromide. Fluorescence was detected after UV excitation. Free siRNA was detected only in nanoplex samples treated with PAA. All nanoplexes were stable in deionized water (data provided by dr. L. Schuster, NMI) [49].

The complexation of siRNA and chitosan_PEG was also characterized in terms of the hydrodynamic diameter, charge and size distribution of the nanoplexes (Table 7, Figure 26). The unmodified chitosan exhibited a particle size of ~200 nm while Chi_PEG formed nanoplexes with a mean size between 140 nm and 170 nm. With a nanoplex diameter lower than 200 nm and a polydispersity index in the 0.1 – 0.2 range, all complexes were optimal candidates for successful cell uptake via endocytosis. Furthermore, in agreement with the gel retardation results, all chitosan/PEGylated chitosans formed stable complexes protecting the negatively charged siRNA and yielding a positive charge on the surface of the nanoplexes. An increasing percentage of grafted PEG displayed a reduced, but still positive zeta potential. Unmodified chitosan: siRNA complexes showed a surface charge of 18 mV, while nanoplexes with Chi_PEG 8% DS exhibited a positive charge of only 8 mV.

Table 7. z-Average diameter and polydispersity index (PDI) of the nanoplexes formed when using different degrees of PEGylation to compact siRNA at a constant N/P ratio at 25.

<i>RN</i>	<i>0% PEG</i>	<i>1.5% PEG</i>	<i>3% PEG</i>	<i>4% PEG</i>	<i>6% PEG</i>	<i>8% PEG</i>
Size \pm S.D* [nm]	203 \pm 11	151 \pm 51	168 \pm 3	150 \pm 4	145 \pm 10	140 \pm 3
PDI \pm S.D*	0.11 \pm 0.06	0.14 \pm 0.03	0.14 \pm 0.06	0.12 \pm 0.04	0.19 \pm 0.03	0.23 \pm 0.01

*S.D = standard deviation between three independent experiments each performed in triplicates

3.2.5. PEGylated chitosans cell viability

Before testing the cytotoxicity of the nanoplexes, it was important to evaluate if chitosan and PEGylated chitosans have an impact on the cell viability (data provided by L. Schuster NMI, Figure 4.20, page 74) [49]. The cytotoxicity results for all chitosans were in the accepted limits of 70% viability (Figure 24). As the chitosans or PEGylation had no negative effect on cell viability, all samples were considered biocompatible and non-toxic.

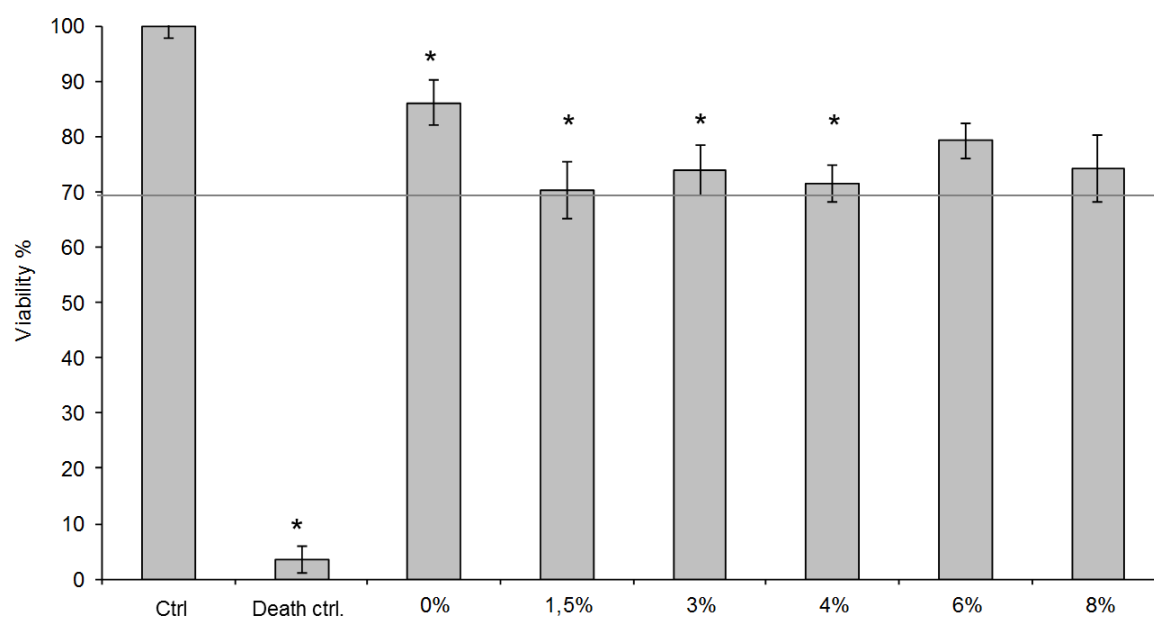


Figure 24. Cell viability of different PEG-modified chitosan. H1299-GFP cells were seeded the day before in medium without antibiotics and incubated on the following day with the tested chitosan for 6 h, followed by a change of medium. 48 h after the addition the vitality of the cells was determined by means of resazurin assay. Untreated cells (100% vital) were used as reference and the DMSO-treated cells were used as a death control. All measurements were based on the viable control. Three independent experiments were done in triplicates. (Statistics based on untreated cells, Nonparametric ANOVA, Kruskal-Wallis test, $p < 0.01$) (data provided by L. Schuster NMI, Figure 4.20, page 74) [49].

3.2.5.1. Chitosan and Chi_PEG:siRNA nanoplexes cell viability

The nanoplexes formed with scrambled siRNA at NP 25 were also tested for biocompatibility to exclude cytotoxic effects (data provided by L. Schuster NMI, Figure 4.22, page 77) [49]. The cytotoxicity results of the nanoplexes were similar to the results of the chitosans alone as shown in Figure 25. Although there were significant differences compared to the live-control, the vitality values were within the acceptable range of minimum 70% vitality.

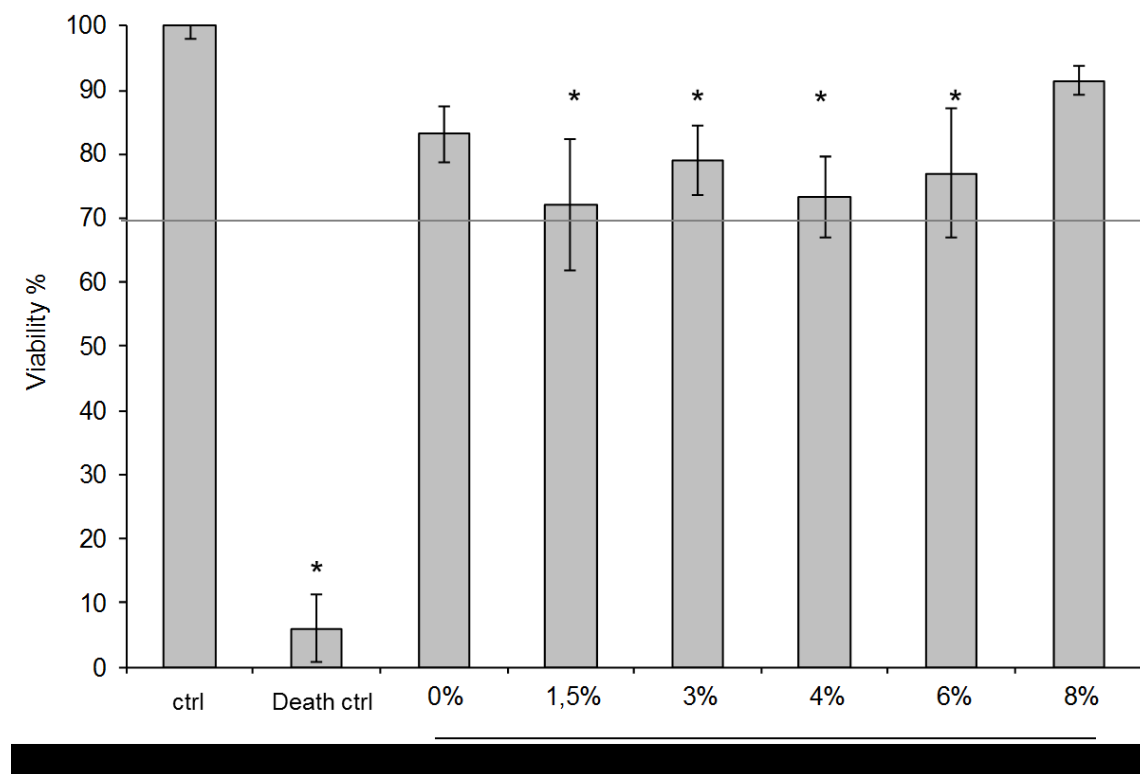


Figure 25. Vitality assay after transfection of H1299 cells with chitosan siRNA nanoparticles. The transfection was carried out with 200 nM siRNA for 6 h, the measurement of cell viability 48 hours after transfection. Untreated cells (100% vital) and DMSO-treated cells (death control) were used as reference. All measurements were based on the viable control. Three independent experiments were done in triplicates. (Statistics based on live control, Nonparametric ANOVA, Kruskal-Wallis test, $p < 0.01$) (data provided by L. Schuster NMI, Figure 4.22, page 77) [49].

3.2.6. Effect of the dynamic cell environment on the properties of PEGylated chitosan:siRNA nanoplexes properties

Chitosan and PEG grafted chitosan:siRNA nanoplexes were designed to enter the cells and be actively translocated across biological barriers. At the point of action they should release siRNA causing the knockdown of the targeted mRNA. Thus nanoplexes will be exposed to cell culture medium and dynamic cell environments with a complex mixture of proteins at

different pH values. Therefore, it was important to analyze their physicochemical parameters in a cell culture medium (CCM) containing RPMI, 1% L – Glutamate and 10% fetal calf serum (FCS). The ratio of nanoplex in aqueous buffer to CCM volume was exactly the one used for the *in vitro* experiments: 1 part nanoplex suspension and 3 parts of CCM.

For nanoplexes exposed to CCM it was expected that proteins adhere to the surface of the complexes forming the so called ‘protein corona’ [222]. The size and charge of the nanoplexes were characterized via dynamic light scattering (DLS) and analysis of the zeta potential of the nanoplexes while the siRNA complexation by the different chitosans was investigated with the dye quenching assay.

3.2.6.1. CCM influences on the nanoplex surface charge

Unmodified chitosan nanoplexes had the lowest zeta potential (-1.6 mV), followed closely by the 1.5% PEG grafted chitosan copolymer with an almost neutral charge of 0.8 mV (Figure 26). The zeta potential was starting to rise when PEG density increased. Chi_PEG 6% nanoplexes reached the positive charge of +6.6 mV and chi_PEG 8% nanoplexes a slightly lower positive charge of +4 mV in zeta potential.

To double check the influence of the ‘protein corona’ on the charge of the nanoplexes, the complexes were also characterized in absence of the CCM, but at a similar pH in PBS (Figure 26). Except for the chi_PEG 8% sample, all the other nanoplexes had a zeta potential similar to the one in buffer at pH 5.5. Therefore, the adsorbed proteins at the surface of the nanoplexes proved to have a much greater impact on the overall charge of the nanoplexes than the pH of the medium. At higher PEGylation ratios the zeta potential reached a quite small range of positive values between 2.4 up to 8 mV. Thus the zeta potential became more and more independent from the composition of the medium. The zeta potential was regulated by the PEG groups at higher PEGylation ratios.

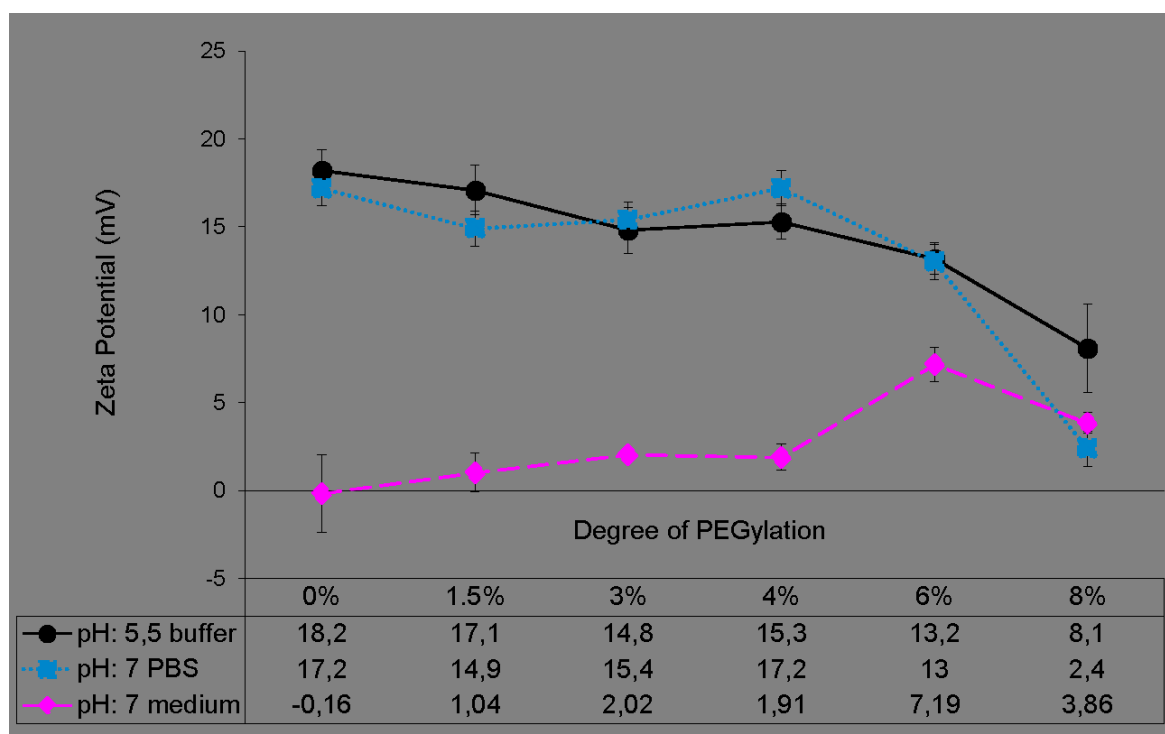


Figure 26. Zeta potential of chitosan and chi_PEG:siRNA nanoplexes with increasing DS measured in buffer at pH 5.5, CCM at pH 7.0 and in PBS at pH 7.0. The nanoplexes were formed in buffer at pH 5.5, after 15 min of stabilization they were directly measured or added over to PBS or CCM in a volume ratio of 1:3. With increasing PEGylation ratio the zeta potential converged to a small range of positive values at 2 – 8 mV.

3.2.6.2. CCM influence on the nanoplex size

The evaluation of the z-average diameter in the serum rich CCM was not as straightforward as in the aqueous buffer due to the exceeding presence of proteins which bound to the nanoplex surfaces. DLS size measurements showed a broad size distribution resulting in different nanoplex species which made it difficult to determine the overall size and charge of the nanoplexes.

When measuring the CCM alone, two peaks were seen: one protein peak at 9 nm and a broader peak at ~77 nm, probably from larger aggregates of FCS proteins (Figure 27 a.). Signal intensities of the blank CCM sample could be compared to the ones measured in the nanoplex samples. When measuring the unmodified chitosan siRNA nanoplexes in CCM, however, the broad peak at ~77 nm, in CCM blanks was drifted to lower size of about 20 nm (Figure 27 c). Furthermore, the presences of two other peaks at about 1000 nm and 600 nm indicated the formation of large aggregates between the proteins and nanoplexes. A dominant nanoplex peak was detected at about 150 nm.

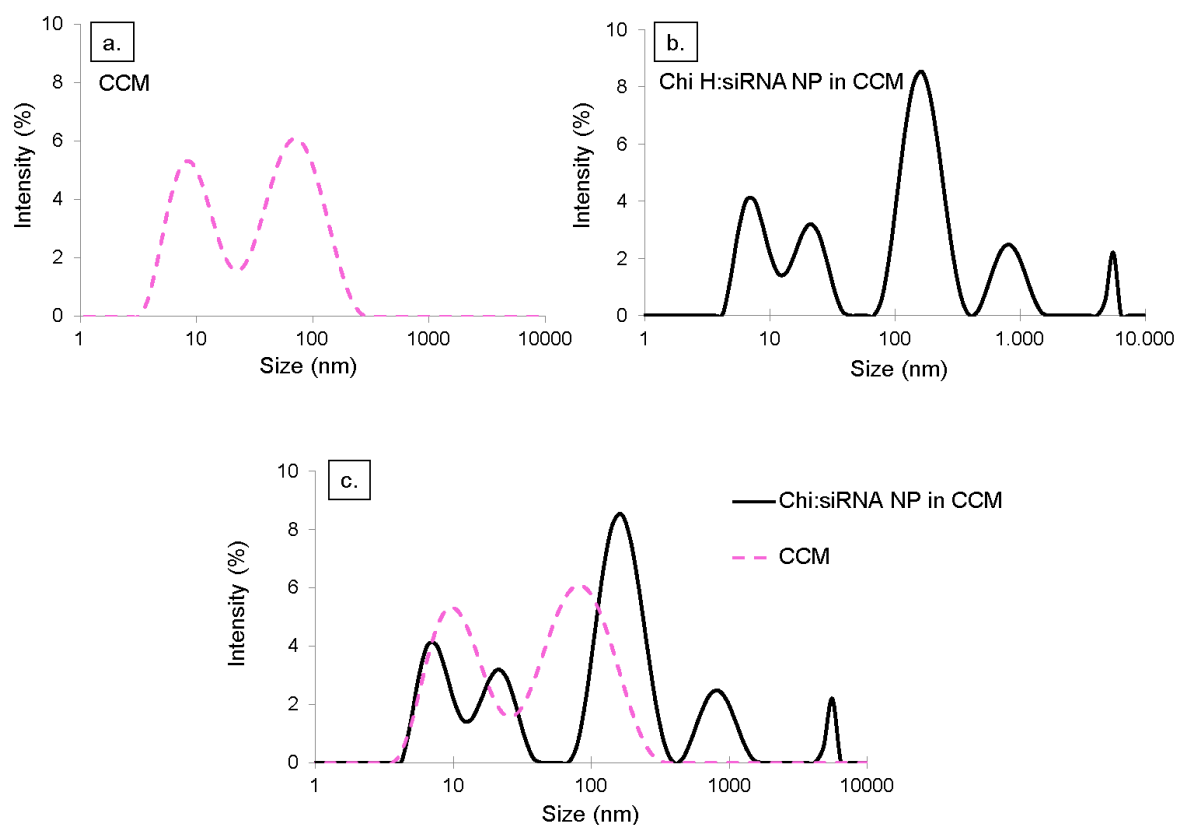


Figure 27. Intensity size distribution of a) CCM (RPMI+10%FCS+1%L-Glu) with a size of ~10 nm and 77 nm, b) chitosan:siRNA NP in CCM, c) overlay of the CCM with the chitosan:siRNA nanoplexes in CCM. The DLS data showed multiple nanoplex populations which made it difficult to determine the precise particle size in the mixture.

All the nanoplexes showed a high polydispersity in CCM and similar intensity peaks as the ones in Figure 27a. Therefore, a precise measurement of the average size was not possible via photon correlation spectroscopy. It was, however, possible to investigate the agglomeration behaviour of the nanoplexes with and without PEG in CCM by DLS. Furthermore, an estimate of the particle size of the nanoplex was possible which was quite similar to the nanoplex size found in pure buffer (Table 7).

Since the nanoplexes in solution exhibit Brownian motion, small random fluctuations in the scattering intensities can be observed and measured across μs time scales. The physical confinement of the nanoplexes, meaning the limited movement in the extremely short time scale makes it possible to correlate the degree of non-randomness in an apparent random data set. The correlation coefficients can be calculated as shown in equation (1) [223]:

$$G(\tau) = \int_0^{\infty} I(t)I(t + \tau)dt; \quad t - \text{initial time}; \tau - \text{delay time} \quad (1)$$

In contrast to separation techniques, where nanoplexes are separated by size and then counted, the dynamic light scattering technique measures all the size information for the whole ensemble of nanoplexes within the same single correlation curve (Figure 28) [223]. Smaller nanoplexes will move faster than larger nanoplexes, which is reflected in the faster fluctuations of the scattered light intensities. Therefore, by comparing the decay rate in the correlation curve the size of the nanoplexes can also be compared. As proteins from FCS in the CCM also scatter light, DLS data referred to proteins, protein aggregates, protein-nanoplexes, and nanoplex aggregates. The overlay of the correlation curve can also give information about the polydispersity of the nanoplexes. An increase in gradient indicates an increase in the distribution of the nanoplexes. However, the most important and reliable information is found over the baseline of the correlation graph. When the nanoplexes agglomerate, or the proteins aggregate the baseline is no longer smooth [224].

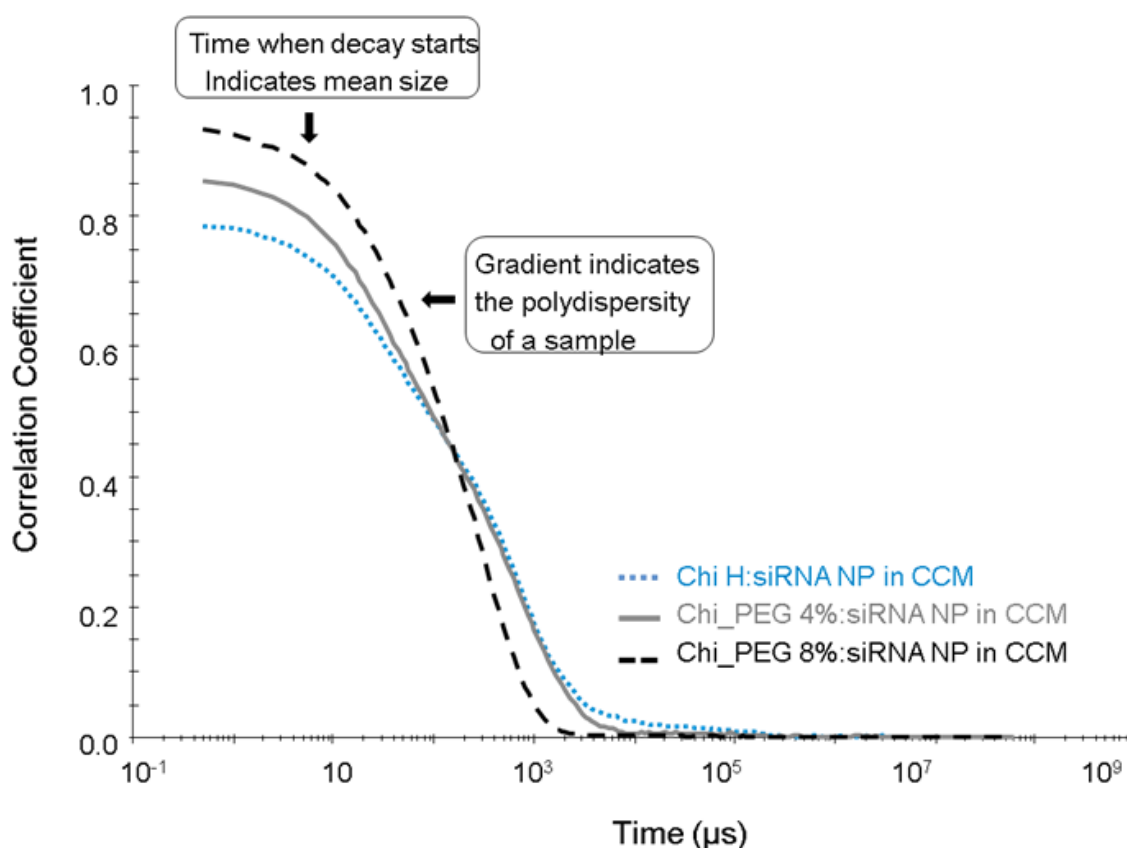


Figure 28. Intensity correlation curves for nanoplexes with increasing percentage of PEG grafted to the chitosan copolymer in CCM (RPMI+10%FCS+1%L-Glu). The three samples were measured after 15 min in CCM at a volume ratio of nanoplexes: CCM of 1:3. (See figure 29)

Same as for the zeta potential measurements nanoplexes were prepared first in 0.3 M CH₃COONa pH 5.5 and then added to the CCM in a volume ratio of nanoplex suspension: CCM of 1:3. After 15 minutes incubation the nanoplexes were analyzed and correlation coefficient curves shown in Figure 28 were compared. In comparison to the chitosan PEG 8% DS nanoplexes, both unmodified chitosan and 4% PEGylated samples showed a curve with three different decay rates. The fast decay rates seen at delay times up to 100 μs were interpreted as arising from the nanoplexes with no protein corona. The slower decay rates seen at delay times up to 1000 μs for the smaller chi_PEG 8% nanoplexes were probably due to the nanoplexes with a protein corona. Decay rates next to the baseline indicated the presence of larger agglomeration of nanoplexes and proteins. The sample with an 8% DS with PEG revealed a standard correlation curve with a smooth baseline, but with a large gradient. This means that the sample was still too dispersed [223].

As the nanoplexes were incubated for 6h in the cell culture in the *in vitro* assay, it was important to evaluate the behavior of the nanoplexes in CCM over time.

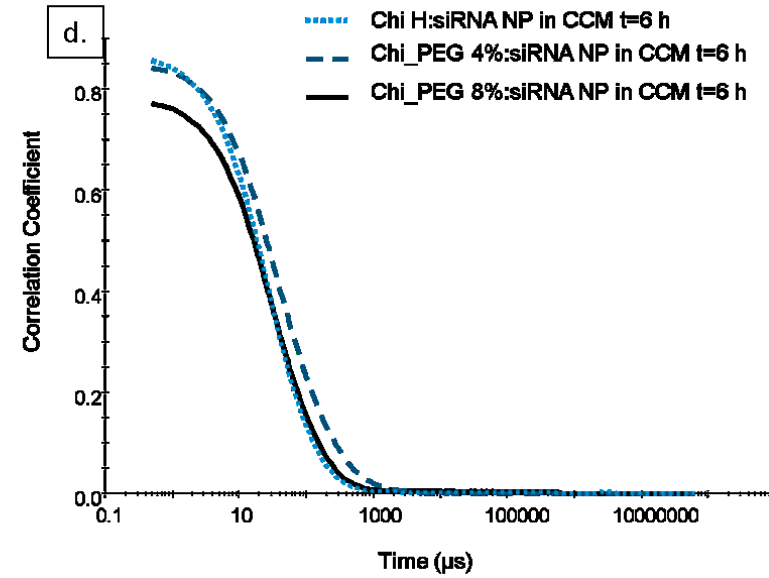
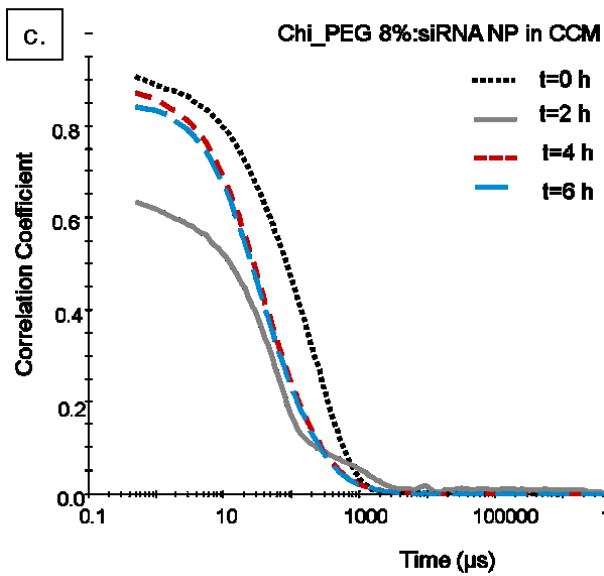
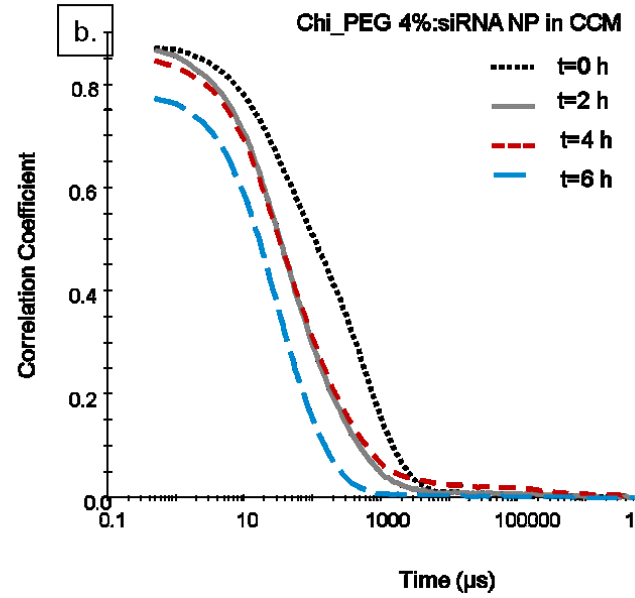
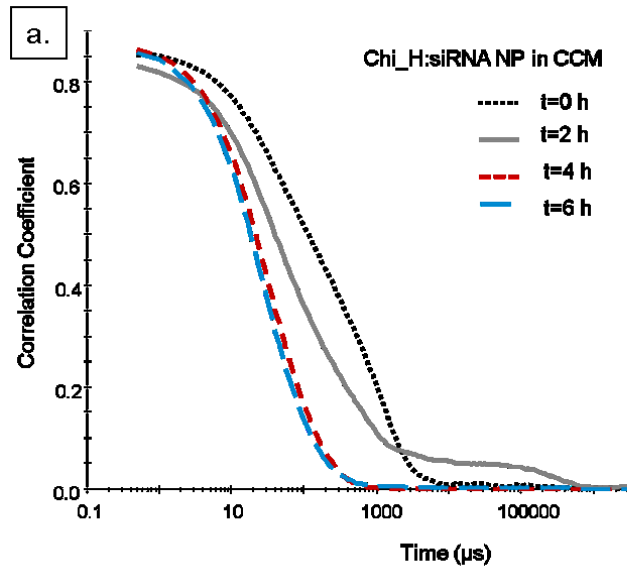


Figure 29. Correlation coefficient curves for nanoplexes with increasing percentage of PEG grafted to the chitosan copolymer kept in CCM (RPMI+10%FCS+1%L-Glu). Curves are shown for a) *chi_H* siRNA NP in CCM measured every 2 h, b) *chi_PEG* 4% siRNA NP in CCM measured every 2 h, c) *chi_PEG* 8% siRNA NP in CCM measured every 2 h, d) overlay of a)b)c) measured at 6h.

Independent of the PEG density increase, all nanoplexes had slower decay rates at time 0 compared to the decay rates after 2, 4 and 6 h as shown in Figure 29. At 2 h the correlation curve showed more than one decay rate for unmodified chitosan and 8% PEGylated chitosan. *Chi_PEG* 4% nanoplexes indicated a similar behavior to the other two samples only after 4 h, as the correlation curve showed the formation of larger agglomerates near the baseline. However, the correlation curve for all 3 nanoplexes, at 6 h, revealed no agglomerates near the baseline and only one decay rate for each sample. These results could reflect the competitive adsorption of the proteins in the FCS to the nanoplex surfaces. Further information for the 3 different samples was obtained by the overlay of the correlation curve after 6 h which indicated slightly higher decay rates when the PEG density of the chitosan was higher.

Given the changes in nanoplexes zeta potential and size parameters once added to the CCM, there was a pending question of whether the complexation of siRNA would be changed due to different PEGylation ratios of chitosan. Merkel *et al.* [225] used the fluorescent quenching assay approach to assess the condensation efficiency at different N/P ratios by using Tye563-labeled siRNA. At a minimum of fluorescence signal a large number of fluorescently labeled siRNA molecules are entrapped in a complex, quenching each other due to close spatial proximity. However when fluorescence intensity increases the close proximity of the dyes decreases, indicating a weaker binding of the siRNA in the nanoplex. In the current work the same approach was used for comparing the behavior of the siRNA complexation in different environments at the same N/P ratio of 25.

The nanoplexes were formed with Tye563-labeled siRNA in 0.3 M CH₃COONa buffer at pH 5.5 before being added to the CCM in a volume ratio of 1 part nanoplexes and 1 part CCM resulting in 200 nM Tye563-labels as final concentration. The dye quenching assay was performed over 6 h in order to analyze the siRNA complexation changes during the cell uptake. Our findings indicated, independent from the nanoplexes formed, that after more than 2 h, the degree of siRNA complexation was almost the same for all types of samples (Figure 30). The relative fluorescence intensities were high, meaning that a very small amount of the labeled siRNA was self-quenched due to decreased spatial proximity. However, the relative

fluorescence intensity was still under 100% was stable enough. Even if siRNA was very tightly bound inside the nanoplexes, the entire complex was stable enough to protect the siRNA in the CCM.

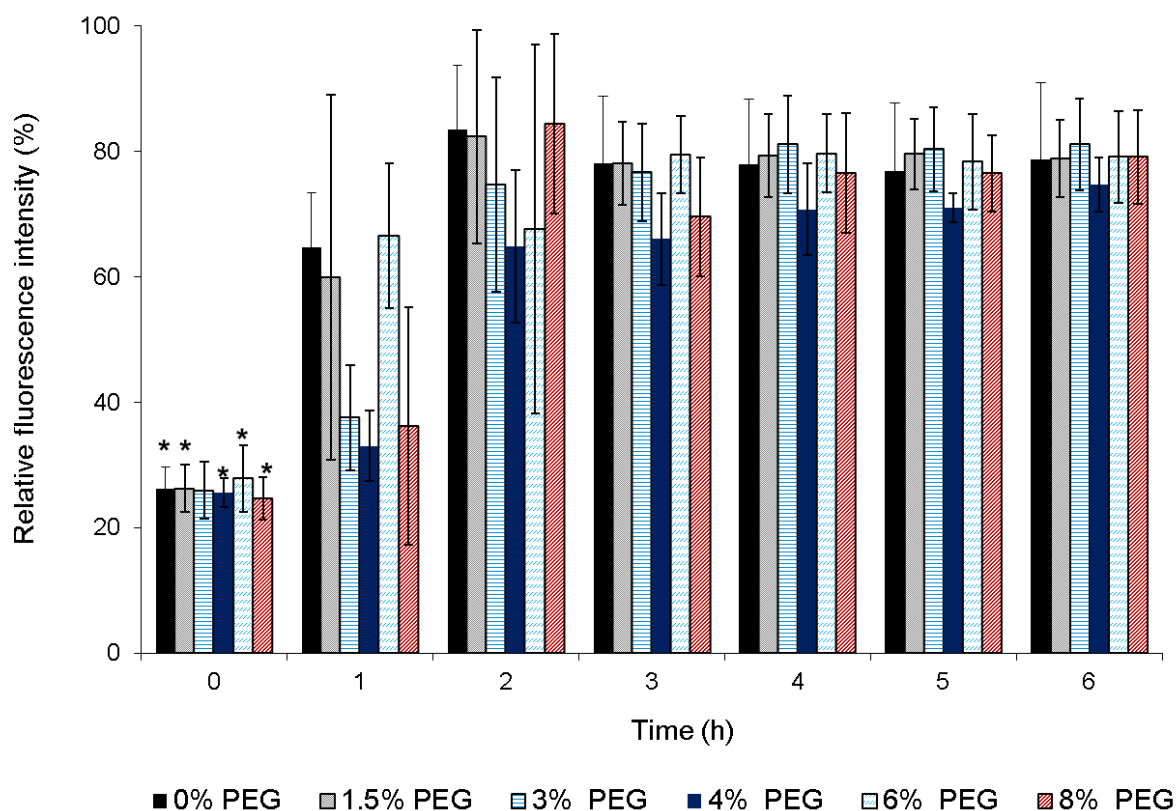


Figure 30. Dye quenching assay of the chitosan:siRNA and chi_PEG:siRNA nanoplexes with increasing PEG grafting in CCM at pH 7.0 over 6 h. At time 0 the fluorescence of Tye-563 siRNA molecules were strongly quenched due to close spatial proximity of the fluorophores. Over time the nanoplexes seemed to enlarge their volume which lead to a decrease in spatial proximity of the dyes and increased in the relative fluorescence intensity, reaching a plateau after 2 h at 80% fluorescence intensity. The relative fluorescence intensity was calculated using Tye-563 siRNA in CCM (200nM - same concentration as for the nanoplexes) as a control (100% fluorescence) and CCM alone as blank (0% fluorescence). Three independent experiments were done in triplicates. (Statistics based on results at $t=6$ h, Nonparametric ANOVA, Kruskal-Wallis test, $p < 0.01$).

3.2.6.3. Intracellular environment

During the cellular uptake experiments, nanoplexes see very different environments. They go from their preparation in pH 5.5 buffer to pH 7.0 in the extracellular CCM. After cellular uptake the nanoplexes are exposed to different subcellular locations (endosome, lysosome, and cytosol). The intracellular environment of the endosome has a pH of 5-5.5 as the vacuolar

ATPase pumps promote the influx of protons from the cytosol. The lysosome compartments are connected to the endosome and have even a more acidic environmental pH of ~ 4.5 [99]. Tribault *at al.* [104] showed in colocalization studies that intracellular trafficking of chitosan based nanoplexes was taken place in the endo-lysosomes, making the endo-lysosome release a crucial step in efficient siRNA delivery. Therefore, the change in zeta potential for nanoplexes at different pH was investigated in detail (

Figure 31). For these analyses, the nanoplexes formed from the different chitosans and scrambled siRNA were first added to the CCM in a volume ratio of 1 part nanoplex to 3 parts CCM. Then the pH was lowered to pH ~ 4.5 and the zeta potential was measured.

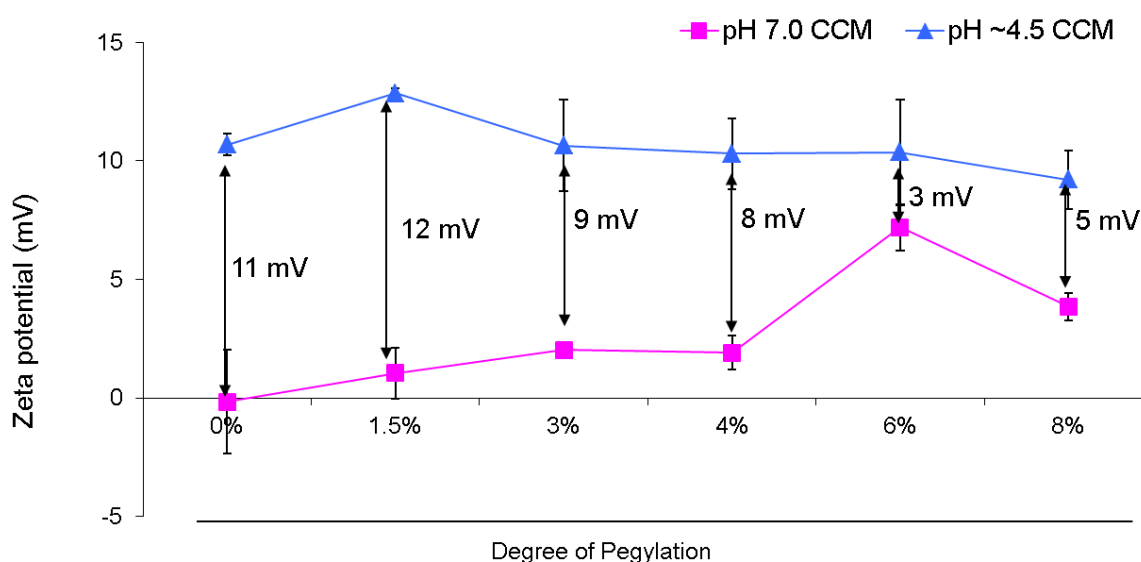


Figure 31. Zeta potential measurements of chi-siRNA and chi_PEG siRNA nanoplexes with increasing PEG grafting in CCM at pH 7.0 and at pH ~ 4.5 . The nanoplexes were formed in 0.3 M CH_3COONa buffer at pH 5.5 then added to CCM (pH of 7.0). The pH was decreased with acetic acid to a pH of ~ 4.5 and the zeta potential was determined immediately. For highly PEGylated chitosan the differences in zeta potential for the nanoplexes at pH 7.0 and 4.5 were much smaller than for low grafted PEG-chitosan nanoplexes.

All samples showed an increase of the positive charge with values between 10 and 13 mV at low pH compared to pH 7.0. Chitosan and chi_PEG nanoplexes with small DS (up to 4%) revealed a higher increase in the zeta potential at low pH than nanoplexes with higher PEG densities. The difference between extracellular and intracellular pH may play an important

role in the endosome release. When highly protonable nanoplexes invade the endo-lysosome the osmotic swelling of the endo-lysosome might be faster and more efficient.

3.2.7. Cellular uptake of chitosan and Chi_PEG:siRNA

In previous chapters it was shown that the grafting of PEG on chitosan improved chitosan solubility. Also, due to the steric hindrance and shielding of the nanoplex surface it can have an effect on charge and could influence the protein corona formation on the nanoplexes once in cellular culture medium. Therefore, it was important to investigate the transfection efficiency of nanoplexes without and with increasing amounts of PEG on the surface

H1299 cell line, which naturally exhibits no fluorescence, were transfected with nanoplexes formed from chitosan/chitosan_PEG at increasing DS and fluorescently labeled siRNA with a final concentration of 200 nM siRNA. The N/P ratio used was 25/1, the same as in the physico-chemical characterization. The transfection was carried out as in the previous experiments for 6 h before the medium was changed and the cells were incubated for another 48 h. The transfection results were assessed via microscopy (data provided by L. Schuster NMI, Figure 4.23, page 78) [49], and the internal intensity inside the cells of the fluorescence signal was determined by flow cytometry (data provided by L. Schuster NMI, Figure 4.24, page 79) [49]. To minimize false positive signals by the adhesion of the nanoplexes to the outer layer of the cell membrane, the extracellular green fluorescence was quenched before cell harvest by treatment of the cells with trypan blue.

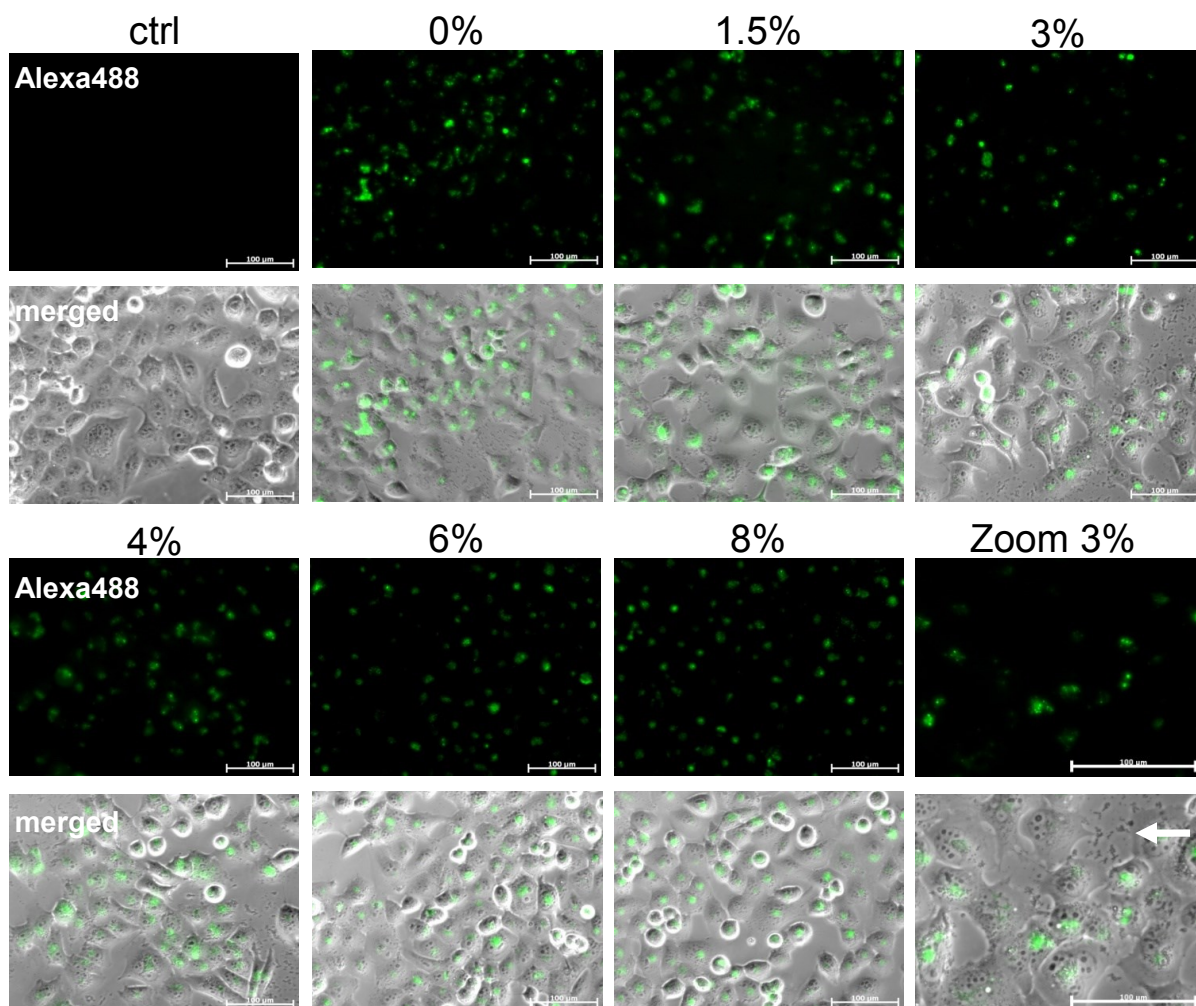


Figure 32. Fluorescence microscopy of H1299 cells after transfection with chitosan/chi_PEG: fluorescently-labeled siRNA nanoplexes. H1299 cells were transfected for 6 h before the medium change. After 48 h, the cells were quenched by trypan blue and the uptake of the nanoplexes in the cells was examined microscopically (scale bar 100 microns) (data provided by L. Schuster NMI, Figure 4.23, page 78) [49].

The microscopy recorded signals for all the chitosan/chi_PEG:fluorescently labeled- siRNA nanoplexes indicating a successful uptake for all 6 samples. In addition, the 3% zoom in Figure 32 indicated the presence of some agglomerates in the cell culture which were successfully quenched showing no green fluorescence. Even though the punctual fluorescent signals can be seen in the cells, it was hard to quantify the transfection efficiency based only on the microscope pictures. Therefore, the cells were further analyzed by flow cytometry.

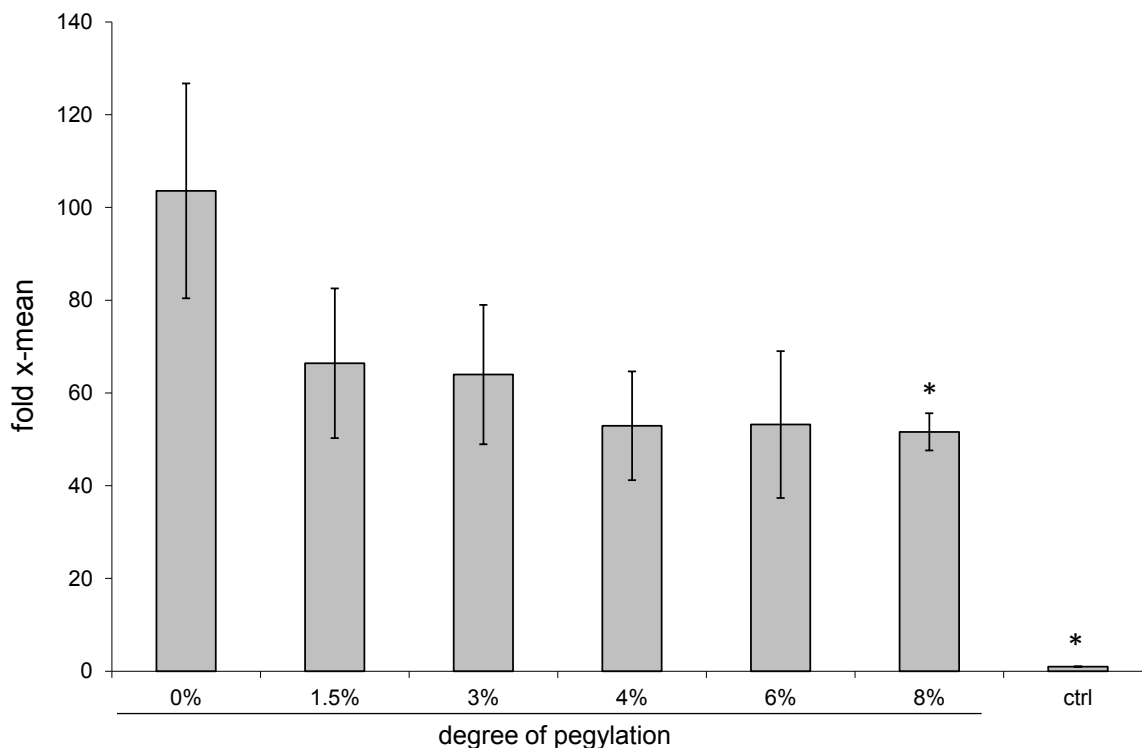


Figure 33. Flow cytometry analysis of chitosan/chi_PEG: fluorescently-labeled siRNA nanoplexes uptake. H1299 cells were transfected with nanoparticles consisting of different chitosans and a fluorescent Alexa488-siRNA for 6 before the medium change. 48 h after transfection, the cells were harvested and the fluorescence in the cells was determined by flow cytometry. Three independent experiments were done in triplicates. (Statistics based on 0% PEG, Nonparametric ANOVA, Kruskal-Wallis test, $p < 0.05$) (data provided by L. Schuster NMI, Figure 4.24, page 79) [49].

The mean fluorescence of the untransfected control was set to 1 as well as for all other analysis based on it. Flow cytometry results showed apparent differences in the measured fluorescence between cells that were transfected with unmodified chitosan and cells that were transfected with PEGylated chitosans. However, according to the statistical analysis no statistically significant difference was detected between the different chitosan and chi_PEG nanoplexes with DS up to 6%. The increase in PEG grafting above 6% indicated a statistically significant decrease in the chi_PEG_8% nanoplex uptake compared to unmodified chitosan nanoplexes. Therefore, it appears that a small degree of PEG substitution did not significantly interfere with the nanoplex uptake. Given these results, the siRNA knockdown results should only be influenced by the intracellular barriers.

3.3. Knockdown of chitosan and chi_PEG:siRNA nanoplexes

The nanoplexes used for the knockdown experiments were prepared similar to the uptake experiments at an N/P ratio 25/1 and a siRNA final concentration of 200 nM siRNA. The transfection of both scrambled and GFP silencer siRNA nanoplexes was measured for 6 h before the medium change. The knockdown efficiency was measured after 48 h in cell culture (data provided by L. Schuster NMI, Figure 4.25, page 81) [49].

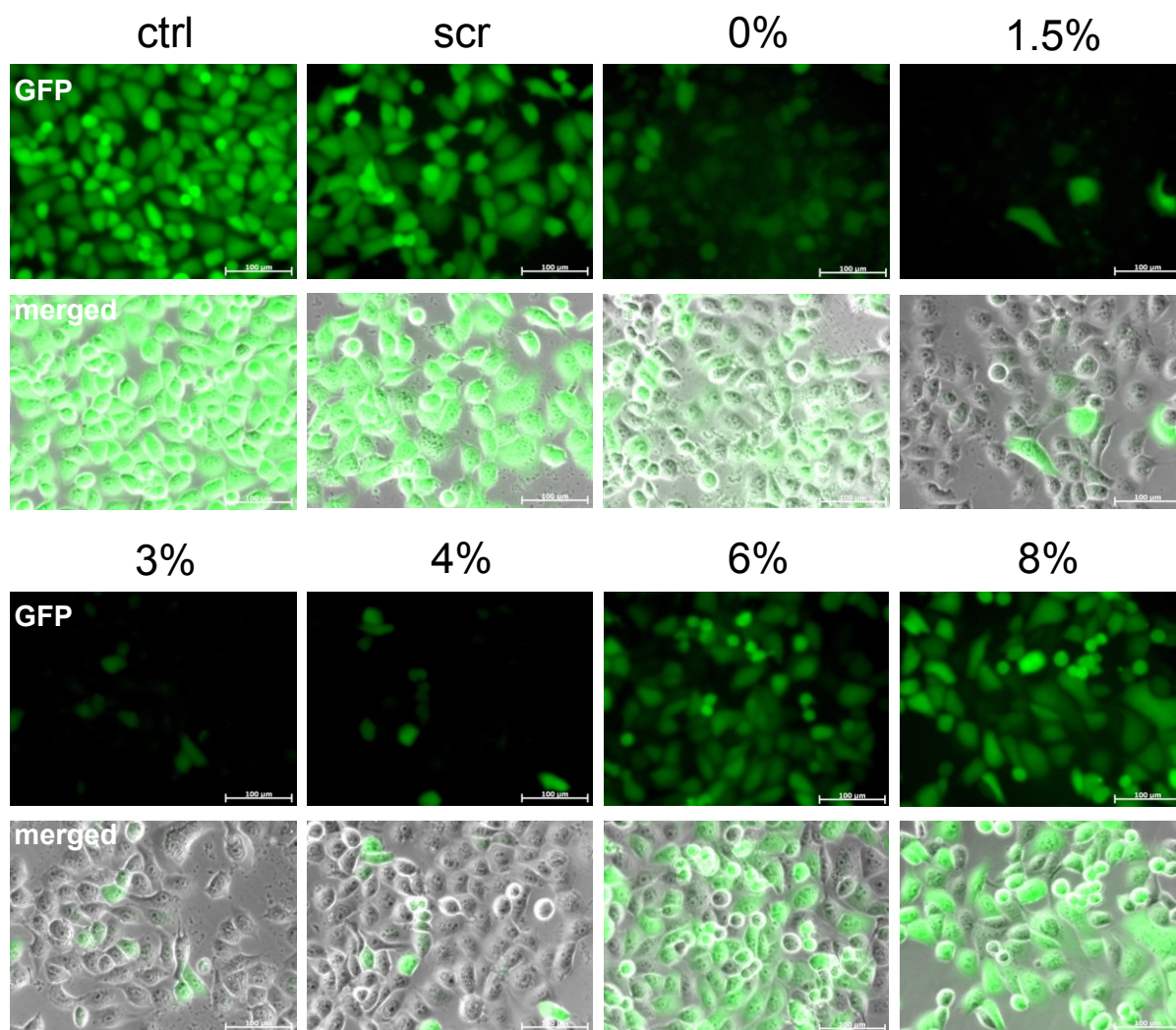


Figure 34. Knockdown efficiency of different chitosan / siRNA nanoparticle formulations in H1299-GFP cells. Transfection was carried out for 6 h with a GFP silencer and a scr siRNA (200 nM). 48 h after transfection reduction of fluorescence was analyzed by microscopy (scale bar 100 microns).

Microscopy showed for all the 6 samples a decrease in fluorescence meaning a successful knockdown of GFP mRNA in targeted cells. The knockdown was more efficient with a smaller amount of GFP expressed from the cells, so that the fluorescence decreased. Unmodified and PEGylated chitosan nanoplexes with a DS smaller than 6% showed very good knockdown results. The increasing PEG percentage seemed to considerably affect the knockdown results. Therefore, only a small amount of PEG was necessary to increase solubility and to prevent the agglomeration of the nanoplexes as seen in Figure 32. On the other hand a too high PEG substitution influenced both the knockdown and the uptake as seen in Figure 33.

As the microscopic results were more qualitative than quantitative, the cells and the remaining fluorescence after successful knockdown was investigated by flow cytometry (data provided by L. Schuster NMI, Figure 4.26, page 82) [49].

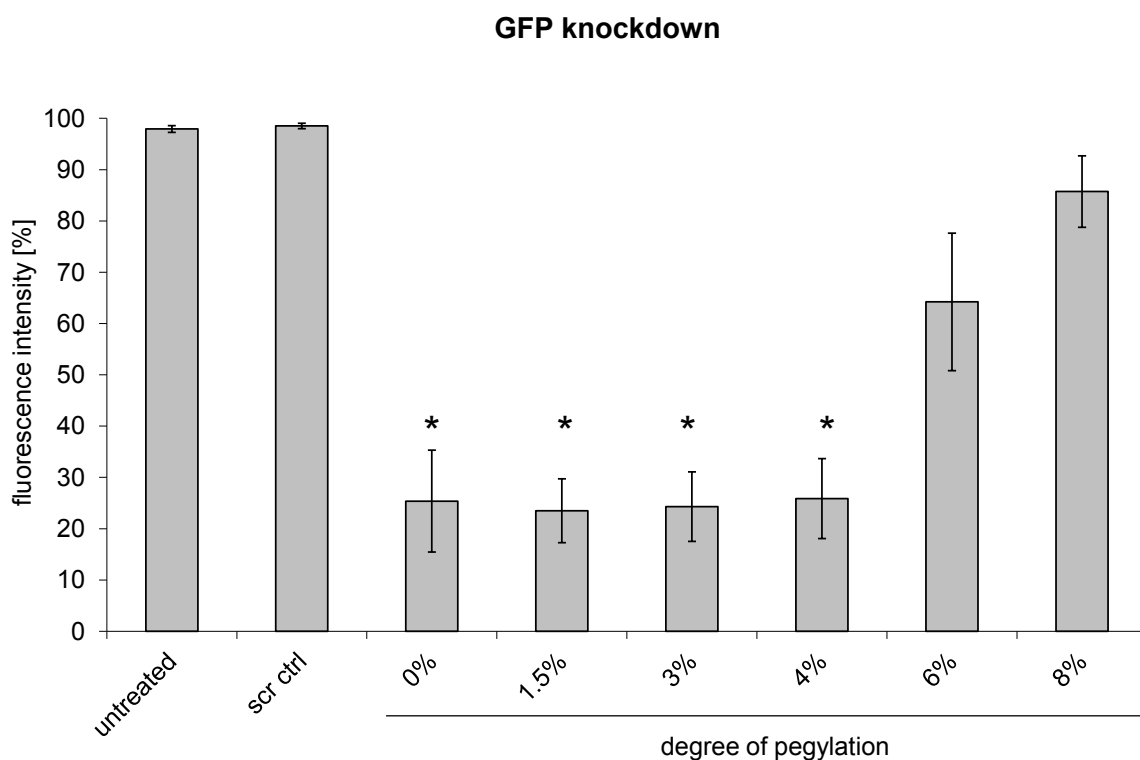


Figure 35. Analysis of the GFP signal by flow cytometry. H1299-GFP cells were transfected with various chitosans: GFP silencer or scr siRNA nanoplexes. The incubation time was 6 h and the cells were harvested after 48 h. The fluorescence of the cells directly correlated to the knockdown efficiency. Statistical analysis was calculated based on the untreated control. Three independent experiments were done in triplicates. (Statistics: Nonparametric ANOVA, Kruskal-Wallis test, $p < 0.01$).

The flow cytometry results were very similar to the microscopy results. The unmodified chitosan and chi_PEG nanoplexes with a DS smaller than 6% showed a knockdown of ~75%. The GFP knockdown of the higher PEGylated chitosans is significantly lower. Chi_PEG nanoplexes with a 6% DS showed a knockdown of ~30%, while chi_PEG nanoplexes with 8% DS showed almost no knockdown. For the last type of nanoplexes it is important to mention also the lower uptake that might have influenced such a low knockdown efficiency.

3.4. Targeted delivery of siRNA nanoplexes to specific cells

The specific delivery of the nanoplexes would not only prevent the side effects of siRNA being delivered to random cells, but will also ensure a concentrated uptake of the nanoplex in the cell of interest increasing the efficiency of the delivery system. PEG was grafted on chitosan in order to increase solubility and to shield the nanoplexes from unspecific interactions. In addition, PEG could be used as a spacer to bind the targeting molecule on the surface of the nanoplex without interfering with complex formation.

3.4.1. Electrostatic interaction of scFv'LCH3 target protein and nanoplex surface

The single chain antibody fragment of the fibroblast activation protein (scFv'LCH3) was chosen as a targeting molecule for fibroblast cells (see 1.7.2.1). The charge of the nanoplexes in 0.3 M CH₃COONa buffer pH 5.5 was previously measured (Figure 26) and yielded a positive zeta potential for all chitosan and PEGylated chitosan nanoplexes. Therefore, the scFv'LCH3 should be negatively charged in order to interact via electrostatic interactions with the nanoplex surface.

The zeta potential of the targeting molecule scFv'LCH3 was measured in the ZetaSizer at a concentration of 1mg/mL and revealed a negative charge of -9.18 mV. After mixing of scFv'LCH3 (1mg/mL) with the chi_PEG 6%:siRNA nanoplexes, the overall charge of the nanoplexes decreased from 16.8 mV to 2.7 mV which indicates the presence of electrostatic interactions between nanoplexes and scFv (Figure 36). The zeta potential decreased at lower concentrations of scFv'LCH3 reaching a reduction in charge of only 3 mV at a concentration of 0.1 mg/mL of scFv. The mixing of the targeting molecule and nanoplexes was performed in a constant 2:1 nanoplex:scFv'LCH3 volume ratio. Therefore, to prevent the electrostatic

interactions the ratio can be increased. Furthermore, in the CCM, the proteins in the medium will probably compete with the scFv'LH3 reducing even more the risk of undesired nanoplex:scFv electrostatic interactions.

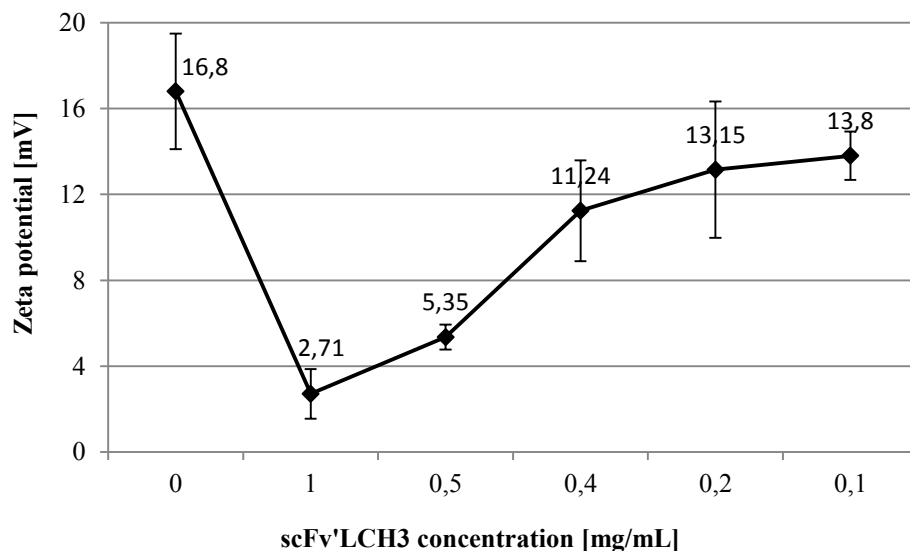


Figure 36. Zeta potential measurement of chi_PEG DS 6%:siRNA nanoplexes at N/P 50 in buffer (0.3M CH₃COONa pH 5.5) at increasing concentrations of scFv'LCH3. The nanoplex solution was mixed with scFv'LCH3 solutions of different concentrations at a constant volume ratio of 2:1. The neighboring charged protein built up a surface layer on the positively charged nanoplexes.

3.4.2. Chemistry of the linker system

The purpose was to find a linker system to conjugate a bio-macromolecular ligand as well as a small chemical inhibitor to the surface of chitosan nanoplexes for specific cell targeting. A too close binding of the ligand/inhibitor to the surface of chitosan would result in a shielding effect and therefore the risk for inactivation of the targeting moiety (Figure 37). PEG as a spacer between the targeting moiety and chitosan was chosen as linker system.

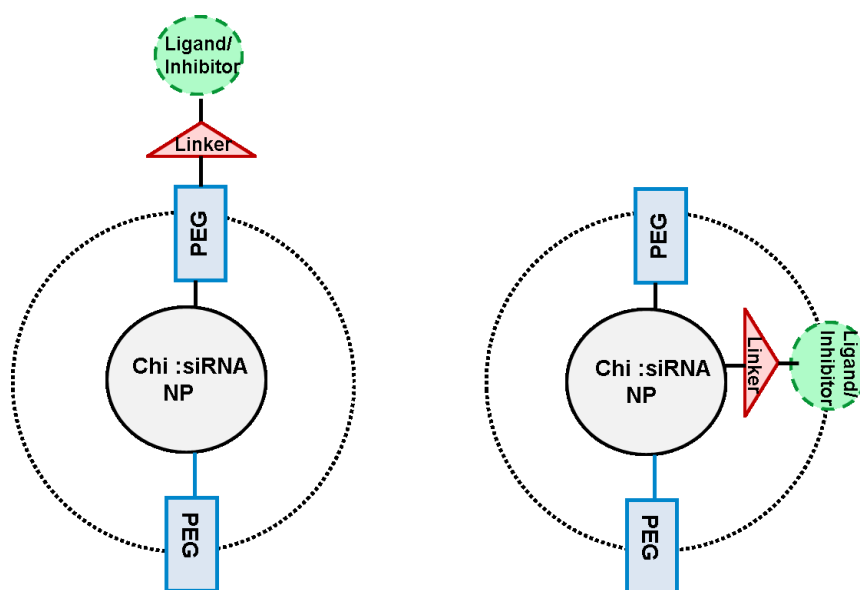


Figure 37. Principle concept of the ligand/inhibitor attachment to chitosan nanoplexes. PEG of different lengths can be used to modify siRNA chitosan nanoplexes with macromolecular ligands or small inhibitor molecules at optimal distance for nanoplex- cell interaction (left). If the linker is too short the specific ligand might be shielded by the nanoplex surface (right).

In order to bind the linker to the spacer, PEG can be modified with an azide group, offering more versatility and efficient coupling yields for the targeting system. The encapped azide functionality can react via “click-chemistry” with substituted alkynes to stable triazoles in a site specific manner as shown in Figure 38. This binding concept allows a high yielding conjugation under mild conditions resulting in a stable covalent linkage.

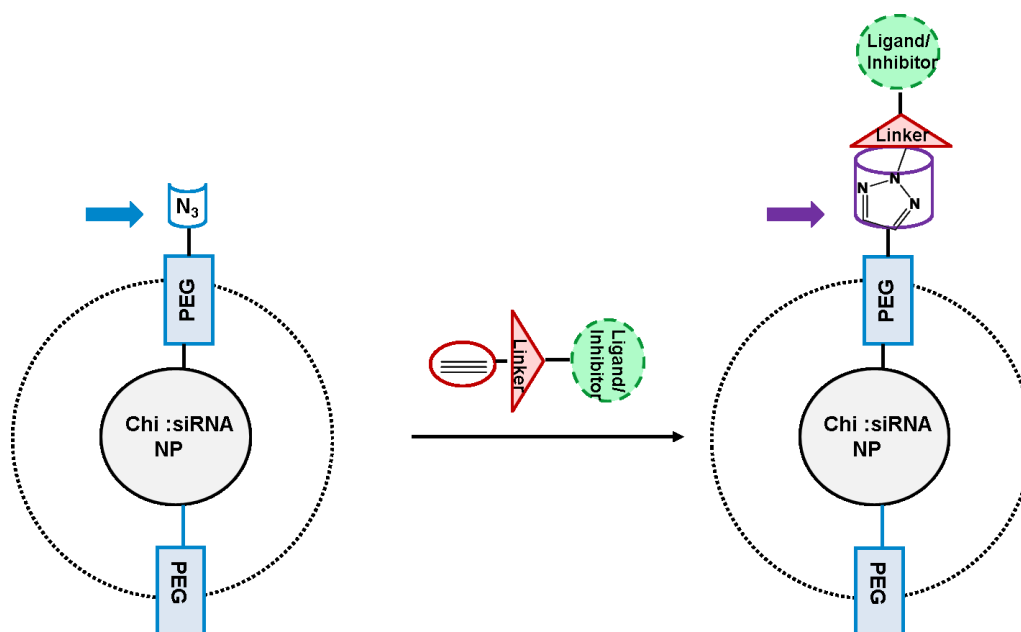


Figure 38. Conjugation concept for the linker-ligand/inhibitor system based on azide modified chitosan_PEG. Azide groups at the PEG terminal end allow specific and mild covalent coupling of alkynes to the nanoplex surface.

3.4.2.1. Synthesis of the PEG/benzoate-cyclooctyne

The first linker system chosen was based on the work of the Bertozzi [188] group with benzoate as spacer and linkage functionality (compound **8**). However, due to the low yields (<20%), not corresponding to the procedures described by Bertozzi, and also the limited expectations derived from the structural properties, such as spacer length and solubility, the focus was changed to a second linker system.

In the second approach a small PEG (n=4) spacer was coupled to the cyclooctyne moiety based on the work of Lallana E. *et al.* [226]. PEG can increase the solubility of the entire system, improve the spacer length and offers the possibility to modify the number of ethylene glycol repeating units if space length should be changed.

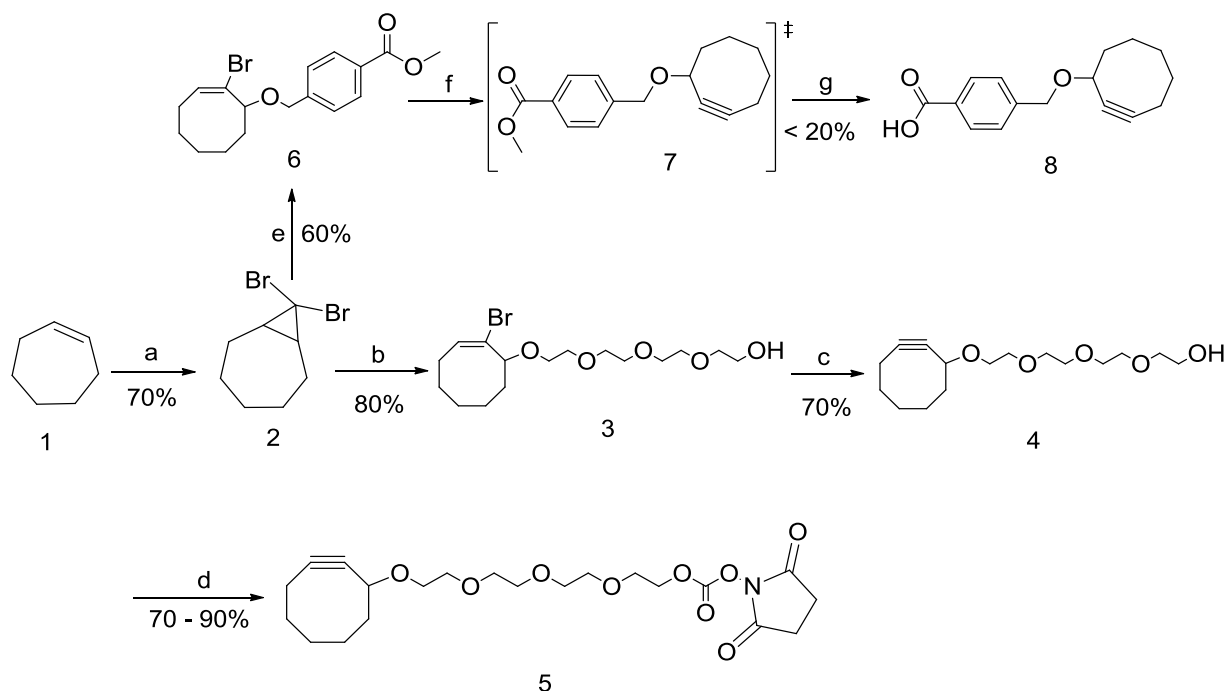


Figure 39. Synthesis of activated cyclooctyne linkers with intermediates. a) *t*-BuOH, H₂CBr₂, pentane anhydride, RT; b) AgClO₄, tetraethylene glycol, toluene/pyridine, overnight, reflux; c) *t*-BuOH, *i*-PrOH/pyridine, RT; d) *N,N'*-Disuccinimidyl carbonate, Et₃N, MeCN, RT; e) AgClO₄, methyl 4-hydroxymethylbenzoate, toluene, no light, RT; f) NaOMe, anhydrous DMSO, RT; g) HCl (1M), 20% H₂O/dioxane, LiOH, RT;

The dibromocyclopropanation of cycloheptene **1** to intermediate **2** was performed via a classical cheletropic reaction, a subclass of pericyclic reactions. Bromoform serves as

carbene precursor, which is released under basic conditions. The *in situ* formed carbene, reacts with the cycloheptene in a concerted [2+1] cycloaddition, yielding compound **2** in a good yield (70%)

Silver perchlorate was then used to carry out the electrocyclic ring-opening of **2** to the allylic cation, which was captured with tetraethylen glycol, affording bromo-cyclooctene **3** as shown in Figure 40 in an 80% yield

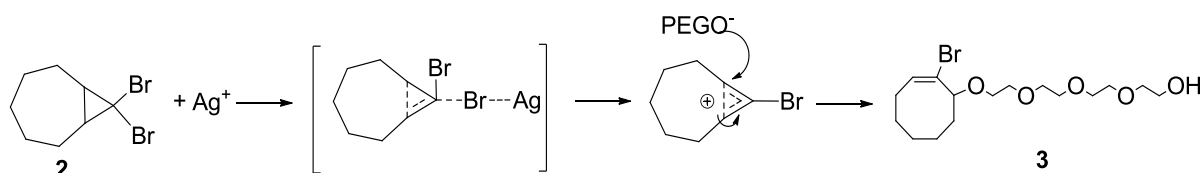


Figure 40. Synthesis of 1-Bromo-8-tetraethylenglycol-cyclooctene. Ag^{2+} catalyzed electrocyclic rearrangement of **2** leads to compound **3** in a good yield (80%)

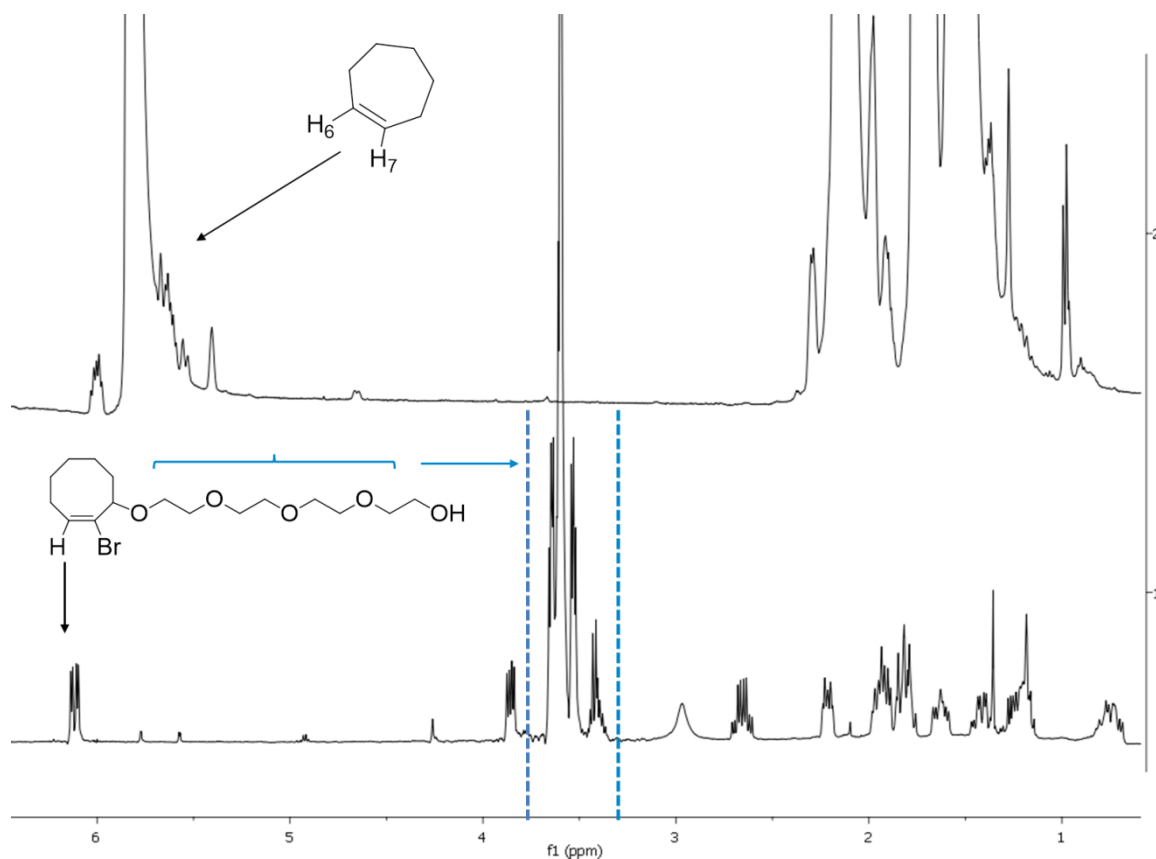


Figure 41. ^1H NMR spectrum of compound **3** (400MHz, CDCl_3). It showed the characteristic vinyl signals at 6.1 ppm and the PEG protons in the range of 3 -3.6 ppm .

^1H NMR spectra of compound **3** showed the characteristic vinyl signal with its anisotropic downfield shift at 6.1 ppm and the following alkyne formation yielding cyclooctyne **4** was performed by dehydrohalogenation via E_2 elimination using $\text{KO}t\text{Bu}$ as base in an isopropanol/pyridine mixture at room temperature. Monitoring of the reaction was difficult via TLC as no clear differences in R_f -values were achieved. HPLC analysis suffered from the low active chromophore and the very similar retention times of educt and product. Therefore, the reaction progress was monitored via in-process ^1H NMR analysis. Characteristic signals were found at 6.1 ppm where the vinyl signal is disappearing and a new signal was seen at 4.21 ppm ($\text{C}\equiv\text{C}-\text{CH}-\text{PEG}$), indicating the alkyne formation Figure 42.

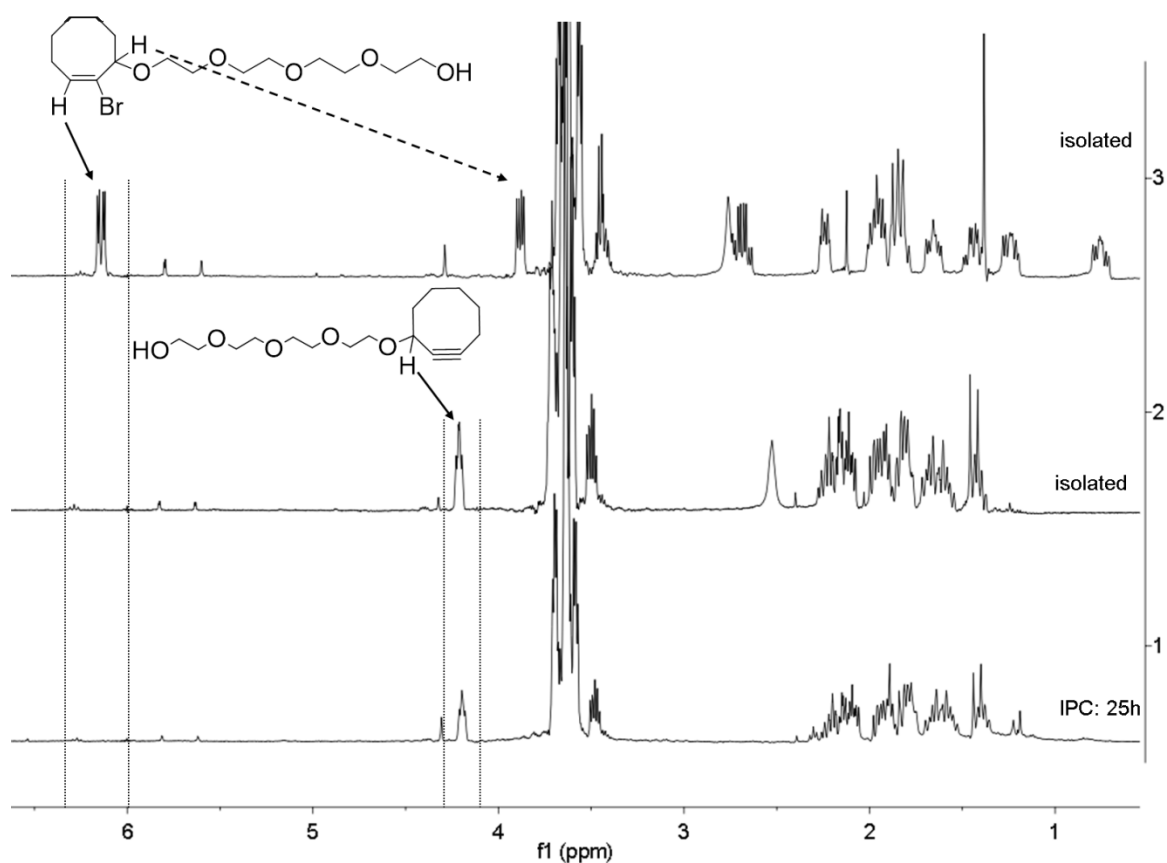


Figure 42. In situ ^1H NMR (400 MHz, CDCl_3) monitoring of cyclooctyne formation after 25 h reaction time (IPC= in process control), pure isolated cyclooctyne (middle) and pure isolated octene (top). The vinyl signal ($\text{CH}=\text{CHBr}$) at 6.1 ppm disappeared within 25h of reaction time whereas the proton of the PEG substituted tertiary carbon atom showed a characteristic new signal at 4.21 ppm ($\text{C}\equiv\text{C}-\text{CH}-\text{PEG}$) which was used to follow the alkyne formation. Sample preparation of the IPC was done by evaporating a small portion of the reaction mixture and subsequent ^1H NMR measuring in CDCl_3 .

According to literature, reaction times of ~60 h were needed [226]. However, it was proven via ^1H NMR that reaction times of 25 hours were by far sufficient and could be further reduced. The yield of the reaction performed for 60 h was actually ~10% less (54% yield) as one of the 25 hours experiment (66% yield) probably due to side reactions. Nevertheless, side products were not quantified or identified in this study.

In the final step, the PEG side chain was transformed to the corresponding activated succinimidyl carbonate ester **5** with N,N'-Disuccinimidyl carbonate (DSC). The carbonate ester **5** served as broad and robust linker platform for further modifications with an acceptable stability profile for storage.

3.4.2.2. Synthesis of the PEG-cyclooctyne-maleimide

As maleimide allows the specific and covalent binding to thiols under physiological conditions, it was decided to use the specific Michael system as a protein capturing moiety on the linker system. Therefore, the succinimidyl carbonate ester **5** was reacted with aminoethane maleimide (TFA salt) in dichloromethane and triethylamine at room temperature to yield the target compound **9**.

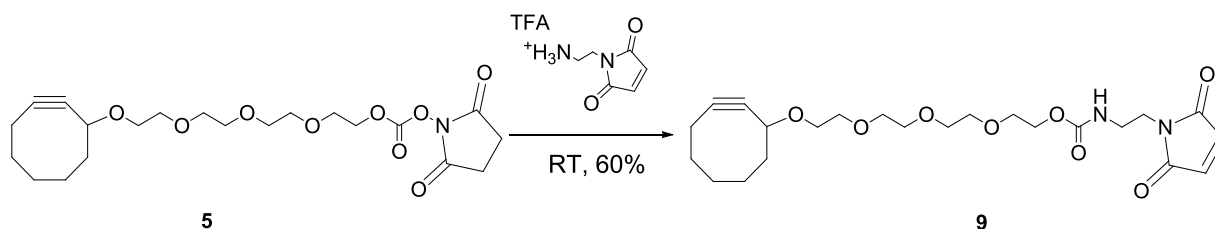


Figure 43. Synthesis of cyclooctyne_PEG-maleimide, compound **9** in DCM, RT (~60% yield)

The maleimide compound **9** was purified via column chromatography and yielded a yellow oil (Figure 44a). The linker was stored at -20°C under argon atmosphere and under light exclusion. Despite these special precautions in storage, a polymerization was observed within ~1-2 days. At room temperature polymerization took place within hours (Figure 44b).

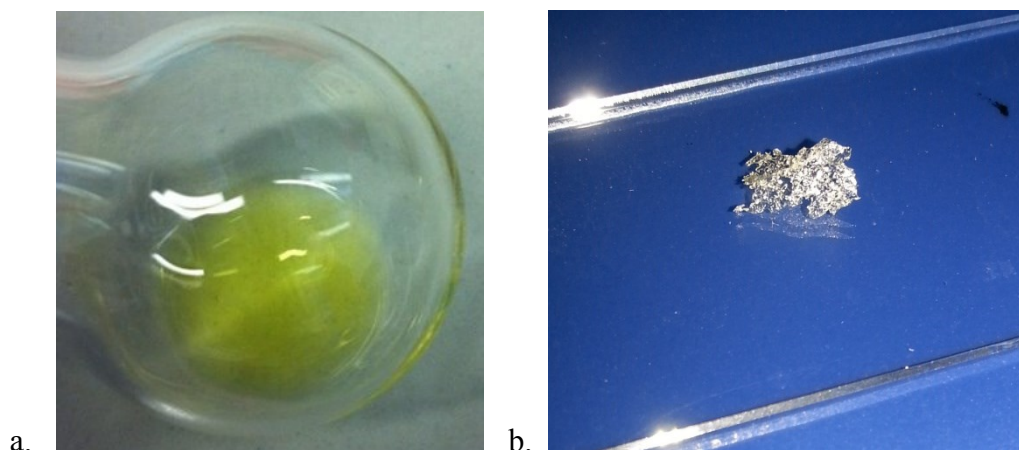


Figure 44. a) Freshly prepared maleimide_linker b) Polymerized maleimide_linker after storage at -20°C under light and oxygen exclusion.

The polymerization of maleimide is known in literature [227] for alkenes, via photocyclization, which can be excluded in our case as storage was done under light protection. Furthermore, systems like furane react under thermal conditions with maleimide as dienophile in Diels Alder reactions even at room temperature at significant reaction rates [228].

For our observations, a thermal [2+2] cycloaddition reaction mechanism like shown in Figure 45 is the most feasible explanation leading to the observed polymer **10** with the structure shown below.

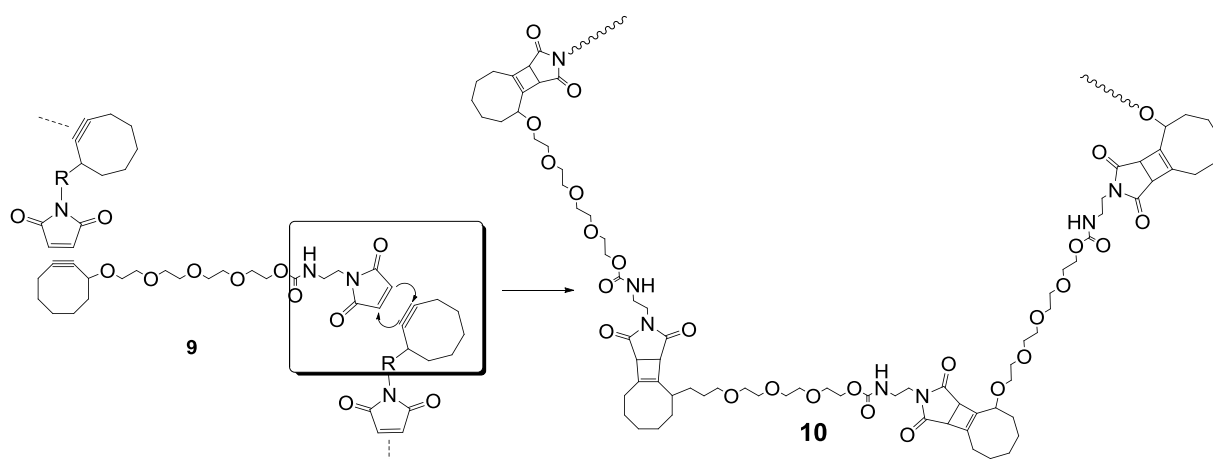


Figure 45. Probable polymerization of compound **9** via [2+2] cycloaddition between the octyne and the maleimide group could lead to the polymer type **10**.

Usually the [2+2] cycloaddition between alkynes and alkenes needs catalysts [229] or UV irradiation [230]. The en (alkyne) and enophil (maleimide) in the present system are differing to usual systems as both have to be seen as highly activated. The HOMO of the cyclooctyne is increased (due to the ring strain activation), whereas the LUMO of maleimide is significantly lowered (due to the high electron deficiency), which is resulting in a lowered HOMO-LUMO energy gap and therefore lowered activation energy barrier, which might enable the [2+2] cycloaddition reaction without any catalysts, heat or photoactivation.

Nevertheless the cyclooctyne_PEG_maleimide compound **9** can be used as a linker to attach the specific cell targeting moiety to the nanoplex. Unfortunately it has to be just freshly prepared. In order to further improve the linker moiety and its stability, the octyne was kept as linkage functionality for the azide substituted chitosan. Only the functional moiety, linking the target to the nanoplex was changed. Therefore, a functional group specific towards thiols and inert to the ring strained activated alkyne was needed.

Iodoacetamide was chosen as an alternative functional group for bioconjugation because of its high reactivity towards thiols and low hydrolysis profile in aqueous systems.

The thiol specific iodoacetamide coupling mechanism is based on the nucleophilic attack of the thiol to the electrophilic iodinated carbon of the iodoacetamide. Interactions, as observed with the Michael acceptor – (maleimide) could be excluded due to the changed mechanism from Michael addition to nucleophilic substitution.

The synthetic strategy was starting with tetraethylenglycole oct-2-yne **4** which was already synthesized before. However, in this case a second linker was introduced to connect the iodoacetamide to the octyne derivative **4**. As coupling strategy for the endcapped hydroxy functionality, we decided for a Steglich esterification with EDC as carbodiimid and DMPA as organocatalyst. The linkage of the acetamide was planned to be introduced as already linked intermediate **12** with an endcapped carboxyl group. The synthesis of intermediate **12** was performed via chlor-iodoacetic acid and 6-aminohexanoic acid (Figure 46).

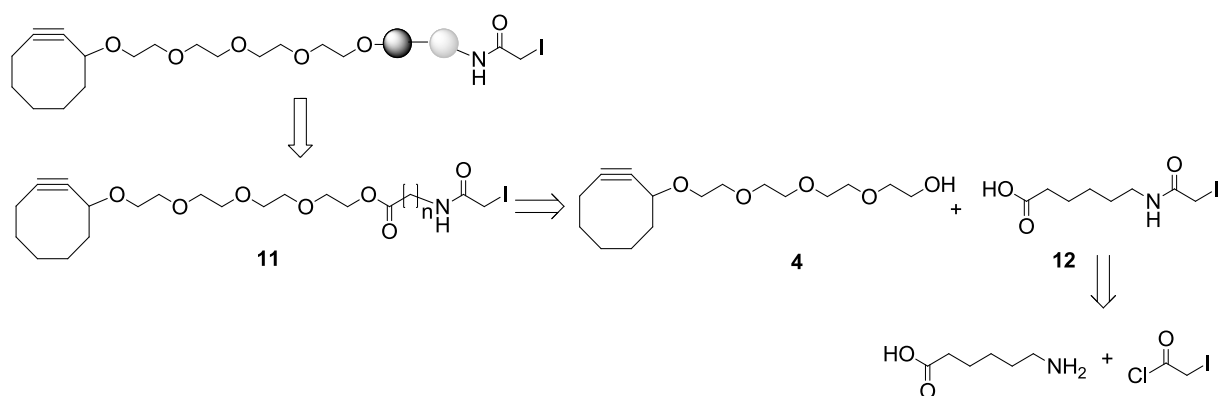


Figure 46. Retrosynthetic analysis of the octyne-iodoacetamide linker system. The synthesis route was developed based on the tetraethylene oct-2-yne **4** which was synthesized earlier. Esterification with 6-[(iodoacetyl)amino]hexanoic acid yielded the desired product **11** (52 %)

The synthesis of compound **11** was performed according to the retrosynthetic concept in a yield of 52% (Figure 47).

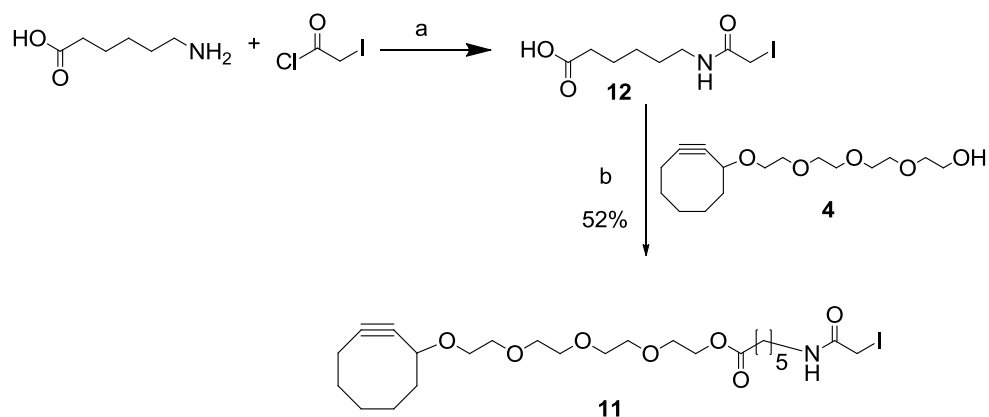


Figure 47. Synthesis of the octyne-PEG-iodoacetamide ester linker (compound **11**). a) THF, 0°C – RT; b) EDC, DMAP, THF, RT.

As an alternative to the iodoacetamide **11**, the corresponding iodoacetic acid ester **13** was also prepared via direct Steglich esterification of iodoacetic acid and tetraethyleneglycole oct-2-yne **4** as shown in Figure 48.

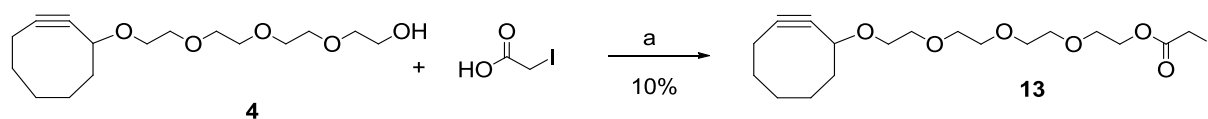


Figure 48. Synthesis of the octyne-PEG-iodoacetic acid ester linker. Reaction conditions: a. **DMAP, EDC, THF, RT**. Direct esterification of the tetraethylenglycol oct-2-yne **4** with iodoacetic acid yielded the compound **13** (10 % yield).

3.4.3. Bioconjugation of biological targets via a free thiol group to the maleimide linker system

The maleimide linker system **9** can be added directly to the chitosan_PEG copolymers. Then the target molecule can be attached to the bound linker via the thiol group (Figure 49a). The alternative synthesis, the system that was chosen, was based on the reaction of the maleimide linker group **9** with the targeted molecule prior to the chitosan_PEG binding via 1,3-dipolar cycloaddition to the azide groups on PEGylated chitosan (Figure 49b).

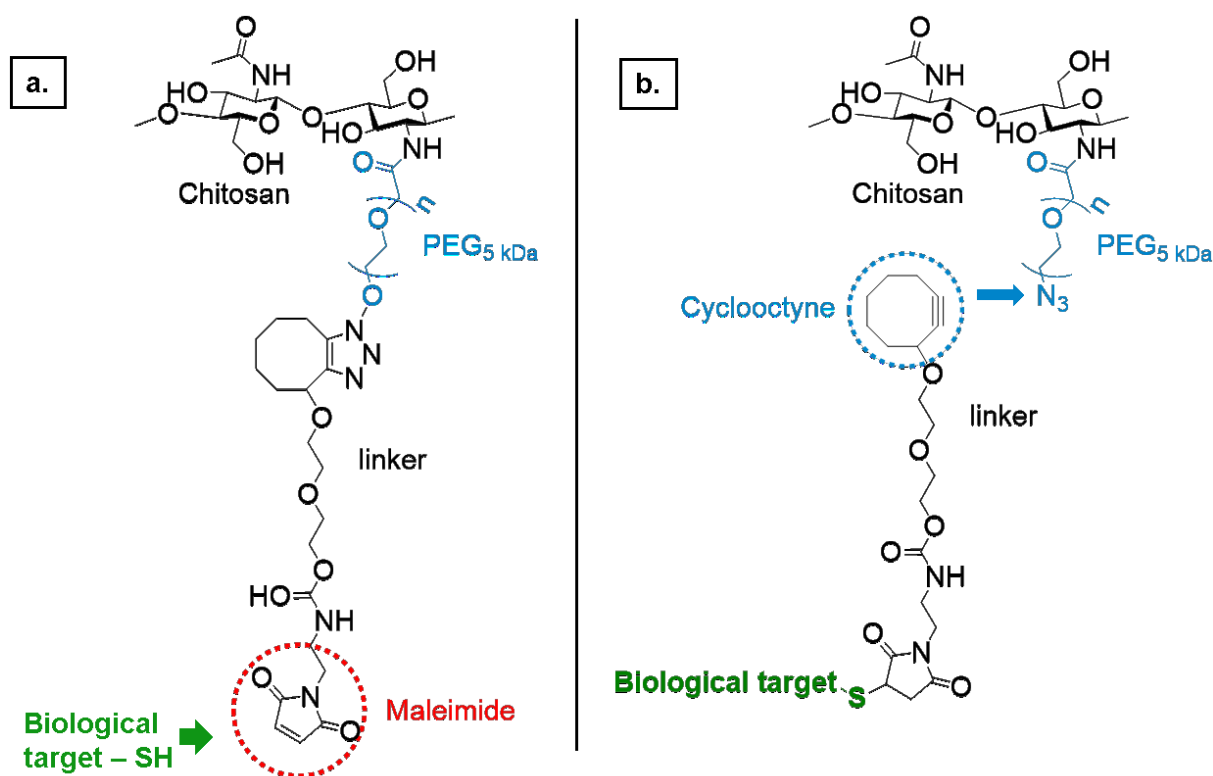


Figure 49. Bioconjugation concepts of biological targets via their free thiol group to the maleimide linker system of compound **9**. a) bind first the linker to the PEGylated chitosan by 1,3 – dipolar cycloaddition of the octyne to the azide groups. Then the thiol group of the biological target can be couples to the maleimido groups on the polymer. b) The coupling of the biological target to the maleimido groups of the linker can be done first followed by the coupling of the whole construct to the azide groups of the PEGylated chitosan. The second approach was chosen for development.

The concern with the first approach (Figure 49 a) was that due to reduced accessibility of the thiol to the linker system with the maleimide moiety at the distal end of the chitosan_PEG_linker the reaction could show low yields. In addition it was much easier to identify and quantify the covalently bound target molecules on the small and well define linker systems compared to the polymeric systems with a broad M_w distribution.

3.4.3.1. Bioconjugation of H-CDoaDoaEQKLISEEDL-OH to the cyclooctyne_maleimide linker system

The first step was to prove the bioconjugation of a small peptide to the linker system via thiol linkage to the maleimide. The chosen peptide was H-CDoaDoaEQKLISEEDL-OH also named Cys-DoaDoa-Myc epitope with a free cysteine at the N-terminus and a molecular weight of 1596.77 g/mol.

As previously mentioned, the double bond of maleimides undergoes a Michael reaction with sulfhydryl groups to form stable thioether bonds. The maleimide on the cyclooctyne linker was reacted with the free thiol group of the H-CDoaDoaEQKLISEEDL-OH peptide at a pH of 6.5 (Figure 50). Another very important aspect was the immediate use of the cyclooctyne_maleimide linker and short reaction times in order to avoid its polymerization (see Figure 45). The reaction was stopped after 2h by adding L-cysteine which could bind to the remaining unreacted maleimide or the free thiol groups on the peptide via disulfide bond formation.

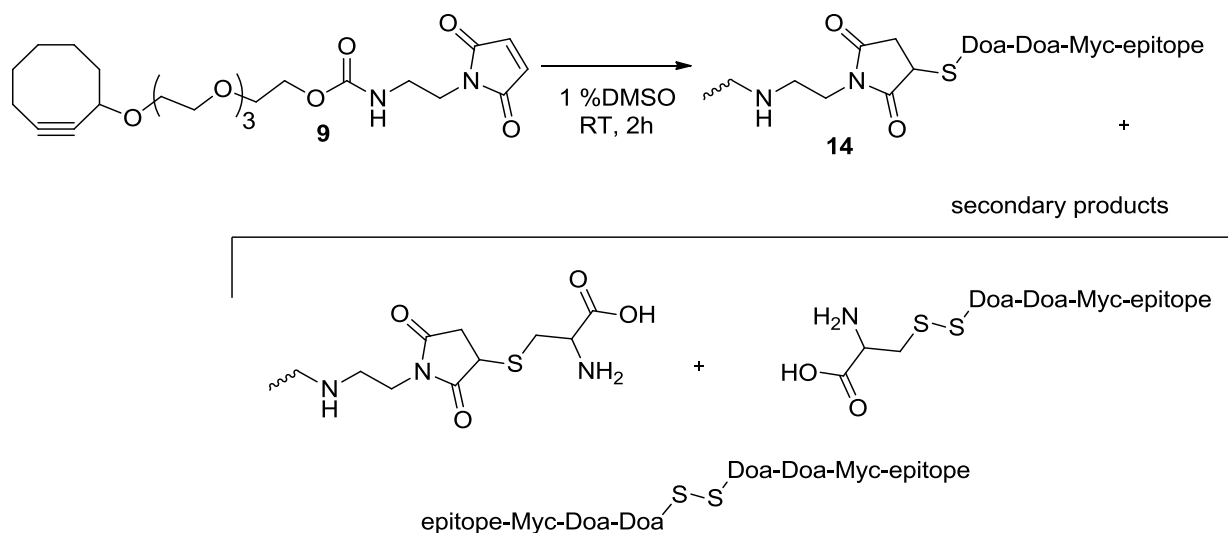


Figure 50. Synthesis of the cyclooctyne-PEG-succ-DoaDoaMyc epitope. Compound 9 was mixed in PBS buffer with 1% DMSO and the H-CDoaDoaEQKLISEEDL-peptide for 2 h at room temperature. The thiol of the N-terminal cysteine was added to the maleimide double bond in a Michael addition reaction. The resulting 3-thio succinimidyl moiety forms a stable linkage of the peptide to the cyclooctyne group. After 2h, cysteine was added which reacted with the remaining maleimido groups or free thiols of the unreacted peptide yielding the secondary products shown.

The crude product was purified via preparative HPLC with a GromSil 120 ODS-4 HE, 7 μ m 125x30mm column. The purified product was compared via analytical HPLC with the raw materials: peptide and cyclooctyne linker system, compound 9 (Figure 51). In the HPLC analysis of the purified compound 14 (pink chromatogram), H-CDoaDoaEQKLISEEDL-OH peptide peak cannot be observed and only a small amount for the dimer peptide can be identified. Furthermore, compound 9 (Peak 5) was not seen and a new compound peak could be observed at a retention time of 3.88 minutes. The binding of the peptide increased the polarity of the bioconjugate. Therefore, from the overlay it was concluded that the new peak represented compound 14 in a 32% yield.

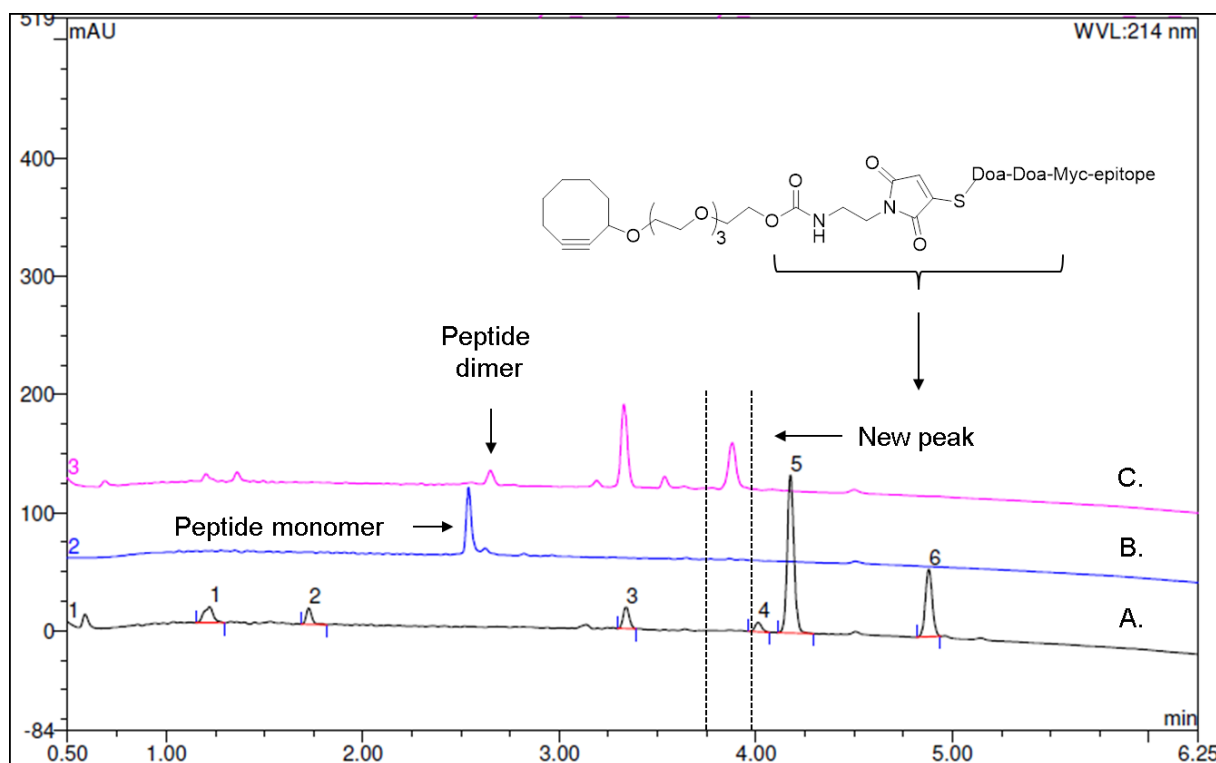


Figure 51. Analytical HPLC comparison of cyclooctyne_maleimide linker (A), H-CDoaDoaEQKLISEEDL-OH peptide (B) and cyclooctyne_succ_CD0aDoaEQKLISEEDL-OH, compound **14** (C). The PEG maleimide showed two prominent peaks (5, 6) in the HPLC separation which shifted to shorter retention times after reaction with the thiopeptide. The later eluting peak was isolated and further characterized by MALDI ToF MS (Figure 52) (column: Chromolith Performance RP-18e 100x3 mm; solvents: 0.1% TFA in water (solvent A), 0.08% TFA, 100% acetonitrile (solvent B); gradient: 5-65% solvent B in 5.8 min, wavelength: 214 nm).

The purified compound **14** was further analysed via the standard ‘dried droplet’ MALDI-ToF MS. The fraction was co-crystallized with α -Cyano-4-hydroxy-cinnamic acid (HCCA) matrix which is used in the majority of proteomics applications for the analysis of peptides[231]. Figure 52 shows the mass spectra of compound **14** yielding the characteristic $[M+H]^+$ signal at m/z 2062.602, the $[M+Na]^+$ signal at m/z 2084.609 and an $[M+K]^+$ signal at m/z 2100.588 which are consistent with the expected monoisotopic mass $[M]$ of 2061 g/mol.

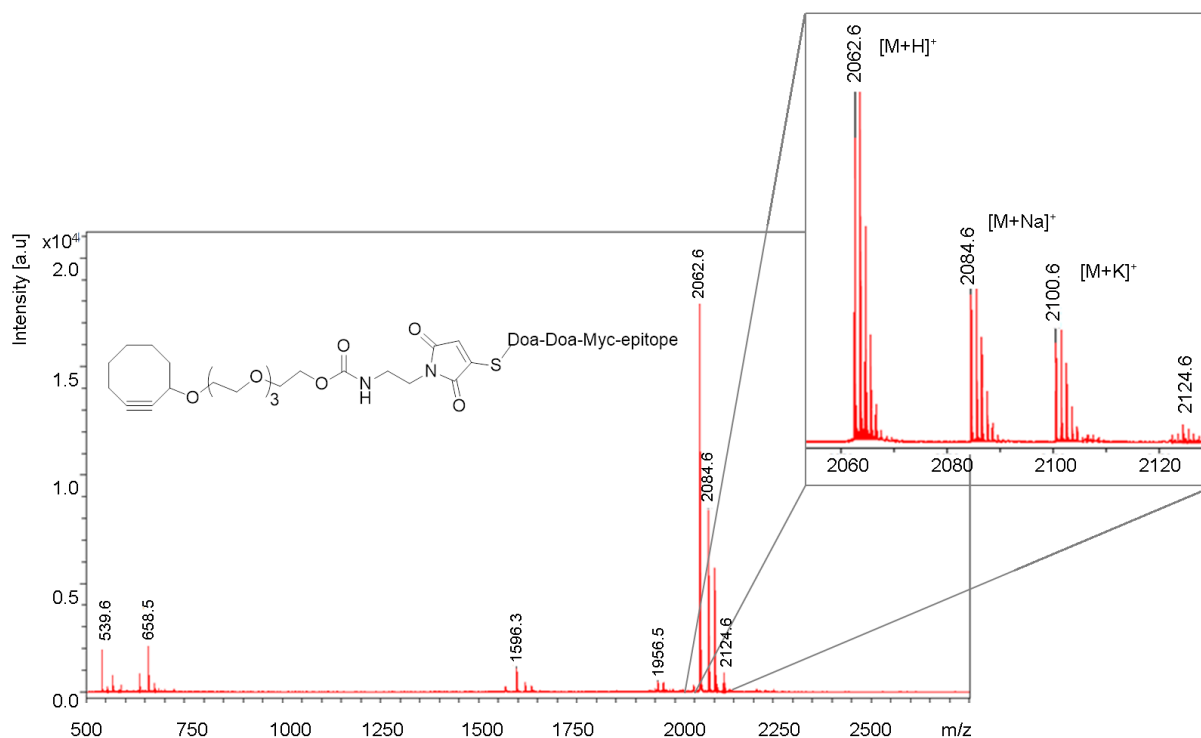


Figure 52. Maldi ToF MS of compound **14** (cyclooctyne_succ_CD₂DoaDoaEQKLISEEDL-OH). The found mass of 2062.62 $[M+H]^+$ and the masses of $[M+Na]^+$ and $[M+K]^+$ fitted well to the calculated monoisotopic mass of 2061 Da (Ultraflex III, Bruker Daltonics, dried droplet preparation with HCCA in ACN + 0.1% TFA:H₂O 2:1).

3.4.3.2. Conjugation of scFv'LCH3 to the cyclooctyne_maleimide linker (**9**)

Given the successful bioconjugation to the small peptide, the next step was to add a larger biological target to the cyclooctyne_maleimide linker (**9**). Therefore, the single chain fragment antibody (scFv'LCH3) directed against of the fibroblast activation protein (FAP) was chosen to target fibroblast cells in a highly specific manner [49, 177]. ScFv'LCH3 expressed and purified from *E.coli* lysates revealed both a monomeric form with a free thiol from the cysteine residue and a dimeric form with disulfide bonds between the free thiols of two monomeric forms (see 1.7.2.1). Therefore, prior to bioconjugation, the disulfide bonds were reduced with an excess of *tris*(2-carboxyethyl)phosphine (TCEP). Unlike commonly used dithiothreitol (DTT), TCEP is more stable and does not have to be removed before the following step. The bioconjugation of the scFv'LCH3 to the maleimide linker was performed in 1% DMSO PBS at a pH of 7.2 over 2 h under argon (Figure 53). As in the case of the small peptide, the reaction was stopped after 2 h by adding L-cysteine which could bind to the remaining unreacted maleimide linker, compound **14** or the free thiol groups on the scFv'LCH3 monomer.

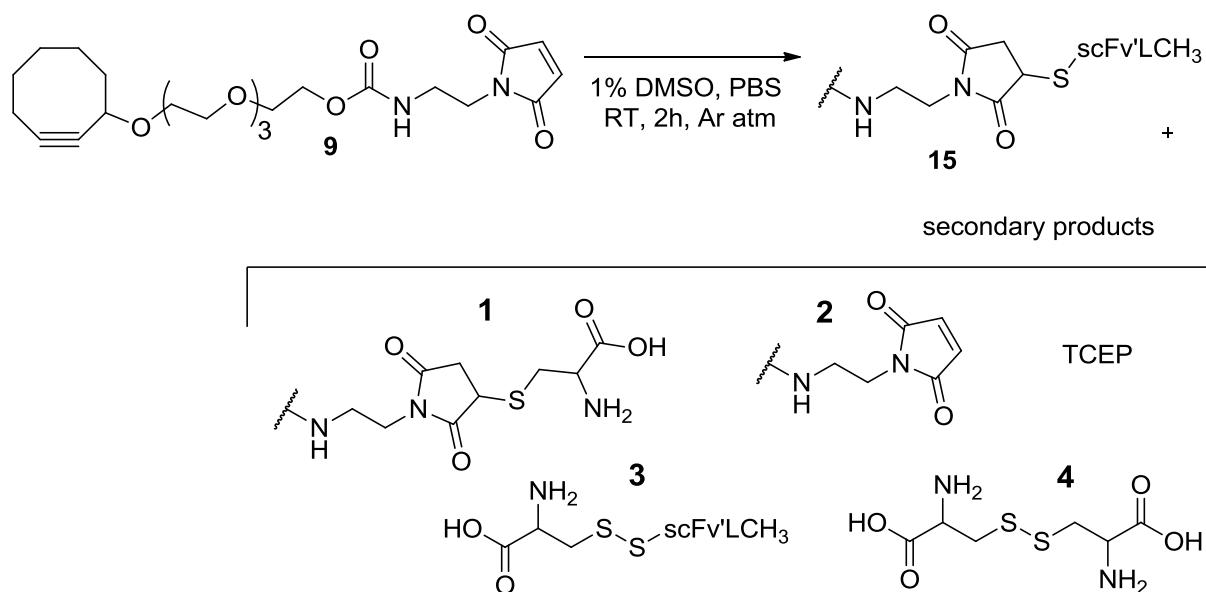


Figure 53. Synthesis of cyclooctyne-PEG-succ-scFv'LCH3 in PBS with 1% DMSO for 2 h at room temperature. Side products of the reaction due to the final quenching step with cysteine are shown. Secondary product 1 and 2 could couple to azide groups in the following 1,3 dipolar cycloaddition and should therefore be removed. Due to the large difference in size this could be easily done by centrifugal ultrafiltration.

The excess of unreacted maleimide_linker, TCEP, L-cysteine and bioconjugated L-cysteine_maleimide linker were removed by centrifugal ultrafiltration with a 10 kDa cutoff membrane. It was noticed that the scFv'LCH3 precipitated in the retentate solution. To prevent scFv'LCH3 precipitation, 0.005% Tween20 was added to the reaction mixture. This kept the final bioconjugated product in solution and increased the overall yield. SDS-PAGE analysis showed an increased amount of scFv'LCH3 in the retentate collected from the ultracentrifugal filters (Figure 54).

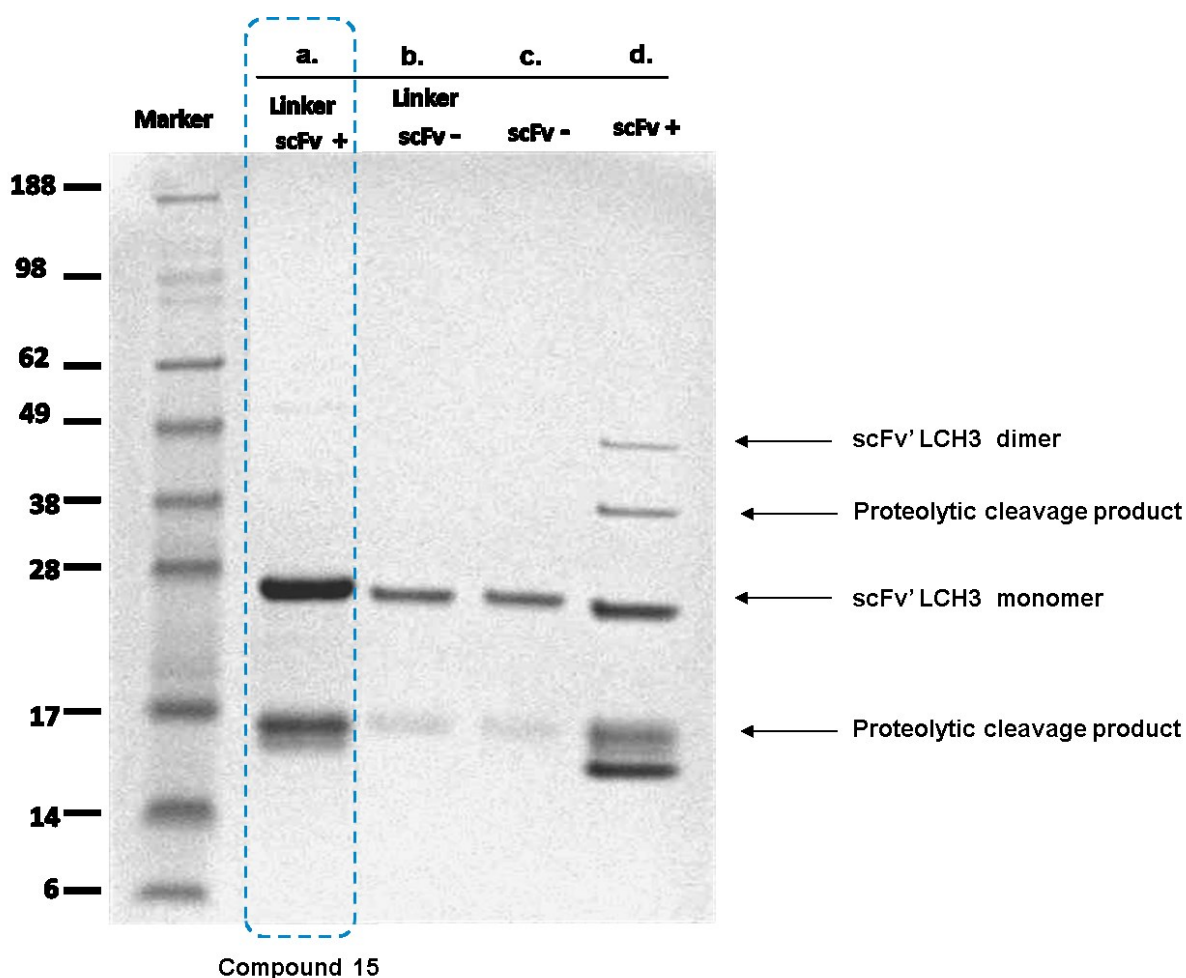


Figure 54. Non-reducing SDS-PAGE analysis of scFv'LCH3 conjugates and unconjugated scFv'LCH3 after ultrafiltration. **a)** Cyclooctyne_succ_scFv'LCH3 (compound 15) with 0.005% Tween20 (**Linker scFv +**), **b)** cyclooctyne_maleimide_scFv'LCH3 (compound 15) without 0.005% Tween20 (**Linker scFv -**), **c)** scFv'LCH3 without 0.005% Tween20 (blank reaction: same conditions but no maleimide_linker (compound 9) was added (**scFv'LCH3 -**), **d)** scFv'LCH3 with 0.005% Tween20 (blank reaction: same conditions but no maleimide_linker (compound 9) was added (**scFv'LCH3 +**). Addition of low amounts of mild detergent improved the protein recovery from the ultrafiltration retentate significantly. The analysis showed smaller potentially fragmented protein at about 16 – 17 kDa and some additional protein bands at higher Mw in the unmodified scFv'LCH3 when Tween20 was added (**d**).

After optimization of the bioconjugation reaction with 0.005% Tween20, compound 15 was produced in higher amounts. The identification of the next batch of compound 15 was done again via SDS-PAGE analysis. Increasing concentrations of BSA were applied to the same gel in order to have an estimate for the concentration of compound 15 obtained in the ultrafiltration retentate (Figure 55).

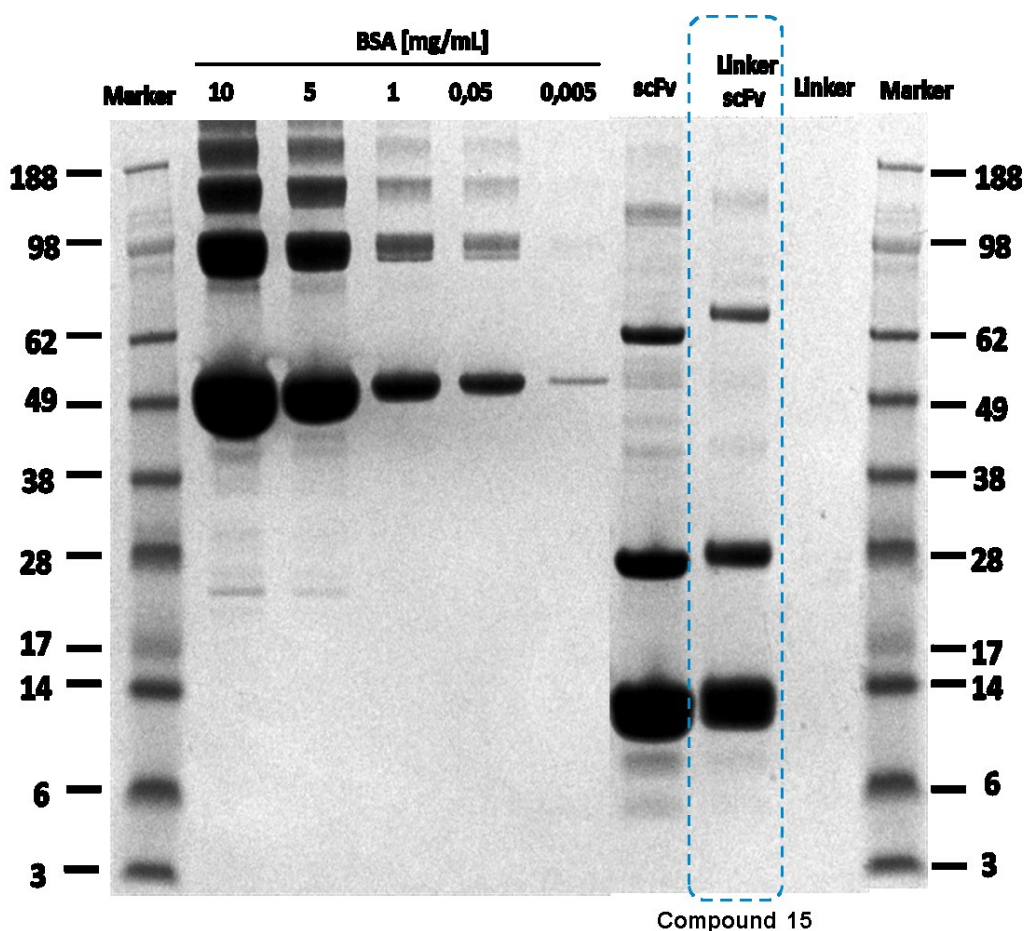


Figure 55. Non-reducing SDS-PAGE analysis of scFv'LCH3 with and without cyclooctyne linker and BSA for determination of total protein yield. BSA was added with increasing concentrations: 0.05 mg/ml to 10 mg/ml, scFv'LCH3, cyclooctyne_succ_scFv'LCH3 (compound 15) and cyclooctyne_maleimide (compound 9) were analyzed. The linker with a M_W of 466,59 g/mol showed no band. scFv'LCH3 showed a slightly lower M_W than the modified cyclooctyne_succ_scFv'LCH3 at about 28 kDa. Stray bands were detected for modified and unmodified scFv'LCH3 at about 64 kDa and very strong bands at about 14 kDa.

Together with the scFv'LCH3 at 28 kDa some potential proteolytic cleavage products of scFv'LCH3 were also detected at 14 kDa. Depending on the scFv'LCH3 fraction collected from the purification column the concentration of these low M_W products was sometimes lower or higher. In the batch shown in Figure 55 it seemed that their concentration was in the range of 5 mg/ml, about 5 times higher than the scFv'LCH3 itself. As SDS-PAGE analysis was performed under non-reducing conditions, the presence of scFv'LCH3 dimers was also seen at ~56kDa in the scFv lanes. However, the successful bioconjugation of the scFv'LCH3 to the maleimide linker seemed to generate a peak shift at the 27 kDa band. Additionally, the mass shift at about 14 kDa on the linker_scFv band, might be from the reaction of a potential proteolytic cleavage product with compound 9. As the scFv'LCH3 is purified via the His-Tag

situated next to the free cysteine it is quite likely that proteolytic cleavage products kept the His-Tag sequence with the cysteine (see 1.7.2.1), which can be modified by the maleimide of compound **9**. The mass shift in the non-reducing SDS-PAGE analysis is much larger than expected for a 476 Da modification. The effect might be due to differences in the 3D structure of the modified and unmodified scFv'LCH3.

Compound **15** was further analyzed via HPLC-ESI-MS with a Poroshell 300SB-5 μ m-C18-1.0x74mm column at 75°C. As the concentration of the proteolytic cleavage products was 5 times higher than the scFv'LCH3, they were detected with a high response. Indeed only the proteolytic cleavage products with and without maleimide linker were identified, but not the full length scFv'LCH3 with an average mass of 26794 Da and a monoisotopic mass of 26778 Da (calculated with the Sequence Editor Software from Bruker). It was not possible to determine whether the full length protein was not transferred through the C18 column or whether it was further fragmented in the highly acidic buffer. The different fractions eluting from the column could be clearly identified as scFv'LCH3 fragments. Fragmentation took place in the His₆ tag linking the two domains V_H and V_L of the original scFv-fragment. Fraction 1 contained the cysteine residue inserted next to the His₆ linker in the protein. The monoisotopic mass of the fragment was calculated without the periplasmic localization sequence of 13775 Da (C₆₀₇H₉₃₁N₁₇₃O₁₈₇S₅). Fraction 2 contained part of the His-Tag and the second part of the peptide linker sequence with the deconvoluted mass of 13019 Da (C₅₇₄H₈₈₄N₁₆₂O₁₇₈S₄). In Figure 56b fraction 1 was increased to the deconvoluted mass of 14241 Da and fraction 2 was increased to the deconvoluted mass of 13485 Da (also masses were calculated with the Sequence Editor software from Bruker).

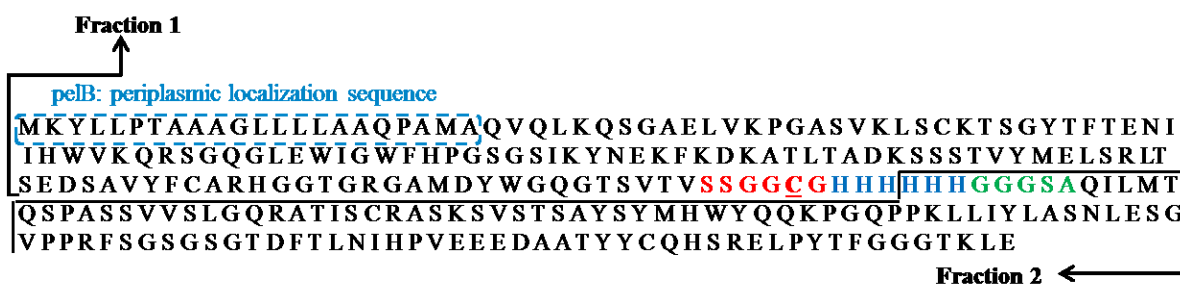
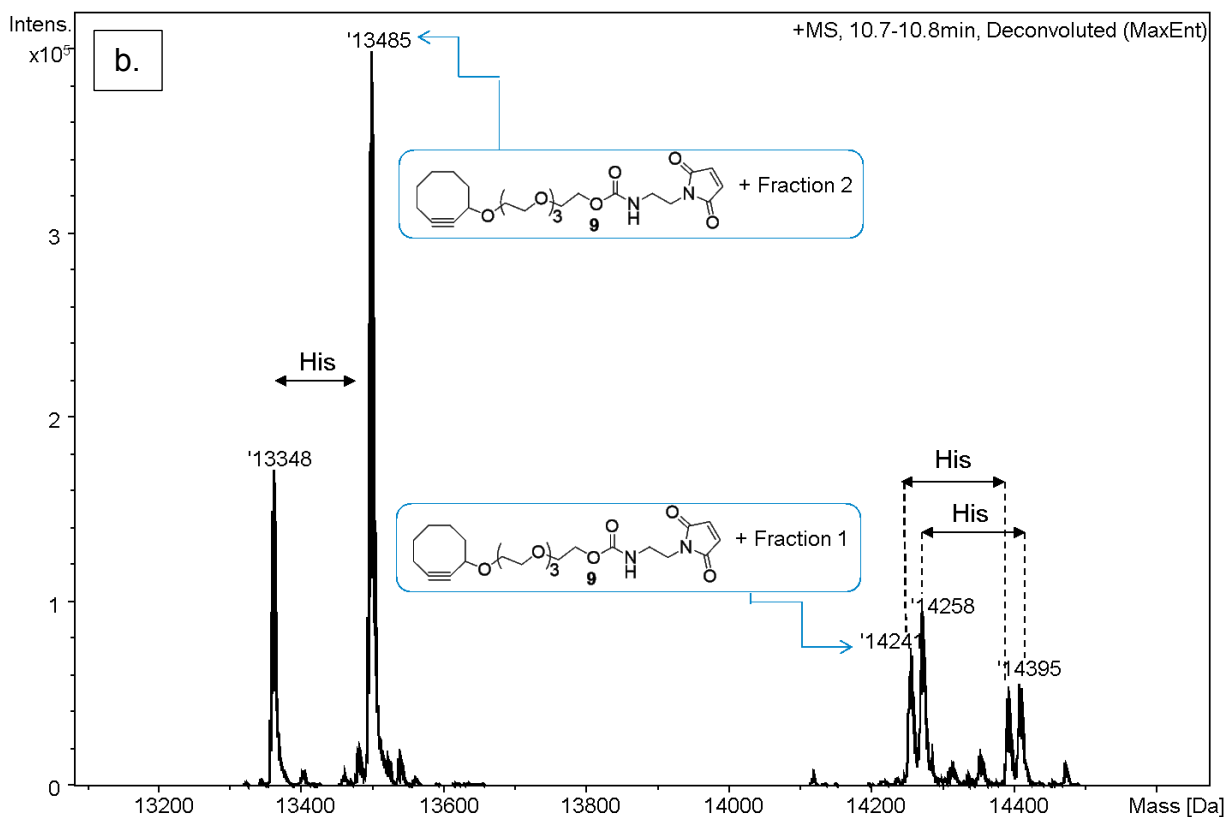
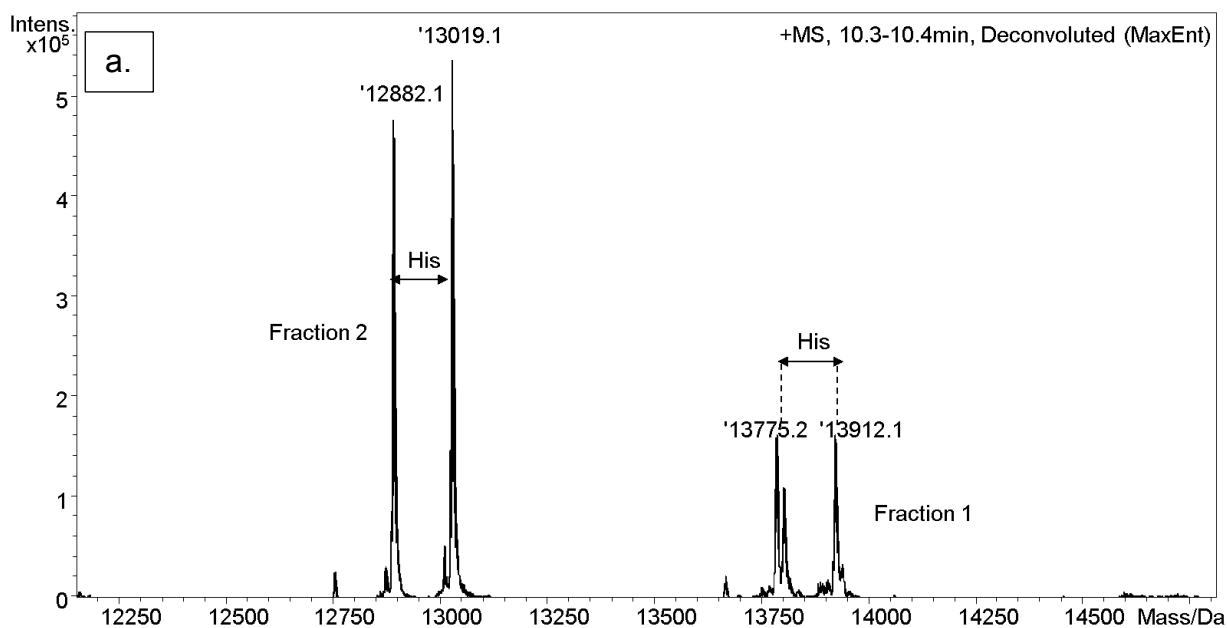


Figure 56. ESI-MS of cyclooctyne_succ_scFv'LCH3 (compound 15) cleavage product with and without cyclooctyne linker. a) proteolytic cleavage products of scFv'LCH3. Four charge fragments were detected in the two fraction elution from the column, The protein was cleaved in the His₆-linker-sequence b) proteolytic cleavage products + cyclooctyne_maleimide_linker (compound 9). The linker peptide sequence in scFv'LCH3 is SSGGCGHHHHHGGGSA, with the cysteine residue in the first part of the sequence in red, the His-tag in blue and the second part of the linker peptide sequence in green. The periplasmic localization sequence was not used for mass calculation.

The increase in mass of both fractions was 466 g/mol, which represents the exact molecular weight of compound **9**. The first proteolytic cleavage product (fraction 1) reacted with the maleimide on the linker via the free cysteine on the first part of the peptide-linker (SSGGCGHHH). The second proteolytic cleavage product (fraction 2) also reacted with compound **9**. The maleimide_linker (compound **9**) can also react with amine groups in the protein. However, this reaction is kinetically disfavored compared to the thioether formation and was not detected for other protein fragments.

The SDS-PAGE and LC-MS ESI results indicate the versatility of the compound **9** to bind to larger peptides (of ~13 kDa), via specific Michael addition reaction with the thiol groups of free cysteine groups, and to single chain antibody fragments with a molecular weight of ~26 kDa (proved by SDS-PAGE, Figure 55). Together with the small peptide bioconjugation results in subchapter Bioconjugation of H-CDoaDoaEQKLISEEDL-OH to the cyclooctyne_maleimide (proved by MALDI, Figure 52), it could be concluded that compound **9** could be used to bind to any biological target with a free thiol.

3.4.4. Chemical inhibitor for specific cell targeting

The highly potent and selective FAP inhibitor received from the Van der Veken group (University of Antwerp) was conjugated to the cyclooctyne_linker system and could be ultimately conjugated to chitosan. The group in Antwerp provided no structural details of the inhibitor besides the long chained endcapped azide that could be used as functional group for linkage to further systems without interfering with the potency or selectivity of the chemical inhibitor. Therefore, the existing cyclooctyne linker system was modified in order to bind both to the FAP chemical inhibitor via the available azide moiety as well as being able to react with the azide substituted chitosan_PEG as shown in Figure 57.

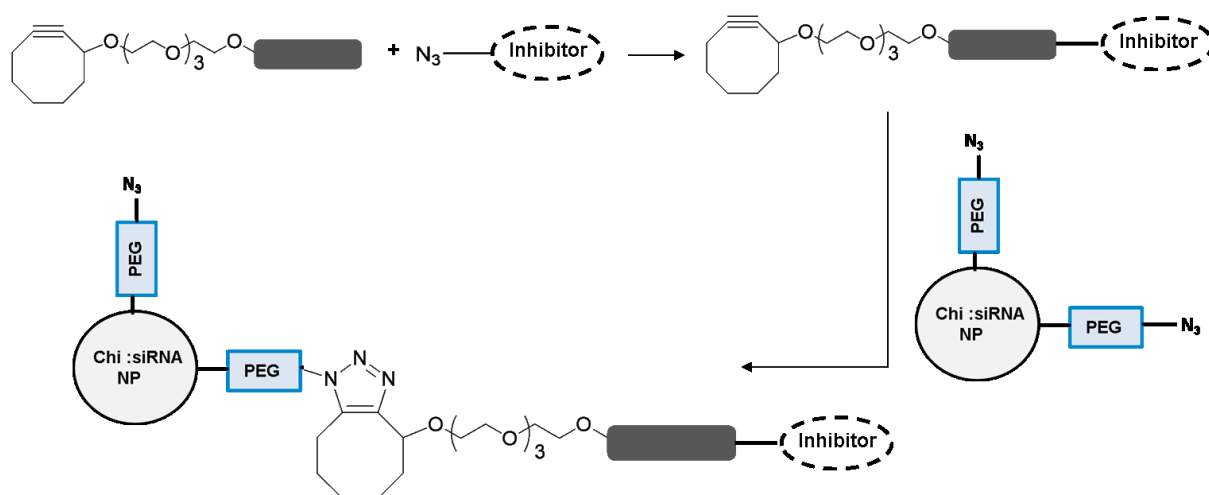


Figure 57. Concept for inhibitor binding to chitosan azide. The inhibitor had to be attached via an azide group to the cyclooctyne linker which should react with the azide groups of the modified chitosan as well.

The FAP inhibitor_linker system was synthesised as shown below.

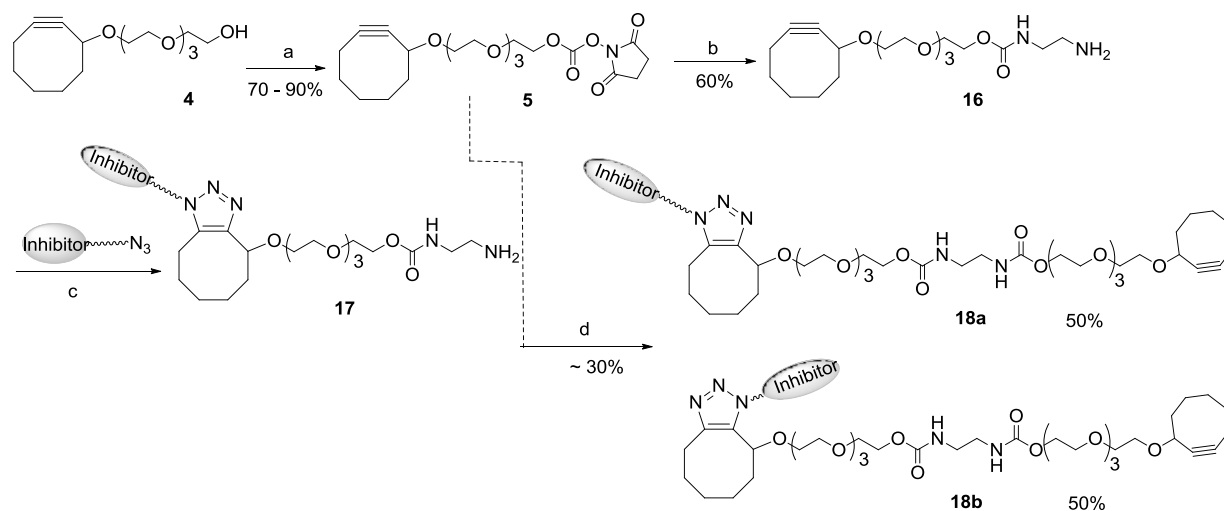


Figure 58. Synthesis of cyclooctyne-FAP inhibitor linker. a) *N,N'*-Disuccinimidyl carbonate, Et₃N, MeCN, RT; b) Ethylenediamine, CH₂Cl₂, RT; c) THF, 50°C; d) CH₂Cl₂, RT.

After activation of compound 4 to the carbonate ester 5, diaminoethan was reacted with 5 to yield the corresponding carbamate 16. The ongoing cycloaddition yielded the triazole coupled inhibitor system 17. The endcapped amine was reacted with the carbonate ester 5, which

serves as dual intermediate in this strategy to the target compound **18** as two regioisomers **18a** and **18b**, which can be coupled to the azide modified chitosan.

The crude product was purified via preparative HPLC with a GromSil 120 ODS-4 HE, 7 μ m 150x50mm column. The regioisomers **18a** and **18b** were obtained with a purity of ~90% (

Figure 59). The exact molecular weight was determined via direct injection ESI-MS analysis resulting in a m/z of 619.3409 [M+2H]²⁺ for regioisomer **18a** and 619.3407 [M+2H]²⁺ for regioisomer **18b** corresponding to a calculated monoisotopic molecular mass of 1238 Da.

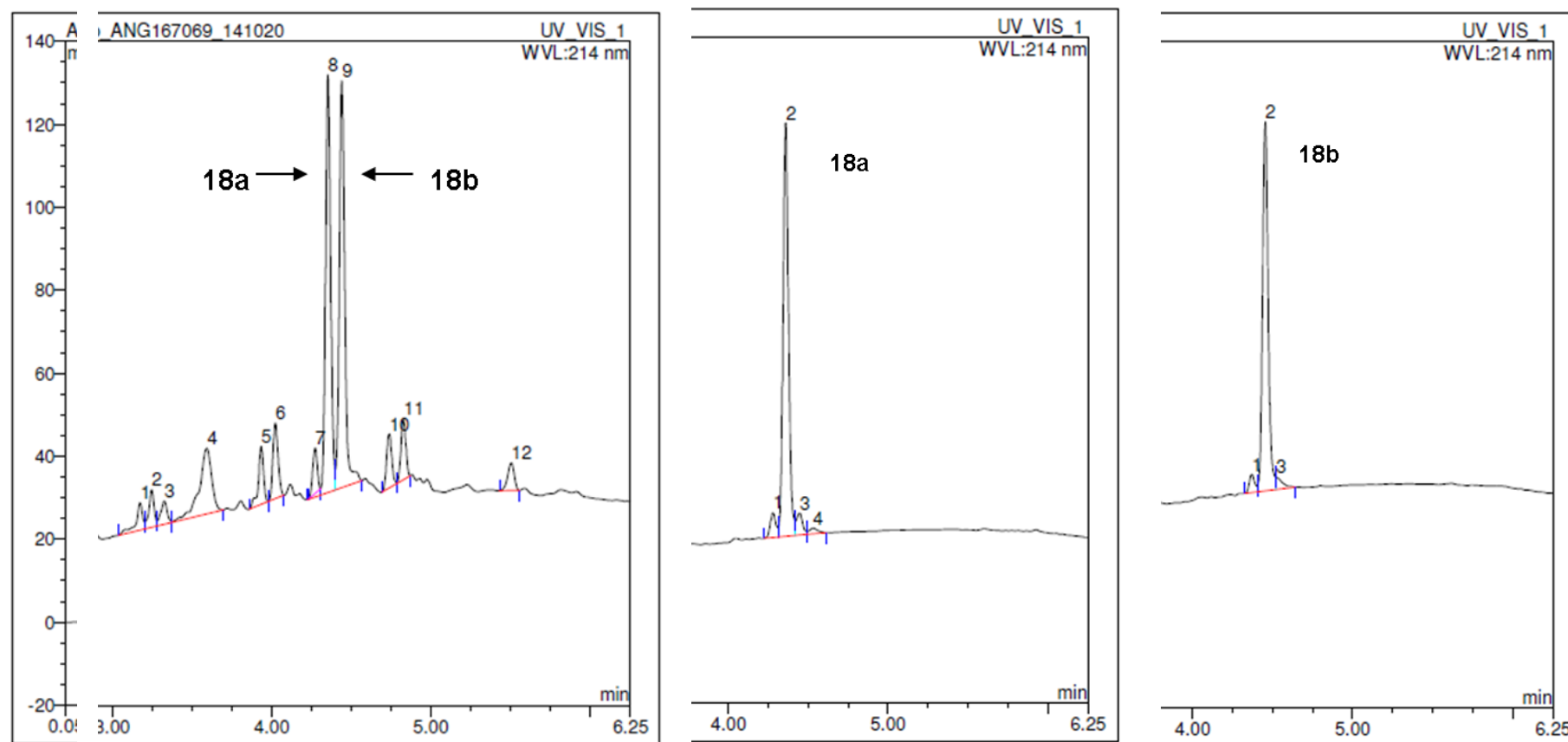


Figure 59. Analytical HPLC before and after purification of the regioisomers a) crude product b) regioisomer **18a** with 91.9% purity c) regioisomer **18b** with 87.5% purity (GromSil 120 ODS-4 HE, 7 μ m 150x50mm column, 5 to 65% solvent B, 25°C, temperature, solvent A: H₂O+0.1% TFA, B: ACN+0.1%TFA).

3.4.5. Chitosan_PEG_N3

The selective functionalization of the nanoplex surface can be achieved by incorporating an azide moiety at the distal end of the PEG spacer. This implies the use of a heterobifunctional PEG spacer which such as compound **20**, with a carboxylic group at one end and an azide the opposite end. The carboxylic acid functionalized PEG was grafted to the N-glucosamine unit of chitosan via amidation. The synthesized was based on the work of Lallana et al. [226]. The grafting linkage was selected because of the high yield and reproducibility of the process under physiological conditions [232]. Compound **20** was synthesized from another heterodifunctional PEG (compound **19**) by reaction with glutaric anhydride as shown below (Figure 60).

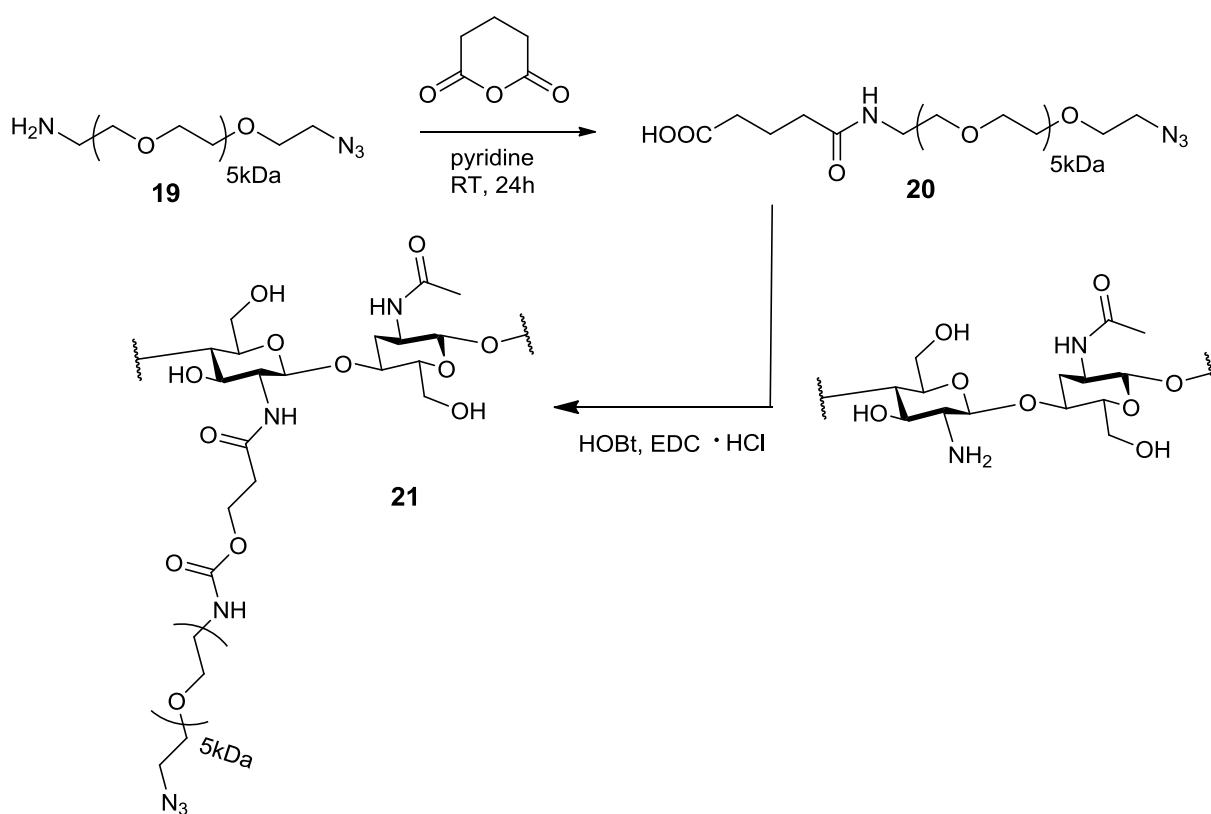


Figure 60. Synthesis scheme of chitosan_PEG_N₃. The commercially available PEG with distal amino and azide groups (**19**) was selectively functionalized with glutaric anhydride yielding compound **20** which was coupled in aqueous solution to the amino groups of deacetylated chitosan with EDC and HOBt.

Table 8. Chitosan_PEG parameters measured and calculated by gel permeation chromatography; number average molecular weight M_N , weight-average molecular weight M_W , intrinsic viscosity η , hydrodynamic radius R_h , degree of substitution DS

<i>RN</i>	<i>Mw</i> [kDa]	<i>Mw</i> / <i>Mn</i>	η [dL/g]	<i>Rh</i> [nm]	* <i>DS</i> [%]
Chi (152; 92,6)	152 ±1,1	1,3 ±0,01	3,75 ±0,19	20,4 ±0,13	-
1.5 % PEG	158 ±1,9	1,3 ±0,01	2,91±0,01	18,9 ±0,08	1,7

$$*DS = \frac{(Mw_{Chi_{PEG}} - Mw_{Chi})/3900}{DP_{Chi}}; DP_{Chi} = Mw_{Chi}/Mn_{Chi}$$

The DS and Mw of compound **20** were determined via GPC and IR analysis (Table 8).

According to the GPC results, the PEG_N₃ grafting to the amino group of chitosan was low (1.7% DS). As the PEG_N₃ grafting was achieved at the primary amino group of the deacetylated chitosan unit, it was important to make sure that there are still enough primary amines were still available for electrostatic interactions stabilizing the final nanoplexes. Therefore, no PEG_N₃ chitosan grafting with higher DS was pursued.

The successful modification of chitosan with the PEG_N₃ group was also be detected via IR analysis (Figure 61).

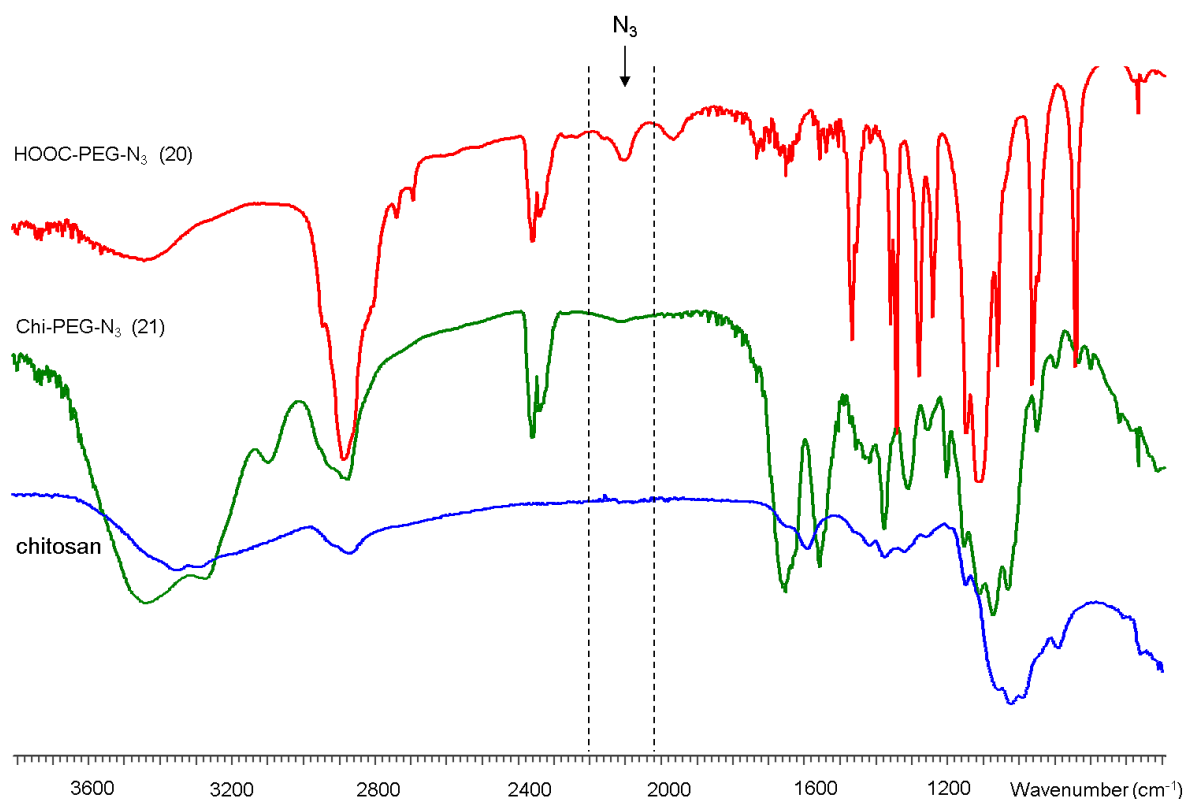


Figure 61. IR spectra overlay of chitosan, Chi_PEG_N3 and HOOC-PEG_N3

3.4.5.1. Proof of concept for azide_cyclooctyne linkage formation

Having established the strain-promoted azide-cyclooctyne [3+2] cycloaddition conditions for the functionalization of chitosan_PEG_N₃, compound **21**, the next step was to prove the formation of the conjugation of the cyclooctyne linker to the chitosan. Therefore, HOOC_PEG_N₃, compound **20**, was reacted with an excess of hydroxyl cyclooctyne linker at room temperature for 52 h (Figure 62).

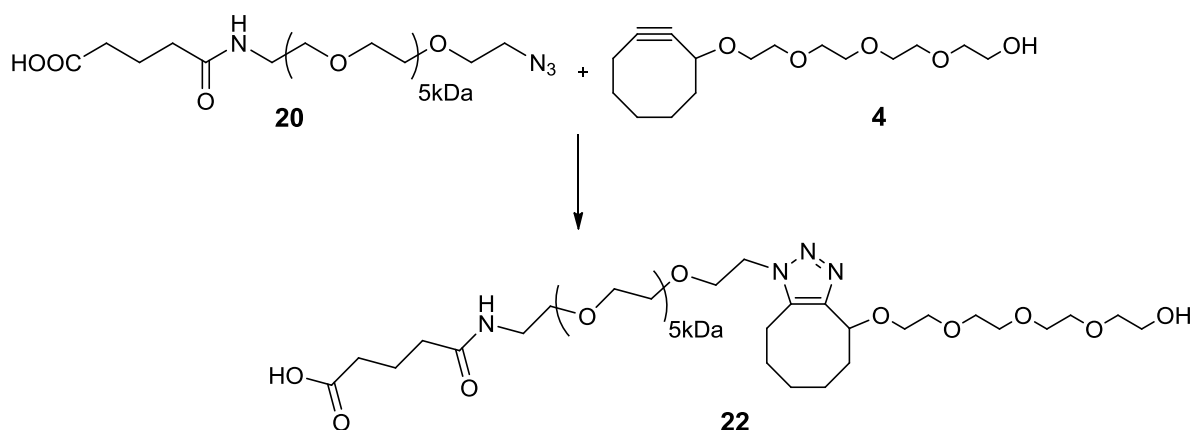


Figure 62. Synthesis of cyclooctyne_linker_PEG_COOH. As proof of concept the azide compound **20** was reacted with the cyclooctyne compound **4** at RT for 52 h to yield product **22** via selective [3+2] azide_cyclooctyne click chemistry.

Both HOOC_PEG_N₃, compound **20**, and the triazole conjugated PEG_linker system, compound **22**, were analyzed via dry droplet MALDI-ToF-MS. The expected mass shift was 301.2 amu in compound **22** MALDI-ToF mass spectrum and a shift of 299.9 was observed. The adjacent peaks in both compound **20** and compound **22** differed in mass one PEG monomer unit ($\Delta M = 44.03$ (CH₂CH₂O)).

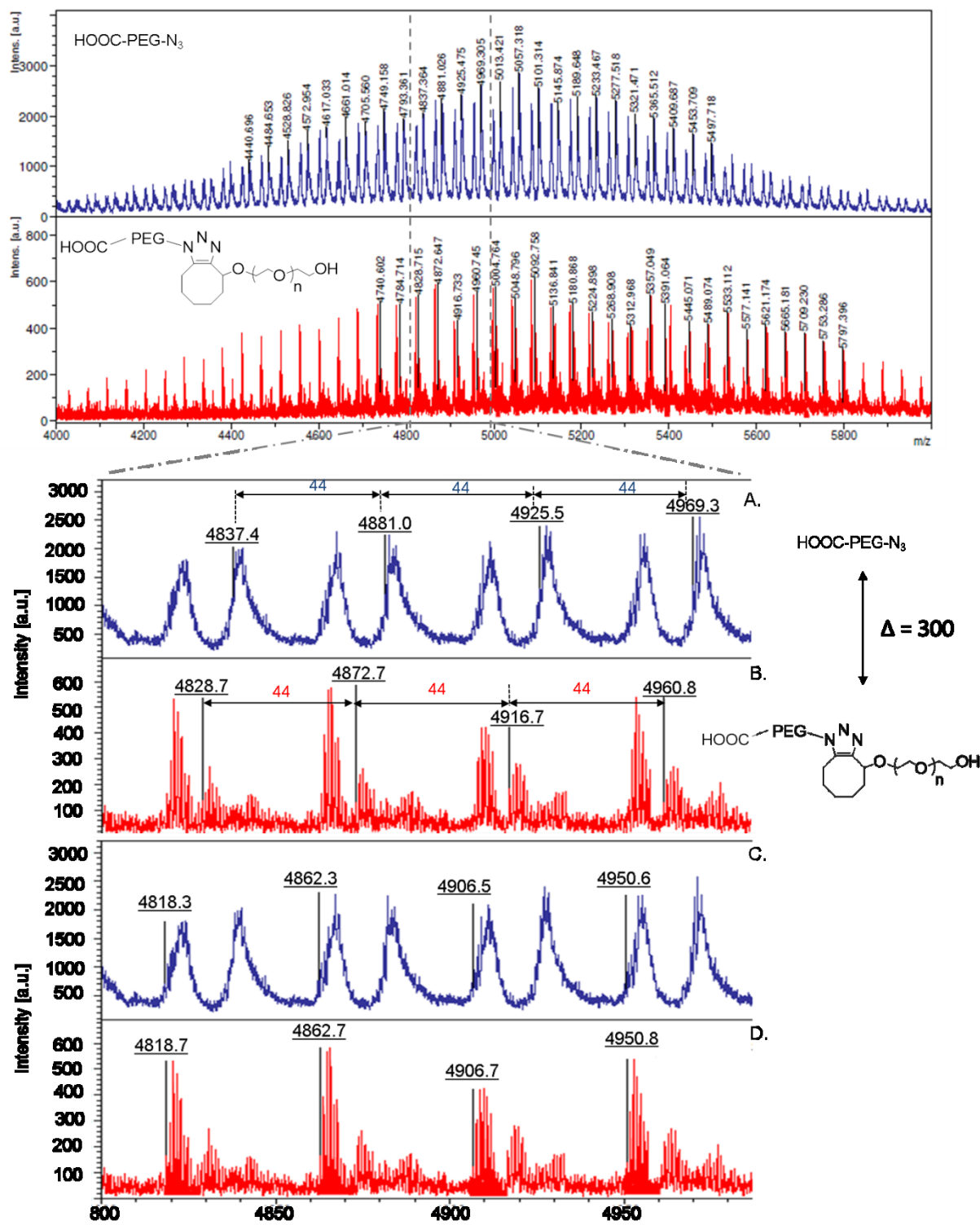


Figure 63. MALDI-MS spectra of reagent HOOC_PEG_N3 and product $\text{triazole_PEG_linker}$ system, compound **22**. The found mass shift between the product and the reagent ion series of the polymer was 300 Da. This corresponded exactly to the mass of the cyclooct-2-yne-tetraethyleneglycol ($\text{C}_{16}\text{H}_{28}\text{O}_5$) attached to the polymer azide. The mass difference between adjacent peaks in both reagent and product related to the mass of the ethylene glycol monomer unit ($\Delta M = 44.03$ ($\text{CH}_2\text{CH}_2\text{O}$)).

3.4.6. Functionality of the scFv'LCH3 after bioconjugation to the linker system

The binding of the scFv'LCH3 to FAP expressing cells was successfully tested by Dr. Schuster* in human fibrosarcoma HT1080 cell line, both the wild type (HT1080wt) and a FAP overexpressing stably transfected variant (HT1080FAP #33)[49]. The bioconjugation of the scFv'LCH3 to the linker system might affect the functionality of the targeting molecule. Therefore, we tested compound **15** (Figure 64) in the same two cell lines together with the scFv'LCH3 as a positive control (Figure 65).

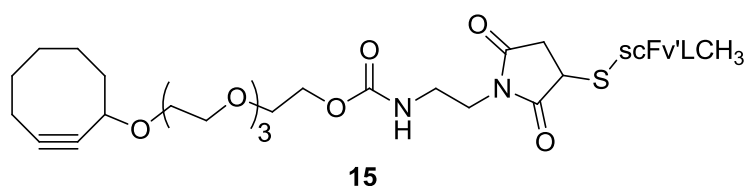


Figure 64. Structure of the scFv'LCH3 bioconjugate succinyl_cyclooctyne_PEG

The integrated His-Tag makes it easier to purify scFv'LCH3 via Ni-affinity chromatography and to identify it with an anti-His primary antibody. In this study, the cells were stained with a Cy3 (red) – labeled secondary antibody in order to detect the binding of the scFv'LCH3 before and after bioconjugation yielding compound **15**. The nuclei were stained with DAPI (blue) in order to be better localize the cell and the binding of the scFv'LCH3 on the cell surface. Therefore, successful binding of scFv'LCH3 was expected to be illustrated by a strong Cy3 (red) signal on the HT1080 cell surface. As a negative control compound **15** was also incubated without the anti-His primary antibody which should correlate with no Cy3 (red) signal. As the optimization of the bioconjugation reaction was performed with 0.01% Tween20, the cells were also incubated with 0.01% Tween20 as a negative control.

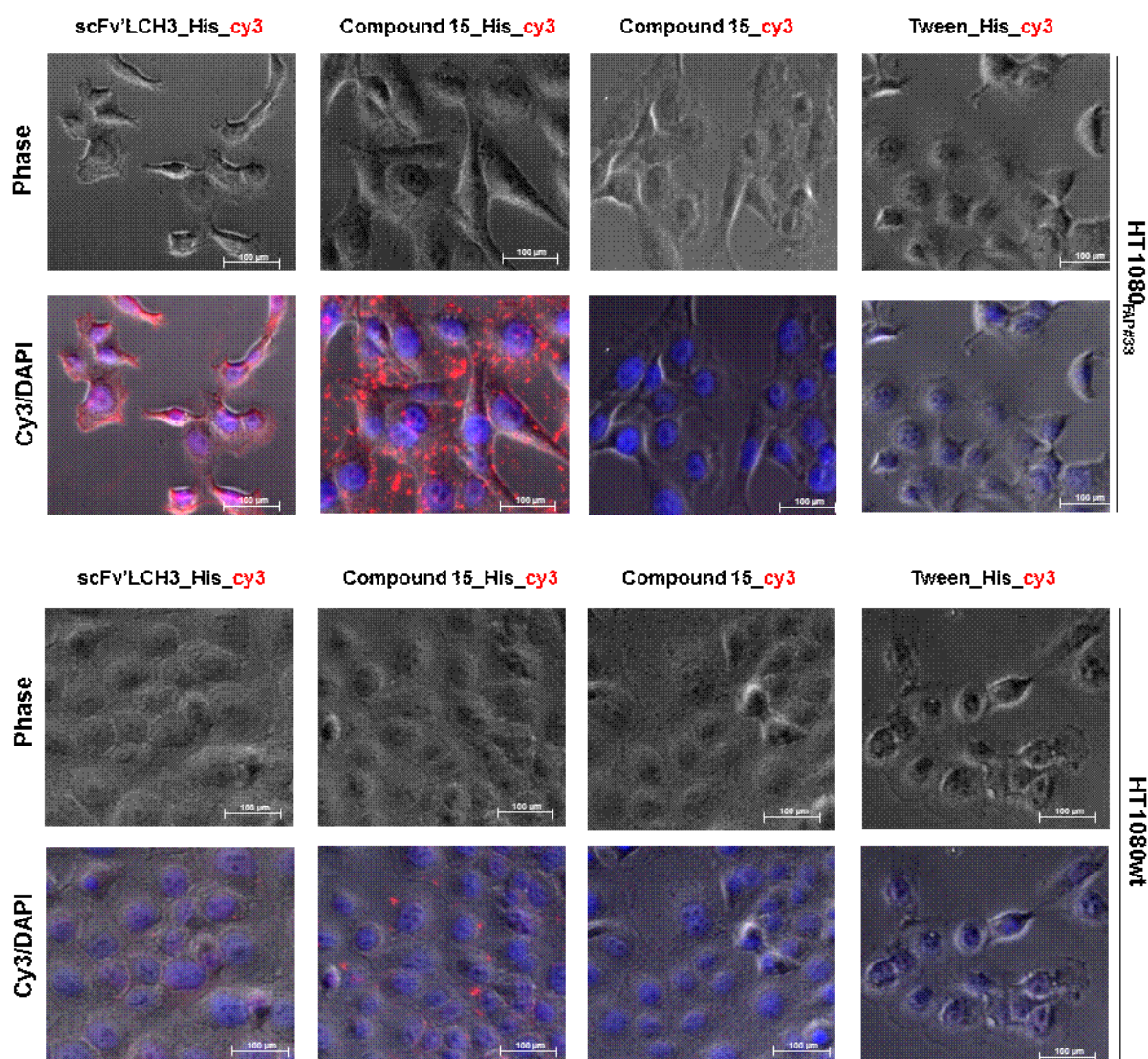


Figure 65. Cell assay to test the functionality of scFv'LCH3 bioconjugated to the maleimide linker system. HT1080FAP # 33 and HT1080wt cells were fixed with PFA before adding compound 15, unconjugated scFv'LCH3 as a positive control, 0.01% Tween20 as a negative control. Detection of bound scFv'LCH3 was performed by an anti-His primary antibody and staining with Cy3 labeled secondary antibody. As a negative assay control compound 15 was added without anti-His primary antibody. The nuclei were stained with DAPI (scale bar 100 microns). Whereas the pure FAP_ligand scFv'LCH3 was located only at the cell membrane. The scFv'LCH3 coupled to the cyclooctyne linker showed strong signals between cells as well (compound_15_His_cy3).

The Cy3 signal in the HT1080FAP cells indicated that scFv'LCH3 was still functional even when coupled to the linker system. Furthermore, the assay data showed that it was specifically bound to the FAP target after the bioconjugation to the linker system. The two negative controls, compound 15 without the anti-His primary antibody and the Tween20, showed that the Cy3 signal was specific to the specific binding of the scFv'LCH3 to its target on FAP expressing cells.

3.5. Layer by layer

3.5.1. Build-up of (HA/Ch)₂ (HA/NP)_n PEM layer

The polyelectrolyte multilayer (PEM) build-up consisted of two bilayers of HA and chitosan (HA/Chi)₂, and several bilayers of HA and Chi/Chi_PEG:siRNA nanoplexes (HA/NP)_n. The first two bilayers were formed in 5.5mM CH₃COONa buffer (pH 5.5), while the HA/NP bilayers were added in 0.3M CH₃COONa buffer (pH 5.5) due to the NP formation. As previously measured at pH 5.5 chitosan and NP (Table 7) have a positive charge. Therefore, the HA was deposited as a negatively charged layer and chi/NP as a positively charge layer in alternative order. The overcompensation of charge resulted in the adsorption of each layer, at which stage the charge on the surface of the layer was reversed.

The multilayer assembly was proven by QCM measurements carried out on PEI-coated gold crystals[44]. The constant increasing frequencies in Figure 66 indicated the continuous building up process. The (HA/NP)_n bilayers revealed smaller frequencies compared to (HA/Chi)₂. However, the steady increase with each (HA/NP)_n bilayer added, confirmed the build-up process. The decreased zeta potential with increasing PEG densities (Table 7) correlated with the lower deposition of NP. The number of HA/NP bilayers decreased from 5 in the case of unmodified chitosan:siRNA NP to 3 – 4 for NP formed with chi_PEG 3 and 4% DS, with only 2 nanoplex bilayer deposition in the case of chi_PEG 8% DS.

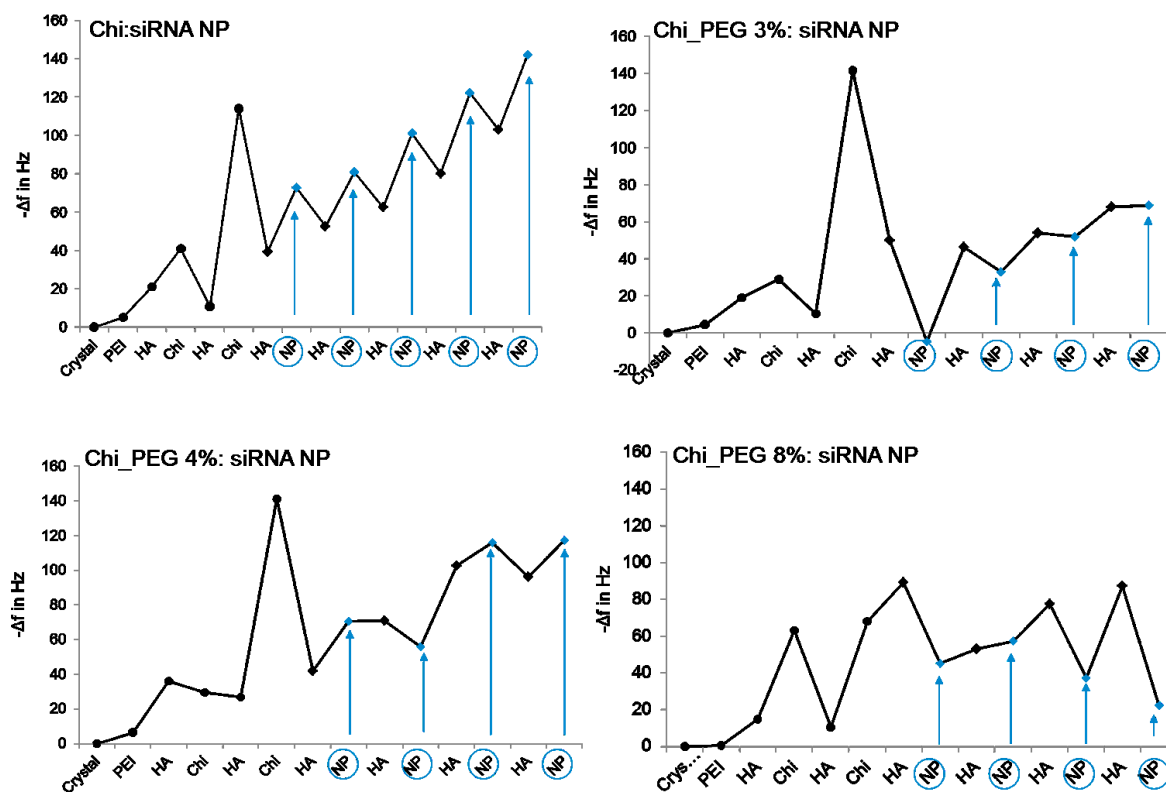


Figure 66. Build-up of (HA/Chi)-layers with Chi:siRNA NP and Chi_PEG:siRNA NPs. Frequency shifts ($-\Delta f$) measured with quartz crystal microbalance after successive injections of polyelectrolytes (hyaluronic acid:HA or chitosan:Chi) and Chi or Chi_PEG:siRNA NPs (indicated by arrows).

3.5.2. NPs release over time

The release of the NPs with Chi_PEG 4 and 8% immobilized PEMs was followed by using Tye563 labeled siRNA (Figure 67). The PEM were build-up analogues to the QCM films, $PEI/(HA/Ch)_2(HA/NP^{Tye563})_n$, with both negative control siRNA and labeled siRNA, and were deposited on 96-well plates. The wells were washed with PBS every 24h and the decreasing fluorescent intensity of the collected supernatant was compared to the negative controls. The data revealed linear release for both PEM assemblies. The higher number of NP bilayers in the case of chi_PEG 4% DS was reflected also in the release data. In the first 24h the relative intensity of PEMs with chi_PEG 4% was higher in comparison to chi_PEG 8%, however after 48 both PEMs showed similar fluorescent absorbance at 600 nm. The PEM complete degradation and NP release was achieved after 96h.

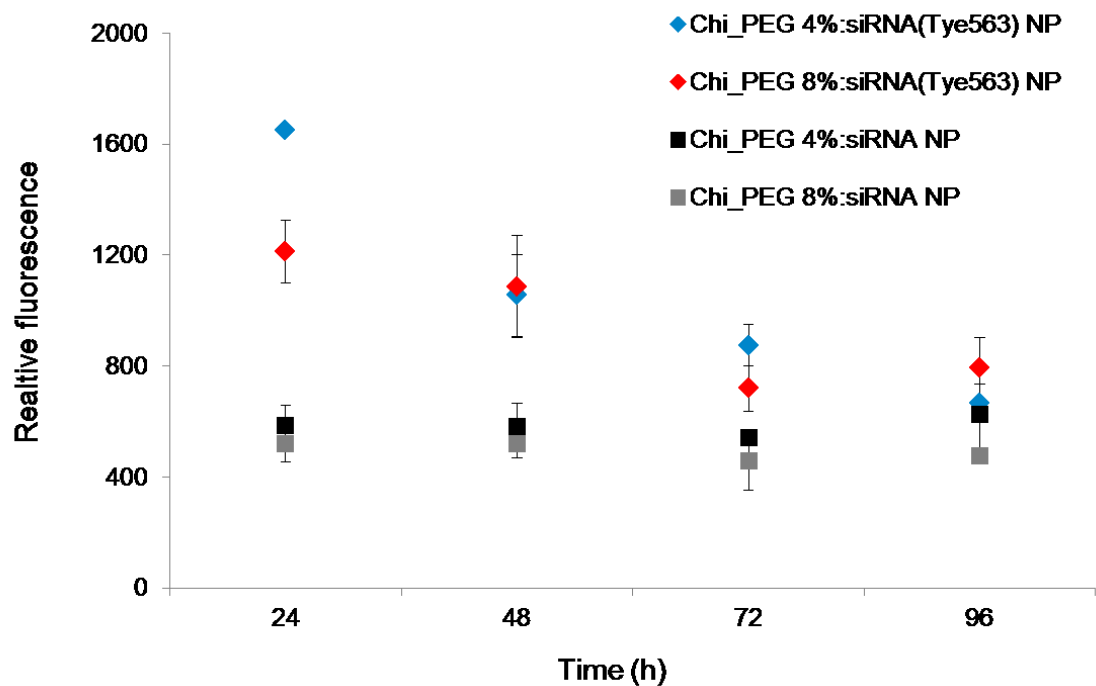


Figure 67. NPs release from $PEI/(HA/Ch)_2(HA/NP^{Tye563})_n$, $PEI/(HA/Ch)_2(chi_PEG\ 4\%:siRNA^{Tye563})_4$ and $PEI/(HA/Ch)_2(chi_PEG\ 8\%:siRNA^{Tye563})_2$ films were incubated in PBS at 37°C for 96h. The fluorescent intensity was measured every 24 h. As a negative control the similar procedure was performed for $PEI/(HA/Ch)_2(chi_PEG\ 4\%:siRNA)_4$ and $PEI/(HA/Ch)_2(chi_PEG\ 8\%:siRNA^{Tye563})_2$.

4. Discussion

4.1. The optimal chitosan for siRNA delivery

Given the cationic nature, biodegradability, biodistribution, low immunogenicity and ease of manufacturing, chitosan was chosen as a natural non-viral siRNA nanocarrier. As it was already used in various studies for the delivery of DNA, many of the tactics used to improve the DNA delivery can be transferred to siRNA delivery. However, it is important to take into consideration that in comparison to DNA, siRNA is much more sensitive to nuclease degradation in the biological environment [233], it has a much smaller size (20-25 base pairs, ~14kDa) [91] and it targets the mRNA in the cytosol instead of the nucleus. Therefore, the physicochemical parameters of chitosan need to be optimized in order to have a subtle balance between sufficient siRNA protection complex, stability and intracellular release of siRNA into the cytosol. As DNA has a higher M_w than siRNA, the polymer length of chitosan can be reduced for the successful DNA condensation from 10 kDa [234] to even ~4.7 kDa [235]. The longer DNA chains might be able to build a stable polymer backbone and compensate for the higher mobility of shorter chitosan chains [58]. siRNA, however, is a lot stiffer and might not be able to condense further [236]. Also the limited number of negative charges per molecule may not be sufficient for stable binding resulting in incomplete association of chitosan and siRNA [237]. As a consequence longer chitosan chains with a higher degree of deacetylation (DD) have to be considered for siRNA complexation. Simultaneously with siRNA protection, the polyplex cell uptake has also to be considered also. A chitosan with a too high molecular weight (M_w) might form polyplexes too large for cell uptake. From literature it seems that chitosan molecules with 5-10 times the chain lengths of siRNA form suitable polyplexes [53, 69]. Katas *et al.* [88] could form 276 nm nanoparticles from siRNA and 160 kDa chitosan and Liu *et al.* [69] showed that a DD higher than 80% is necessary for higher siRNA binding capacity.

In the current study a library of chitosans with DD between 80 – 94% and M_w between 73 – 379 kDa was synthesized and characterized. The chitosan/siRNA nanoplexes formed were characterized according to size and zeta potential in order to choose the chitosan with the best DD and M_w values for an efficient siRNA based knockdown in the current study. The nanoplexes were formed at N/P ratios of 50/1 and 100/1. For both ratios the size of the nanoplexes was never higher than 250 nm. The zeta potential was always positive, but lower than the charge of the chitosans alone before nanoplex formation. This indicated the

successful interaction with the negatively charged siRNAs. The results pointed towards a balance between DD and M_w which influences nanoparticle formation. The chitosans with M_w lower than 165 kDa and higher than 250 kDa as well as DD smaller than 90%, formed nanoplexes with a size of ~250 nm at both N/P ratios. Conversely, the chitosans with higher DD (90-94%) and M_w in the range of 165 – 280 kDa formed smaller nanoplexes. Therefore, chitosan Heppe 95/50 was used further on as the structural characteristics (M_w (140-200 kDa and the DD (~95%)), as well as the more detailed biological testing for side effects due to contaminants in comparison to the Aldrich products were optimal for biological applications. Chitosan Heppe was microbiologically tested and had a protein content of 0.5%. The exact structural parameters (M_w of 152 and DD of 92.6%) were determined via GPC and ^1H NMR.

4.2. Impact of the PEGylation on the chitosan siRNA delivery system

The two drawbacks of chitosan nanoplexes are the need for slightly acidic conditions for solubilization and the lower transfection efficiency compared to other cationic polymers such as polyethylene imine (PEI) [165]. However, chitosan structure offers the possibility for broad and straightforward modifications to overcome these limitations. By conjugating chitosan with poly(ethylene glycol) (PEG), the solubility can be improved at pHs higher than 6.5 [139]. The steric shielding provided by the PEG chains could reduce the inter-particle aggregation or prevent unspecific interactions with proteins or cells. PEG can also be used as linker or spacer to attach groups on the nanoplex surface for specific targeting of the chitosan:siRNA nanoplexes resulting in an increased transfection efficiency.

Taking into consideration the previous investigations with PEG, which state that small chains (550Da) can interfere with the nanoplex formation and stability [150], it was decided to conjugate chitosan with slightly larger 5 kDa PEG. The longer PEG chains (5 kDa) stick on the surface of the nanoplexes and can induce stealth shielding [138, 150]. Furthermore, they can better facilitate the addition of a targeting moiety at the distal end of the PEG chains [238]. The PEG density was also taken into consideration because of its impact on the biological activity. According to Zheng *et al.* [138] a PEG density higher than 7% is necessary for a sufficient shielding against unspecific interactions with proteins or cells. Also the chitosan solubility increases with a higher PEG grafting. The drawback is that a too high PEG density on the nanoplex surface is also known to decrease the transfection efficiency due to the reduce cellular uptake [239]. Furthermore, a certain percentage of primary positively

charged amino groups necessity for nanoplex formation is lost due to PEGylation. Therefore, chitosan was conjugated with 1.5% PEG to 8% PEG (mol %) in this study.

A clear increase in solubility could be noticed even from 1.5% PEG grafting in comparison to unmodified chitosan. However, chitosans with 4 and 8% PEG grafting showed lower turbidity at pH 7.0. This increase in solubility can be explained by the increase of hydrophilicity. Investigations of PEG in solution have shown that PEG typically binds 2-3 water molecules per ethylene oxide unit of the two polymers forming the nanoplex [141, 221]. Furthermore, the PEG substitution on the primary amines of the deacetylated unit can deform the rigid crystalline structure of chitosan, disturbing the hydrogen bonding and leading to an enhancement in hydrophilicity [221, 240].

The nanoplexes were formed spontaneously at pH 5.5 in aqueous buffer, at an N/P ratio of 25/1. The N/P was calculated taking into consideration the replacement of the primary amino groups with increasing PEG amounts. Therefore, the stability of the nanoplexes was not influenced by the increasing PEG density due to the constant ratio of positive and negative charges. The size of the nanoplexes at N/P 25/1 was smaller than 200 nm for all PEGylation ratios. Actually, a decrease in size was noticed for increasing amounts of PEG. The nanoplexes formed with chitosan_PEG 8% degree of substitution (DS) had a size of 140 nm, 60 nm smaller compared to the nanoplexes formed with unmodified chitosan. The increase in PEG density led to a decrease in zeta potential of the nanoplexes. Chitosan_PEG 8% had a zeta potential of ~ 8 mV, 10 mV smaller in comparison to unmodified chitosan nanoplexes. As the ratio between protonable amino groups (N) and phosphate groups (P) was kept constant for all nanoplexes, the decrease in zeta potential may be due to the spatial shielding of the surface charges by the PEG chains [220, 241, 242]. The hydrophilic PEG chains may cause a thicker stationary layer on the nanoplexes and the replacement of the slipping plane further away from the nanoplex surface. Fewer ions in that stationary layer would then lead to a decrease in zeta potential. The mobility of the nanoplexes could also be decreased by changes of the local dynamic viscosity. Furthermore, the addition of the hydrogen bonds between PEG chains and water on the complex surface might also lead to a decrease in zeta potential [224].

The nanoplex characteristics started to change in the biological environment. The proteins in the cell culture medium (CCM) are likely to interact with the nanoplex surface. In recent years several groups have been investigating the formation of a so called “protein corona” on the surface on different nanoparticles, defining two entities: the hard and the soft corona [92,

^{243, 244]}. The proteins with higher affinity for the nanoparticle surface form the hard corona, while the soft corona consists of a more loosely associated and rapidly exchanging layer of biomolecules [244]. Some investigations showed that even with PEG surface modifications some protein interactions may still occur. Due to the reduced amount of surface grafted PEG, higher degrees of conformational freedom and hydration could enable easier binding of proteins in the PEG layer. In a smaller percentage protein binding could be due to the interactions with the methoxy distal end of the PEG chains [148, 244-247]. Therefore, the formation of the protein corona depends on the nanoplexes size, charge, stability, and PEG density.

The charge of the nanoplexes in CCM decreased significantly, especially in the case of unmodified chitosan and low PEG grafted chitosan nanoplexes. For chitosan siRNA nanoplexes the zeta potential dropped to a slight negative value (-1.6 mV), while for chitosan_PEG 6% and 8% DS the difference between buffer and CCM was of only 6 and 4 mV respectively. The investigations showed that the charge differences were not influenced by the increase in pH from 5.5 to 7.0. The measurements in PBS at pH 7.0 resulted in charge values similar to the ones in buffer at pH 5.5. Therefore, it can be assumed that proteins from CCM interacted with the nanoplex surface decreasing the overall surface charge. Furthermore, the increase in PEG density correlated to the higher positive charges for chitosan_PEG 6% and 8% nanoplexes. This might be due to the steric sheilding of unspecific interactions of the nanoplex surface with some of the proteins in the CCM.

The dynamic light scattering results for the size of the nanoplexes measured in CCM only offered an indication of the formation of a protein corona. As previously mentioned, when nanoplexes are incubated in CCM, the proteins with the highest concentration (e.g. albumin) will bind first to the nanoplex surface. The formation of a weak protein corona could explain the slower decay rates in the intensity correlation curve of the ZetaSizer noticed immediately after adding the nanoplexes in CCM ($t=0$). However, these proteins did not necessarily have the highest affinity for the chitosan siRNA complexes. With time the higher affinity proteins, which might have a lower concentration in the CCM, will compete with and likely replace the initially bound proteins. This could also be noticed in our results. After 2 and 4 h the formation of larger agglomerates was noticed as well as a faster decay of the autocorrelation curve in comparison to the initial state. Once the high affinity proteins reached the surface, they formed a hard corona, which was more stable over time and had a well-defined layer thickness resulting in a lowered polydispersity of the particles. In our case, at 6 h nearly the

same progression of the correlation curve could be detected and the larger aggregates were no longer present independent from the ratio of PEGylation (Figure 29). The investigations of the nanoplexes in CCM over time, as well as the zeta potential results reinforced the idea that even with the PEG chains attached to the surface some proteins are still able to bind to the nanoplexes. From the DLS measurements it is not clear whether the proteins bind inside the PEG layer between the PEG chains or at the distal end of the PEG chains. A higher shielding of the nanoplex might be possible with an increased PEGylation ratio. However, as previously mentioned, an increased shielding could lead to a decrease in cell transfection efficiency.

Zheng *et al.* [248] used a dye-quenching assay to investigate the self-assembly of siRNA with PEI at different N/P ratios. In the current work the same assay was used with a different purpose. TyeTM563 labeled siRNA was used to investigate its complexation with the different PEGylated chitosan samples over time in CCM at a constant N/P ratio of 25/1. The results showed an immediate formation of siRNA chitosan nanoplex by a reduction of fluorescence intensity to about 25%. But after 1h and even more after 2 and more hours TyeTM563 fluorescence increased up to 60 – 80% (Figure 30). This indicates a loosened entrapment of the siRNA after 1h. However, the fluorescent intensity was stable until the 6h of cell uptake and still smaller than 100% in comparison to free labeled siRNA in CCM. As a consequence chitosan was still able to protect the siRNA against degradation in CCM over the 6 h of preparation time up to cell uptake independent of the PEG density grafted to chitosan. As a consequence, transfection could be started after 3h of preparation time.

Once inside the intracellular environment the pH is becoming more and more acidic during endocytosis. In the extracellular environment the main concern was the stability and the protection of the siRNA in the CCM at a pH of ~ 7.0 . Inside the cell the balance between stability until the release from the endo-lysosomal compartment is very important. However, the release of the siRNA from the nanoplexes once released into the cytosol has to also be taken into consideration for nanoplex optimization.

Thibault *et al.* [104] traced the intracellular trafficking of chitosan/DNA systems via the dextran pulse-chase fluorescent dextran lysosomal staining which revealed the very fast transport (~ 4 h) of the nanoplexes from the endosome to the lysosome in HEK293 cells and a colocalization in the lysosome for 8-12h until they were gradually released in the cytosol. The mechanism for endo-lysosomal escape discussed in literature relies on the osmotic pressure generated by the ‘proton sponge’ effect [102] or by a rise in lysosomal enzyme-induced

degradation products of the polycation [235] [108]. Chitosan can be degraded in the lysosome by lysozymes which can hydrolyze the $\beta(1-4)$ linkages between *N*-acetylglucosamine and glucosamine [114, 249]. Therefore, it was important to analyse the nanoplexes charge difference between pH 7.0 and pH \sim 4.5 in CCM for different PEGylation ratios. At a pH of \sim 4.5 all nanoplexes showed zeta potentials higher than 10 mV. Whereas, at pH 7.0 PEGylation influenced the nanoplex charge significantly (Figure 31). The charge difference between the two pHs decreased with increasing PEG densities, revealing for chitosan_PEG 6% and 8% charge differences of only 4 mV and 6mV respectively. Given the mechanism of endo-lysosomal escape, the positive zeta potential of the nanoplexes with higher PEGylation rate at pH 4.5 in CCM should reduce the proton sponge effect. Therefore, it might be that the two higher PEGylated chitosan nanoplexes will show lower endosomal release rates and maybe final knockdown efficiency compared to the other samples. Nevertheless, a detailed analysis of endosomal release rates could not be performed.

The comparison of the physicochemical parameters of the modified chitosans and the nanoplexes formed thereof with the biological results offered a better understanding of our delivery system. Cytotoxicity assays of the chitosans before and after nanoplex formation all showed cell viabilities above 70%. In fact, the unmodified chitosan had slightly higher cell viability (\sim 85%) in comparison to all PEGylated chitosans and it stayed the same also after the nanoplex formation. The only improvement in cell viability after the nanoplex formation was for chitosan_PEG 8% DS. Cell viability increased from \sim 75% to \sim 90% in comparison to the untreated cells set at 100% cell viability (Figure 24, Figure 25).

The cellular uptake was tested with fluorescently labeled siRNA in H1299 cells which naturally exhibited no fluorescence. Both, fluorescent microscopy and flow cytometry measurements showed for all samples a cell uptake in the range of 50-60% (Figure 32, Figure 33). Even when these results could not reach statistical significance they correlated very well with the protein corona hypothesis. Chi_PEG 6% and 8% resulted in smaller zeta potential decrease in the CCM indicating some shielding against unspecific interactions. However, as it is known from literature [146, 147] and was already mentioned in the introduction (1.6), the proteins from CCM are still able to bind to the nanoplexes. Actually, the protein corona might even facilitate the nanoplex cell uptake. Furthermore, the uptake results indicated a good nanoplex stability and siRNA protection for all nanoplexes in the extracellular environment during the entire cell uptake period of 6h.

During her PhD work Dr. Liane Schuster established a cellular assay system to test the functional delivery of siRNA using the stable EGFP-expressing cell line, H1299-GFP (Figure 68). The nanoplexes were formed from the different PEGylated chitosans. Instead of fluorescently-labeled siRNA, siRNA against GFP was chosen for nanoplex formation. Therefore, the efficiency of the siRNA knockdown could be traced by the GFP downregulation which was easily analyzed via fluorescence microscopy and flow cytometry. The controls used for this test system were the nanoplexes formed with scrambled siRNA which are not able to downregulate GFP mRNA, keeping the fluorescent signal at the same level as for untreated cells and indicating unspecific RNAi side effects as well.

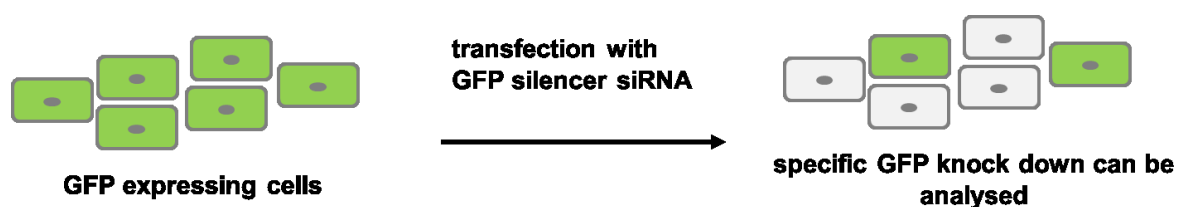


Figure 68. siRNA based knockdown assay system based on the H1299-GFP cell line stably expressing GFP. GFP siRNA silencer loss of fluorescence shows efficient mRNA knockdown. The cellular assay detects the final end point of the different processes of siRNA based knockdown starting from cellular uptake of siRNA nanoplexes to endosomal release of siRNA in the cytosol, binding of siRNA to the Dicer complex and degradation of GFP mRNA [49].

Both fluorescent microscopy and flow cytometry results revealed an identical knockdown of 75% for nanoplexes built with unmodified chitosan, chitosan_PEG 1.5%, 3% and 4%. Chitosan_PEG 6% and 8% nanoplexes showed much lower knockdown of only 35% and 15% respectively. Therefore, assuming a similar cellular uptake for all PEGylation ratios of chitosan:siRNA nanoplexes, which was shown with fluorescent siRNA (Figure 32), the efficient knockdown of mRNA was only influenced by the intracellular behavior of the nanoplexes. Thibault *et al.* [104, 108] showed that an excess of chitosan can protect the siRNA in the lysosome from degradation. At the same time the degradation of some of the extra chitosan not bound to the nanoplexes could induce a faster destabilization of the nanoplexes leading to a faster siRNA release from the nanoplexes once in the cytosol. In the current study, one hypothesis could be, that the lower number of charges on chitosan_PEG 6 and 8% might not be enough to promote a strong proton sponge effect to induce efficient endo-lysosomal siRNA release. The other hypothesis could be, that the lower positive charge

number of the higher PEGylated nanoplexes might influence the stability of the nanoplexes in the lysosome and reduce the protection of the siRNA. These knockdown results contradict other studies, which hypothesize that a higher PEG density leads to a higher transfection efficiency [250]. Nevertheless, a comparison of results generated with different assays is difficult, as different processes involved in the whole RNAi process might show different dependencies on the PEGylation rate of chitosan.

As outlook, further experiments should be carried out to understand the protein corona formed on the nanoplexes, once in CCM. Also the DLS information regarding the size determination in CCM needs to be improved and alternative methods such as single particle tracking [251] and flow cytometry-based size determination [77, 252] should be tested. Furthermore, as the zeta potential was only characterized according to different pHs and different cell environments, a time dependence could offer more information about the charge changes at the nanoplexes once inside the cell. Furthermore, detailed analyses of intracellular trafficking [104] and stability of the nanoplexes could give a better understanding of the whole RNAi process which could help to improve nanoplexes further. All these further detailed physical chemical characterization should be again correlated to more detailed biological studies, such as knockdown measurements at different time points.

4.3. Targeting of the chitosan_PEG siRNA delivery system

The lack of efficient methods to specifically deliver siRNA represents one of the major obstacles for the therapeutic applications of RNA interference (RNAi). A selective targeting of specific cells could improve the specific cellular uptake, decrease the overall dosage of siRNA required for effective RNAi and minimize off-target silencing and side effects in other cells [174].

In this study chitosan_PEG siRNA nanoplexes were synthesized and characterized with the aim to coat pharmaceutical implants and prevent the prolonged foreign body response. Therefore, FAP was chosen as a selective target for activated fibroblasts in tissues undergoing remodeling of their ECM due to chronic inflammation or fibrosis [253]. The scFv'LCH3 developed by Messerschmidt *et al.* [176] to target FAP, was chosen as one specific ligand for our nanoplexes. The cysteine residue incorporated in the flexible peptide linker (LCH) of the scFv'LCH3 offered the possibility to selectively bind the targeting ligand molecule to the

surface of the delivery system. The thiol bearing cysteine is located opposite to the antigen-binding site, as shown by structural analysis, and should therefore be highly accessible for site-directed coupling without interference with the FAP binding ability [177].

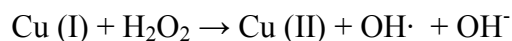
In order to bind the scFv'LCH3 to the nanoplexes a heterobifunctional linker was synthesized. One end of the linker had to be selective to the cysteine residue of scFv'LCH3 and the other end had to be reactive towards one moiety of the chitosan_PEG siRNA nanoplex, not present on the targeted molecule or in the reaction environment. The bioconjugation of the scFv'LCH3 required also mild reaction conditions in aqueous solutions, at pH values close to neutral and temperatures lower than 55°C [254] in order to prevent protein denaturation or precipitation. For the bioconjugation with the scFv'LCH3, maleimide was chosen as an excellent thiol-selective reagent. Messerschmidt *et al.* [177] also successfully functionalized polystyrene particles with a maleimide sulfo-SMCC linker and immunoliposomes with maleimide_PEG_DSPE. Other groups also choose the activated NHS ester_PEG_Maleimide heterobifunctional linker for the reaction of the NHS ester with an amino-functionalized surface and the relatively stable, but highly reactive maleimide group for the coupling to biological targeting molecules [255]. However, due to the high reactivity NHS ester with amino groups [256] and its fast hydrolysis in aqueous buffers [257], it is imperative to react the NHS ester first with the primary amino groups of chitosan. Conjugation to the scFv'LCH3 is performed afterward. Such an approach is not ideal. The coupling of the chitosan_PEG_maleimide to the single specific cysteine thiol groups of the protein ligand is much more difficult than the conjugation of the scFv'LCH3 to the low molecular weight NHS_PEG_maleimide prior to chitosan attachment. Furthermore, the identification and characterization of the scFv'LCH3 bound only to the NHS_PEG_maleimide, would be much easier in comparison to the analysis of a chitosan_PEG_maleimide_scFv'LCH3 polymer. Therefore, the first step was to modify the chitosan with an azide group enabling click chemistry based bioconjugation with several ligand proteins at the polymer. The azide moiety is stable, extremely small and biologically inert. Therefore it has no competing chemical reaction.

Furthermore, azide moieties are well characterized 1,3-dipoles for high region and stereoselective 1,3-dipolar cycloaddition reactions. Such reactions can be performed as so called "Click Chemistry" under mild aqueous conditions compatible with biological systems even in the presence of cells [258, 259] or inside cells [190, 260]. Even when the covalent attachment of the ligands was not performed in the presence of cells, copper ions could either

be bound to the chitosan moieties and could influence cell behavior in the bioassays in a negative manner. Therefore, copper free click reaction were developed for applications in biology [261, 262].

As chitosan represents a biopolymer with metal complexing character, the use of copper represents a disadvantage in terms of residual copper, with cytotoxic properties (class 2 metal acc. to ICH guideline). The effect of copper binding to chitosan was investigated by Lallana *et. al* [226] and it was revealed that even after several work-up procedures trying to remove the residual copper, a content of 200-700 ppm could still be found attached to the chitosan polymer. As the ICH guideline limits oral exposure to 250 ppm and parenteral exposure to 25 ppm the copper contamination is not acceptable for drugs or chemicals used in biology.

Another disadvantage of Cu (I) catalysis is the degradation of chitosan via OH· radicals formed via a Cu (I) based oxygen radicals generation analog to the iron catalyzed Fenton reaction. H₂O₂ is generated by copper mediated formation of a superoxide anion radical [O₂]⁻, which finally leads to hydrogen peroxide disproportionation [263]. The formed hydrogen peroxide serves as substrate for the Fenton analog reaction, initializing the radical mediated decomposition of chitosan.



Due to the tight complexation of copper ions to the amino functionalities of chitosan, the generation of the OH· radicals takes place next to the polymer backbone. The direct interaction of the OH· radical with the neighboring hydrogen atom at C₁ of the glucosamine in chitosan results in an effective degradation of the polymer. The close proximity of generated radicals to the polymer backbone makes the use of radical scavengers ineffective as shown by Riguera *et. al* [226]. The mechanism involves an exceedingly rapid abstraction of C-bonded hydrogen atoms accompanied by the formation of new radicals, resulting in breaking glycosidic bonds as shown in Figure 69.

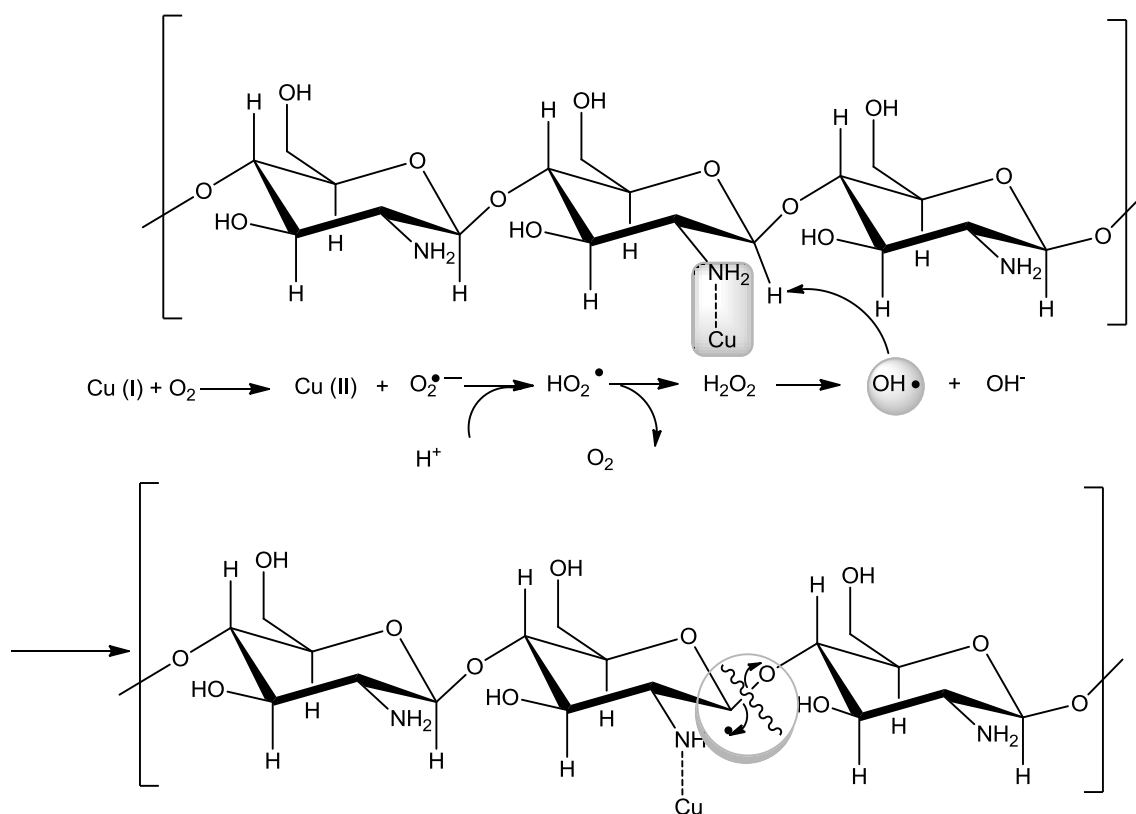


Figure 69. Copper mediated degradation of chitosan. Cu (I) can be oxidized by molecular oxygen to Cu (II) resulting in a superoxide anion radical which shows disproportionation to oxygen (O_2) and hydrogen peroxide (H_2O_2). H_2O_2 is oxidizing Cu (I) to Cu (II) in a Fenton analog reaction yielding OH and hydroxyl radical which reacts to water with the neighboring hydrogen at C_1 of the glucosamine moiety. This further leads to radical depolymerisation of the chitosan by breaking the β -1,4-glycosidic bond.

As we already optimized the chitosan_PEG siRNA nanoplexes and as the targeting ligand should be located on the surface of the nanoplexes, the azide group was incorporated at the distal end of the PEG chain, not of directly on the chitosan backbone [232]. The second step in the linker modification was to replace the chemically stable NHS ester with a stable cyclooctyne moiety [261]. We relied on the orthogonality of the click chemistry via strain-promoted alkyne azide cycloaddition (SPAAC). This coupling technique proceeds in high yields under mild physiological conditions [226]. The last modification of the linker system was the introduction of a tetra PEG spacer between the two reactive distal end groups to offer more flexibility to the linker [226] (Figure 70). The length of the PEG chain can be further modified for a better exposure to the biological environment.

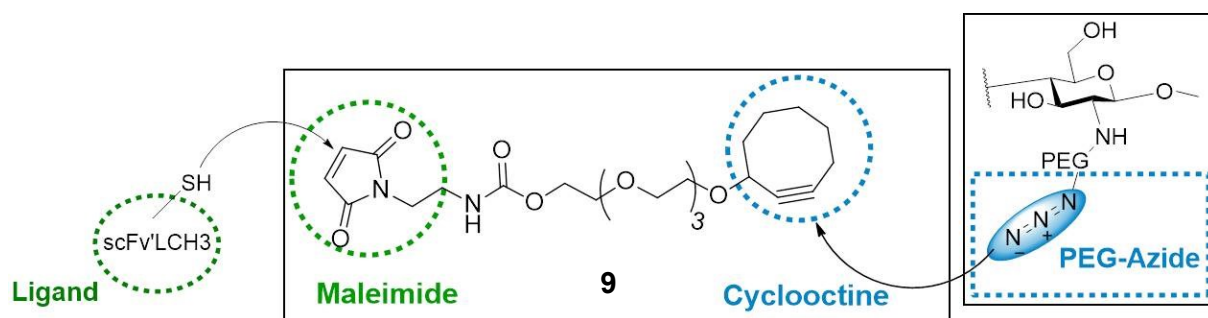


Figure 70. Chitosan_PEG_N₃ modification with scFv'LCH3 using heterobifunctional linker system developed for optimization of nanoplexes delivery to activated fibroblasts. The scFv'LCH3 protein ligand can be easily attached to linker (9) via specific Michael reaction with the free thiol group of the scFv'LCH3 protein. The modified protein can be coupled to azide groups at the distal end of PEG chains grafted to chitosan. This 1,3 dipolar cycloaddition is specific as well and can be performed under physiological conditions.

The site-direct coupling of the cyclooctyne_PEG_maleimide linker, compound **9**, was tested first with a small peptide, HC-Doa-Doa-EQKLISEEDL-OH (~1.5kDa). The bioconjugation took place under physiological conditions and was characterized via analytical HPLC and MALDI-ToF MS. Given the successful binding of the peptide, the bioconjugation of the scFv'LCH3 to compound **9** was performed under the same conditions. However, after purification via centrifugal ultrafiltration the bioconjugated scFv'LCH3 precipitated. Aggregation or precipitation of the proteins [264, 265] e.g. monoclonal antibodies [266] is a common issue. One option to prevent such precipitation is to use additives preventing protein aggregation [267]. Tween20 (polysorbate 20) was used as a surfactant [268]. As the critical micelle concentration of Tween20 is 0.007%, we used 0.01% for the bioconjugation. The surfactant seemed to have formed micelles with the bioconjugate scFv'LCH3 and successfully prevented its precipitation during purification. The concentration of the scFv'LCH3 with 0.01% Tween20 compared to a control sample without Tween20 was much higher with than without 0.01% Tween20 after ultrafiltration. The micelle formation around scFv'LCH3 prevented its binding to the filter membrane successfully. The modified scFv'LCH3, compound **15**, was successfully identified via SDS-PAGE and also analyzed by LC-MS. However, in the LC-MS analysis of the full length modified scFv'LCH3 only proteolytic cleavage products from the scFv'LCH3 production, could be detected. Together with these secondary products two additional products were identified with a mass difference of exactly 466 Da, the mass of the cyclooctyne_PEG_maleimide linker. The proteolytic cleavage products (~17 kDa) with cysteine groups also reacted with the maleimide moiety of the linker system. Therefore, compound **9** proved its versatility to bind specifically to biological

targeting ligands with Mw from 1.5 kDa to 28 kDa, with an available free thiol group. For further applications it was important to take into consideration the possibility of a polymerization of compound **9** via cycloaddition of maleimide and cyclooctyne. For long term storage of the bifunctional linker **9** a protection of the maleimide functionality is recommended. For example furans can be used to protect the maleimide group via a Diels-Alder and the corresponding retro Diels-Alder reaction [228]. Also, in order to completely avoid the polymerization of the linker system **9**, the maleimide functionality was replaced with an iodo ester and iodoacetamide groups, which were stable in solution at 4°C. However, the binding to large biological molecules with free thiol groups was not tested so far.

FAP is not a cell surface receptor, but it is a membrane associated gelatinase. It is still unclear how the scFv'LCH3_immunoliposomes in the investigations of Messerschmidt *et al.* [177] were internalized. Kelly *et al.* [269] indicated that FAP executes its biological function through a combination of the protease activity and the ability to form complexes with other membrane-bound signaling molecules. Therefore, an alternative to target FAP via the scFv'LCH3 antibody, could be the attachment of a FAP selective chemical inhibitor of the gelatinase activity. Prof. Van der Veken and his group have designed and synthesized such FAP selective chemical inhibitors [167, 178] and provided us with one of their high affinity inhibitors modified with an endcap azide. In order to bind this small chemical inhibitor to the nanoplexes, the linker system was further modified. The maleimide group was replaced by another cyclooctyne moiety and both ends were reacted with the azide groups. First the FAP chemical inhibitor was conjugated to one end of the cyclooctyne forming a stable triazole bond. The other cyclooctyne end can be bound to the chitosan_PEG_N₃ before or after the nanoplex formation.

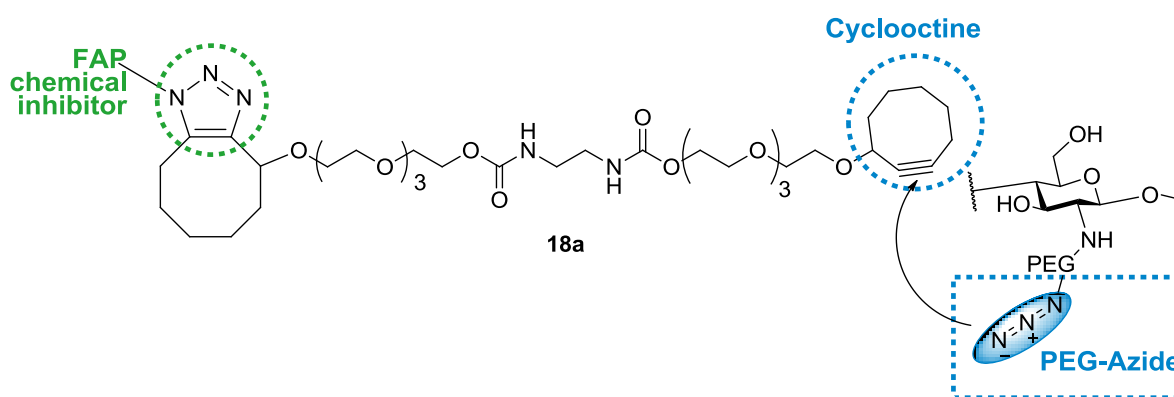


Figure 71. Chitosan_PEG_N₃ modified with a FAP selective chemical inhibitor using a homobifunctional linker system with cyclooctynes at both ends of the linker molecule. Stoichiometric balance of octyne and azide groups enables attachment of

the chemical FAP inhibitor to one end of the linker. This modified inhibitor was still active and could be attached to azide-modified chitosan in a separate 1,3-dipolar cycloaddition reaction.

The potency and selectivity of compound **18a** was tested at the Univ.of Antwerp (Table 18). With an IC_{50} of 0.05 μ M, compound **18a** maintained a high binding activity and selectivity towards FAP and dipeptidylpeptidase (DPP) 8, DPP9, DPPII and showed a lower selectivity towards DPP IV and PREP (prolyl oligopeptidase).

The bifunctional linker system **18a** was designed and synthesized to bind to the chitosan_PEG_N3 before or after the nanoplex formation. Therefore, the reaction between the cyclooctyne and the chitosan_PEG_azide was tested As a proof of concept PEG-azide was reacted with the cyclooctyne and the azide groups in 1% DMSO/D₂O over 72 h at room temperature. The successful triazole formation was analyzed via MALDI-ToF-MS which showed a mass shift of the polymer mass distribution of 300 Da corresponding to the linker mass. Therefore, the linker system can be attached to the chitosan_PEG_N₃ before or after the nanoplex formation in an aqueous buffer within 72h. For the coupling directly to the nanoplexes a time control reaction at 4⁰C should be considered to investigate the potential degradation of the scFv'LCH3 and of the nanoplex.

As an outlook, a dual-targeting strategy on the surface of the siRNA delivery system could be advantageous for specific siRNA delivery to specifically activate fibroblasts [194]. Based on the new linker systems, both the biological targeting ligand and the small chemical inhibitor molecule can be attached to siRNA chitosan nanoplexes to target FAP on the surface of active fibroblasts which could lead to better transfection efficiency.

4.4. Local delivery via LBL coating and release

Although the bulk properties of biomaterials should not be ignored, surface functionalization is of utmost important with respect to biomedical applications [270]. Therefore, polymers such as chitosan have great potential to coat implants in order to change the chemical and physical properties, as well as incorporating active substances at the surface material. One critical issue with pharmaceutical implantable devices the foreign body response (FRB) (Figure 1). Therefore, the bioactive surface of implantable devices could be coated with chitosan:siRNA

nanoplexes targeting the mRNA knockdown of the hsp47 chaperon in order to trigger the healing process, but prevent it from evolving to the formation of the fibrous capsule (see 1.2).

One possibility to immobilize the chitosan:siRNA nanoplexes on implant surfaces is to incorporate them into polyelectrolyte multilayers (PEMs) via LbL assembly. Previously in our group, biocompatible and biodegradable polymers HA and Chi were used for solid surface coatings due to their low toxicity [271]. Furthermore, PEM chi:siRNA nanoplexes at N/P ratio 50 were successfully used for neuronal implant coatings [44] and coronary stent coatings [272]. In the current work chi:siRNA nanoplexes and PEG modified chi:siRNA nanoplexes were used at N/P ratio 25. Therefore, the N/P ratio 25 and the PEG influence on the multilayer assembly and release was tested. The examined continuous adsorption of five bilayers of HA/chi:siRNA nanoplex via QCM was successful and similar to literature [44] (Figure 66). However, PEG modified chi:siRNA nanoplexes PEM incorporation revealed a decrease in bilayer adsorption with increasing nanoplex PEG grafting. The bilayer deposition decreased from 4 layers for nanoplexes formed with chi_PEG 3% DS to 3 layers for chi_PEG 4% DS and 2 layers for chi_PEG 8% DS Figure 66. As the LbL assembly is achieved via electrostatic interaction [201], the charge of the polyelectrolytes forming the coating is extremely important. The zeta potential of chi_PEG:siRNA nanoplexes was shown to decrease with increasing PEG grafting, chi_PEG 8% DS having the smallest zeta potential of 8 mV in comparison to 18 mV for unmodified chi:siRNA nanoplexes (Figure 26).

The release of the nanoplexes immobilized in non-fluorescent PEMs was followed by using Tye563 labeled siRNA. The decrease in chi_PEG:siRNA NP layer build-up with increasing PEG densities on the nanoplex surface correlated to the release behaviour in the first 24h. The nanoplex release was slower for the coatings with HA/Chi_PEG 4% nanoplexes when compared to HA/Chi_PEG 8% nanoplexes and revealed a uniform release up to 96h (Figure 67).

For specific targeting of the activated fibroblasts chitosan was modified with PEG_azide with a DS of 1.7 %. Therefore, the DS is small enough to not affect the successful nanoplex layer build-up. This approach can be directly translated to nanoplexes using FAP small chemical inhibitor as a targeting moiety. However, for the biological molecule (e.g. scFv'LCH3) targeting molecule, the nanoplex formation should be tested in PBS at pH ~7.0.

5. Conclusions

The goal of the work was to establish a chitosan siRNA delivery system which is able to target fibroblast cells and specifically inhibit the collagen synthesis in these cells via RNAi knockdown of hsp47.

As there were no in house chitosan characterization methods and no chitosan synthesis experience available, first such standard procedures were established. From a variety of spectroscopic and conventional methods for the characterization of chitosan, we established and optimized the characterization of chitosan via infrared spectrometry, gel permeation chromatography, and ^1H NMR. Then a library of chitosans with different molecular weights and degrees of deacetylation was synthesized and characterized. It was shown that all of these chitosans could form nanoplexes with siRNA via electrostatic interactions. However, the size and charge of these nanoplexes needed to be taken into consideration for the transfection and knockdown efficiency. The correlation of structural chitosan characteristics with nanoplexes formation allowed to choose an optimal commercially available chitosan (Heppe) with a molecular weight of 152 kDa and a degree of deacetylation of 92.6%, and low protein content (0.5%).

Chitosan solubility at higher pH values was improved by further grafting chitosan with PEG at different degrees of substitution, between 1.5 and 8% (mol %). The properties of the nanoplexes with increasing PEG densities was tested in buffer and cell culture medium, at different pH values and over time. Several trends were noticed and correlated well with biological results. In buffer, PEG grafting led to the formation of smaller size nanoplexes. In cell culture medium, the zeta potential of the nanoplexes showed, that increased PEGylation can minimize unspecific interactions with the proteins present in cell culture medium. However, DLS experiments in cell culture medium indicated towards the formation of a protein corona even at higher PEG substitution. The biological characterization of the nanoplexes indicated that increased PEGylation actually had no effect on cell uptake efficiency. The successful uptake of all different nanoplexes with a similar efficiency could be due to the similar protein corona formed on the nanoplex surfaces. Further characterization of the PEGylated nanoplexes at lower pHs indicated a decrease in the charge difference between pH 7.0 (extracellular pH) and ~ 4.5 (endo-lysosomal pH). Chitosan_PEG 6 and 8% showed the lowest decrease in charge difference which also correlated to the knockdown efficiency found in the GFP cell model. Unmodified chitosan and chitosan PEGylated nanoplexes with a

low degree of substitution of 1.5 to 4% showed a knockdown of ~75%, while for chitosan_PEG 6 and 8% the knockdown was only 35% and 15% respectively.

PEG was used as a spacer, which offered the flexibility to add the targeting molecules on the surface of the nanoplexes before or after the nanoplex formation. The distal end of the PEG chain was modified with an azide and a cyclooctyne_linker was synthesized with maleimide functionality for binding the biological targeting molecule (compound **9**). A single chain antibody scfv'LCH3 was chosen to target the FAP protein on the surface of active fibroblast cells. Furthermore, a *novel* linker system with a small FAP chemical inhibitor was synthesized as an alternative targeting molecule (compound **18**). The highly selective FAP inhibitor was modified with an azide end group. Therefore the heterobifunctional linker was changed to a homobifunctional linker with two cyclooctyne groups. Both targeting molecules, the scFv'LCH3 antibody as well as the small inhibitor molecule, were successfully attached to the same linker system and yielded an activated targeting ligand with a conserved chemical functionality and selectivity for the FAP target.

The binding between the linker and the chitosan_PEG_N₃ was proven by the reaction between HOOC_PEG_N₃ and the hydroxy cyclooctyne_linker and could be confirmed by MALDI-ToF-MS analysis of the molecules.

Therefore, the system for the specific siRNA delivery to activated fibroblast cells was fully established (Figure 72). Functional assay in activated fibroblast cells could not be performed so far.

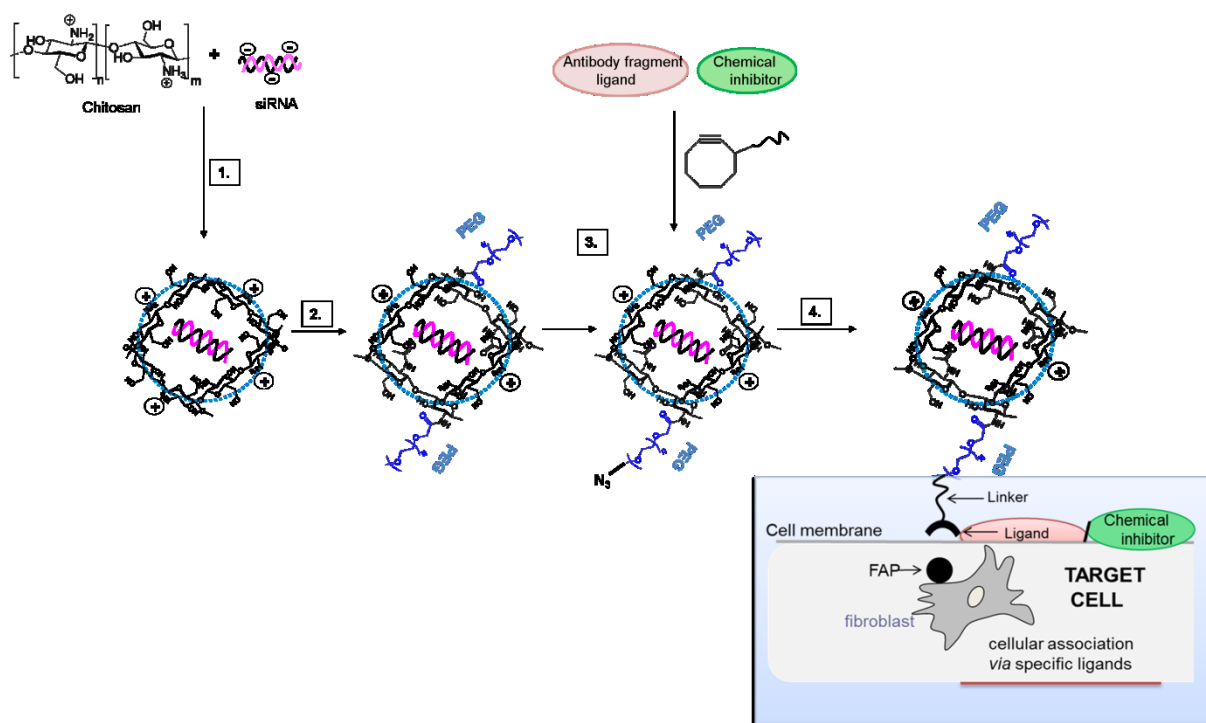


Figure 72. Scheme of the established chitosan siRNA delivery system for targeted siRNA in activated fibroblast cells. 1) Nanoplex formation from chitosan siRNA for knockdown of hsp47 in collagen synthesis 2) Nanoplex PEGylation 3) The PEGylated nanoplex was modified with the targeting ligand, which reacts with terminal azide groups of the PEG nanoplexes via 1,3-dipolar cycloaddition with cyclooctyne 4) The modified nanoplexes recognize activated fibroblasts by specific binding of the targeting ligand to the FAP gelatinase at the cell surface. After internalization endo-lysosomal release and RNAi based knockdown of the hsp47 mRNA collagen synthesis would be reduced;

The chemical uniformity of siRNAs as a molecular class with similar physicochemical properties means that the know-how from the development of one siRNA drug candidate can be applied to nearly every other oligonucleotide delivery. Furthermore, the linker system synthesized proved its versatility by binding biological targets with various masses and chemical inhibitors as *novel* targeting molecules.

Furthermore, the proof-of concept with Chi_PEG:siRNA nanoplex coatings of solid surfaces can further be used for incorporation of nanoplexes with the targeting moieties and developing implant coatings with bioactive properties.

6. Materials and methods

6.1. Materials

Table 9. Table of chemicals and reagents

Chemicals/Reagents	Company
30 % Acryl amide	Carl Roth, Karlsruhe
30 vol.% H ₂ O ₂ :70 vol.% H ₂ SO ₄ 1:1,	Carl Roth, Karlsruhe
Agarose	Carl Roth, Karlsruhe
Ammoniumperoxidisulfate (APS)	Merck, Darmstadt
Ampiciline	Carl Roth, Karlsruhe
Bovine Serum Albumin (BSA)	PAA, Cölbe
Bromoform	Sigma-Aldrich, Taufkirchen
Chitosan 95/50	Heppe Medical Chitosan ,Halle (Saale)
Coomassie Brilliant Blue R-250	Sigma-Aldrich, Taufkirchen
Cycloheptene	TCI, Eschborn
DAPI (4',6'-Diamidino-2-phenylindol)	Sigma-Aldrich, Taufkirchen
Dimethylsulfoxide (DMSO)	Sigma-Aldrich, Taufkirchen
di-Sodiumhydrogenphosphate	Carl Roth, Karlsruhe
Dithiothreitol (DTT)	Carl Roth, Karlsruhe
Dulbecos Modified Eagle Medium (DMEM)	PAA, Cölbe
Fetal Calf Serum (FCS)	PAA, Cölbe
Geneticinsulfate (G-418)	Carl Roth, Karlsruhe

Gentamycine	PAA, Cölbe
Glucose	Carl Roth, Karlsruhe
H ₂ N-PEG-N ₃ , PEG Mw 5000 Da	Rapp Polymere, Marktredwitz
Hyaluronic acid, 360 kDa	Lifecore Biomedical, Chaska, USA
Inhibitorcocktail His-tag	Carl Roth, Karlsruhe
Isopropyl-D-thiogalactopyranosid (IPTG)	Carl Roth, Karlsruhe
L-Glutamine	PAA, Cölbe
N-(2-Aminoethyl)maleimid Trifluoroacetic acid (TFA)	Sigma-Aldrich, Taufkirchen
N-(2-Aminoethyl)maleimide TFA	Sigma-Aldrich, Taufkirchen
N,N'-Disuccinimidyl carbonate	Sigma-Aldrich, Taufkirchen
Normal Goat Serum (NGS)	Jackson ImmunoResearch, Baltimore, USA
Paraformaldehyde (PFA)	Carl Roth, Karlsruhe
Penicilin/Streptomycin	PAA, Cölbe
Phenylmethylsulfonylfluoride (PMSF)	Sigma-Aldrich, Taufkirchen
Phosphat-gepufferte Saline (PBS)	PAA, Cölbe
Poly-Aspartic Acid (PAA)	Santa Cruz, Heidelberg
Polyethylene glycol (Mw = 21 kDa)	Malvern Instruments, Herrenberg
Polystyrolsulfonat Natriumsalz	Sigma-Aldrich, Taufkirchen
Resazurin	Sigma-Aldrich, Taufkirchen
Ultrapure 18.2 MΩ water	Satorius, Goettingen,

All other chemicals and reagents were purchased from Sigma Aldrich, Carl Roth, ACROS and Merck.

Table 10. Table of consumables

Consumables	Company
Millipore column	Merck, Darmstadt
Microtiter plates	Greiner, Frickenhausen
Ni-NTA Agarose Beads	Qiagen, Hilden
Sterile filter (0,2 µm, 0,45µm)	Satorius, Göttinge
Fluotrac 96-well plates	Greiner Bio-One GmbH, Frickenhausen,
ViscoGel A6000M (mixed Bed) column	Malvern Instruments GmbH, Herrenberg
Folded capillary cells	Malvern Instruments, Herrenberg
Chromolith Performance RP-18e,	Phenomenex, Aschaffenburg
GromSil 120 ODS-4 HE, 7µm 125x30mm	Chromspec, Brockville, Canda
GromSil 120 ODS-4 HE, 7µm 150x50mm	Chromspec, Brockville, Canda
GromSil 120 ODS-4 HE, 7µm 30x30mm	Chromspec, Brockville, Canda
D-Tube Dializer, Midi,, MWCO 3,5 kDa	VWR, Darmstadt

Table 11. Table of instruments

Instrumentts	Company
Microscope Axiovert 200M	Carl Zeiss AG, Oberkochen
Äktar UPC900	GE Healthcare, Freiburg
Cell counter Casy	Schärfe System, Reutlingen
Centrifuge 5415C	Eppendorf AG, Hamburg
Centrifuge Rotofix 32 A	Hettich Zentrifugen, Tuttlingen
Flow cytometer Beckmann Coulter Cytomics FC 500	Beckmann Coulter Krefeld
FTIR	Thermoscientific, Munchen
GPC Viscotek Triple Detector Array max system	Malvern Instruments, Herrenberg
HPLC Dionex Ultimate 3000	Thermoscientific, Munchen
HPLC Varian Prep Star	Thermoscientific, Munchen
Maxis U3000 UHR-ToF	Thermoscientific, Munchen
Nanodrop 2000C Spectrophotometer	Thermoscientific, Munchen
PHERASTAR	BMG Labtech, Offenburg
Q-Sense AB,	Göteborg, Sweden
Typhoon Trio	GE Healthcare, Freiburg
Ultraflex III MALDI-TOF	Bruker, Daltonik, Bremen
UV/VIS spectrometer	Jesko, Munchen
Zetasizer Nano ZS particle analyzer	Malvern Instruments, Herrenberg

Table 12. Different antibodies

Antigen	Specie	Use and dilution	Reference source
FAP	Mouse	IF 1:300 IC 1:100	Santa Cruz
His-tag	Mouse	WB: 1:5000 IC: 1:100	Santa Cruz

(WB = Western blot, IF = immunofluorescence microscopy)

Table 13. Secondary antibody

Name/Specie	Use and dilution	Reference source
Goat-anti-Mouse Cy3	IF 1:300 FC 1:100	Jackson Immuno Research

(IF = immunofluorescence microscopy, FC= flow cytometry)

6.1.1. Table 14. Different siRNA's

siRNA	Stock concentration	Reference source
GFP	50 μ M	Applied Biosystems
Negative control	50 μ M	Applied Biosystems
Negative control Alexa 488	20 μ M	Qiagen
TYE 563 DsiRNA Transfection Control	5 mM	Integrated DNA Technologies

				Ingelheim Pharma KG
HT1080 FAP	HT1080wt transfected with with human pFAP .38(Klone #33)	DMEM	10% FCS, 1%L-Glutamin, 0,5% Gentamycin, G418	Wolfgang J. Rettig, Boehringer Ingelheim Pharma KG

6.1.4. Buffers and solutions

1xRunning Buffer SDS-PAGE	50 mL 20x NuPAGE MES in 1 L H ₂ O
1% BSA/PBS	10 g BSA in 1 L PBS
5x Bradford reagent	100 mg Coomassie Brilliant Blue 47 ml Methanol (100%) 100 ml Phosphoric Acid (85%) in 200 ml H ₂ O
5 µg/ml DAPI	1,5 ml DAPI in 148,5 ml PBS
4% PFA/PBS	40 g PFA in 1 L PBS pH 7.4
300 mM Sodium Acetate Buffer	2,72 g Acetic Acid 20,89 g Sodiumacetate in 1L H ₂ O pH 5,5, steril filter (0,2µm)

5x Sodium Phosphate Buffer

37.38 g $\text{Na}_2\text{HPO}_4 \cdot 2\text{H}_2\text{O}$

6.24 g $\text{NaH}_2\text{PO}_4 \cdot 2\text{H}_2\text{O}$

1.25 M NaCl, pH 7.5

in 1 L H_2O

Periplasma-Lysis Buffer

30 mM Tris-HCl pH 8.0

1 mM EDTA

20 % Sucrose

in H_2O

6.2. Biological and biochemical methods

6.2.1. Chi, Chi_PEG and NP cell viability

The cytotoxicity of chitosan, modified chitosan, and linker system was evaluated via the resazurin assay (data provided by L. Schuster NMI, page 73) [49]. H1299-GFP cell were used. Once the cells reached ~70% confluence, the samples were added. The medium was changed after 6 h and the cells were cultured for another 48 h before addition of resazurin. Depending on the cell type, the cells were left for 4 h to 6 h in the incubator until clear color change from blue to pink was evident. This was followed by photometric measurement. Untreated cells were considered as 100% viable and the viability of the remaining samples was normalized to the signal from the untreated cells measured as absorbance at 570 nm. DMSO-treated cells were used as a death control. For the analysis, the blank value was subtracted from all values and all other values normalized to the untreated cell control. These samples were incubated in H1299-GFP cell in triplicates at a concentration of 0.18 mg/mL, left as in a transfection experiment for 6 h before changing the medium. The cytotoxicity measurements were performed after 48 h.

The resazurin assay was performed in an analogue manner to the the chitosan and Chi_PEG samples in H1299 with a 200 nM siRNA final concentration in each well of 200 nM.

6.2.2. Cell culture for immunocytochemistry

The cultivation of human fibrosarcoma cell lines HT1080 FAP (HT1080#33) as well as HT1080 wild-type cells were performed by Dr. Liane Schuster and Dr. Dominic Stadel in uncoated tissue culture flasks. The medium was changed every two or three days or if necessary the cells were passaged. The cells were seeded with 2.5×10^4 cells/cm² (HT1080 wild-type) or 5×10^4 cells/cm² (HT1080 FAP) in 48-well plate, in 250 µl of medium, at 37°C and 5 % CO₂.

6.2.3. Immunocytochemistry

For fluorescence microscopy the cells were cultured and stained directly in 48-well plates. First, the cells were washed once with PBS and subsequently fixed with 4 % paraformaldehyde in PBS, for 30 min at RT. They were then washed 3 times with PBS to remove the residues of fixing agent. To prevent non-specific antibody binding the cells were

blocked with 5 % NGS and 1 % BSA in PBS, at RT for 45 minutes. Then, the primary antibodies (10 µg/ml) were diluted (1:100) with 1 % BSA in PBS and stained for 1 h at RT or overnight at 4 °C. After three washes with PBS, the secondary antibody (goat-anti-mouse Cy3) was diluted (1:300) with 1 % BSA in PBS and added on the cells for 45 minutes. The cells were washed again three times with PBS before the staining of the nuclei with DAPI (5 µg/ml) for 10 minutes. As the coloring was directly into well plates, two PBS washing steps were necessary before measuring the sample via fluorescent microscopy.

6.2.4. Expression and purification of scFv'36LCH3

6.2.4.1. Periplasmic protein expression in *Escherichia coli*

FAP-specific antibody fragment, scFv'36 LCH3, was expressed using the *Escherichia coli* TG1 bacterial strain. The scFv'36 LCH3 construct was amplified at the University of Stuttgart from pAB1 scFv36 with the primers stop-*EcoRI*-For and LCH3-*XhoI*-Back. The PCR products were digested with *XhoI* and *EcoRI* and cloned into pAB1 scFv36 digested with the same enzymes [177]. For protein expression, a preculture of the TG1 bacteria were first inoculated from the glycerol stock in LB medium with ampicillin (100 µg/mL) and 1 % glucose and then incubated under gentle shaking (140 rpm) overnight at 37°C.

For 2 x 2 L scale production, 40 mL of the overnight culture were added to 4 L of 2 x TY medium with 0.1 % glucose and ampicillin (100 µg/mL) in 5 L baffled flasks. The bacteria culture was then cultivated on a rotary shaker (140 rpm) at 37°C until an optical density (OD₆₀₀) of about 0.6 – 0.8 was reached. Induction of scFv'LCH3 was started by addition of IPTG (end concentration 1 mM). Expression of the antibody fragment was carried out overnight at 20°C (120 rpm) to keep the scFv'36LCH3 soluble and prevent the accumulation of the overexpressed protein in inclusion bodies.

The next day, bacteria were harvested at 4°C *via* centrifugation (5 min at 6000 g). The cell pellet was either processed immediately or stored for a longer period in at -80°C.

The pellet was resuspended in 40 mL periplasmic lysis buffer. Fresh lysozyme (10 g/L), protease inhibitor cocktail (100x), PMSF and DNase (25 mg/mL) were added to the resuspended cell pellet and left to incubate while rolling the tube for 1 h at 4°C. Subsequently, cells were completely disrupted by ultrasonication pulses, (5 times pulsing for 30 seconds followed by 1 minute incubation on ice) to prevent heat denaturation of the protein. Protein extract was isolated as supernatant after ultracentrifugation (12000 rpm, 4°C, for 20 min) in

falcon tubes (50 mL) and immediately purified either by metal ion affinity chromatography (IMAC) or fast protein liquid chromatography (FPLC).

6.2.4.2. Purification by IMAC

Table 16. Purification buffers for IMAC and FPLC

Buffer	Na-Phosphate Buffer pH 7.5	NaCl	Imidazole
Washing buffer/ Binding buffer	50 mM	250 mM	35 mM
Elution buffer	50 mM	250 mM	250 mM

Ni-NTA agarose beads (500 μ L for 10 mL lysate) were added to the protein extract supernatant and left to incubate while rolling the tube for 3 h at 4°C. Then the agarose beads were transferred to separating columns (1 mL) and washed with washing buffer (10 mL) for a minimum of 4 times. The presence of unbound proteins in the flow through fraction was checked using Bradford reagent (90 μ L Bradford reagent per 10 μ L of eluate incubated in 96 well plate). The scFv'36 LCH3 was collected by the addition of 500 μ L elution buffer. This step was repeated 4 to 5 times until there were no or only small amounts of proteins in the eluate (tested with Bradford reagent). The fractions with the highest protein concentration were pooled and dialysed overnight against PBS at 4°C and concentrated using (500 μ L).

6.2.4.3. Purification by FPLC

The collected supernatant of the bacteria lysate after ultracentrifugation, containing the histidine tagged scFv'36 LCH3, was purified on an ÄKTA system in two steps. First the His-tagged protein was captured on a 1 mL HisTrap FF (GE) column. Then the eluted protein fraction was further purified, using gel filtration chromatography, on a Superdex_75_10/300 GL column.

To avoid column clogging, the protein extracts had to be fully dissolved and were filtered through a 0.45 μ m filter to remove cell debris or other particulate material which might be present in the protein extract supernatant.

As a general rule first you have to equilibrate the column with 3-5 bed volumes equilibration buffer so as to provide optimum binding conditions (in cases where protein will bind to

column matrix first and will be eluted later). Then you can load your protein. After that you can elute the protein with elution buffer which is again dependent on the column (e.g. increasing concentration of salt (NaCl) or change of pH in case of ion exchange, increasing concentration of ethylene glycol in case of hydrophobic interaction chromatography). Needless to mention every buffer has to be used 3-5 bed volumes. Before elution you may include one wash step where unbound or loosely bound proteins may elute.

Purification #1 (HisTrap FF)

Flash system with 3 to 5 column volumes of binding buffer for 2 minutes at a flow rate of 10mL/min. Then equilibrate the column with 5 column volumes with a flow rate of 1mL/min.

Inject sample in sample loop using a 2 mL syringe and leave flow to 0.5ml/min until the binding buffer reaches port valve 2. Then put the flow at 10mL/min to put the HisTrap FF on to the UV chamber and connect it to valve 1.

Method: HisPurification 10mL Gradient 25mL >row by row.

Wash with binding buffer until the absorbance reaches the baseline. Then start eluting with the elution buffer using a linear gradient. The flow rate is fixed at 0.5mL/min for 4 column volumes.

After elution regenerate the column by washing it with 5 column volumes of binding buffer.

Run SDS-PAGE of the collected fraction that contain the scFv'LCH3.

Purification #2 (SEC)

Flash the system with PBS with a flow of 10mL/min for 30mL buffer.

Flow for the column 0.5mL/min and equilibrate the column with 1 column volume (approximately 23.5mL).

Inject 4 mL of PBS in the sample loop before adding the HisTrap purified fractions. Then inject the sample, with a syringe (minimum 2.2mL volume with no bubbles), into the sample loop without completely emptying the syringe.

The elution will run with a flow of 0.5mL/min for 1.5 column volumes.

Run SDS-PAGE and then Western-Blot before concentrating the samples for further use.

6.2.5. Antibody fragment characterization

6.2.5.1. Determination of the protein concentration

- a. The concentration of scFv-LCH3 was determined using the following formula from the UV absorption at 280 nm:

$$c \left[\frac{mg}{mL} \right] = M \left[\frac{mol}{L} \right] * MW \left[\frac{g}{mol} \right] = \left(\frac{OD280}{\epsilon} \right) * MW$$

where ϵ was calculated based on the amino acid sequence results [177] in:

$$\epsilon = (\text{number Trp} * 5540) + (\text{number Tyr} * 1480) + (nCys * 125)$$

(M = molarity, MW = molecular weight [g/mol = Da], ϵ = molar extinction coefficient)

- b. The concentration of scFv-LCH3 was determined by nanodrop using the extension coefficient (see a).

6.2.5.2. SDS-PAGE identification

Under non-reducing conditions 2.5 μ L of sample were added to 2.5 μ L of NuPAGE LDS sample buffer (4X) and 5 μ L of water. For reducing conditions 1 μ L NuPAGE reducing agent (10X) and 4 μ L of water were additionally added. The mixtures were heated for 10 min at 95 ° C, which further causes reduction and denaturation of the proteins. The whole sample was transferred to a gel pocket. In addition, a protein standard sample was applied as a M_w reference on each gel.

Electrophoresis was carried out in 4-12% Bis-Tris SDS-PAGE gel for 35 min at 200 V using MES running buffer.

The gels were then either stained by Coomassie or used for Western blot.

6.2.5.3. Coomassie brilliant blue gel staining

SDS polyacrylamide gels were stained using Coomassie Brilliant Blue G-250. Gels were incubated for 30 to 60 min at RT in Coomassie staining solution (0.25 % Coomassie Blue R250 in Coomassie destain solution). Subsequently, the excess stain was removed by multiple washes with Coomassie destaining solutions I and II. First, for about 30 minutes the gels were incubated under gentle shaking at RT in destaining solution I (500 mL Ethanol, 200 mL acetic acid in 1 L double distilled H₂O) and afterwards in destaining solution II (100 mL Ethanol, 50

mL acetic acid in 1 L double distilled H₂O) until low signal background and a good intensity of the protein bands was reached.

6.3. Physico-chemical methods

6.3.1. Nanoplex formation and characterization

6.3.1.1. Nanoplex formation

Chitosan and PEG-chitosans were dissolved overnight in an acidic aqueous solution (MQ water 5 ml and 25 μ l CH₃COOH). The next day the pH was adjusted to 5.5 with CH₃COONa*3H₂O; a final chitosan concentration of 1 mg/mL was obtained via the addition of H₂O. Prior to mixing, chitosan solution was sterile-filtered through a 0.45 μ m syringe filter. siRNA was added to the chitosan solutions under intense stirring at 1.200 rpm for 1 h to allow nanoplex formation, with a resulting 800 nM siRNA concentration. The nanoplexes were then left to stabilize for 15 minutes prior to characterization and further use. The nanoplexes were formed at a N:P ratio of 25:1 (defined as the molar ratio of chitosan amino groups:RNA phosphate groups) for all experiments.

6.3.1.2. Polyplex characterization Zeta Sizer

Nanoplex size and zeta potential were determined using a Zetasizer Nano ZS particle analyzer (Malvern Instruments, Herrenberg, Germany) at 22°C, 173° scattering angle by cumulative analysis. Size measurements were analyzed in CONTIN mode, in triplicates and reproduced minimum three times (N = 3 experiments and n = 9 total measurements). The absence of aggregates was assessed on basis of the correlation coefficient curve. Zeta potential analysis based on the electrophoretic mobility of the nanoplexes in aqueous buffer were performed using folded capillary cells (Malvern Instruments, Herrenberg, Germany) in automatic mode and calculated using the Smoluchowski equation. Zeta potential measurements were done in doublets and reproduced minimum three times (N = 3 experiments and n = 6 total measurements).

6.3.2. Stability measurement of chitosan/siRNA nanoplexes

Nanoplexes stability and siRNA integrity were investigated using a gel retardation assay. For this purpose, nanoplexes were either incubated with RNase free water or with polyaspartic acid (PAA) at 37°C for 30 min. PAA (5 mg/ml, Sigma, Taufkirchen, Germany) was used as a destabilizing control as it competes and displaces anionic siRNA from polycationic chitosan.

The stability of chitosan/siRNA nanoplexes was determined by 4% agarose (Promega, low melting point, Mannheim, Germany) gel electrophoresis containing ethidium bromide. Electrophoresis was carried out at a constant voltage of 55 V for 1.5 h in TAE buffer (2 M Tris, 250 mM sodium acetate, 50 mM EDTA, pH 7.8). The siRNA bands were visualized in a UV transilluminator.

6.3.3. Fluorescence Quenching Assay

The assay was completed in accordance with a previous study published by Merkel *et al.* [225]. In essence, Tye563-labeled DsiRNA (20 μ M) (IDT Leuven, Belgium) was complexed with chitosan and PEG-chi with the differing degrees of substitution analogue to the siRNA nanoplexes previously described. All nanoplexes were first formed in 0.3 M CH₃COONa buffer at pH 5.5, as described above, and only after PBS or cell culture medium (RPMI with 10% fetal calf serum and 1% L-Glutamate) were added in a ratio of 1:3 (volume ratio) with a final siRNA concentration of 200 nM. The nanoplexes were pipetted into opaque Fluotrac 96-well plates (Greiner Bio-One GmbH, Frickenhausen, Germany). Remaining fluorescence of the polyplex solution was quantified using a fluorescence plate reader (FLUOstar Optima, BMG Labtech, Ortenberg, Germany) at 545 nm excitation and 580 nm emission wavelengths. The experiments were performed in multiple series of three, and the results are given as mean relative fluorescence intensity values \pm SD. For normalization purposes, free siRNA in buffer or cell culture medium represents 100% fluorescence, while PBS or cell culture medium were subtracted as blanks.

6.3.4. Build-up of (HA/Chi)₂(HA/NP)_n PEM

The PEM films were deposited onto QCM quartz crystals. Before, starting the build-up, the quartz crystals were cleaned by ultrasonication in acetone, followed by isopropanol (2 min, each) and plasma cleaned for 10 min. PEMs were prepared manually using the LbL technique [200]. First, an activating monolayer of PEI (10–2 monomer mol/l, pH \sim 7) was deposited onto the glass slides for 10 min and extensively rinsed with ultrapure 18.2 M Ω water (Satorius,arium 611VF, Goettingen, Germany) (3 \times 2 min). Next, a precursor layer of two bilayers of (HA/Chi)₂ was deposited, in 5 mM sodium acetate buffer at pH 5.5, by alternate deposition on the quartz crystals in the flow chamber HA (1mg/mL, 10 min deposition) and chi (1mg/mL, 10 min deposition) solutions with an intermediate washing step (2 \times 3 min) in

buffer (5 mM sodium acetate buffer at pH 5.5). Subsequently, layers of (HA/NP)_n were adsorbed on the (HA/Chi)₂ precursor layers in 0.3 M sodium acetate buffer at pH 5.5. Each deposition step for the NPs was carried out for 20 min. The deposition steps were repeated until the desired number of bilayers were formed. In the case of Chi_PEG:siRNA NP, the PEM build-up stop when no more NP deposition was noticed in the QCM.

6.3.5. Release of chi_PEG:siRNA^{Tye563} over time

Two 96 well-plates coated with (HA/Ch)₂ (HA/Chi_PEG:siRNA^{Tye563} NPs)₅ and (HA/Ch)₂ (HA/Chi_PEG:siRNA NPs)₅ (as control) films were incubated in 300 μL phosphate buffered saline (PBS), pH 7.4 at 37 °C for 96h with gentle agitation. Every day, the supernatant was replaced with 300 μL of fresh PBS solution. The fluorescence intensity of the collected supernatants was measured (Phera Star, BMG Labtech, Offenburg, Germany).

6.4. Analytical chemistry methods

6.4.1. NMR – Spectroscopy

Bruker Advance 200 (Proton resonance frequency: 200MHz)

Bruker Advance 400 (Proton resonance frequency: 400MHz)

The chitosan and chitosan modified samples were diluted in CD₃COOD/D₂O and were measured at 400MHz.

The degree of acetylation (DA), the fraction or percentage of acetylated glucosamine units (GlcNAc), was determined using the Equation (1) and the degree of deacetylation (DD), the fraction or percentage of acetylated glucosamine units (GlcN) was determined using the Equation (2):

$$DA = \frac{\left(\frac{1}{3} \times I_{CH3}\right)}{\left(\frac{1}{6} \times I_{(H2-H6)}\right)} \times 100 \quad (1)$$

$$DD = 100 - DA \quad (2)$$

I_{CH3} is the intensity of CH₃ signal in ¹H NMR

$I_{(H2-H6)}$ is the summation intensities of H₂%, H₃%, H₄%, H₅%, and H₆% of the sugar protons in ¹H NMR

The height of the area of the signal is proportional to the number of protons.

The DS of PEG-chi was determined using the integration of the OCH₃ singlet (I_{OCH_3}) together with the degree of acetylation (DA) as shown in Equation (3):

$$\text{DSPEG-chi (\%)} = I_{\text{OCH}_3} \times \text{DAchitosan (\%)} \quad (3)$$

I_{OCH_3} – integration of the acetyl protons in the N-acetyl-glucosamine monomer

6.4.2. Gel permeation chromatography (GPC)

The molecular weight (M_w) was determined by gel permeation chromatography (GPC), on a Viscotek Triple Detector Array max system using a ViscoGel A6000M (mixed Bed) column (Malvern Instruments GmbH, Herrenberg, Germany). The set up consisted of a size exclusion chromatograph connected to a light scattering cell, a refractive index detector, and a viscometer that allowed for simultaneous determination of the absolute polymer molecular weight, hydrodynamic radius and intrinsic viscosity. The analyses were performed at 35°C with 0.3 M sodium acetate pH 4.5 (adjusted with acetic acid) 1% ethylene glycol as running buffer, using a flow rate of 0.5 mL/min and a dn/dc of 0.165 mL/g. The concentration of the polymer samples was 1 mg/mL in the same buffer and the injection volume was 100 μ L. Polyethylene glycol ($M_w = 21$ kDa) (Malvern Instruments GmbH, Herrenberg, Germany) was used to calibrate the detectors. For the evaluation of the physical data OmniSEC software (Viscothek) was used. Every polymer was measured in a triplicate.

The DS of the PEGylated conjugates was also determined using the GPC results as shown in Eq (4):

$$\text{DS} = \frac{M_{\text{nPEG-chi}} - M_{\text{nchitosan}}}{5000} / \text{DPchitosan} \quad (4)$$

M_n = Number Average Molecular Weight

DP = degree of polymerization; $DP = \frac{M_w}{M_n}$

6.4.3. Fourier transform infrared (FT-IR)

FTIR spectra were recorded with potassium bromide (KBr) pressed disks on a Bruker Vector 22 FTIR spectrometer using 4 cm^{-1} resolution and 32 scans with a frequency range of $4000 - 400\text{ cm}^{-1}$.

The chitosan sample was prepared with 40-60 mg of chitosan powder and 120 mg of KBr by blended and triturated with mortar and pestle for 5 min. The mixture was compacted using a hydraulic press at a pressure of 8 tons for 30 s.

6.4.4. Solubility measurement via UV/VIS

The solubility of chitosan and PEGylated conjugates was evaluated at different pH values (4.0, 7.0 and 9.6) at a concentration of 1 mg/mL. The chitosan samples were solubilized overnight in 0.3 M CH_3COONa at pH 5.5, PBS at pH 7.0 and carbonate buffer at pH 9.6. The transmittance of the solution was recorded as a function of pH on the UV/VIS spectrometer (Jesko, Munchen Germany) using a quartz cell with an optical path length of 1 cm at $\lambda = 600\text{ nm}$.

6.4.5. LC-MS/ESI and direct injection ESI

I want to thank Sandra Maier from the Bioanalytics department at NMI for measuring the small FAP inhibitor_linker regioisomers **18a** and **18b** via direct injection ESI and for measuring the scFv'LCH3 and FAP_cyclooctyne_linker compound **15** via LC-MS/ESI.

6.4.6. MALDI

The Mass Spectra have been acquired on a Bruker Ultraflex III MALDI-TOF with reflector in positive ion mode. α -Cyano-4-hydroxycinnamic acid (HCCA) matrix was used. Samples have been prepared with the dried droplet method, using 50% ACN + 0,5%TFA as solvent.

6.4.7. HPLC

	Analytical HPLC	Preparative HPLC	
		Method 1	Method 2:
Column	Chromolith Performance RP-18e, #UM6102/024,	GromSil 120 ODS-4 HE, $7\mu\text{m}$ 125x30mm <u>Pre-column</u> : GromSil	GromSil 120 ODS-4 HE, $7\mu\text{m}$ 150x50mm <u>Pre-column</u> : Gromsil

	100x3mm	120 ODS-4 HE, 7 μ m 30x30mm	120 ODS-4 HE, 7 μ m 30x30mm
Buffer A	0.1% (v/v) TFA in water	0.1% (v/v) TFA in water	0.1% (v/v) TFA in water
Buffer B	100% ACN containing 0.08% (v/v) TFA	100% ACN containing 0.08% (v/v) TFA	100% ACN containing 0.08% (v/v) TFA
Gradient	5 to 65% solvent B	5 to 65% solvent B	5 to 65% solvent B
Temperature	25°C	25°C	25°C
Detection	Dionex – UVD340U 214nm, 254nm	214nm, 254nm	214nm, 254nm
Injection	5 μ L	1 mL	1 mL

6.4.8. Quartz crystal microbalance (QCM)

The polymer/nanoplex film building up was measured *in situ* by QCM. The system measures the changes of oscillation frequency of a quartz crystal when the polymer/nanoplexes are adsorbed on the crystal surface. The measured shift of the resonance frequency (Δf) is directly proportional to the adsorbed amount of polymer/nanoplexes.

The measurements were the polyelectrolyte multilayer (PEM) adsorption was performed in flow chamber system using an “open module” system which allows film assembly using very small amounts of reagent.

The QCM crystals were cleaned with Pirania solution (30% H_2O_2 :70% H_2SO_4 : 1:1(v/v))

6.5. Statistical analysis

The experiments were repeated a minimum of three times, and the GraphPad InStat3 software was used for statistical analyses. The non-parametric Kruskal–Wallis test was applied. The data are expressed as the mean \pm SD. A statistically significant difference was assumed at $P < 0.05$.

Injection: 1 mL

7. Experimental section

7.1. Deacetylated chitosan

Various concentrations of NaOH_{aq} solutions were added to commercially available chitosan (Aldrich low and medium molecular weight) and stirred at different temperatures over a certain period of time. The mixture was either filtered and again treated with 50% (w/v) NaOH_{aq} for 24h at 60°C or filtered and lyophilized. (All the variable parameters are given in Table 17).

Table 17. Variable parameters for the chitosan deacetylation reaction: NaOH_{aq} , temperature (T) and time.

<i>RN</i>	<i>Batch number</i>	<i>SM</i>	<i>NaOH (w/v) %</i>	<i>T (° C)</i>	<i>Time (h)</i>
Chi (80;165)	Aldrich Low	-	-	-	-
Chi (85;335)	Aldrich Medium	-	-	-	-
Chi (90;56)	ANG115235a	Aldrich Low	40	110	8
Chi (87;62)	ANG115235b	Aldrich Low	40	110	4
Chi (85;78)	ANG115236a	Aldrich Low	40	60	8
Chi (83;81)	ANG115236b	Aldrich Low	40	60	4
Chi (94;116)	ANG115251b	Aldrich Low	50	60	24
Chi (93;61)	ANG115251a	Aldrich Low	40/50	110/60	8/24
Chi (94;200)	ANG115275a	Aldrich Medium	50	110	4
Chi (90;240)	ANG115275b	Aldrich Medium	50	110	8

7.2. Synthesis of mPEG grafted chitosan: Reaction conditions

<i>RN</i>	<i>Batch number</i>	<i>Chi H [mg]</i>	<i>Chi NH₂ [mmo]^a</i>	<i>mPEG-NHS [mg]</i>	<i>mPEG-NHS</i>	<i>mPEG/Chi-NH₂ [mol/mol]</i>
-----------	---------------------	-------------------	---	----------------------	-----------------	--

		<i>[mmol]</i>				
1.5 % PEG	ANG142958	50	0,28	90,9	0,018	0,06
3 % PEG	ANG142960	50	0,28	151,2	0,030	0,11
4 % PEG	ANG142961	50	0,28	181,8	0,036	0,13
6 % PEG	ANG142897	100	0,56	400	0,080	0,14
8 % PEG	ANG142953	50	0,28	227	0,045	0,16

^aMmol of chitosan Hepe free amino groups, considering the degree of deacetylation 92.6% and the M_w of the deacetylated monomer: 165 [g/mol]

7.3. Synthesis of the linker system

Compound 2: 8,8-dibromobicyclo[5.1.0]octane

C_7H_{12} 10.05g (0.105 mol)

$CHBr_3$ 24.6g (0.219 mol)

C_4H_9KO 57.5 (0.223 mol)

$C_8H_{12}Br_2$ 26.78g (0.099 mol) 95%

In a dry 250mL 3 neck round bottom flask, anhydrous pentane (75mL) was added over cycloheptane and potassium *tert*-butoxide, *t*-BuOK. The reaction mixture was then placed in ice with salt ($T < 5^\circ C$) and stirred vigorously. Then the bromoform was added dropwise (~20min). The reaction mixture was left to stir overnight at RT under N_2 . The next day H_2O (150mL) was added and neutralized with HCl (1M). The organic phase was extracted with pentane (3x60mL) and then pentane phase was washed with H_2O (3x60mL). After drying over $MgSO_4$, the solvent was evaporated on the rotavap.

The crude product was then purified twice on a 20g normal silica column *via* extraction with 250mL hexan/AcOEt 5% to afford the pure compound as a yellow oil.

Analytically

1H NMR (400MHz, $CDCl_3$): δ [ppm] 0.98-1.29 (m, 3 H), 1.34 (qq, $J=1-7,5$ Hz, 2 H), 1.73 (ddd, $J=1,5-4-10,5$ Hz, 2 H), 1,75-1,82 (m, 3 H), 2,26

(dtq, $J=14.6-1$ Hz, 2 H)

^{13}C NMR (400MHz, CDCl_3): δ [ppm] 27.9 (2, C_{3-5}), 29.1 (2, C_{2-6}), 32.2 (C_4),
34.7 (2, C_{1-7}), 40.6 (C_8)

Compound 6: (Z)-methyl 4-(((2-bromocyclooct-2-en-1-yl)oxy)methyl)benzoate

$\text{C}_8\text{H}_{12}\text{Br}_2$ 500mg (1.866 mmol)

$\text{C}_9\text{H}_{10}\text{O}_3$ 3.7g (22.38 mmol)

AgClO_4 1.2 (5.6 mmol)

$\text{C}_{17}\text{H}_{21}\text{BrO}_3$ 379mg (1.073 mmol) 57%

AgClO_4 was added to a solution of **8,8-dibromobicyclo[5.1.0]octane (1)** and methyl 4-hydroxymethylbenzoate dissolved in toluene (8mL) protected from light. The reaction was stirred for 2h, diluted with pentane (20mL), and filter to remove insoluble silver salts. The crude product was concentrated and purified *via* flash chromatography with 4-8% EtOAc: pet ether to yield the pure compound as a colorless oil ($R_{f8\%EtOAc:pet\ ether}=0.33$).

Analytatics

^1H NMR (400MHz, CDCl_3): δ [ppm] 0.8 (m, 1H), 1.3 (m, 1H), 1.51 (app dq, 1H, $J=5.5$ 12 Hz), 1.75 (m, 1H), 1.9-2.1 (m, 4H), 2.35 (m, 1H), 2.8 (app dq, 1H, $J=5-8$), 3.8-4.05 (m, 4H), 4.4 (d, 1H, $J=12.5$ Hz), 4.8 (d, 1H, $J=12.5\text{Hz}$), 6.2 (dd, 1H, $J=4-11.5$ Hz), 7.4 (d, 2H, $J=8$ Hz), 7.9 (d, 2H, $J=8$ Hz)

Compound 7: 4-((cyclooct-2-yn-1-yloxy)methyl)benzoic acid

$\text{C}_{17}\text{H}_{21}\text{BrO}_3$ 240mg (0.68 mmol)

NaOMe 41.8mg (0.77 mmol)

LiOH 610mg (25.4 mmol)

$\text{C}_{16}\text{H}_{18}\text{O}_3$ 40mg (0.136 mmol) 20%

(Z)-methyl 4-(((2-bromocyclooct-2-en-1-yl)oxy)methyl)benzoate (2) was dissolved in 1mL DMSO and 1mL NaOMe (30% in MeOH) was added under a constant flow of nitrogen at

room temperature. The solution turned immediately to a first deeply brown solution then a turbid brown thick solution. Constant flow of nitrogen was stopped after 15min. The reaction was quenched with 200mL 1M HCl affording a white solution. The combined organic extracts were washed with 80mL brine (saturated solution) and the organic layer was evaporated at 52°C, yielding a slightly brown oil which was solidifying with cooling. The remaining crude product was dissolved in H₂O/Dioxan (7.6mL/30.4mL), LiOH were added to this solution and the reaction mixture was stirred overnight. The reaction was acidified with 100mL 1M HCl and extracted twice with 80mL ethylacetate (each portion). The organic layer was dried over sodium sulfate, filtered and evaporated. The crude product was purified *via* flash chromatography (EtOAc/petrolether/AcOH 25/75/1, flow 15mL/min) $R_f = 0.38$ (mean of two experiments), $R_{f\text{byproduct}} = 0.12$ (same eluent as for chromatography).

¹H NMR (400MHz, CDCl₃): δ [ppm] 2.10- 2.27 (m, 1H), 2.5 (m, 1H), 4.25 (m, 1H), 4.49 (d, 1H, $J=13\text{Hz}$), 4.74 (d, 1H, $J=12.5\text{ Hz}$), 7.45 (d, 1H, $J=8\text{ Hz}$), 8.07 (d, 1H, $J=8.5\text{ Hz}$).

Compound (3): (E)-2-(2-(2-(2-((2-bromocyclooct-2-en-1-yl)oxy)ethoxy)ethoxy)ethoxy)ethanol

C₈H₁₂Br₂ 4g

AgClO₄ 10g (0.048 mol)

C₈H₁₈O₅ 69.5g (0.358 mol)

C₁₆H₂₉BrO₅ 4.2g (mol) (0.011 mol) 74%

8,8-dibromobicyclo[5.1.0]octane (1) was added over a solution of AgClO₄ (300mol%) dissolved in toluene (20mL) and tetraethylene glycol (300mol%) in a mixture of toluene (8mL) and pyridine (6mL). The reaction was refluxed (~140°C) in the dark overnight. The next day the solvent was evaporated and then brine (saturated solution) (220mL) was added. The insoluble salts were removed *via* filtration in a big funnel using filter paper. The filter was washed with diethylether (440mL). The aqueous phase was extracted with Et₂O (8x440mL) and the combined organic layers were washed with brine (440mL), H₂O (440mL), dried (Na₂SO₄), and concentrated to give a brown oil pure compound.

¹H NMR (400MHz, CDCl₃): δ [ppm] 0.66 - 0.92 (m, 1 H) 1.18 (s, 2 H) 1.36 (s, 2 H)

1.57 - 1.69 (m, 1 H), 1.78 - 1.86 (m, 2 H) 1.89 - 1.97 (m, 2 H) 2.21 (d, $J=11.73$ Hz, 1 H) 2.58 - 2.73 (m, 1 H) 2.89 - 3.07 (m, 1 H) 3.39 - 3.43 (m, 1 H) 3.51 - 3.57 (m, 3 H) 3.57 - 3.66 (m, 7 H) 3.60 (s, 8 H) 3.78 - 3.94 (m, 1 H) 3.86 (dd, $J=10.17, 5.08$ Hz, 1 H) 6.02 - 6.21 (m, 1 H)

^{13}C NMR (400MHz, CDCl_3): δ [ppm] 26.3, 28.1, 33.2, 36.5, 39.5, 61.7, 70.3, 70.4, 70.5, 70.6, 72.5, 85.2, 131.4, 133.1

Compound 4: 2-(2-(2-(2-(cyclooct-2-yn-1-yloxy)ethoxy)ethoxy)ethoxy)ethanol

$\text{C}_{16}\text{H}_{29}\text{BrO}_5$ 2g (mmol)

$\text{C}_4\text{H}_9\text{KO}$ 3.15 g (mmol)

$\text{C}_{16}\text{H}_{28}\text{O}_5$ 1.05g (mol) 66%

Potassium *tert*-butoxide was added to a solution of compound **5** in a mixture *i*-PrOH (48 mL)/pyridine (7.2 mL). After 60 h of stirring at room temperature, the reaction was neutralized with 5% HCl and partitioned between CH_2Cl_2 (500 mL) and H_2O (200 mL). Then, the aqueous layer was extracted with CH_2Cl_2 (4x500 mL), dried (Na_2SO_4), and concentrated under vacuum to give a crude product that was purified by column chromatography (EtOAc/MeOH 5%) $R_f=0.38$ to yield compound **6** as a colorless oil.

^1H NMR (400MHz, CDCl_3): δ [ppm] 1.46 (s, 2 H) 1.52 - 1.74 (m, 2 H) 1.74 - 2.03 (m, 5 H) 2.05 - 2.30 (m, 4 H) 2.46 - 2.63 (m, 1 H) 3.49 (d, $J=4.69$ Hz, 1 H) 3.65 (d, $J=3.52$ Hz, 21 H) 4.14 - 4.28 (m, 1H)

^{13}C NMR (400MHz, CDCl_3): δ [ppm] 20.7, 26.4, 29.7, 34.3, 42.2, 61.8, 68.5, 70.4, 70.4, 70.5, 70.6, 72.5, 72.7, 92.8, 100.0

Compound 5: 2-(2-(2-(2-(cyclooct-2-yn-1-yloxy)ethoxy)ethoxy)ethoxy)ethyl (2,5-dioxopyrrolidin-1-yl) carbonate

$\text{C}_9\text{H}_8\text{N}_2\text{O}_7$ 767,7mg (3 mmol)

C₁₆H₂₈O₅ 300mg (1 mmol)

C₆H₁₅N 303.2mg (3 mmol)

C₂₁H₃₁NO₉ 388mg (8.8 mmol) 88%

N,N'-Disuccinimidyl carbonate (300 mol%) was added to a solution of compound **6** and triethylamine (300 mol%) in acetonitrile (MeCN, 4 mL). The reaction was left to stir at room temperature for 21h. The solvent was evaporated and the reaction was partitioned between dichloromethane (DCM, 100 mL) and H₂O (50 mL). The aqueous layer was extracted with dichloromethane (DCM, 2x100 mL) and the organic layer was washed with sodium carbonate (NaHCO₃ 5%, 2x50 mL), dried over Na₂SO₄ and concentrated at max. 35°C to give a yellow crude product that was purified *via* flash column chromatography (EtOAc/Hexan: 4/1) R_f=0.6 to give a slight yellow syrupy pure compound.

¹H NMR (400MHz, CDCl₃): δ [ppm] 1.53 – 2.02 (m, 6 H), 2.07 -2.32 (m, 2 H), 2.84 (s, 5 H) 3.11 (s, 1 H), 3.45 – 3.55 (m, 1 H), 3.46 – 3.56 (m, 1H), 3.67 (d, *J*=4.30 Hz, 11 H), 3.80 (d, *J*=4.69 Hz, 2 H), 4.17 – 4.27 (m, 1H), 4.42 – 4.53 (m, 2 H).

Compound 6: 2-(2-(2-(2-(cyclooct-2-yn-1-yloxy)ethoxy)ethoxy)ethoxy)ethyl (2-(2,5-dioxo-2,5-dihydro-1H-pyrrol-1-yl)ethyl)carbamate

C₂₁H₃₁NO₉ 60mg (0.136 mmol)

C₆H₈N₂O₂ · C₂HF₃O₂ 48.3mg (1.4 mmol)

C₆H₁₅N 50.6mg (0.544 mmol)

C₂₃H₃₄N₂O₈ 40mg (mmol) 63%

Triethylamine, and Mal-TFA were added over compound **7** in CH₂Cl₂ (1.5 mL). The mixture was stirred overnight under Ar and then concentrated on the rotavap at a maximum of 35°C. The crude product was purified by column chromatography (EtOAc 100%, R_f= 0.66) and then dried extra on the rotavap with pentane to yield a colorless oil.

¹H NMR (400MHz, CDCl₃): δ [ppm] 0.64-2.95 (m, 12 H) 3.08-3.82 (m, 16 H) 4.09 (m, 2 H), 5.03 (br. s, 1 H) 6.62 (s, 2 H)

Compound 16: 2-(2-(2-(2-(cyclooct-2-yn-1-yloxy)ethoxy)ethoxy)ethoxy)ethyl(2-aminoethyl)carbamate

C₂₁H₃₁NO₉ 283mg (0.641 mmol)

C₂H₈N₂ 770.5mg (12.8 mmol)

C₁₉H₃₄N₂O₆ 154mg (0.4 mmol) 62%

Ethylenediamine (2000 mol%) was added to a solution of compound **7** in CH₂Cl₂ (6.4mL). After 10 minutes the reaction mixture was a white turbid mixture. Reaction was allowed to stir at room temperature overnight and then was concentrated under vacuum. The resulting crude product was purified by column chromatography (CH₂Cl₂/MeOH 33%) R_f=0.13 to give the final compound as a colorless oil.

¹H NMR (400MHz, CDCl₃): δ [ppm] 1.20-2.35 (m, 10 H), 2.92 (t, J = 5.7 Hz), 3.27 (m, 2H), 3.41 (m, 1H), 3.57 (m, 14H), 4.18 (m, 5H), 6.15 (br. s, 1H)

Compound 13: 2-(2-(2-(2-(cyclooct-2-yn-1-yloxy)ethoxy)ethoxy)ethoxy)ethyl 2-iodoacetate

C₁₆H₂₈O₅ 100 mg (0.33 mmol)

C₂H₃IO₂ 80.5 mg (0.43 mmol)

DMAP 0.4 mg (0.003 mmol)

EDC 70.2 mg (0.366 mmol)

C₁₈H₂₉IO₆ 13.5 mg 10%

Iodoacetic acid was added to a solution of compound **4**, N'-ethylcarbodiimide hydrochloride and 4-dimethylaminopyridine in tetrahydrofuran (THF, 5mL). The reaction was left to stir overnight at room temperature. The reaction mixture was concentrated and the organic layer was extracted with 5% NaHCO₃ solution (40 mL) and ethylacetate (50 mL). The aqueous layer was extracted twice with ethylacetate (2x75 mL each). The organic layers were combined, dried over sodium sulfate and evaporated under reduced pressure to yield the crude product as a yellow oil. The crude product was subjected to flash chromatography (EtOAc/n-hexane 4/1, R_f_{product1}=0.80, R_f_{product2}=0.73) to give the pure compound **13** (13.5mg, 10%) as a colorless oil.

¹H NMR (400MHz, CDCl₃): δ [ppm] 1.13-2.22 (m, 10 H) 3.42 (m, 1 H) 3.49-3.76 (m, 13 H) 4.04 (m, 2 H) 4.16 (m, 1 H) 4.23 (m, 1 H) 4.28 (m, 2 H)

Compound 12: 6-(2-iodoacetamido)hexanoic acid

$C_6H_{13}NO_2$ 1.5 g (8.66 mmol)

C_2H_2ClIO 1 g (4.89 mmol)

Na_2CO_3 2.46 (23.21 mmol)

$C_8H_{14}INO_3$ 1.8 g (6 mmol), crude product

To a slurry of 6-aminohexanoic acid and sodium carbonate in anhydrous THF (50 mL) was added a solution of iodoacetyl chloride in THF (1.5 mL) at 0°C. The resulting reaction mixture was warmed to room temperature after 15 min and stirred for 4h. Water was added to the reaction mixture and the resulting solution was acidified with HCl_{aq} (32%) to pH 1.0. The reaction mixture was extracted 5 times with EtOAc (30 mL each). The combined organic layers were dried over Na_2SO_4 and evaporated to yield the crude product as a dark brown oil which was used further without purification.

Compound 11: 2-(2-(2-(2-(cyclooct-2-yn-1-yloxy)ethoxy)ethoxy)ethoxy)ethyl-6-(2-iodoacetamido)hexanoate

$C_{16}H_{28}O_5$ 100 mg (0.333 mmol)

$C_8H_{14}INO_3$ 199 mg (0.666 mmol)

EDC 70.2 mg (0.366 mmol)

DMAP 0.4 mg (0.003 mmol)

$C_{24}H_{40}INO_7$ 100 mg (mmol) 52%

Crude compound **12** was added to a solution of compound **4**, N'-ethylcarbodiimide hydrochloride and 4-dimethylaminopyridine in tetrahydrofuran (5 mL). The reaction was left to stir overnight at room temperature. The reaction mixture was concentrated and the organic layer was extracted with 5% $NaHCO_3$ solution (40 ml) and ethylacetate (50 ml). The organic layer was separated and the aqueous layer was extracted with ethylacetate (2x75 ml each). The organic layers were combined, dried over sodium sulfate and evaporated under reduced

pressure to yield the crude product **12** as yellow oil. The crude product was subjected to flash chromatography (EtOAc 100%, $R_{f_{product}}=0.83$) to give the pure product as a colorless oil.

$^1\text{H NMR}$ (400MHz, CDCl_3): δ [ppm] 0.80-2.35 (m, 14 H) 2.67 (m, 1 H) 3.33-3.74 (m, 20 H) 3.99-4.39 (m, 3 H) 7.15 (br. s, 2 H)

Compound 14: 2-(2-(2-(2-(cyclooct-2-yn-1-yloxy)ethoxy)ethoxy)ethoxy)ethyl (2-(2,5-dioxopyrrolidin-1-yl)ethyl)carbamate-S-Doa-Doa-EQKLISEEDL-OH

$\text{C}_{23}\text{H}_{34}\text{N}_2\text{O}_8$ 8.95mg (19.2 μmol)

H-C-Doa-Doa-EQKLISEEDL-OH 1.6mg (1.00 μmol)

$\text{C}_{23}\text{H}_{36}\text{N}_2\text{O}_8$ - C-Doa-Doa-EQKLISEEDL-OH

H-C-Doa-Doa-EQKLISEEDL-OH was solubilised in H_2O (8.8mL) and compound **8** was solubilised in DMSO (88.2 μL). The two compounds were mixed gently at room temperature for 2h. The reaction was stopped by adding L-Cys (10mM final concentration). The crude product was purified by reversed-phase HPLC.

Purity by HPLC $\lambda=214\text{nm}$;

MALDI: $[\text{M}-\text{H}^+]$ 2062.62

Compound 15: 2-(2-(2-(2-(cyclooct-2-yn-1-yloxy)ethoxy)ethoxy)ethoxy)ethyl (2-(2,5-dioxopyrrolidin-1-yl)ethyl)carbamate – scFv'LCH₃

scFv'LCH₃ 1.26mg/1mL PBS (0.049 μmol)

$\text{C}_9\text{H}_{15}\text{O}_6\text{P}$ 18mg/0.06mL H_2O (71.3 μmol)

$\text{C}_{23}\text{H}_{34}\text{N}_2\text{O}_8$ 1.082 mg (2.42 μmol)

$\text{C}_{23}\text{H}_{34}\text{N}_2\text{O}_8$ – scFv'LCH₃

TCEP was added to scFv'LCH₃ solution and allowed to react for 2h. Then a solution of compound **8** (100mg/mL DMSO) was added and left to stir moderately for another 2h at room temperature under Ar. The reaction was stopped by adding L-Cysteine (10mM final volume).

The excess of unreacted compound **8** was removed by centrifugal ultrafiltration (Amicon Ultra 0.5 – centrifugal filters 10kDa) affording a pure final compound.

Compound 18: Inhibitor conjugate - -2 (2-(2-(2-(cyclooct-2-yn-1-yloxy)ethoxy)ethoxy)ethyl(2-(2-(2-(2-((4,5,6,7,8,9-hexahydro-1H-cycloocta[d][1,2,3]triazol-4-yl)oxy)ethoxy)ethoxy)ethoxy)ethyl) (azanediylbis(ethane-2,1-diyl))dicarbamate

Inhibitor from Belgium 120 mg (0.229 mmol)

C₁₉H₃₄N₂O₆ 280 mg (0.725 mmol)

C₂₁H₃₁NO₉ 300 mg (0.68 mmol)

C₃₈H₆₅N₆O₁₂ – inhibitor conjugate 84 mg (0.068 mmol) 30%

Compound **9** was added to a solution of Belgium inhibitor in THF (4 mL) under N₂. The reaction was left to stir at room temperature over 1 week and then tested by TLC using the EtOAc/MeOH/Et₃N 1/1/1% solvent system. The crude product was used directly for the next step. Compound **7** was prepared freshly and added over the crude product in CH₂Cl₂ (3 mL) and was allowed to stir at room temperature overnight. The reaction mixture was concentrated and the crude product was purified by flash chromatography with EtOAc/MeOH/Et₃N 1/1/1% to yield a yellow green fluorescent oil which was further purified by reversed-phase HPLC.

Purity by HPLC regiosomer1 λ=214nm; 4.4min (94.6 %), 4.5min (5.2 %) (regioisomer2)
 regiosomer2 λ=214nm; 4.5min (96.3 %), 4.4min (3.7 %) (regioisomer1)

ESI-MS: regiosomer1: found [MH²⁺] 619.3409, calculated 1238
 regiosomer1: found [MH²⁺] 619.3407, calculated 1238

8. Appendix

8.1. Functionality of the bioconjugated linker_FAP chemical inhibitor (UAMC 1533)

Table 18. Potency and selectivity of compound 18.

Compd	IC ₅₀ (μM)						SI (FAP/PREP)*
	FAP	DPP IV	DPP8	DPP9	DPP II	PREP	
UAMC 1533	0.0051 ±0.0003	>100	>100	>100	>25	>100	>20
18	0.051 ±0.0030	13.2 ±0.7	>100	>100	>100	7.7 ±1.1	151

*SI stands for "Selectivity Index" (calculated as $[IC_{50}(PREP)/IC_{50}(FAP)]$).

9. References

1. Ramsden, J.J., *1 - Introduction to medical materials and devices*, in *Joining and Assembly of Medical Materials and Devices*, Y. Zhou and M.D. Breyen, Editors. 2013, Woodhead Publishing. p. 3-27.
2. Wiesmann, H.P. and U. Meyer, *Biomaterials*, in *Fundamentals of Tissue Engineering and Regenerative Medicine*, U. Meyer, et al., Editors. 2009, Springer Berlin Heidelberg. p. 457-467.
3. Meyer, U., *The History of Tissue Engineering and Regenerative Medicine in Perspective*, in *Fundamentals of Tissue Engineering and Regenerative Medicine*, U. Meyer, et al., Editors. 2009, Springer Berlin Heidelberg. p. 5-12.
4. Williams, D.F., *On the nature of biomaterials*. *Biomaterials*, 2009. **30**(30): p. 5897-5909.
5. Dee, K.C., D.A. Puleo, and R. Bizios, *Biomaterials*, in *An Introduction To Tissue-Biomaterial Interactions*. 2002, John Wiley & Sons, Inc. p. 2.
6. Battiston, K.G., et al., *Biomaterials in co-culture systems: Towards optimizing tissue integration and cell signaling within scaffolds*. *Biomaterials*, 2014. **35**(15): p. 4465-4476.
7. Metcalfe, A.D. and M.W.J. Ferguson, *Tissue engineering of replacement skin: the crossroads of biomaterials, wound healing, embryonic development, stem cells and regeneration*. *Journal of the Royal Society Interface*, 2007. **4**(14): p. 413-437.
8. Allo, B.A., et al., *Bioactive and Biodegradable Nanocomposites and Hybrid Biomaterials for Bone Regeneration*. *Journal of Functional Biomaterials*, 2012. **3**(2): p. 432-463.
9. Ravi, S. and E.L. Chaikof, *Biomaterials for vascular tissue engineering*. *Regenerative medicine*, 2010. **5**(1): p. 107.
10. Helmus, M.N. and C.M. Cunanan, *5 - Mechanical and bioprosthetic heart valves*, in *Biomaterials for Artificial Organs*, M.L.J. Webster, Editor. 2011, Woodhead Publishing. p. 113-162.
11. Ebert, M.J., et al., *4 - Biomaterials for pacemakers, defibrillators and neurostimulators*, in *Biomaterials for Artificial Organs*, M.L.J. Webster, Editor. 2011, Woodhead Publishing. p. 81-112.
12. Langer, R. and N.A. Peppas, *Advances in biomaterials, drug delivery, and bionanotechnology*. *AIChE Journal*, 2003. **49**(12): p. 2990-3006.
13. Zhong, J., et al., *A smart polymeric platform for multistage nucleus-targeted anticancer drug delivery*. *Biomaterials*, 2015. **65**: p. 43-55.
14. Wang, X., et al., *Delivery of platinum(IV) drug to subcutaneous tumor and lung metastasis using bradykinin-potentiating peptide-decorated chitosan nanoparticles*. *Biomaterials*, 2014. **35**(24): p. 6439-6453.
15. Oral, E., *3 - Polymeric joint bearing surfaces for total joint replacements*, in *Biomaterials for Artificial Organs*, M.L.J. Webster, Editor. 2011, Woodhead Publishing. p. 56-80.
16. Neumann, A. and K. Kevenhoerster, *Biomaterials for craniofacial reconstruction*. *GMS Current Topics in Otorhinolaryngology, Head and Neck Surgery*, 2009. **8**: p. Doc08.
17. Rodella, L.F., G. Favero, and M. Labanca, *Biomaterials in Maxillofacial Surgery: Membranes and Grafts*. *International Journal of Biomedical Science : IJBS*, 2011. **7**(2): p. 81-88.
18. Jensen, T.H.L., *Development of a novel biomaterial: A nanotechnological approach*. 2009, Ph.D. Thesis, University of Aarhus
19. Kenneth Ward, W., *A Review of the Foreign-body Response to Subcutaneously-implanted Devices: The Role of Macrophages and Cytokines in Biofouling and Fibrosis*. *Journal of diabetes science and technology (Online)*, 2008. **2**(5): p. 768-777.
20. Tang, L. and W. Hu, *Molecular determinants of biocompatibility*. *Expert Review of Medical Devices*, 2005. **2**(4): p. 493-500.

21. Dolores, W., et al., *Cellular and molecular composition of fibrous capsules formed around silicone breast implants with special focus on local immune reactions*. Journal of Autoimmunity, 2004. **23**(1): p. 81-91.
22. Frost, M. and M.E. Meyerhoff, *In Vivo Chemical Sensors: Tackling Biocompatibility*. Analytical Chemistry, 2006. **78**(21): p. 7370-7377.
23. Borges, J., et al., *Layer-by-Layer Assembly of Light-Responsive Polymeric Multilayer Systems*. Advanced Functional Materials, 2014. **24**(36): p. 5624-5648.
24. Issa, M.M., et al., *Targeted gene delivery with trisaccharide-substituted chitosan oligomers in vitro and after lung administration in vivo*. Journal of Controlled Release, 2006. **115**(1): p. 103-112.
25. Weiss, W.A., S.S. Taylor, and K.M. Shokat, *Recognizing and exploiting differences between RNAi and small-molecule inhibitors*. Nature chemical biology, 2007. **3**(12): p. 739-744.
26. Bennett, C.F. and E.E. Swayze, *RNA Targeting Therapeutics: Molecular Mechanisms of Antisense Oligonucleotides as a Therapeutic Platform*. Annual Review of Pharmacology and Toxicology, 2010. **50**(1): p. 259-293.
27. Bumcrot, D., et al., *RNAi therapeutics: a potential new class of pharmaceutical drugs*. Nat Chem Biol, 2006. **2**(12): p. 711-719.
28. Lorenzer, C., et al., *Going beyond the liver: Progress and challenges of targeted delivery of siRNA therapeutics*. Journal of Controlled Release, 2015. **203**: p. 1-15.
29. Deng, Y., et al., *Therapeutic potentials of gene silencing by RNA interference: Principles, challenges, and new strategies*. Gene, 2014. **538**(2): p. 217-227.
30. Issa, M.M., *Linear and Branched Chitosan Oligomers as Delivery Systems for pDNA and siRNA In Vitro and In Vivo*. 2006, PhD thesis, Uppsala University p. 64.
31. Kole, R., A.R. Krainer, and S. Altman, *RNA therapeutics: beyond RNA interference and antisense oligonucleotides*. Nature Reviews Drug Discovery, 2012. **11**(2): p. 125-140.
32. Wilson, R.C. and J.A. Doudna, *Molecular Mechanisms of RNA Interference*. Annual Review of Biophysics, 2013. **42**(1): p. 217-239.
33. Hannon, G.J., *RNA interference*. Nature, 2002. **418**(6894): p. 244-251.
34. Nguyen, J. and F.C. Szoka, *Nucleic acid delivery: the missing pieces of the puzzle?* Accounts of Chemical Research, 2012. **45**(7): p. 1153-1162.
35. Lares, M.R., J.J. Rossi, and D.L. Ouellet, *RNAi and small interfering RNAs in human disease therapeutic applications*. Trends in Biotechnology, 2010. **28**(11): p. 570-579.
36. Zhou, Y., C. Zhang, and W. Liang, *Development of RNAi technology for targeted therapy — A track of siRNA based agents to RNAi therapeutics*. Journal of Controlled Release, 2014. **193**: p. 270-281.
37. Dykxhoorn, D.M., D. Palliser, and J. Lieberman, *The silent treatment: siRNAs as small molecule drugs*. Gene Ther, 2006. **13**(6): p. 541-552.
38. Jackson, A.L., et al., *Position-specific chemical modification of siRNAs reduces “off-target” transcript silencing*. RNA, 2006. **12**(7): p. 1197-1205.
39. Sioud, M., *Overcoming the Challenges of siRNA Activation of Innate Immunity: Design Better Therapeutic siRNAs*, in *RNA Interference*, M. Sioud, Editor. 2015, Springer New York. p. 301-319.
40. Sioud, M., *Recent advances in small interfering RNA sensing by the immune system*. New Biotechnology, 2010. **27**(3): p. 236-242.
41. Whitehead, K.A., et al., *Silencing or Stimulation? siRNA Delivery and the Immune System*. Annual Review of Chemical and Biomolecular Engineering, 2011. **2**(1): p. 77-96.
42. Robbins, M., et al., *2[prime]-O-methyl-modified RNAs Act as TLR7 Antagonists*. Mol Ther, 2007. **15**(9): p. 1663-1669.
43. Judge, A.D., et al., *Design of Noninflammatory Synthetic siRNA Mediating Potent Gene Silencing in Vivo*. Mol Ther, 2006. **13**(3): p. 494-505.

44. Hartmann, H., et al., *Hyaluronic acid / chitosan multilayer coatings on neuronal implants for localized delivery of siRNA nanoplexes*. *Journal of Controlled Release*, 2013. **168**(3): p. 289-297.
45. Martens, P.J., et al., *In vivo delivery of functional Flightless I siRNA using layer-by-layer polymer surface modification*. *Journal of Biomaterials Applications*, 2015.
46. Balasubramanian, P., et al., *Collagen in Human Tissues: Structure, Function, and Biomedical Implications from a Tissue Engineering Perspective*, in *Polymer Composites – Polyolefin Fractionation – Polymeric Peptidomimetics – Collagens*, A. Abe, et al., Editors. 2013, Springer Berlin Heidelberg. p. 173-206.
47. Taguchi, T. and M.S. Razzaque, *The collagen-specific molecular chaperone HSP47: is there a role in fibrosis?* *Trends in Molecular Medicine*. **13**(2): p. 45-53.
48. Ishida, Y. and K. Nagata, *Chapter nine - Hsp47 as a Collagen-Specific Molecular Chaperone*, in *Methods in Enzymology*, C.W. James and I.B. Phillip, Editors. 2011, Academic Press. p. 167-182.
49. Schuster, L., *Neue Wirkstoff-Transport-Systeme zur Verhinderung fibrotischer Reaktionen*, in *Cell Biologie und Immunologie Institut*. 2014, PhD thesis, Stuttgart University. p. 127.
50. Tasab, M., M.R. Batten, and N.J. Bulleid, *Hsp47: a molecular chaperone that interacts with and stabilizes correctly-folded procollagen*. *The EMBO Journal*, 2000. **19**(10): p. 2204-2211.
51. Brown, K.E., et al., *Expression of HSP47, a collagen-specific chaperone, in normal and diseased human liver*. *Lab Invest*, 2005. **85**(6): p. 789-797.
52. Sato, Y., et al., *Resolution of liver cirrhosis using vitamin A-coupled liposomes to deliver siRNA against a collagen-specific chaperone*. *Nat Biotech*, 2008. **26**(4): p. 431-442.
53. Ragelle, H., G. Vandermeulen, and V. Préat, *Chitosan-based siRNA delivery systems*. *Journal of Controlled Release*, 2013. **172**(1): p. 207-218.
54. Couto, L.B. and K.A. High, *Viral vector-mediated RNA interference*. *Current Opinion in Pharmacology*, 2010. **10**(5): p. 534-542.
55. Lee, Y. and K. Kataoka, *Delivery of Nucleic Acid Drugs*, in *Nucleic Acid Drugs*, A. Murakami, Editor. 2012, Springer Berlin Heidelberg. p. 95-134.
56. Ghosn, B., *Development and evaluation of an imidazole-modified chitosan for nucleic acid and contrast agent delivery*, in *Biomedical Engineering*. 2009, PhD Thesis, University of Texas at Austin. p. 253.
57. Aliabadi, H.M., et al., *Supramolecular assemblies in functional siRNA delivery: Where do we stand?* *Biomaterials*, 2012. **33**(8): p. 2546-2569.
58. Mao, S., W. Sun, and T. Kissel, *Chitosan-based formulations for delivery of DNA and siRNA*. *Adv Drug Deliv Rev*, 2010. **62**(1): p. 12-27.
59. Balazs, D.A. and W. Godbey, *Liposomes for Use in Gene Delivery*. *Journal of Drug Delivery*, 2011. **2011**.
60. Barichello, J.M., et al., *Agitation during lipoplex formation harmonizes the interaction of siRNA to cationic liposomes*. *International Journal of Pharmaceutics*, 2012. **430**(1–2): p. 359-365.
61. Dabkowska, A.P., et al., *Effect of Helper Lipids on the Interaction of DNA with Cationic Lipid Monolayers Studied by Specular Neutron Reflection*. *Biomacromolecules*, 2012. **13**(8): p. 2391-2401.
62. Mosca, M., A. Ceglie, and L. Ambrosone, *Effect of membrane composition on lipid oxidation in liposomes*. *Chemistry and Physics of Lipids*, 2011. **164**(2): p. 158-165.
63. Ozcan, G., et al., *Preclinical and clinical development of siRNA-based therapeutics*. *Advanced Drug Delivery Reviews*, 2015. **87**: p. 108-119.
64. Hu, J., et al., *Cytoplasmic Reactive Cationic Amphiphiles for Efficient Intracellular Delivery and Self-Reporting Smart Release*. *Macromolecules*, 2015.
65. Urban-Klein, B., et al., *RNAi-mediated gene-targeting through systemic application of polyethylenimine (PEI)-complexed siRNA in vivo*. *Gene Ther*, 2004. **12**(5): p. 461-466.

66. Breunig, M., et al., *Breaking up the correlation between efficacy and toxicity for nonviral gene delivery*. Proceedings of the National Academy of Sciences of the United States of America, 2007. **104**(36): p. 14454-14459.
67. Kawata, E., et al., *Administration of PLK-1 small interfering RNA with atelocollagen prevents the growth of liver metastases of lung cancer*. Molecular Cancer Therapeutics, 2008. **7**(9): p. 2904-2912.
68. Iwaki, K., et al., *A small interfering RNA targeting proteinase-activated receptor-2 is effective in suppression of tumor growth in a Panc1 xenograft model*. International Journal of Cancer, 2008. **122**(3): p. 658-663.
69. Liu, X., et al., *The influence of polymeric properties on chitosan/siRNA nanoparticle formulation and gene silencing*. Biomaterials, 2007. **28**(6): p. 1280-8.
70. Singla, A. and M. Chawla, *Chitosan: some pharmaceutical and biological aspects - an update*. The Journal of Pharmacy and Pharmacology 2001. **53**(8): p. 1047-67.
71. Kas, H.S., *Chitosan: Properties, preparations and application to microparticulate systems*. Journal of Microencapsulation, 1997. **14**(6): p. 689-711.
72. Singha, K., R. Namgung, and W.J. Kim, *Polymers in Small-Interfering RNA Delivery*. Nucleic Acid Therapeutics, 2011. **21**(3): p. 133-147.
73. Strand, S.P., et al., *Molecular design of chitosan gene delivery systems with an optimized balance between polyplex stability and polyplex unpacking*. Biomaterials, 2010. **31**(5): p. 975-987.
74. Lee, M., et al., *Water-soluble and low molecular weight chitosan-based plasmid DNA delivery*. Pharmaceutical research, 2001. **18**: p. 427-431.
75. Nordtveit, R.J., K.M. Varum, and O. Smidsrod, *Degradation of partially N-acetylated chitosans with hen egg white and human lysozyme*. Carbohydrate Polymers, 1996. **29**: p. 163-167.
76. Hoemann, C.D., et al., *Scaffold-Guided Subchondral Bone Repair: Implication of Neutrophils and Alternatively Activated Arginase-1+ Macrophages*. The American Journal of Sports Medicine, 2010. **38**(9): p. 1845-1856.
77. Buschmann, M.D., et al., *Chitosans for delivery of nucleic acids*. Advanced Drug Delivery Reviews, 2013. **65**(9): p. 1234-1270.
78. Jean, M., et al., *Chitosan-plasmid nanoparticle formulations for IM and SC delivery of recombinant FGF-2 and PDGF-BB or generation of antibodies*. Gene Therapy, 2009. **16**(9): p. 1097-1110.
79. Malmo, J., et al., *siRNA delivery with chitosan nanoparticles: Molecular properties favoring efficient gene silencing*. Journal of Controlled Release, 2012. **158**(2): p. 261-268.
80. Trung, T.S., et al., *Functional characteristics of shrimp chitosan and its membranes as affected by the degree of deacetylation*. Bioresource Technology, 2006. **97**(4): p. 659-663.
81. Fernandes, J.C., et al., *Low molecular weight chitosan conjugated with folate for siRNA delivery in vitro: optimization studies*. International Journal of Nanomedicine, 2012. **7**: p. 5833-5845.
82. Alameh, M., et al., *Low molecular weight chitosan nanoparticulate system at low N:P ratio for nontoxic polynucleotide delivery*. International Journal of Nanomedicine, 2012. **7**: p. 1399-1414.
83. Howard, K.A., et al., *RNA Interference in Vitro and in Vivo Using a Chitosan/siRNA Nanoparticle System*. Molecular Therapy, 2006. **14**(4): p. 476-484.
84. Csaba, N., M. Köping-Höggård, and M.J. Alonso, *Ionicly crosslinked chitosan/tripolyphosphate nanoparticles for oligonucleotide and plasmid DNA delivery*. International Journal of Pharmaceutics, 2009. **382**(1-2): p. 205-214.
85. Ji, A.M., et al., *Functional gene silencing mediated by chitosan/siRNA nanocomplexes*. Nanotechnology, 2009. **20**(40): p. 405103.
86. Malhotra, M., et al., *Ultrafine chitosan nanoparticles as an efficient nucleic acid delivery system targeting neuronal cells*. Drug Development and Industrial Pharmacy, 2009. **35**(6): p. 719-726.

87. Rojanarata, T., et al., *Chitosan-Thiamine Pyrophosphate as a Novel Carrier for siRNA Delivery*. *Pharmaceutical Research*, 2008. **25**(12): p. 2807-2814.
88. Katas, H. and H.O. Alpar, *Development and characterisation of chitosan nanoparticles for siRNA delivery*. *Journal of Controlled Release*, 2006. **115**(2): p. 216-225.
89. Andersen, M.Ø., K.A. Howard, and J. Kjems, *RNAi using a chitosan/siRNA nanoparticle system: in vitro and in vivo applications*. *Methods Molecular Biology*, 2009. **555**: p. 77-86.
90. Peer, D. and J. Lieberman, *Special delivery: targeted therapy with small RNAs*. *Gene Therapy*, 2011. **18**(12): p. 1127-1133.
91. Zhang, S., et al., *Cationic lipids and polymers mediated vectors for delivery of siRNA*. *Journal of Controlled Release*, 2007. **123**(1): p. 1-10.
92. Lundqvist, M., et al., *Nanoparticle size and surface properties determine the protein corona with possible implications for biological impacts*. *Proceedings of the National Academy of Sciences*, 2008. **105**(38): p. 14265-14270.
93. Nel, A., et al., *Understanding biophysicochemical interactions at the nano-bio interface*. *Nature Materials*, 2009. **8**: p. 543 - 557.
94. Erbacher, P., et al., *Chitosan-Based Vector/DNA Complexes for Gene Delivery: Biophysical Characteristics and Transfection Ability*. *Pharmaceutical Research*, 1998. **15**(9): p. 1332-1339.
95. Ishii, T., Y. Okahata, and T. Sato, *Mechanism of cell transfection with plasmid/chitosan complexes*. *Biochimica et Biophysica Acta (BBA) - Biomembranes*, 2001. **1514**(1): p. 51-64.
96. Nimesh, S., et al., *Enhanced Gene Delivery Mediated by Low Molecular Weight Chitosan/DNA Complexes: Effect of pH and Serum*. *Molecular Biotechnology*, 2010. **46**(2): p. 182-196.
97. Sato, T., T. Ishii, and Y. Okahata, *In vitro gene delivery mediated by chitosan. Effect of pH, serum, and molecular mass of chitosan on the transfection efficiency*. *Biomaterials*, 2001. **22**(15): p. 2075-2080.
98. Zhao, X., et al., *Transfection of primary chondrocytes using chitosan-pEGFP nanoparticles*. *Journal of Controlled Release*, 2006. **112**(2): p. 223-228.
99. Pack, D.W., et al., *Design and development of polymers for gene delivery*. *Nature Reviews Drug Discovery*, 2005. **4**(7): p. 581-593.
100. Knutson, V.P., *Endosomes/Acidification*, in *Molecular Biology of Membrane Transport Disorders*. 1996. p. 303-314.
101. Behr, J.-P., *The Proton Sponge: a Trick to Enter Cells the Viruses Did Not Exploit*. *CHIMIA International Journal for Chemistry*, 1997. **51**(1-2): p. 34-36.
102. Sonawane, N.D., F.C. Szoka, and A.S. Verkman, *Chloride Accumulation and Swelling in Endosomes Enhances DNA Transfer by Polyamine-DNA Polyplexes*. *Journal of Biological Chemistry*, 2003. **278**(45): p. 44826-44831.
103. Richard, I., et al., *Ionization Behavior of Chitosan and Chitosan-DNA Polyplexes Indicate That Chitosan Has a Similar Capability to Induce a Proton-Sponge Effect as PEI*. *Biomacromolecules*, 2013. **14**(6): p. 1732-1740.
104. Thibault, M., et al., *Intracellular Trafficking and Decondensation Kinetics of Chitosan-pDNA Polyplexes*. *Molecular Therapy*, 2010. **18**(10): p. 1787-1795.
105. Koping-Hoggard, M., et al., *Chitosan as a nonviral gene delivery system. Structure-property relationships and characteristics compared with polyethylenimine in vitro and after lung administration in vivo*. *Gene Therapy*, 2001. **8**(14): p. 1108-1121.
106. Itaka, K., et al., *In situ single cell observation by fluorescence resonance energy transfer reveals fast intra-cytoplasmic delivery and easy release of plasmid DNA complexed with linear polyethylenimine*. *The Journal of Gene Medicine*, 2004. **6**(1): p. 76-84.
107. Bowman, K. and K.W. Leong, *Chitosan nanoparticles for oral drug and gene delivery*. *International Journal of Nanomedicine*, 2006. **1**(2): p. 117-128.
108. Thibault, M., et al., *Excess polycation mediates efficient chitosan-based gene transfer by promoting lysosomal release of the polyplexes*. *Biomaterials*, 2011. **32**(20): p. 4639-4646.
109. Huang, M., et al., *Transfection efficiency of chitosan vectors: Effect of polymer molecular weight and degree of deacetylation*. *Journal of Controlled Release*, 2005. **106**(3): p. 391-406.

110. Kiang, T., et al., *Formulation of chitosan-DNA nanoparticles with poly(propyl acrylic acid) enhances gene expression*. Journal of Biomater Science Polymer Edition 2004. **15**(11): p. 1405-21.
111. Steen, M., T. Kirchberger, and A.H. Guse, *NAADP Mobilizes Calcium from the Endoplasmic Reticular Ca²⁺ Store in T-lymphocytes*. Journal of Biological Chemistry, 2007. **282**(26): p. 18864-18871.
112. Akinc, A., et al., *Exploring polyethylenimine-mediated DNA transfection and the proton sponge hypothesis*. The Journal of Gene Medicine, 2005. **7**(5): p. 657-663.
113. Labat-Moleur, F., et al., *An electron microscopy study into the mechanism of gene transfer with lipopolyamines*. Gene Therapy, 1996. **3**(11): p. 1010-7.
114. Aiba, S.-i., *Studies on chitosan: 4. Lysozymic hydrolysis of partially N-acetylated chitosans*. International Journal of Biological Macromolecules, 1992. **14**(4): p. 225-228.
115. Dehousse, V., et al., *Development of pH-responsive nanocarriers using trimethylchitosans and methacrylic acid copolymer for siRNA delivery*. Biomaterials, 2010. **31**(7): p. 1839-1849.
116. Dehousse, V., et al., *Comparison of chitosan/siRNA and trimethylchitosan/siRNA complexes behaviour in vitro*. International Journal of Biological Macromolecules, 2010. **46**(3): p. 342-349.
117. Zhang, J., et al., *Ternary Polymeric Nanoparticles for Oral siRNA Delivery*. Pharmaceutical Research, 2013. **30**(5): p. 1228-1239.
118. Varkouhi, A.K., et al., *Gene Silencing Activity of siRNA Polyplexes Based on Thiolated N,N,N-Trimethylated Chitosan*. Bioconjugate Chemistry, 2010. **21**(12): p. 2339-2346.
119. Huh, M.S., et al., *Tumor-homing glycol chitosan/polyethylenimine nanoparticles for the systemic delivery of siRNA in tumor-bearing mice*. Journal of Controlled Release, 2010. **144**(2): p. 134-143.
120. Lee, S.J., et al., *Tumor-Homing Poly-siRNA/Glycol Chitosan Self-Cross-Linked Nanoparticles for Systemic siRNA Delivery in Cancer Treatment*. Angewandte Chemie International Edition, 2012. **51**(29): p. 7203-7207.
121. Raviña, M., et al., *Hyaluronic Acid/Chitosan-g-Poly(ethylene glycol) Nanoparticles for Gene Therapy: An Application for pDNA and siRNA Delivery*. Pharmaceutical Research, 2010. **27**(12): p. 2544-2555.
122. Malhotra, M., C. Tomaro-Duchesneau, and S. Prakash, *Synthesis of TAT peptide-tagged PEGylated chitosan nanoparticles for siRNA delivery targeting neurodegenerative diseases*. Biomaterials, 2013. **34**(4): p. 1270-1280.
123. Luo, Y., et al., *An inhalable β_2 -adrenoceptor ligand-directed guanidinylated chitosan carrier for targeted delivery of siRNA to lung*. Journal of Controlled Release, 2012. **162**(1): p. 28-36.
124. Germershaus, O., et al., *Gene delivery using chitosan, trimethyl chitosan or polyethylenglycol-graft-trimethyl chitosan block copolymers: Establishment of structure-activity relationships in vitro*. Journal of Controlled Release, 2008. **125**(2): p. 145-154.
125. Loubaki, E., M. Ourevitch, and S. Sicsic, *Chemical modification of chitosan by glycidyl trimethylammonium chloride. characterization of modified chitosan by ¹³C- and ¹H-NMR spectroscopy*. European Polymer Journal, 1991. **27**(3): p. 311-317.
126. Kim, C.-H., S.-Y. Kim, and K.-S. Choi, *Synthesis and Antibacterial Activity of Water-soluble Chitin Derivatives*. Polymers for Advanced Technologies, 1997. **8**(5): p. 319-325.
127. Mao, S., et al., *Synthesis, characterization and cytotoxicity of poly(ethylene glycol)-graft-trimethyl chitosan block copolymers*. Biomaterials, 2005. **26**(32): p. 6343-6356.
128. Chang, K.-L., et al., *Development of lysine-histidine dendron modified chitosan for improving transfection efficiency in HEK293 cells*. Journal of Controlled Release, 2011. **156**(2): p. 195-202.
129. Jiang, H.-L., et al., *Galactosylated poly(ethylene glycol)-chitosan-graft-polyethylenimine as a gene carrier for hepatocyte-targeting*. Journal of Controlled Release, 2008. **131**(2): p. 150-157.

130. Lee, J.I., K.-S. Ha, and H.S. Yoo, *Quantum-dot-assisted fluorescence resonance energy transfer approach for intracellular trafficking of chitosan/DNA complex*. *Acta Biomaterialia*, 2008. **4**(4): p. 791-798.
131. Park, Y.K., et al., *Galactosylated chitosan-graft-dextran as hepatocyte-targeting DNA carrier*. *Journal of Controlled Release*, 2000. **69**(1): p. 97-108.
132. Tiera, M.J., et al., *Synthesis and Characterization of Phosphorylcholine-Substituted Chitosans Soluble in Physiological pH Conditions*. *Biomacromolecules*, 2006. **7**(11): p. 3151-3156.
133. Tømmeraas, K., et al., *Preparation and characterisation of fluorescent chitosans using 9-anthraldehyde as fluorophore*. *Carbohydrate Research*, 2001. **336**(4): p. 291-296.
134. Strand, S.P., et al., *Tailoring of Chitosans for Gene Delivery: Novel Self-Branched Glycosylated Chitosan Oligomers with Improved Functional Properties*. *Biomacromolecules*, 2008. **9**(11): p. 3268-3276.
135. Morris, V.B. and C.P. Sharma, *Folate mediated in vitro targeting of depolymerised trimethylated chitosan having arginine functionality*. *Journal of Colloid and Interface Science*, 2010. **348**(2): p. 360-368.
136. Kim, T.H., et al., *Efficient gene delivery by urocanic acid-modified chitosan*. *Journal of Controlled Release*, 2003. **93**(3): p. 389-402.
137. Moreira, C., et al., *Improving chitosan-mediated gene transfer by the introduction of intracellular buffering moieties into the chitosan backbone*. *Acta Biomaterialia*, 2009. **5**(8): p. 2995-3006.
138. Zheng, J.N., et al., *Chitosan-g-MPEG-Modified Alginate/Chitosan Hydrogel Microcapsules: A Quantitative Study of the Effect of Polymer Architecture on the Resistance to Protein Adsorption*. *Langmuir*, 2010. **26**(22): p. 17156-17164.
139. Casettari, L., et al., *PEGylated chitosan derivatives: Synthesis, characterizations and pharmaceutical applications*. *Progress in Polymer Science*, 2012. **37**(5): p. 659-685.
140. Kolate, A., et al., *PEG — A versatile conjugating ligand for drugs and drug delivery systems*. *Journal of Controlled Release*, 2014. **192**(0): p. 67-81.
141. Roberts, M.J., M.D. Bentley, and J.M. Harris, *Chemistry for peptide and protein PEGylation*. *Advanced Drug Delivery Reviews*, 2002. **54**(4): p. 459-476.
142. Varum, K.M., M.H. Ottoy, and O. Smidsrod, *Water-solubility of partially N-acetylated chitosans as a function of pH: effect of chemical composition and depolymerisation*. *Carbohydrate Polymers*, 1994. **25**: p. 65-70.
143. Veronese, F.M. and G. Pasut, *PEGylation, successful approach to drug delivery*. *Drug Discovery Today*, 2005. **10**(21): p. 1451-1458.
144. Lee, J.H., H.B. Lee, and J.D. Andrade, *Blood compatibility of polyethylene oxide surfaces*. *Progress in Polymer Science*, 1995. **20**(6): p. 1043-1079.
145. Jeong, J.H., T.G. Park, and S.H. Kim, *Self-Assembled and Nanostructured siRNA Delivery Systems*. *Pharmaceutical Research*, 2011. **28**(9): p. 2072-2085.
146. Jeong, J.H., et al., *Intracellular Delivery of Poly(ethylene glycol) Conjugated Antisense Oligonucleotide Using Cationic Lipids by Formation of Self-Assembled Polyelectrolyte Complex Micelles*. *Journal of Nanoscience and Nanotechnology*, 2006. **6**(9-10): p. 2790-2795.
147. Jeong, J.H., S.W. Kim, and T.G. Park, *A new antisense oligonucleotide delivery system based on self-assembled ODN-PEG hybrid conjugate micelles*. *Journal of Controlled Release*, 2003. **93**(2): p. 183-191.
148. Pozzi, D., et al., *Effect of polyethyleneglycol (PEG) chain length on the bio-nano-interactions between PEGylated lipid nanoparticles and biological fluids: from nanostructure to uptake in cancer cells*. *Nanoscale*, 2014. **6**(5): p. 2782-2792.
149. Ebbesen, M.F., et al., *Surface Analysis of PEGylated Nano-Shields on Nanoparticles Installed by Hydrophobic Anchors*. *Pharmaceutical Research*, 2013. **30**(7): p. 1758-1767.
150. Mao, S., et al., *Influence of polyethylene glycol chain length on the physicochemical and biological properties of poly(ethylene imine)-graft-poly(ethylene glycol) block copolymer/sirna polyplexes*. *Bioconjugate Chemistry*, 2006. **17**(5): p. 1209-1218.

151. Zhou, Y., et al., *Chitosan-N-poly(ethylene oxide) brush polymers for reduced nonspecific protein adsorption*. Journal of Colloid and Interface Science, 2007. **305**(1): p. 62-71.
152. Fang, C., et al., *In vivo tumor targeting of tumor necrosis factor- α -loaded stealth nanoparticles: Effect of MePEG molecular weight and particle size*. European Journal of Pharmaceutical Sciences, 2006. **27**(1): p. 27-36.
153. Valencia, P.M., et al., *Effects of Ligands with Different Water Solubilities on Self-Assembly and Properties of Targeted Nanoparticles*. Biomaterials, 2011. **32**(26): p. 6226-6233.
154. Lee, M. and S.W. Kim, *Polyethylene Glycol-Conjugated Copolymers for Plasmid DNA Delivery*. Pharmaceutical Research, 2005. **22**(1): p. 1-10.
155. Suh, W., et al., *An Angiogenic, Endothelial-Cell-Targeted Polymeric Gene Carrier*. Molecular Therapy, 2002. **6**(5): p. 664-672.
156. Choi, Y.H., et al., *Lactose-Poly(ethylene Glycol)-Grafted Poly-L-Lysine as Hepatoma Cell-Targeted Gene Carrier*. Bioconjugate Chemistry, 1998. **9**(6): p. 708-718.
157. Choi, Y.H., et al., *Characterization of a Targeted Gene Carrier, Lactose-Polyethylene Glycol-Grafted Poly-L-Lysine, and Its Complex with Plasmid DNA*. Human Gene Therapy, 1999. **10**(16): p. 2657-2665.
158. Sagara, K. and S.W. Kim, *A new synthesis of galactose-poly(ethylene glycol)-polyethylenimine for gene delivery to hepatocytes*. Journal of Controlled Release, 2002. **79**(1-3): p. 271-281.
159. Leamon, C.P., D. Weigl, and R.W. Hendren, *Folate Copolymer-Mediated Transfection of Cultured Cells*. Bioconjugate Chemistry, 1999. **10**(6): p. 947-957.
160. Bennis, J.M., et al., *Folate-PEG-folate-graft-polyethylenimine-based gene delivery*. Journal of Drug Targeting, 2001. **9**(2): p. 129-39.
161. Bennis, J.M., R.I. Mahato, and S.W. Kim, *Optimization of factors influencing the transfection efficiency of folate-PEG-folate-graft-polyethylenimine*. Journal of Controlled Release, 2002. **79**(1-3): p. 255-269.
162. Wang, H., et al., *Folate-PEG coated cationic modified chitosan – Cholesterol liposomes for tumor-targeted drug delivery*. Biomaterials, 2010. **31**(14): p. 4129-4138.
163. Aktaş, Y., et al., *Development and Brain Delivery of Chitosan-PEG Nanoparticles Functionalized with the Monoclonal Antibody OX26*. Bioconjugate Chemistry, 2005. **16**(6): p. 1503-1511.
164. Wang, F., et al., *Nanoscaled Polyion Complex Micelles for Targeted Delivery of Recombinant Hirudin to Platelets Based on Cationic Copolymer*. Molecular Pharmaceutics, 2010. **7**(3): p. 718-726.
165. Noh, S.M., et al., *Pegylated poly-L-arginine derivatives of chitosan for effective delivery of siRNA*. Journal of Controlled Release, 2010. **145**(2): p. 159-164.
166. Scanlan, M.J., et al., *Molecular cloning of fibroblast activation protein alpha, a member of the serine protease family selectively expressed in stromal fibroblasts of epithelial cancers*. Proceedings of the National Academy of Sciences of the United States of America, 1994. **91**(12): p. 5657-5661.
167. Jansen, K., et al., *Extended Structure-Activity Relationship and Pharmacokinetic Investigation of (4-Quinolinoyl)glycyl-2-cyanopyrrolidine Inhibitors of Fibroblast Activation Protein (FAP)*. Journal of Medicinal Chemistry, 2014. **57**(7): p. 3053-3074.
168. Niedermeyer, J., et al., *Targeted Disruption of Mouse Fibroblast Activation Protein*. Molecular and Cellular Biology, 2000. **20**(3): p. 1089-1094.
169. Garin-Chesa, P., L.J. Old, and W.J. Rettig, *Cell surface glycoprotein of reactive stromal fibroblasts as a potential antibody target in human epithelial cancers*. Proceedings of the National Academy of Sciences of the United States of America, 1990. **87**(18): p. 7235-7239.
170. Aertgeerts, K., et al., *Structural and Kinetic Analysis of the Substrate Specificity of Human Fibroblast Activation Protein α* . Journal of Biological Chemistry, 2005. **280**(20): p. 19441-19444.
171. Han, H.D., et al., *Targeted Gene Silencing Using RGD-Labeled Chitosan Nanoparticles*. Clinical cancer research 2010. **16**(15): p. 3910-3922.

172. Delehanty, J.B., et al., *Peptides for specific intracellular delivery and targeting of nanoparticles: implications for developing nanoparticle-mediated drug delivery*. Therapeutic Delivery, 2010. **1**(3): p. 411-33.
173. Benfer, M., et al., *Folic Acid-Decorated Nanocomposites Prepared by a Simple Solvent Displacement Method*. Macromolecular Bioscience, 2012. **12**(4): p. 438-445.
174. Lu, H., et al., *Site-Specific Antibody–Polymer Conjugates for siRNA Delivery*. Journal of the American Chemical Society, 2013. **135**(37): p. 13885-13891.
175. Lee, J., et al., *T Cell-Specific siRNA Delivery Using Antibody-Conjugated Chitosan Nanoparticles*. Bioconjugate Chemistry, 2012. **23**(6): p. 1174-1180.
176. Messerschmidt, S.K.E., et al., *Novel Single-Chain Fv' Formats for the Generation of Immunoliposomes by Site-Directed Coupling*. Bioconjugate Chemistry, 2008. **19**(1): p. 362-369.
177. Messerschmidt, S., *Targeted Lipid-Coated Nanoparticles: Delivery of Tumor Necrosis Factor-Functionalized Particles to Tumor Cells.*, in *Institute for Cell Biology and Immunology*. 2009, PhD Thesis, University of Stuttgart. p. 107.
178. Ryabtsova, O., et al., *Acylated Gly-(2-cyano)pyrrolidines as inhibitors of fibroblast activation protein (FAP) and the issue of FAP/prolyl oligopeptidase (PREP)-selectivity*. Bioorganic & Medicinal Chemistry Letters, 2012. **22**(10): p. 3412-3417.
179. Hermanson, G.T., *Bioconjugate Techniques*. Vol. 2 nd edition. 2008, Rockford, Illinois, USA.
180. Schoonen, L. and J.C.M. van Hest, *Functionalization of protein-based nanocages for drug delivery applications*. Nanoscale, 2014. **6**(13): p. 7124-7141.
181. Lallana, E., et al., *Click Chemistry for Drug Delivery Nanosystems*. Pharmaceutical Research, 2012. **29**(1): p. 1-34.
182. Kolb, H.C., M.G. Finn, and K.B. Sharpless, *Click Chemistry: Diverse Chemical Function from a Few Good Reactions*. Angewandte Chemie International Edition, 2001. **40**(11): p. 2004-2021.
183. Tang, W. and M.L. Becker, *"Click" reactions: a versatile toolbox for the synthesis of peptide-conjugates*. Chemical Society Reviews, 2014. **43**(20): p. 7013-7039.
184. Majireck, M.M. and S.M. Weinreb, *A Study of the Scope and Regioselectivity of the Ruthenium-Catalyzed [3+2]-Cycloaddition of Azides with Internal Alkynes*. The Journal of organic chemistry, 2006. **71**(22): p. 8680-8683.
185. Himo, F., et al., *Copper(I)-Catalyzed Synthesis of Azoles. DFT Study Predicts Unprecedented Reactivity and Intermediates*. Journal of the American Chemical Society, 2005. **127**(1): p. 210-216.
186. Sustman, R., *Orbital energy control of cycloaddition reactivity*. Pure and Applied Chemistry 1974. **40**(4): p. 569-593.
187. Brückner, R., *Organic Mechanisms - Reactions, Stereochemistry and Synthesis*, ed. M. Harmata. 2010, Berlin Heidelberg: Springer
188. Agard, N.J., J.A. Prescher, and C.R. Bertozzi, *A Strain-Promoted [3 + 2] Azide–Alkyne Cycloaddition for Covalent Modification of Biomolecules in Living Systems*. Journal of the American Chemical Society, 2004. **126**(46): p. 15046-15047.
189. Gobbo, P., et al., *Interfacial strain-promoted alkyne-azide cycloaddition (I-SPAAC) for the synthesis of nanomaterial hybrids*. Chemical Communications, 2013. **49**(38): p. 3982-3984.
190. Xie, R., S. Hong, and X. Chen, *Cell-selective metabolic labeling of biomolecules with bioorthogonal functionalities*. Current Opinion in Chemical Biology, 2013. **17**(5): p. 747-752.
191. Ning, X., et al., *Visualizing Metabolically Labeled Glycoconjugates of Living Cells by Copper-Free and Fast Huisgen Cycloadditions*. Angewandte Chemie, 2008. **120**(12): p. 2285-2287.
192. Baskin, J.M., et al., *Copper-free click chemistry for dynamic in vivo imaging*. Proceedings of the National Academy of Sciences of the United States of America, 2007. **104**(43): p. 16793-16797.
193. Codelli, J.A., et al., *Second-Generation Difluorinated Cyclooctynes for Copper-Free Click Chemistry*. Journal of the American Chemical Society, 2008. **130**(34): p. 11486-11493.

194. Ledin, P.A., N. Kolishetti, and G.-J. Boons, *Multifunctionalization of Polymers by Strain-Promoted Cycloadditions*. *Macromolecules*, 2013. **46**(19): p. 7759-7768.
195. Debets, M.F., et al., *Synthesis of DIBAC analogues with excellent SPAAC rate constants*. *Organic & Biomolecular Chemistry*, 2014. **12**(27): p. 5031-5037.
196. Gordon, C.G., et al., *Reactivity of Biarylazacyclooctynones in Copper-Free Click Chemistry*. *Journal of the American Chemical Society*, 2012. **134**(22): p. 9199-9208.
197. Dommerholt, J., et al., *Highly accelerated inverse electron-demand cycloaddition of electron-deficient azides with aliphatic cyclooctynes*. *Nat Commun*, 2014. **5**.
198. Patterson, D.M., L.A. Nazarova, and J.A. Prescher, *Finding the Right (Bioorthogonal) Chemistry*. *ACS Chemical Biology*, 2014. **9**(3): p. 592-605.
199. Decher, G. and J. Schmitt, *Fine-Tuning of the film thickness of ultrathin multilayer films composed of consecutively alternating layers of anionic and cationic polyelectrolytes*, in *Trends in Colloid and Interface Science VI*, C. Helm, M. Lösche, and H. Möhwald, Editors. 1992, Steinkopff. p. 160-164.
200. Decher, G., *Fuzzy Nanoassemblies: Toward Layered Polymeric Multicomposites*. *Science*, 1997. **277**(5330): p. 1232-1237.
201. Ariga, K., J.P. Hill, and Q. Ji, *Layer-by-layer assembly as a versatile bottom-up nanofabrication technique for exploratory research and realistic application*. *Physical Chemistry Chemical Physics*, 2007. **9**(19): p. 2319-2340.
202. Jewell, C.M. and D.M. Lynn, *Multilayered Polyelectrolyte Assemblies as Platforms for the Delivery of DNA and Other Nucleic Acid-Based Therapeutics*. *Advanced drug delivery reviews*, 2008. **60**(9): p. 979-999.
203. Lu, Y., et al., *Self-defensive antibacterial layer-by-layer hydrogel coatings with pH-triggered hydrophobicity*. *Biomaterials*, 2015. **45**: p. 64-71.
204. Pavluchina, S. and S. Sukhishvili, *Polymer assemblies for controlled delivery of bioactive molecules from surfaces*. *Advanced Drug Delivery Reviews*, 2011. **63**(9): p. 822-836.
205. Kharlampieva, E., V.A. Izumrudov, and S.A. Sukhishvili, *Electrostatic Layer-by-Layer Self-Assembly of Poly(carboxybetaine)s: Role of Zwitterions in Film Growth*. *Macromolecules*, 2007. **40**(10): p. 3663-3668.
206. Kim, B.-S., et al., *All-Star Polymer Multilayers as pH-Responsive Nanofilms*. *Macromolecules*, 2009. **42**(1): p. 368-375.
207. Labouta, H.I. and M. Schneider, *Tailor-made biofunctionalized nanoparticles using layer-by-layer technology*. *International Journal of Pharmaceutics*, 2010. **395**(1-2): p. 236-242.
208. Monika, S., *Layered polyelectrolyte complexes: physics of formation and molecular properties*. *Journal of Physics: Condensed Matter*, 2003. **15**(49): p. R1781.
209. Qi, Z., et al., *Layer-by-Layer Fabrication and Characterization of Gold-Nanoparticle/Myoglobin Nanocomposite Films*. *Advanced Functional Materials*, 2006. **16**(3): p. 377-386.
210. Göse, M., P. Pescador, and U. Reibetanz, *Design of a Homogeneous Multifunctional Supported Lipid Membrane on Layer-by-Layer Coated Microcarriers*. *Biomacromolecules*, 2015. **16**(3): p. 757-768.
211. Saurer, E.M., et al., *Polyelectrolyte Multilayers Promote Stent-Mediated Delivery of DNA to Vascular Tissue*. *Biomacromolecules*, 2013. **14**(5): p. 1696-1704.
212. Deng, Z.J., et al., *Layer-by-Layer Nanoparticles for Systemic Codelivery of an Anticancer Drug and siRNA for Potential Triple-Negative Breast Cancer Treatment*. *ACS Nano*, 2013. **7**(11): p. 9571-9584.
213. Dimitrova, M., et al., *Sustained delivery of siRNAs targeting viral infection by cell-degradable multilayered polyelectrolyte films*. *Proceedings of the National Academy of Sciences*, 2008.
214. Zhang, H., et al., *Gold Nanoparticles for Neural Prosthetics Devices*. *Nano letters*, 2012. **12**(7): p. 3391-3398.

215. Dimzon, I.K.D. and T.P. Knepper, *Degree of deacetylation of chitosan by infrared spectroscopy and partial least squares*. International Journal of Biological Macromolecules, 2015. **72**: p. 939-945.
216. Duarte, M.L., et al., *An optimised method to determine the degree of acetylation of chitin and chitosan by FTIR spectroscopy*. International Journal of Biological Macromolecules, 2002. **31**(1-3): p. 1-8.
217. Vårum, K.M., et al., *Determination of the degree of N-acetylation and the distribution of N-acetyl groups in partially N-deacetylated chitins (chitosans) by high-field n.m.r. spectroscopy*. Carbohydrate Research, 1991. **211**(1): p. 17-23.
218. Hirai, A., H. Odani, and A. Nakajima, *Determination of degree of deacetylation of chitosan by ¹H NMR spectroscopy*. Polymer Bulletin, 1991. **26**(1): p. 87-94.
219. Reischl, D. and A. Zimmer, *Drug delivery of siRNA therapeutics: potentials and limits of nanosystems*. Nanomedicine, 2009. **5**(1): p. 8-20.
220. Hu, Y., et al., *Effect of PEG conformation and particle size on the cellular uptake efficiency of nanoparticles with the HepG2 cells*. Journal of Controlled Release, 2007. **118**(1): p. 7-17.
221. Sugimoto, M., et al., *Preparation and characterization of water-soluble chitin and chitosan derivatives*. Carbohydrate Polymers, 1998. **36**(1): p. 49-59.
222. Cedervall, T., et al., *Understanding the nanoparticle-protein corona using methods to quantify exchange rates and affinities of proteins for nanoparticles*. Proceedings of the National Academy of Sciences of the United States of America, 2007. **104**(7): p. 2050-2055.
223. Kevin Mattison, A.M., and Michael Kaszuba, *A Primer on Particle Sizing Using Dynamic Light Scattering*. American biotechnology laboratory 2003: p. 20-22.
224. Malvern, I.L., *Zetasizer Nano User Manual*. MAN0485 Issue 11. 2013, Worcestershire, Uk.
225. Merkel, O.M., et al., *Nonviral siRNA Delivery to the Lung: Investigation of PEG-PEI Polyplexes and Their In Vivo Performance*. Molecular Pharmaceutics, 2009. **6**(4): p. 1246-1260.
226. Lallana, E., E. Fernandez-Megia, and R. Riguera, *Surpassing the Use of Copper in the Click Functionalization of Polymeric Nanostructures: A Strain-Promoted Approach*. Journal of the American Chemical Society, 2009. **131**(16): p. 5748-5750.
227. Booker-Milburn, K.I., et al., *Stereoselective Intermolecular [2+2] photocycloaddition reactions of tetrahydrophthalic anhydride and derivatives with alkenols and alkynols*. Tetrahedron, 1999. **55**(18): p. 5875-5888.
228. Chen, X., et al., *A Thermally Re-mendable Cross-Linked Polymeric Material*. Science, 2002. **295**(5560): p. 1698-1702.
229. López-Carrillo, V. and A.M. Echavarren, *Gold(I)-Catalyzed Intermolecular [2+2] Cycloaddition of Alkynes with Alkenes*. Journal of the American Chemical Society, 2010. **132**(27): p. 9292-9294.
230. Hook, B.D.A., et al., *A Practical Flow Reactor for Continuous Organic Photochemistry*. The Journal of Organic Chemistry, 2005. **70**(19): p. 7558-7564.
231. Franz, H., W.J. Thorsten, and K. Michael, *The MALDI process and method in MALDI MS: A practical guide to instrumentation, methods, and applications*. **2014**, Wiley-VCH Verlag, Weinheim. p. 1-39.
232. Fernandez-Megia, E., et al., *Conjugation of Bioactive Ligands to PEG-Grafted Chitosan at the Distal End of PEG*. Biomacromolecules, 2007. **8**(3): p. 833-842.
233. Sioud, M., *On the delivery of small interfering RNAs into mammalian cells*. Expert Opinion on Drug Delivery, 2005. **2**(4): p. 639-651.
234. Lavertu, M., et al., *High efficiency gene transfer using chitosan/DNA nanoparticles with specific combinations of molecular weight and degree of deacetylation*. Biomaterials, 2006. **27**(27): p. 4815-4824.
235. Koping-Hoggard, M., et al., *Improved chitosan-mediated gene delivery based on easily dissociated chitosan polyplexes of highly defined chitosan oligomers*. Gene Therapy, 2004. **11**(19): p. 1441-1452.

236. Gary, D.J., N. Puri, and Y.-Y. Won, *Polymer-based siRNA delivery: Perspectives on the fundamental and phenomenological distinctions from polymer-based DNA delivery*. *Journal of Controlled Release*, 2007. **121**(1–2): p. 64–73.
237. Bloomfield, V.A., *DNA condensation by multivalent cations*. *Biopolymers*, 1997. **44**(3): p. 269–282.
238. Knorr, V., et al., *An Acetal-Based PEGylation Reagent for pH-Sensitive Shielding of DNA Polyplexes*. *Bioconjugate Chemistry*, 2007. **18**(4): p. 1218–1225.
239. Sung, S.-J., et al., *Effect of Polyethylene Glycol on Gene Delivery of Polyethylenimine*. *Biological and Pharmaceutical Bulletin*, 2003. **26**(4): p. 492–500.
240. Yang, T.-C., C.-C. Chou, and C.-F. Li, *Preparation, water solubility and rheological property of the N-alkylated mono or disaccharide chitosan derivatives*. *Food Research International*, 2002. **35**(8): p. 707–713.
241. Malvern, I.L. *Liposomes and the use of zeta potential measurements to study sterically stabilized liposomes using malvern instruments*. 2013.
242. Mosqueira, V.C., et al., *Relationship between complement activation, cellular uptake and surface physicochemical aspects of novel PEG-modified nanocapsules*. *Biomaterials*, 2001. **22**(22): p. 2967–79.
243. Hühn, D., et al., *Polymer-Coated Nanoparticles Interacting with Proteins and Cells: Focusing on the Sign of the Net Charge*. *ACS Nano*, 2013. **7**(4): p. 3253–3263.
244. Monopoli, M.P., et al., *Biomolecular coronas provide the biological identity of nanosized materials*. *Nature Nanotechnology*, 2012. **7**(12): p. 779–786.
245. Kingshott, P., H. Thissen, and H.J. Griesser, *Effects of cloud-point grafting, chain length, and density of PEG layers on competitive adsorption of ocular proteins*. *Biomaterials*, 2002. **23**(9): p. 2043–2056.
246. Unsworth, L.D., H. Sheardown, and J.L. Brash, *Protein-Resistant Poly(ethylene oxide)-Grafted Surfaces: Chain Density-Dependent Multiple Mechanisms of Action*. *Langmuir*, 2008. **24**(5): p. 1924–1929.
247. Walkey, C.D., et al., *Nanoparticle Size and Surface Chemistry Determine Serum Protein Adsorption and Macrophage Uptake*. *Journal of the American Chemical Society*, 2012. **134**(4): p. 2139 – 2147.
248. Zheng, M., et al., *Targeting the Blind Spot of Polycationic Nanocarrier-Based siRNA Delivery*. *ACS nano*, 2012. **6**(11): p. 9447 – 9454.
249. <https://www.rndsystems.com/research-area/lysosomal-enzymes>. *R&D systems, Lysosomal Enzymes*.
250. Maurstad, G., et al., *PEGylated chitosan complexes DNA while improving polyplex colloidal stability and gene transfection efficiency*. *Carbohydrate Polymers*, 2013. **94**(1): p. 436–443.
251. Braeckmans, K., et al., *Sizing Nanomatter in Biological Fluids by Fluorescence Single Particle Tracking*. *Nano Letters*, 2010. **10**(11): p. 4435–4442.
252. van Gaal, E.V.B., et al., *Flow cytometry for rapid size determination and sorting of nucleic acid containing nanoparticles in biological fluids*. *Journal of Controlled Release*, 2010. **141**(3): p. 328–338.
253. Jacob, M., L. Chang, and E. Pure, *Fibroblast Activation Protein in Remodeling Tissues*. *Current Molecular Medicine*, 2012. **12**(10): p. 1220–1243.
254. Messerschmidt, S.K.E., et al., *Targeted lipid-coated nanoparticles: Delivery of tumor necrosis factor-functionalized particles to tumor cells*. *Journal of Controlled Release*, 2009. **137**(1): p. 69–77.
255. Zimmermann, J.L., et al., *Thiol-based, site-specific and covalent immobilization of biomolecules for single-molecule experiments*. *Nat. Protocols*, 2010. **5**(6): p. 975–985.
256. Mädler, S., et al., *Chemical cross-linking with NHS esters: a systematic study on amino acid reactivities*. *Journal of Mass Spectrometry*, 2009. **44**(5): p. 694–706.

257. Morpurgo, M., E.A. Bayer, and M. Wilchek, *N-hydroxysuccinimide carbonates and carbamates are useful reactive reagents for coupling ligands to lysines on proteins*. Journal of Biochemical and Biophysical Methods, 1999. **38**(1): p. 17-28.
258. Sletten, E.M. and C.R. Bertozzi, *Bioorthogonal Chemistry: Fishing for Selectivity in a Sea of Functionality*. Angewandte Chemie (International ed. in English), 2009. **48**(38): p. 6974-6998.
259. Best, M.D., *Click Chemistry and Bioorthogonal Reactions: Unprecedented Selectivity in the Labeling of Biological Molecules*. Biochemistry, 2009. **48**(28): p. 6571-6584.
260. Yao, J.Z., et al., *Fluorophore targeting to cellular proteins via enzyme-mediated azide ligation and strain-promoted cycloaddition*. Journal of the American Chemical Society, 2012. **134**(8): p. 3720-3728.
261. Jewett, J.C. and C.R. Bertozzi, *Cu-free click cycloaddition reactions in chemical biology*. Chemical Society Reviews, 2010. **39**(4): p. 1272-1279.
262. Jewett, J.C., E.M. Sletten, and C.R. Bertozzi, *Rapid Cu-Free Click Chemistry with Readily Synthesized Biarylazacyclooctynones*. Journal of the American Chemical Society, 2010. **132**(11): p. 3688-3690.
263. Bar-Or, D., et al., *An Analog of the Human Albumin N-Terminus (Asp-Ala-His-Lys) Prevents Formation of Copper-Induced Reactive Oxygen Species*. Biochemical and Biophysical Research Communications, 2001. **284**(3): p. 856-862.
264. Chang, B.S. and B. Yeung, *Physical Stability of Protein Pharmaceuticals*, in *Formulation and Process Development Strategies for Manufacturing Biopharmaceuticals*. 2010, John Wiley & Sons, Inc. p. 69-104.
265. Mahler, H.-C., et al., *Protein aggregation: Pathways, induction factors and analysis*. Journal of Pharmaceutical Sciences, 2009. **98**(9): p. 2909-2934.
266. Vázquez-Rey, M. and D.A. Lang, *Aggregates in monoclonal antibody manufacturing processes*. Biotechnology and Bioengineering, 2011. **108**(7): p. 1494-1508.
267. Bondos, S.E. and A. Bicknell, *Detection and prevention of protein aggregation before, during, and after purification*. Analytical Biochemistry, 2003. **316**(2): p. 223-231.
268. Bam, N.B., et al., *Tween protects recombinant human growth hormone against agitation-induced damage via hydrophobic interactions*. Journal of Pharmaceutical Sciences, 1998. **87**(12): p. 1554-1559.
269. Kelley, S.K. and A. Ashkenazi, *Targeting death receptors in cancer with Apo2L/TRAIL*. Current Opinion in Pharmacology, 2004. **4**(4): p. 333-339.
270. v. Klitzing, R., *Internal structure of polyelectrolyte multilayer assemblies*. Physical Chemistry Chemical Physics, 2006. **8**(43): p. 5012-5033.
271. Nolte, A., et al., *Impact of polyelectrolytes and their corresponding multilayers to human primary endothelial cells*. Journal of Biomaterials Applications, 2013. **28**(1): p. 84-99.
272. Hossfeld, S., et al., *Bioactive coronary stent coating based on layer-by-layer technology for siRNA release*. Acta Biomaterialia, 2013. **9**(5): p. 6741-6752.

CURRICULUM VITAE

Persönliches

Geboren am 09 April 1987
Geburtsort: Galați, Rumänien
Familienstand: ledig

Studium und Ausbildung

- Seit Jul 2011, Naturwissenschaftliches und medizinisches Institut an der Universität Tübingen (NMI)
Promotion unter der Betreuung von Prof. Stefan Laufer und Prof. Dieter Stoll
Titel: *Entwicklung von Target spezifischen siRNA-Nanotransportern*
Schwerpunkte:
- Organische Chemie (Biokonjugatchemie, Polymerchemie)
 - Biochemie (Darstellung von Antikörperfragmenten aus Zellkulturen)
 - Physikalische Chemie (Charakterisierung von Nanopartikeln)
 - Arbeiten unter GMP Bedingungen
 - Führen kleiner Arbeitsgruppen
- Sep 2009 – Sep 2010 Mathematisch – Physikalische Fakultät, Universität Leeds
Masterarbeit in Chemie/Biochemie,
„*Synthese potenter und selektiver Inhibitoren von Glutamat Transportern*“ („*Synthesis of potent and selective inhibitors of glutamate transporters*“); Betreuer: Prof. Adam Nelson
Schwerpunkte:
- Organische Chemie
 - Zellkulturen
- Okt 2006 – Jun 2009 Chemische Fakultät, Universität Bukarest
Bachelorarbeit „*Neue katalytische Syntheseroute zur Darstellung von Vitamin K₃*“
Betreuerin: Prof. Dr. Mihaela Florea
Abschlussnote: 8.75 von 10

Stipendien

- Mai 2012 – Mai 2014 DAAD Stipendium, Kooperationsprojekt mit der technischen Universität Lissabon, Zentrum für Strukturaufklärung (Forschungsaufenthalt)
- Sep 2013 Deutsche Gesellschaft für Biomaterialien, Reisestipendium zum Jahreskongress der European Society of Biomaterials (ESB) in Madrid
- Sep 2009 – Sep 2010 AstraZeneca Stipendium

Sep 2009 – Sep 2010 Biotechnology and Biological Sciences Research Council Stipendium

Okt 2006 – Jun 2009 Universität Bukarest Stipendium

Weiterbildungen / Praktika

Okt 2008 – Jan 2009 Laborpraxis molekulare Zellbiologie, Institut für Biochemie, Bukarest

Jun – Jul 2008 Praktikum organische Chemie, Institut für Forschung und Entwicklung in der chemisch pharmazeutischen Industrie, Bukarest

Ehrenamtliche Tätigkeiten

Seit Feb 2014 Projektleiter (Kontaktmanagement und konzeptionelle Begleitung) "Galati2020" – Projekt zur Wirtschaftsförderung, Kommunikationskoordination von Politik, Wirtschaft und Kirche
Projektpartner: Ministerium für Kultus; Jugend und Sport Baden-Württemberg; Steinbeis Transferzentrum; Rumänische orthodoxe Metropole für Deutschland, Zentral und Nordeuropa; Fairventures Worlwide GmbH

Qualifikationen / Zusätzliches

Sprachen **Rumänisch:** Muttersprache
Englisch: fließend, IELTS Prüfung (Note: 7.0)
Französisch: fließend, DELF B2
Deutsch: fortgeschritten (Niveau B1)
Spanisch: fließend (Niveau B1)
Italienisch: fortgeschritten

EDV Sehr gute Kenntnisse in MS Excel, MS PowerPoint, MS Word, Outlook, Mind Map, Endnote, Origin

Publikationen

1. Andra Guțoaia, Liane Schuster, Simona Margutti, Dieter Stoll, Burkhard Schlosshauer, Stefan Laufer, Hanna Hartmann, Rumen Krastev, *Pre-programmed nanocarriers for implant coatings*, Bionanomaterials, **2014**
2. Andra Guțoaia, Liane Schuster, Dieter Stoll, Burkhard Schlosshauer, Stefan Laufer, Hanna Hartmann, Rumen Krastev, *Increased transfection efficiencies by PEGylation of chitosan/siRNA nanoplexes*, 25th European Conference of Biomaterials, **2013**, p.61
3. Andra Guțoaia, Liane Schuster, Simona Margutti, Dieter Stoll, Burkhard Schlosshauer, Stefan Laufer, Hanna Hartmann, Rumen Krastev, *PEG-functionalized chitosan/siRNA nanoplexes for gene delivery*, 11th International Congress of the European Chitin Society, **2013**, p.124
4. Andra Guțoaia, Liane Schuster, Simona Margutti, Dieter Stoll, Burkhard Schlosshauer, Stefan Laufer, Hanna Hartmann, Rumen Krastev, *Novel chitosan polymer – based system to target cell delivery of siRNA*, Bionanomaterials, **2012**, 13:1-4, p.221